JPL Publication 87-14

Proceedings of the NASA Workshop on Atomic Oxygen Effects

November 10 –11, 1986

David E. Brinza
Editor

June 1, 1987

National Aeronautics and
Space Administration

Jet Propulsion Laboratory
California Institute of Technology
Pasadena, California

JPL Publication 87-14

Proceedings of the NASA Workshop on Atomic Oxygen Effects

November 10 –11, 1986

David E. Brinza
Editor

June 1, 1987

National Aeronautics and
Space Administration

Jet Propulsion Laboratory
California Institute of Technology
Pasadena, California

This publication was prepared by the Jet Propulsion Laboratory, California Institute of Technology, under a contract with the National Aeronautics and Space Administration.

ABSTRACT

A workshop was held November 10-11, 1987 in Pasadena, California addressing the scientific issues concerning the effects of atomic oxygen on materials in the low earth orbital (LEO) environment. The workshop program included eighteen invited speakers plus contributed posters covering topics such as LEO spaceflight experiments, interaction mechanisms, and atomic oxygen source development. Discussion sessions were also held to organize a test program to evaluate atomic oxygen exposure facilities. The key issues raised in the workshop are: 1) the need to develop a reliable predictive model of the effects of long-term exposure of materials to the LEO environment, 2) the ability of ground-based exposure facilities to provide useful data for development of LEO durable materials, and 3) accurate determination of the composition of the LEO environment. These proceedings include manuscripts submitted by the authors of the invited papers, the abstracts for the contributed posters, and an account of the test program discussion sessions.

Foreword

This workshop, hosted by the Jet Propulsion Laboratory, was held November 10-11, 1986 in Pasadena, California. The focus of the workshop was the effect of atomic oxygen on materials in the low earth orbit (LEO) environment. The primary goal of the workshop was to provide a forum for scientific discussion to define the elements necessary in a research program to fully characterize atomic interactions with materials. A secondary goal of the workshop was to formulate a test program which would evaluate the various atomic oxygen exposure facilities. The workshop was attended by over one hundred participants representing a very broad spectrum of technical areas relevant to the atomic oxygen problem.

Since the identification of atomic oxygen as a key element in the erosion of thermal blanketing materials in early shuttle missions, the degradation of materials caused by long-term exposure to atomic oxygen impacting material surfaces at LEO velocities (8 km/sec) has become an area of major concern in material selection for Space Station and other long projected life LEO missions. This workshop was organized to present the current level of understanding of the problem to an audience of widely varying areas of expertise such as experimental and theoretical chemical physics, chemistry, polymer and material sciences, spacecraft hardware design, etc. A more important aim, though, was to gain insight from experts in the above areas whose work has not been focussed on the atomic oxygen problem. These participants offered fresh, innovative points of view to the issues addressed during the workshop and often led some very stimulating discussions. The key issues raised in the workshop lie in three areas:

1) The ability to develop a reliable predictive model to assess the effects of long-term exposure of materials to the LEO environment;

2) The ability of ground-based simulation facilities to provide meaningful data in the development of LEO durable materials; and

3) Aeronometric determination of the compositional details of the low earth orbital environment.

The presentations at the workshop demonstrated the significant effort under way in NASA centers, at various universities and in private corporations attempting to address the above issues. A subsequent workshop, to be held about a year from now, should provide an indication of progress in these areas, particularly in the ground-based simulation aspect, through presentation of the results of the facilities test program.

The technical program of the workshop consisted of eighteen invited speakers, a contributed poster session, and an open discussion session. The invited presentations addressed issues relevant to atomic oxygen interactions within the topics of past and future spaceflight experiments, experimental and theoretical aspects of mechanistic model development, and LEO simulation source development. Contributed posters were presented in the above topics in an informal environment which encouraged interaction among the participants. The workshop ended with a discussion session in which a test program was defined with the purpose of characterizing the various atomic oxygen exposure facilities in use or under development.

These proceedings document the formal presentations of the workshop via manuscripts as submitted by the authors. The papers are reproduced in the order of presentation at the workshop. The abstracts for the posters presented in the third session are reproduced in Appendix A. Appendix B provides an account of the open and closed discussion sessions led by Dr. Bruce Banks (NASA Lewis Research Center) to organize the atomic oxygen facility test program. The workshop agenda is reproduced in Appendix C. A listing of the names and addresses of registered workshop participants is given in Appendix D.

The workshop coordinator and scientific committee would like to commend the speakers for their highly relevant and stimulating presentations. The presenters of the posters are also to be commended for providing interesting material and engaging in enlightening discussions with the other workshop particpants. Finally, the workshop administrative staff deserves special acknowledgment for their efforts in organizing and conducting this workshop.

David E. Brinza
Workshop Coordinator

TABLE OF CONTENTS

TABLE OF CONTENTS (cont.)

Session I:

Space Flight Experiments

REVIEW OF LEO FLIGHT EXPERIMENTS

L. Leger, B. Santos-Mason, J. Visentine and J. Kuminecz
NASA Lyndon B. Johnson Space Center
Houston, Texas

Introduction

Surfaces of orbiting spacecraft are exposed to a flux of Earth ambient atmospheric species. This flux can be highly directional as a result of spacecraft velocity through the atmosphere. Fluence on the spacecraft is maximized on the ram surface and minimized on the wake surface. The main constituent of this atmosphere is atomic oxygen, and at spacecraft velocities, its kinetic energy, relative to the surface, is approximately 8×10^{-19} J (5 eV). Atomic oxygen flux for typical low Earth orbit conditions is 3×10^{14} atom/cm^2-sec. Since atomic oxygen is a strong oxidizing agent, it might be expected that such a flux would affect exposed organic surfaces, and indeed such effects have been observed on Space Shuttle flights.[1,2,3] The major effect is recession of surfaces exposed to ram conditions. Recession is assumed to result from oxidative attack of the organic polymer chains, producing volatile species and resulting in mass loss. Exposed surfaces are generally roughened on a microscopic scale with some physical property changes occurring. Based on current data, this recession appears to be the most significant change in materials used on spacecraft in the low Earth orbital (LEO) environment.

Limited measurements were made on Orbiter exposed surfaces during early Space Shuttle flights. Low fluence and lack of control specimens precluded obtaining quantitative data from these flights. However, qualitative results do support the observations obtained on later, dedicated flight experiments.

Essentially all quantitative reaction rate data have been obtained on Space Shuttle flights STS-5 and STS-8, which are discussed in the flight experiments summary. Additional limited data obtained on mission STS 41-G are also summarized in the flight experiments summary and discussed in references 4 and 4b. Reaction rate data obtained from these flight experiments have been applied to Space Station exposure conditions and are discussed in the Space Station application section.

Results of measurements made on hardware returned on the Solar Maximum repair mission (Space Shuttle flight 41-C) are reported in reference 5. Quantitative rate data were not available from these measurements because of the difficulty in defining the exposure fluence for the specific surfaces studied.

Additional data may be available with the return of the Long Duration Exposure Facility (LDEF), which was launched in April 1984. Unfortunately, delayed return of the spacecraft may have already lead to significant loss of quantitative results since original experiment design lifetime was one year.

Summary of Flight Experiments

General

All flight experiments conducted to date have essentially provided for passive exposure of samples to oxygen fluences of approximately 1 to 3.5 $\times$ 10^{20} atoms/cm^2. Atmospheric density is used to derive fluence and is dependent on solar activity, which has been on the declining side of the 11-year cycle. Thus, relatively low flight altitudes of <300 km were used to acquire these exposures. In addition, the flight attitudes were selected to provide maximum exposure to ram conditions. Exposure fluence was derived from ambient density predictions obtained using the mass spectrometer incoherent scattering (MSIS) model, together with spacecraft velocity and exposure attitude.[7] After exposure on the flight experiments, the samples were analyzed using various methods ranging from mass loss to extensive scanning electron microscopy and surface analysis techniques.

Experiment Description

STS-5: The fifth Space Shuttle flight (STS-5) was launched in November 1982 with a payload consisting principally of deployable satellites. After deployment of these satellites, an experiment was conducted to further study surface effect found on earlier missions. A detailed description of this experiment and associated results has previously been presented.[8,9,10] Therefore, only a brief summary is included here for completeness.[12.13]

Exposure conditions were selected to provide the largest atomic oxygen fluence and associated surface changes that would facilitate postflight laboratory measurements. These conditions were established during a 40-hr period in which the Orbiter vehicle was maintained in solar inertial attitude. Material samples were exposed on two trays, which were mounted to a support structure located at the payload bay door hinge level and thereby, provided maximum view to the space environment. Specimens in filmstrip form were mounted on six heater plates, which were thermally controlled to temperatures of 297, 338, and 394 K (24°, 65°, and 121° C). A few disk samples were mounted on other regions of the trays.

STS-8: The second dedicated materials/space environment interaction experiment was conducted on the eighth Space Shuttle (STS-8) flight in August 1983. Basically, the same exposure approach as that employed previously was used, except that, in addition two active instruments were added to evaluate the effects of charged species and solar radiation on the reaction rates. Passive fixtures were also added to evaluate mass transfer from specimen to specimen.

Considering that solar activity was approaching a minimum, a rather high fluence was achieved by both lowering the vehicle altitude to 225 km and maintaining the sample surfaces in direct ram conditions throughout the 40-hr exposure period. Such exposure conditions provided a fluence of 3.5 $\times$ 10^{20} atoms/cm^2 to the samples, which were located in the forward region of the payload bay (fig. 1).

Material specimens consisted of both strips and disks as before, but more individual specimens (>300) were included. Samples were selected to

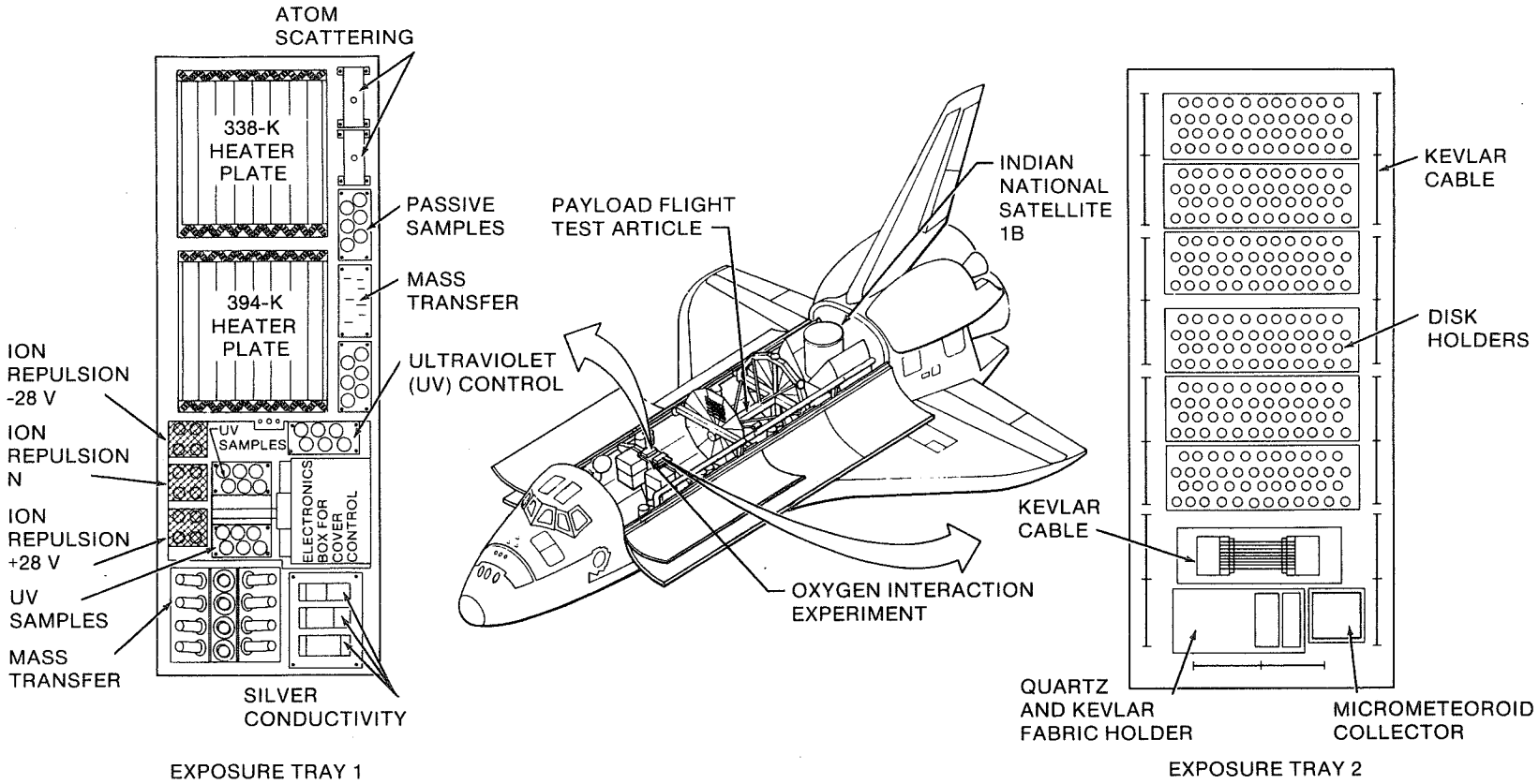

Fig. 1. STS-8 mission exposure configuration.

represent typical spacecraft materials such as polymer films, paints, vapor-deposited coatings, metals, and composites and were provided and analyzed by a number of different laboratories.

In addition to the STS-8 experiments described above, several quartz crystal microbalances (QCM) were exposed on a separate mounting system in the payload bay. Three QCM's were coated to determine the reaction efficiencies of carbon and osmium. A detailed description of this experiment is to be published, however, reaction rates were $\sim 3.5 \times 10^{-25}$ cm^3/atom (0.035 carbon atoms/oxygen atom) for carbon and 2.6×10^{-26} cm^3/atom (1.9×10^{-3} osmium atoms/oxygen atom) for osmium.(11)

STS 41-G: Another exposure opportunity was provided on the Space Shuttle mission (STS 41-G) launched in October 1984. Because Orbiter attitude for this mission did not allow orienting the payload bay into the velocity vector, samples were mounted directly to the remote manipulator system (RMS) using polyimide tape as shown in figure 2. The arm was then deployed over the port side of the vehicle as shown and oriented with the samples facing into the velocity vector for a period of 35 hr. Not all ambient atmosphere exposure occurred in this orientation since the RMS was also used to deploy a satellite. These operations precluded accurate calculation of the exposure flux; however, based on recession of the attachment tape, the exposure flux was determined to be approximately 3×10^{20} atoms/cm^2 on the direct ram-facing surfaces.

Samples for the STS 41-G mission consisted primarily of composite materials and materials used on the Hubble space telescope. Results for composite materials and the space telescope are reviewed in references 4 and 6, respectively.

Experiment Results

A variety of postflight measurements ranging from surface morphology to surface chemistry changes were made on the exposed surfaces by the participating laboratories. The limited scope of this paper does not allow for a complete discussion of the findings, which are reported elsewhere(4 through 10 and 12 through 22); therefore, only a brief summary with sufficient quantitative data for application to following Space Station discussions will be presented.

Of the two general classes of materials: metals and nonmetals, the metals are the least reactive. More than twenty metal surfaces have been exposed on the two experiments and, of these, only two, silver and osmium (Os), interact with sufficient speed to produce macroscopic changes. Silver forms heavy oxide layers, typical of oxidative attack, resulting in loss of material by flaking and spallation. The rate of oxidation is somewhat dependent on the specific silver form. Quantitative interaction rates have not been well established; however, oxide thicknesses of greater than 0.4 μm have been measured.

Osmium loses mass with a reaction efficiency of 2.6×10^{-26} cm^3/atom, (Table 1) apparently through the formation and loss of OsO_4, which has a relatively high vapor pressure.(11) Generally, all the other metals have

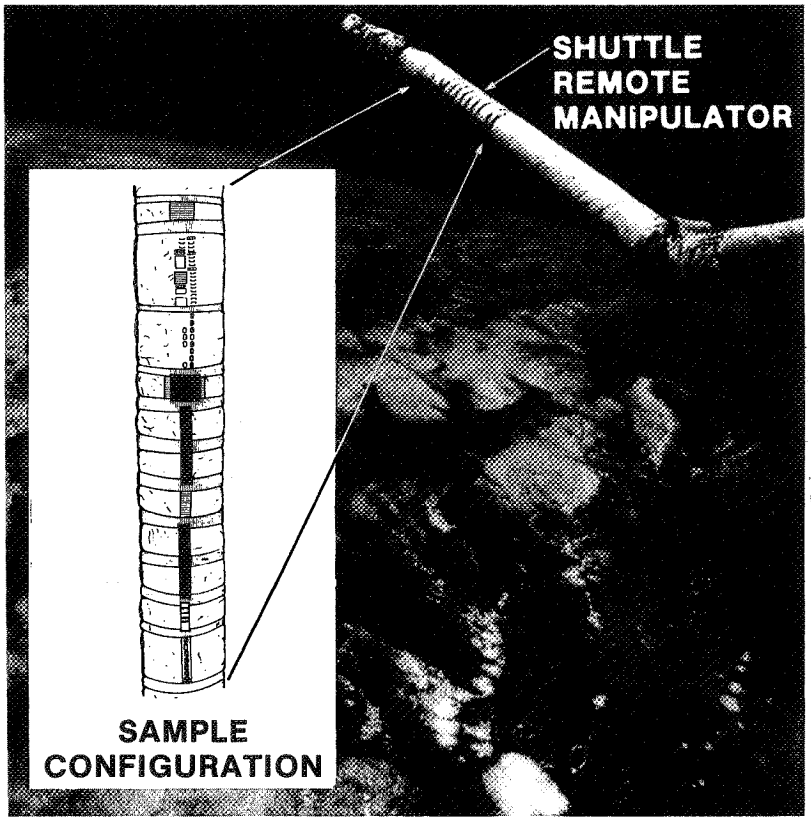

Fig. 2. STS-41G exposure configuration.

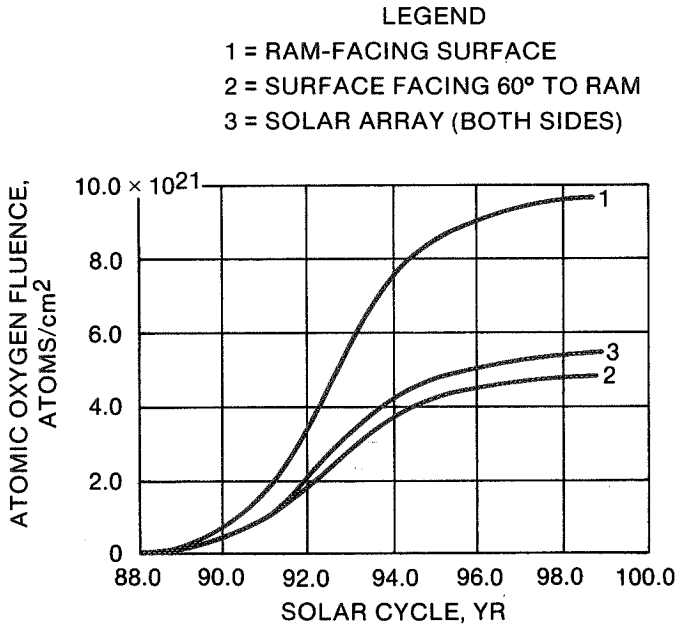

Fig. 3. Atomic oxygen fluence increase with solar activity.

TABLE 1. REACTION EFFICIENCIES OF SELECTED MATERIALS WITH ATOMIC OXYGEN IN LOW EARTH ORBIT

Material	Reaction efficiency, ($\times 10^{-24}$ cm^3/atom)	Material	Reaction efficiency, ($\times 10^{-24}$ cm^3/atom)
Kapton	3×10^{-24}	Silicones	
Mylar	3.4	RTV-560	0.02*
Tedlar (Clear)	3.2	DC6-1104	0.02*
Polyethylene	3.7	T-650	0.02*
Polysulfone	2.4	DC1-2577	0.02*
Graphite/Epoxy		Black paint Z306	0.3-0.4*
1034C	2.1	White paint A276	0.3-0.4*
5208/T300	2.6	Black paint Z302	2.03*
Epoxy	1.7	Perfluorinated polymers	
Polystyrene	1.7	Teflon, TFE	<0.05
Polybenzimidazole	1.5	Teflon, FEP	<0.05
25% Polysiloxane/45% Polyimide	0.3	Carbon (various forms)	0.5-1.3
Polyester 7% 7% Polysilane/93% Polyimide	0.6	Silver (various forms)	Heavily attacked
Polyester	Heavily attacked	Osmium	0.026
Polyester with Antioxidant	Heavily attacked		

*Units of mg/cm^2 for STS-8 mission. Loss is assumed to occur in early part of exposure; therefore, no assessment of efficiency can be made.

TABLE 2. SURFACE RECESSION PREDICTIONS FOR SPACE STATION COMPONENTS

		Constant altitude (465 km)		Constant density (2×10^8 atoms/cm^3)	
Materials	Lifetime, yr	Fluence, atoms/cm^2	Recession, cm (mil)	Fluence, atoms/cm^2	Recession, cm (mil)
Graphite epoxy structural members, forward facing side	30	3.6×10^{22}	8.6×10^{-2} (34)	$*1.4 \times 10^{23}$	3.2×10^{-1} (126)
Solar power arrays front & back, exposure	20	1.3×10^{22}	3.8×10^{-2} (15)	$*5.5 \times 10^{22}$	1.7×10^{-1} (65)
Radiator surfaces front & back, exposure	20	1.5×10^{22}	--	$*6.3 \times 10^{22}$	--

*Constant density results in approximately 4 times more fluence

significantly lower interaction rates than those of silver and osmium. As expected, metal oxides are nonreactive.

Generally all organic materials are reactive with the LEO environment, with interaction rates being apparently independent of chemical structure. The effect of additives is much more significant than chemical structure, since these materials are very often oxides or other low reacting components which shadow the organic matrix from the incoming ambient atomic oxygen beam. Reaction efficiencies for a representative set of organic materials are shown in table 1. These efficiencies are derived by normalizing the sample recession by exposure fluence and represent, principally, data from the STS-8 mission. For some material samples, the STS-5 mission reactivities are lower than those for the STS-8 mission; however, the earlier results may have been affected by sample mounting contaminants combined with the low fluence. Since sample recession for the STS-8 mission was as much as 12 μm, it is felt that these data are more representative of bulk reactivity. Considering errors involved in both recession measurements and atomic oxygen density prediction, the reaction efficiencies have a probable error of 30% to 50%. Errors associated with ambient density predictions appear to be the largest contributor.

Perfluoronated polymers, such as Teflon and silicone polymers are considerably less reactive than organic polymers (Table 1); in fact, their reaction rates are low enough that these materials can be considered as protective coatings. Nonreactive fillers also lower the reactivity of polymers by shadowing the organic matrix; however, the filler particles are then only partially attached through pedestal regions which may be lost in time due to scattered atomic oxygen.

Material reaction rate dependence on surface temperature and charged-species concentrations were evaluated using heated trays and a charged grid apparatus. Based on these measurements, polymer material reactivities show no temperature dependence over the temperature range of 298 to 393 K (25° to 120° C). Additionally, the charged grids did not affect the recession of associated samples, an indication that charged species were not important, as expected, in explaining the exposure effects.

Space Station Application

The extent of degradation caused by exposure to the LEO environment is dependent on surface attitude relative to ram, on altitude, and on solar activity. Even with these parameters, ambient density must be obtained from appropriate models, such as the previously mentioned MSIS model, and the flux integrated over the particular mission. An algorithm has been developed for coupling the results from MSIS and flight parameters to generate mission fluence and has been applied to Space-Station-peculiar flight parameters.[22] For these calculations, it was assumed that the Space Station was oriented in a gravity gradient attitude at 465 to 500 km. In such a flight attitude, some surfaces are always facing ram conditions, notably one side of structural components. Fluence predictions show a buildup as the solar activity increases to a maximum in the 1993 timeframe (fig. 3) and results in one solar cycle exposure for various surfaces as shown in table 2.

Recent Space Station programmatic considerations have resulted in definition of a constant drag flight attitude as a baseline. Such a flight condition would provide a varying Space Station altitude (500 to 350 km), depending on solar activity. This altitude variation results in relatively small velocity variations and, therefore, to a first approximation, constant drag can be considered as providing a constant density condition for environmental considerations. Assuming a density of 2×10^8 atoms/cm^3, which corresponds to the Space Station design requirement of 475 km with a maximum plus 2σ solar activity, the fluence and recession are approximately a factor of four larger than for a constant altitude condition. (See Table 2.)

Effects on Space Station surfaces are derived by multiplying the predicted fluence by the reactivity of the given material being exposed. For example, the forward-facing portion of the structural members is exposed to a total fluence of 1.4×10^{23} atoms/cm^2 for constant density conditions, and if these members are made of graphite epoxy composite with a reactivity of 2.4×10^{-24} cm^3/atom, recession of as much as 0.3 cm can be expected in 30 years. Current conceptual design uses a structural member wall thickness of approximately 0.15 cm; therefore, a loss of 50% of the wall thickness can be expected. Such a large loss of wall thickness is unacceptable and dictates that coatings be developed for protection.

An even more severe system problem arises from environmental exposure for the solar power components. Again, using computed fluence for the solar array exposure from table 2 of 5.5×10^{22} atoms/cm^2 and using a reactivity of 3×10^{-24} cm^3/atom, a typical solar array would experience recession of approximately 0.17 cm for a twenty-year exposure. Since substrates for typical arrays are 8×10^{-3} cm thick, life is very limited and coatings must be developed.

Although the effect on other Space Station materials may not be as severe as that on the photovoltaic power system, similar considerations apply and care must be taken in selecting durable coatings to ensure adequate life. As a result of these considerations, a significant amount of the Space Station materials advanced development activities are dedicated to coating development.

Conclusion

It was assumed for many years that the aspects of the low Earth orbital environment most degrading to materials were ultraviolet radiation and thermal vacuum exposure. With the advent of frequent space flights and opportunities to examine returned surfaces, it now appears that effects of atomic oxygen will be the most damaging by far. In fact, major changes in solar voltaic system design must be made to ensure sufficient life for even one solar cycle.

A preliminary data base has been generated from flight experiments to date, but is limited both in extent of orbital exposure time and, therefore, fluence and in the variety and number of samples studied. With a relatively short time before Space Station design begins, it is imperative that we augment the data base in both scope and quality of rate data. This

augmentation must be done through flight experiments, in which limited studies are possible, and ground-based facilities, where more extensive evaluations can be performed. Such an approach has been conceptually defined and is in program development. Successful implementation of this program will provide a significant increase in our understanding of LEO environment interactions with materials.

References

1. Leger, L. J., "Oxygen Atom Reaction with Shuttle Materials at Orbital Altitudes," NASA TM-58246, 1982.

2. Leger, L. J., "Oxygen Atom Reaction with Shuttle Materials at Orbital Altitudes--Data and Experiment Status," AIAA Paper 83-0073, 1983.

3. Peters, P. N., Linton, R. C. and Miller, E. R., "Results of Apparent Atomic Oxygen Reaction on Ag, C and Os Exposed during the Shuttle STS-4 Orbits," Geophys Res 10, pp. 569-571, 1983.

4. Zimcik, D. G. and Maag, C. R., "Results of Apparent Atomic Oxygen Reactions with Spacecraft Materials during Shuttle Flight STS 41-G", AIAA Paper 85-7020, Shuttle Environment and Operations II Conference, Houston, Texas, Nov. 1985.

5. Proceedings of the SMRM Degradation Study Workshop, Goddard Spaceflight Center Publication 408-SMRM-79-0001, May 1985.

6. Whitaker, A. F., *et al.*, "Protective Coatings for Atomic Oxygen Susceptible Spacecraft Materials - STS 41-G Results," AIAA Paper 85-7017, Shuttle Environment and Operations II Conference, Houston, Texas, Nov. 1985.

7. Hedin, A. E., *et al.*, "A Global Thermospheric Model Based on Mass Spectrometer and Incoherent Scatter Data: MSIS 2 Composition," Geophys Res 10, pp. 2139, 1977.

8. Leger, L. J., *et al.*, "STS Flight 5 LEO Effects Experiment -- Background Description and Thin Film Results," AIAA Paper 83-2361-CP, 1983.

9. Whitaker, A. F., "LEO Atomic Oxygen Effects on Spacecraft Materials," AIAA Paper 83-2632-CP, 1983.

10. Park, J. J., *et al.*, "Effects of Atomic Oxygen on Pint and Optical Coating," AIAA Paper 83-2634, 1983.

11. Triolo, J. J., to be published.

12. Zinner, E., *et al.*, "Erosion of Mylar and Protection by Thin Metal Films," AIAA Paper 83-2636, 1983.

13. Liang, R. and Gupta, A., "Mechanistic Studies of Kapton Degradation in Shuttle Environments," AIAA Paper 83-2656, 1983.

14. Visentine, J. T., Leger, L. J., Kuminecz, J. R. and Spiker, I. K., "STS-8 Atomic Oxygen Effects Experiment," AIAA Paper 85-0415, 1985.

15. Whitaker, A. F., *et al.*, "Orbital Atomic Oxygen Effects on Thermal Control and Optical Materials, STS-8 Results," AIAA Paper 85-0416, 1985.

16. Banks, B. A., *et al.*, "Ion Beam Sputter-Deposited Thin Film Coatings for Protection of Spacecraft Polymers in Low Earth Orbit," AIAA Paper 85-0420, 1985.

17. Smith, K. A., "EOIM STS-8 Atomic Oxygen Effects," AIAA Paper 85-7021-CP.

18. Slemp, W. S., Santos, B. and Sykes, Jr., G. F., "Effects of STS-8 Atomic Oxygen Effects on Composites, Polymer Films and Coatings," AIAA Paper 85-0421, 1985.

19. Liang, R. and Gupta, A., "Mechanistic Studies of Interactions of Materials with Energetic Oxygen Atoms in Low Earth Orbit," AIAA Paper 85-0422, 1985.

20. Gull, T. F., *et al.*, "Effects on Optical Surfaces at Shuttle Altitudes," AIAA Paper 85-0418, 1985.

21. Gregory, J. C. and Peters, P. N., "Measurement of Reaction Rates and Activation Energies of 5 eV Oxygen Atoms with Graphite and Other Solid Surfaces," AIAA Paper 85-0417, 1985.

22. Leger, L. J., Visentine, J. T. and Schliesing, J. A., "A Consideration of Atomic Oxygen Interactions with Space Station," AIAA Paper 85-0476, 1985.

MATERIAL INTERACTIONS WITH THE LOW EARTH ORBITAL ENVIRONMENT: ACCURATE REACTION RATE MEASUREMENTS

BY

JAMES T. VISENTINE AND LUBERT J. LEGER
NASA LYNDON B. JOHNSON SPACE CENTER

Abstract

An understanding of the surface chemistry which gives rise to atom/surface interactions within the orbital environment is crucial to establishing a reliable materials interaction data base for Space Station and verifying the operational capability of ground-based neutral beam facilities which simulate the space environment. One of the more important effects of these interactions is oxidation of material surfaces by atomic oxygen, a major constituent of the low Earth orbital environment. Material interaction studies conducted during flights STS-5 and STS-8 have provided most of the current information regarding the reactivity of spacecraft materials to atomic oxygen, and the results of these studies indicate many materials such as organic films, polymers and many composites, react readily with atomic oxygen and have reactivities in the range 2.5×10^{-24} to 3.0×10^{-24} cubic centimeters per atom.

The data base provided by these flight programs is limited in its application, however, because no information is currently available which adequately explains the basic mechanisms responsible for atom/surface interactions. Another more serious limitation to this data base is the total integrated atomic oxygen flux (fluence) derived for these flights and used to determine material interaction rates that have been estimated using thermospheric models to predict atomic oxygen number densities within the orbital environment. Typically, errors of $\pm 25\%$ or greater can be expected for these density estimations, and since they were used to compute fluence, these errors also appear in the surface recession rates for Space Station materials.

To resolve these uncertainties and provide reaction product compositional data for comparison to data obtained in ground-based laboratories, a flight experiment has been proposed for the Space Shuttle which utilizes an ion-neutral mass spectrometer to obtain in-situ ambient density measurements and identify reaction products from modeled polymers exposed to the atomic oxygen environment. An overview of this experiment will be presented and the methodology of calibrating the flight mass spectrometer in a neutral beam facility prior to its use on the Space Shuttle will be established.

Introduction

A reliable materials interaction data base and an understanding of the surface chemistry which gives rise to the interaction of surfaces with atomic oxygen, the principal constituent within the low Earth orbital (LEO) environment, are crucial to the development of materials and coatings for future spacecraft, such as Space Station, designed to operate for extended

(10 to 30 yr) periods at low (300 to 500 km) orbital altitudes. Previous Space Shuttle flights[1,2,3] have shown that many polymers, organic films, and composite materials used in typical spacecraft applications undergo significant mass loss when exposed at low altitudes to the orbital environment. Polyimide films used as substrates for lightweight, large-area solar arrays, such as those proposed for Space Station, had relatively high rates of surface recession when exposed to atomic oxygen. Polyurethane paints used to suppress stray light within astronomical telescopes and in thermal control coatings for spacecraft structures were found to degrade,[4] with specular paints becoming more diffuse and thermal control paints acquiring a chalky, particulate residue on their surfaces. Metals such as carbon, osmium, and silver were also reactive in the flight environment[5] and underwent significant mass loss, in the case of osmium and carbon, and gross oxidation, in the case of silver. Graphite epoxy composites proposed for lightweight truss members in large space structures lost significant mass[6] when exposed to moderate atomic oxygen fluxes (10^{14} to 10^{15} atoms/cm^2-sec) for limited periods.

An interaction data base has been developed for these and other materials to aid in spacecraft design. The data base provided by previous Space Shuttle flights is limited in its application, however, because total integrated atomic oxygen flux (fluence) used to derive material reaction rates must be estimated using thermospheric models[7] to predict atomic oxygen number densities. Typically, errors of $\pm$25% or greater can be expected for these density estimations, and, since they are used to compute both fluence and reactivity, these errors also appear in the data base. Another limitation is the lack of available information which adequately explains the details of the interaction process and the chemical mechanisms responsible for surface recession. These mechanisms must be understood to enable selection of coatings or new materials that do not readily degrade in the LEO environment.

Proposed Flight Experiment

To resolve many of these uncertainties and provide a more accurate data base, a materials interaction flight experiment designated EOIM-3 (Evaluation of Oxygen Interactions with Materials, third series) has been proposed. The EOIM-3 experiment uses an ion-neutral mass spectrometer and a carousel system (Fig. 1) to conduct aeronomy measurements and to study surface interaction mechanisms. In addition to obtaining accurate reaction rate measurements for materials, this experiment will use the mass spectrometer to measure the local Space Shuttle environment over many orbital passes to develop a more thorough understanding of the ionospheric processes and to obtain correlations of orbital ion/neutral number densities with ambient density models.

To implement these objectives, the mass spectrometer (Fig. 2) will be positioned within the Orbiter bay on a rotatable mount (Fig. 3) to view first along the Orbiter +Z-axis (aeronomy measurements) and then toward materials installed on a rotatable carousel. The carousel will have five sectors, each containing materials with different chemical compositions, which will be rotated sequentially to face the mass spectrometer. Where possible, these materials will be isotopically labeled with carbon-13 and

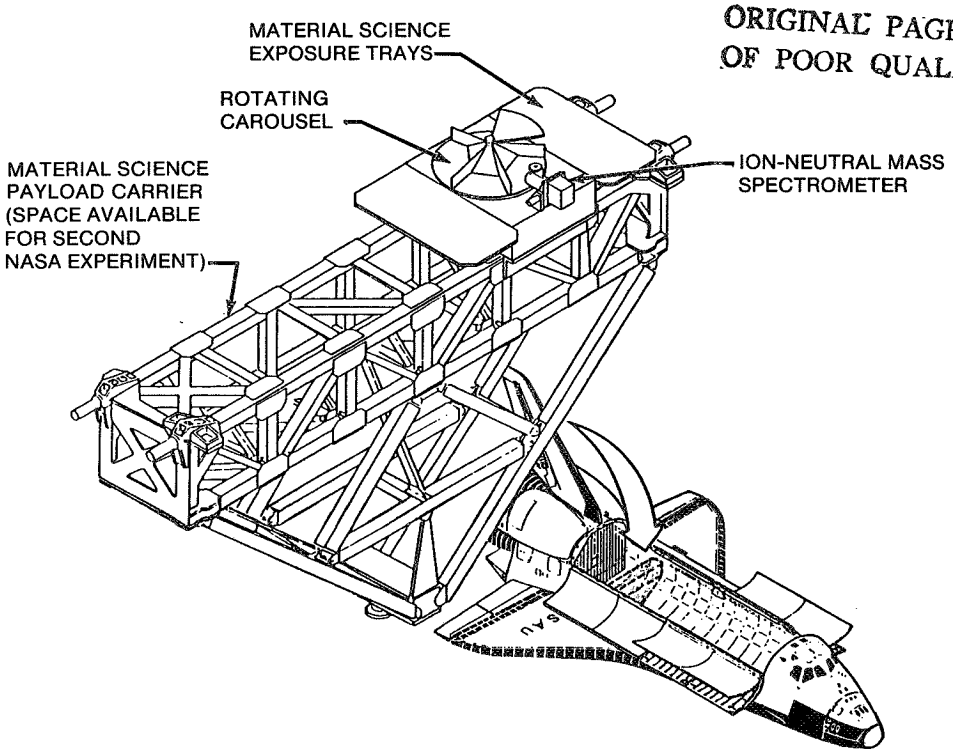

Fig. 1 EOIM-3 atomic oxygen effects experiment.

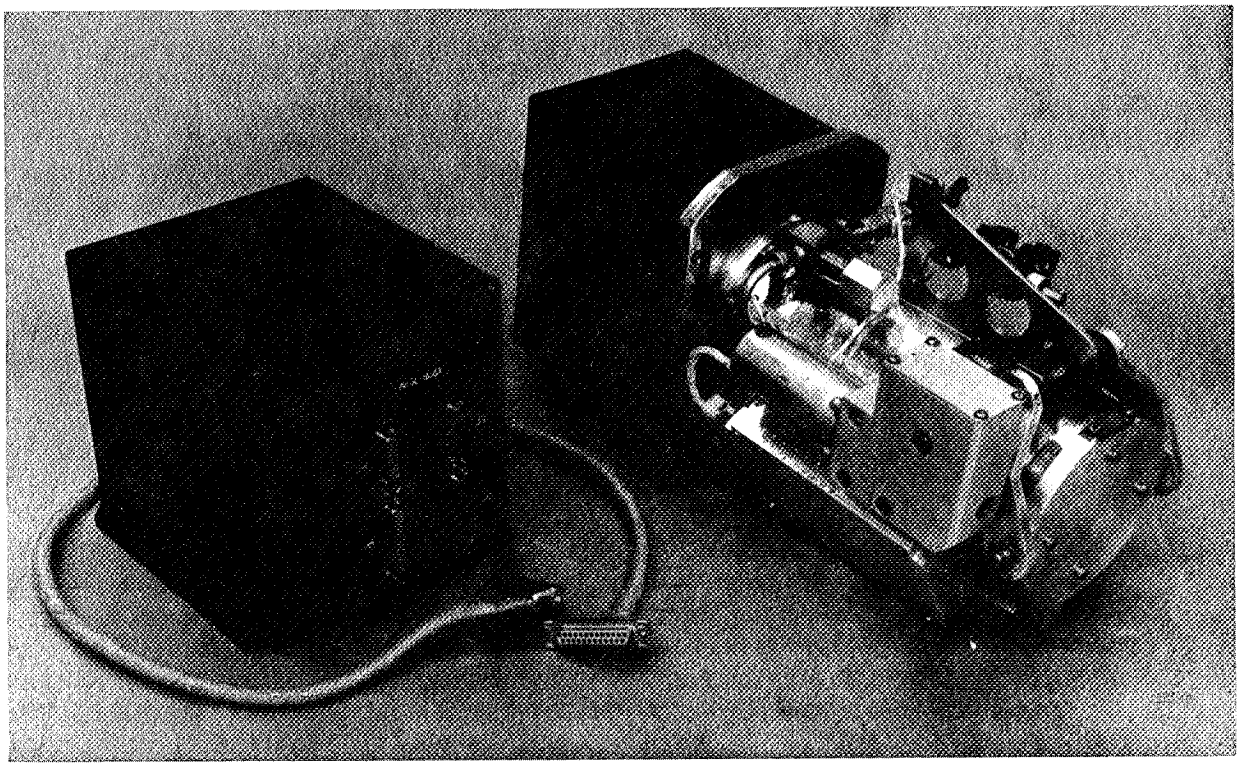

Fig. 2 Ion-neutral mass spectrometer. The control unit to the left of the sensor is preprogrammed prior to flight.

deuterium to differentiate the reaction products from the overall instrument background. Measurements of gases produced by the interaction of atomic oxygen with the carousel materials will aid in identifying chemical mechanisms which give rise to surface recession. Materials proposed for mechanistic studies include polyimide, carbon, polyvinylchloride, polystyrene, labeled polyethylene, polyurethane light-absorbing paint or similar material, and gold or aluminum oxide as a control surface.

Reaction Rate Measurements

Accurate reaction rates for atomic oxygen interactions with materials will be obtained by operating the mass spectrometer in the aeronomy mode (+Z-axis) and orienting the Orbiter such that specimens installed on heated trays and disk holders (Fig. 4) are subjected to direct oxygen impingement. Whereas mass spectrometer density measurements will be made while the flight is in progress, mass loss determinations for highly reactive materials will be obtained when the mission is completed. To obtain the required exposure conditions, it is being requested that the Orbiter be flown for 40 hr in a circular orbit (variable inclination) with its payload bay oriented into the velocity vector (+ZVV) at an altitude of 222 km (120 n. mi.). Computations indicate that this exposure should result in day-night number densities (Fig. 5) sufficiently high to produce atomic oxygen fluxes in the range 1.1×10^{15} to 1.5×10^{15} atoms/cm^2-sec. This flux, in turn, will produce an accumulated fluence of 1.8×10^{20} atoms/cm^2. Using interaction data derived from previous Space Shuttle flights, it is estimated this fluence will result in surface recessions of 3 to 5 μm for materials (organic films, polyimide paints, and composites) that are susceptible to atomic oxygen interactions. A typical mass spectrometer measurement sequence for obtaining accurate reaction rates is shown in Fig. 6.

Less reactive materials, such as fluoropolymers, will be evaluated during this mission using quartz crystal microbalances (QCM's) to measure low rates of surface recession. These instruments have been selected for this application since they have high sensitivity (1×10^{-9} g/cm^2) in comparison to postflight weight loss determinations.[8] Although this exposure is several orders of magnitude less than the fluence Space Station structures will encounter[9] over an 11-yr solar cycle (2.5×10^{21} to 1.2×10^{22} atoms/cm^2), it will be sufficiently high to obtain accurate interaction rates for the materials evaluated.

Additional Measurements

As currently designed, this flight experiment will include additional sensors to study in greater detail the effects of atomic oxygen interactions with surfaces. In addition to the mass spectrometer, the carousel, the QCM's, and the passive disk holders discussed earlier, the experiment will include stress fixtures (Fig. 7) to study the effects of mechanical stress on erosion rates, heated disks and filmstrips to study the effects of temperature on interaction rates, and scatterometers to estimate energy accommodation on surfaces and define surface-atom emission characteristics as related to surface recession. A solar ultraviolet experiment, similar to one flown on the STS-8 mission, will be used to assess the effects of solar radiation on reaction rates. This device will consist of control (uncovered) specimens and specimens that are alternately exposed during the

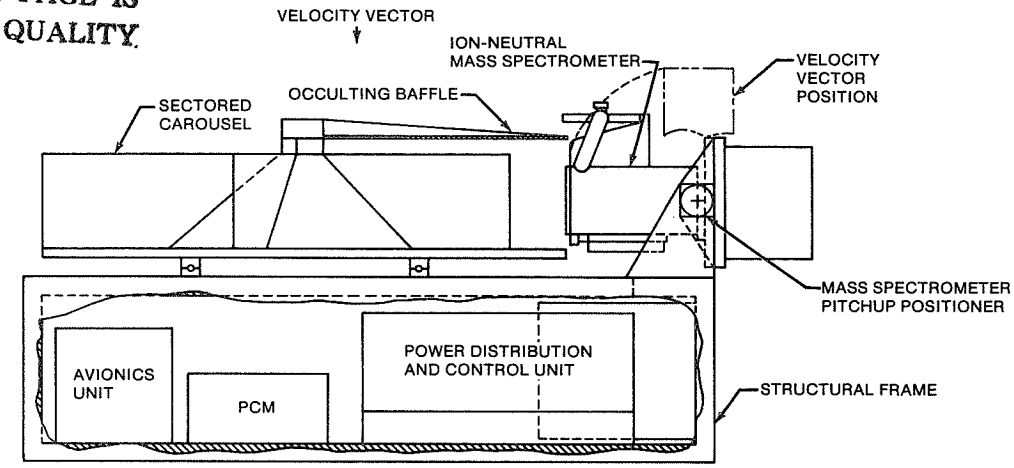

Fig. 3 Mass spectrometer/carousel flight configuration.

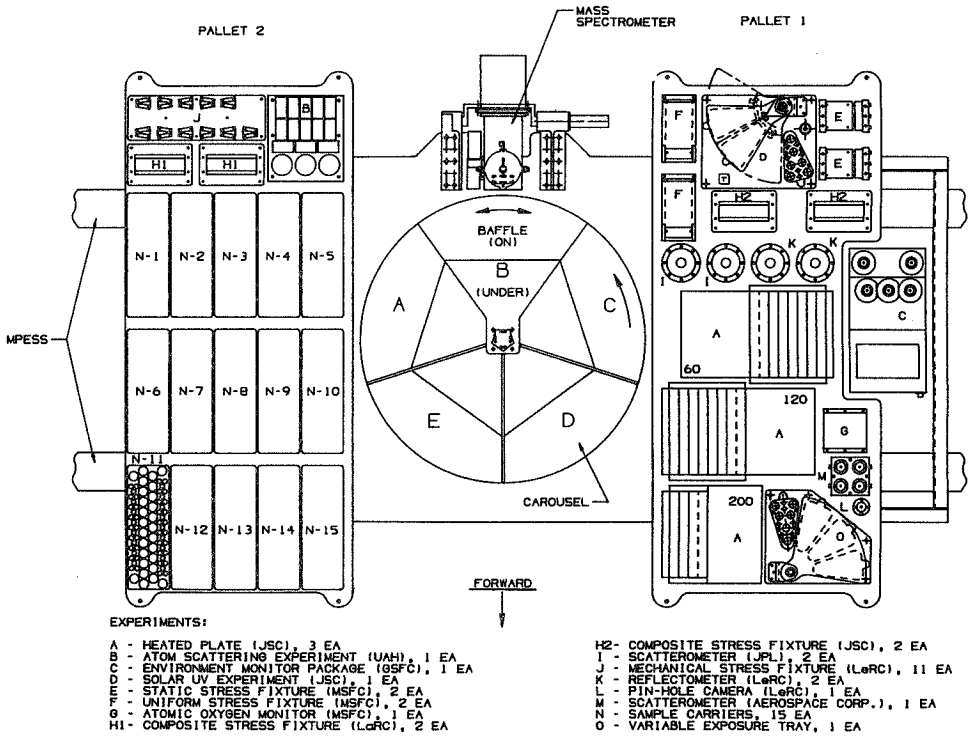

Fig. 4 EOIM-3 atomic oxygen interaction experiment.

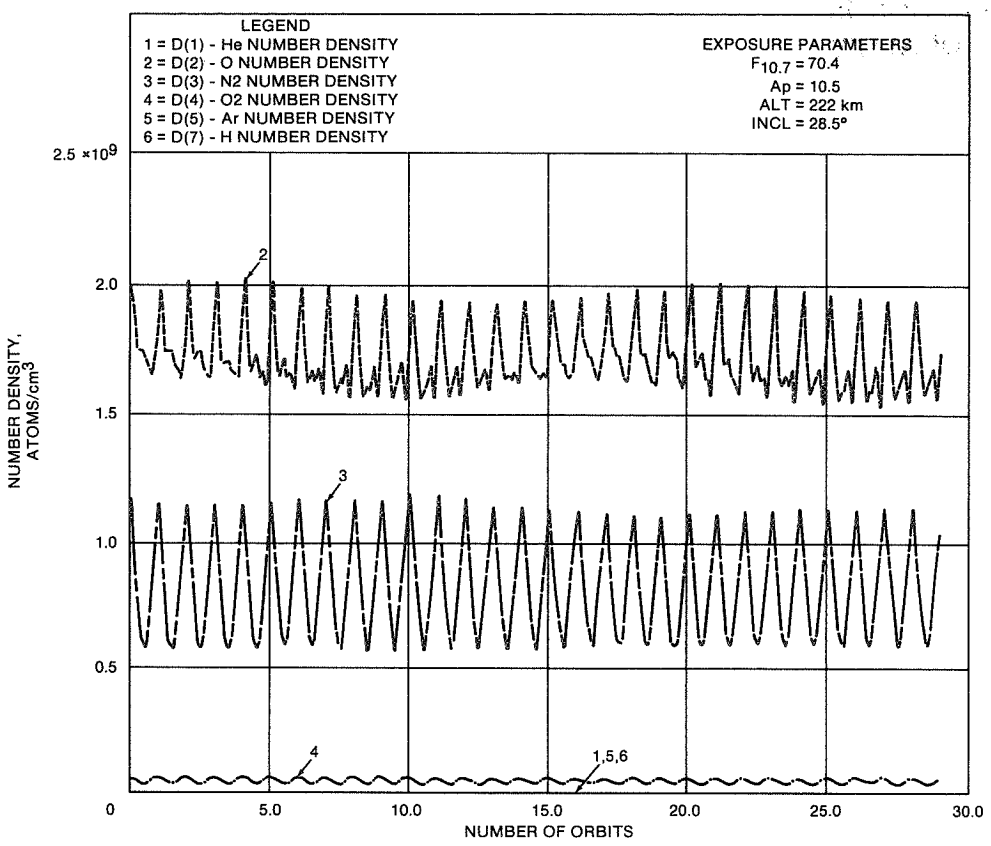

Fig. 5 Atmospheric density estimations for May 6, 1988, launch date.

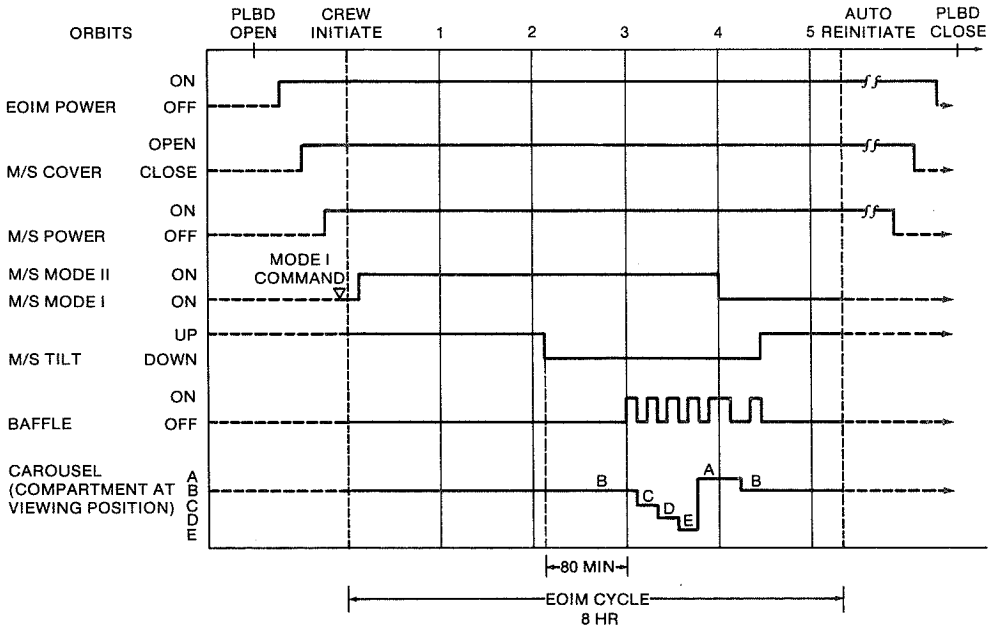

Fig. 6 EOIM-3 mass spectrometer measurement sequence, typical 8-hr exposure cycle.

day and night portions of the 40-hr exposure cycle. A similar device, the variable exposure experiment, will be used to assess the effects of matrix shadowing on reaction rates. Previous flight results have demonstrated nonreactive fillers lower the reactivity of polymers by shadowing the organic matrix. The variable exposure experiment will sequentially expose filled polymers at 5, 10, 20 and 40 hour intervals to evaluate how their surface recession varies with exposure time. Reaction rates will be derived for materials selected for each of these experiments by using the mass spectrometer to measure variations in day-night number densities, by determining the exposure time, and by performing postflight weight loss measurements.

The locations of these devices, as currently proposed for this flight experiment, are shown in Fig. 4. These locations, in addition to the location of the mass spectrometer/carousel system, have been chosen to minimize tray dimensions, to isolate products outgassed from the heated (60°, 120°, 200° C) trays from the mass spectrometer, and to limit uncontrolled scattering of the oxygen beam onto sensitive surfaces.

Experiment Status

Flight hardware is under development at the NASA Lyndon B. Johnson Space Center (JSC) and the U.S. Air Force Geophysics Laboratory. Passive and active experiments and material specimens will be provided by most NASA centers and by the Space Station work package contractors. Experiments under development by the NASA centers (JSC, Goddard Space Flight Center (GSFC), George C. Marshall Space Flight Center (MSFC), Langley Research Center (LaRC), Jet Propulsion Laboratory (JPL), and Lewis Research Center (LeRC)), by an aerospace contractor (Aerospace Corp.), and by the University of Alabama at Huntsville (UAH) are identified, by organization, in Fig. 4, which illustrates the locations of the mass spectrometer and carousel, and the configuration of the active and passive trays discussed earlier.

The experiment program plan and request for flight assignment have been approved by the NASA offices (Space Station and Office of Aeronautics and Space Technology) who will provide funding for hardware development. The flight readiness date for this experiment is tentatively scheduled for May 1988. A flight assignment date has not been established by NASA; however, it may occur as soon as early- to mid- 1988, since these investigations directly support Space Station advanced development.

Mass Spectrometer Preflight Calibrations

The mass spectrometer will be calibrated in an atomic oxygen neutral beam facility, under development at Los Alamos National Laboratory, to obtain accurate aeronomy measurements during the flight. Atomic oxygen is being produced at this facility[10] by sustaining a discharge with a high-intensity continuous-wave (CW) laser in a mixture of rare gas and molecular oxygen. The high-temperature discharge region dissociates the molecular oxygen into atoms, which are allowed to expand through a nozzle into a differentially pumped chamber. The facility in which the mass spectrometer will be calibrated will use a 1.5-kW CW laser to sustain a discharge within

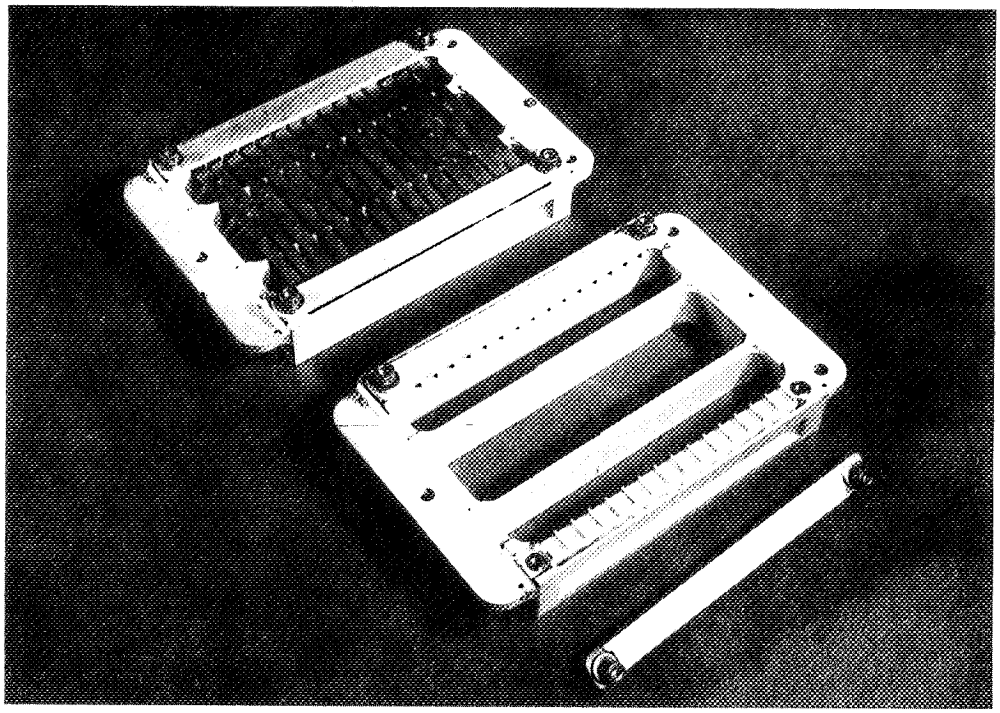

Fig. 7 Mechanical stress fixture for composite materials.

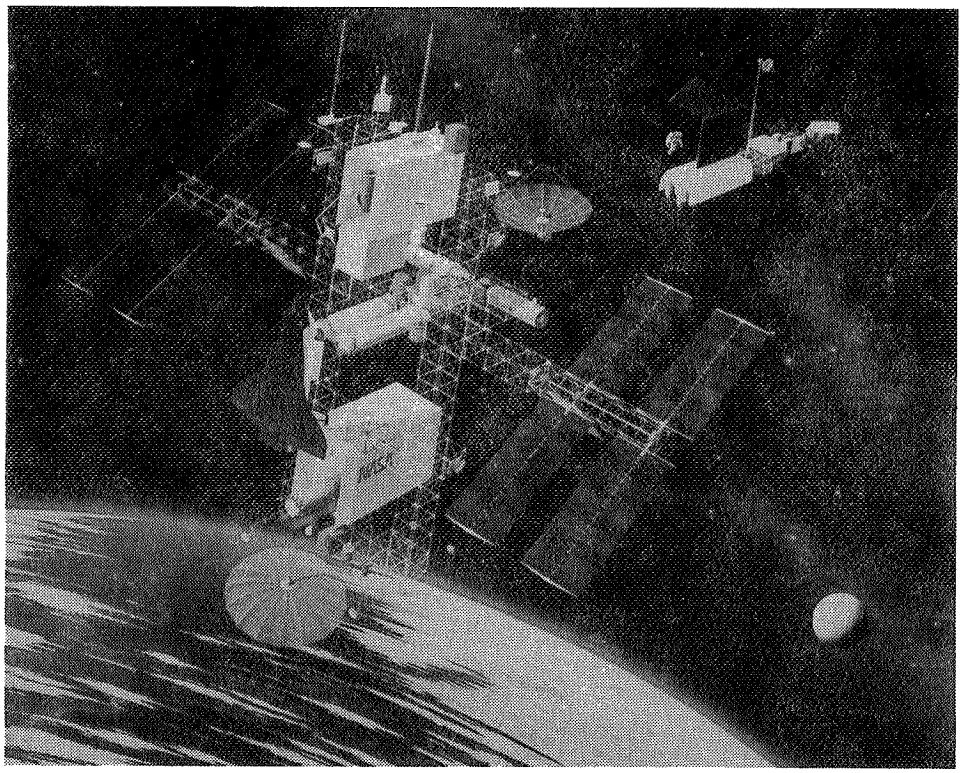

Fig. 8. Space Station dual-keel configuration.

a helium-oxygen mixture. It is anticipated that use of this mixture will produce oxygen atoms in the 5-eV range, as required for the flight simulation. The system will be designed to produce atomic oxygen fluxes of 10^{16} to 10^{17} atoms/cm^2-sec or less to accurately simulate the flight environment and later to provide capability for accelerated testing.

Interaction efficiencies and view factor calculations for carousel surfaces indicate that the amplitude of mass peaks recorded by the mass spectrometer during flight should be in the range 2×10^{-9} to 6×10^{-9} A, sufficiently above the expected instrument background current of 5×10^{-11} A recorded during previous missions.(11) To verify these calculations, materials such as polyimide and polyethylene will be exposed to the neutral oxygen beam, and the mass spectrometer will be oriented inside the target chamber to view products generated during the interaction process. The sensitivity of the instrument will be optimized to detect the interaction products. Final calibration will be performed by exposing the mass spectrometer to a 5-eV neutral oxygen beam to study recombination effects inside the ion source and to derive its measurement sensitivity for atomic oxygen.

Conclusions

The experiment described in this paper will provide a reliable materials interaction data base for future spacecraft design and will furnish insight into the basic chemical mechanisms leading to atomic oxygen interactions with surfaces. The effects of solar radiation and mechanical stress on erosion rates as well as scattering of atomic oxygen by various surfaces will enable derivation of protection techniques to ensure long-lived operation of lightweight Space Station structures and components. Such protective techniques as special coatings for truss structures and lightweight power generation devices, if properly applied, will be important considerations in designing a large, multipurpose Space Station, such as the NASA dual keel configuration shown in Fig. 8, that requires minimum refurbishment and limited component replacement over its lifetime.

References

1. Leger, L. J., Spiker, I. K., Kuminecz, J. F., Ballentine, T. J., and Visentine, J. T., "STS Flight 5 LEO Effects Experiment - Background Description and Thin Film Results," AIAA Paper 83-2631-CP, Shuttle Environment and Operations Meeting, Washington, D.C., Nov. 1983.

2. Leger, L. J., Visentine, J. T., and Kuminecz, J. F., "Low Earth Orbit Atomic Oxygen Effects on Surfaces," AIAA Paper 84-0548, 22nd Aerospace Sciences Meeting, Reno, Nev., Jan. 1984.

3. Visentine, J. T., Leger, L. J., Kuminecz, J. F., and Spiker, I. K., "STS-8 Atomic Oxygen Effects Experiment," AIAA Paper 85-0415, 23rd Aerospace Sciences Meeting, Reno, Nev., Jan. 1985.

4. Whitaker, A. F., Little, S. A., Harwell, R. J., Griner, D. B., and DeHaye, R. F., "Orbital Atomic Oxygen Effects on Thermal Control and Optical Materials - STS-8 Results," AIAA Paper 85-0416, 23rd Aerospace Sciences Meeting, Reno, Nev., Jan. 1985.

5. Gull, T. R., Herzig, H., Toft, A. R., Park, J. J., and Triolo, J. J., "Effects on Optical Surfaces at Shuttle Altitudes," AIAA Paper 85-0418, 23rd Aerospace Sciences Meeting, Reno, Nev., Jan. 1985.

6. Slemp, W. S., Santos-Mason, B., and Sykes, G. F., Jr., "Effects of STS-8 Atomic Oxygen Exposure on Composites, Polymeric Films and Coatings," AIAA Paper 85-0421, 23rd Aerospace Sciences Meeting, Reno, Nev., Jan. 1985.

7. Hedin, A. E., "A Revised Thermospheric Model Based on Mass Spectrometer and Incoherent Scatter Data: MSIS-83," Journal of Geophysical Research, Vol. 88, No. A12, Dec. 1983, pp. 10,170-10,188.

8. Triolo, J., Maag, C., and Kruger, R., "Results from a Small Box Real-Time Molecular Contamination Monitor on STS-3," Journal of Spacecraft and Rockets, Vol. 21, No. 4, July-Aug. 1984, pp. 400-404.

9. Leger, L. J., Visentine, J. T., and Schliesing, J. A., "A Consideration of Atomic Oxygen Interactions with Space Station," AIAA Paper 85-0476, 23rd Aerospace Sciences Meeting, Reno, Nev., Jan. 1985.

10. Cross, J. B., "Atomic Oxygen Surface Interactions - Mechanistic Studies Using Ground-Based Facilities," AIAA Paper 85-0473, 23rd Aerospace Sciences Meeting, Reno, Nev., Jan. 1985.

11. Narcisi, R., Trzcinski, E., Federico, G., Wlodyka, L., and Delorey, D., "The Gaseous and Plasma Environment Around Space Shuttle," AIAA Paper 83-2659, Shuttle Environment and Operations Meeting, Washington, D.C., Nov. 1983.

MASS SPECTROMETERS AND ATOMIC OXYGEN

D. E. Hunton and E. Trzcinski
Air Force Geophysics Laboratory
Hanscom Air Force Base, MA 01731

J. B. Cross, L. H. Spangler, M.H. Hoffbauer and F.H. Archuleta
Los Alamos National Laboratory
Los Alamos, NM 87545

J. T. Visentine
NASA Lyndon B. Johnson Space Center
Houston, TX 77058

ABSTRACT

The likely role of atmospheric atomic oxygen in the recession of spacecraft surfaces and in the Shuttle glow has revived interest in the accurate measurement of atomic oxygen densities in the upper atmosphere. The Air Force Geophysics Laboratory is supplying a quadrupole mass spectrometer for a materials interactions flight experiment being planned by the NASA Johnson Space Center. The mass spectrometer will measure the flux of oxygen on test materials and will also identify the products of surface reactions. The instrument will be calibrated at a new facility for producing high energy beams of atomic oxygen at the Los Alamos National Laboratory. This paper summarizes plans for these calibration experiments.

INTRODUCTION

The measurement of atomic oxygen densities in the atmosphere with mass spectrometers is one of the outstanding problems in aeronomy. The measurements were originally made to investigate the structure of the earth's atmosphere. Recently, atomic oxygen has been implicated in the recession of spacecraft surfaces(1-4) and in the Shuttle glow(5,6). These phenomena have renewed interest in the accurate measurement of atomic oxygen densities.

The accuracy of the mass spectrometer measurements is limited by uncertainties in the response of the instruments to the atomic oxygen. The major technical problems are recombination of the atomic oxygen to the molecular species on the inner surfaces of the ion sources, differences in detection sensitivity between thermal and hyperthermal oxygen atoms, energy equilibration of oxygen with ion source surfaces, and background contributions to the mass 16 and 32 signals.

These problems have been addressed in the past by designing the two types of ion sources sketched in Fig. 1. Open ion sources(7) seek to reduce

recombination as much as possible. Much of the atomic oxygen can pass through the electron beam and into the mass analysis section of the instrument without any surface interactions. In contrast, closed ion sources(8) force complete recombination. The electron beam is surrounded by a closed accommodation volume. The atomic oxygen enters this volume through a pinhole. A baffle deflects the oxygen to the walls of the chamber, where it forms molecular oxygen.

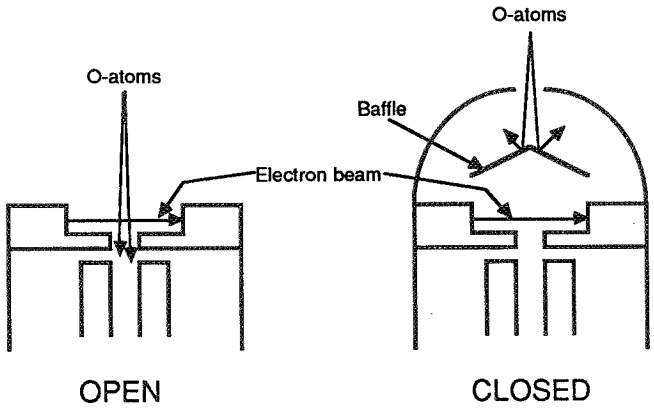

FIG. 1: Types of ion sources used for atmospheric atomic oxygen measurements. Open sources reduce recombination by eliminating surfaces in the beam path. Closed sources force complete recombination.

The sensitivity of closed source mass spectrometers can be calculated from the measured sensitivity to thermal molecular oxygen and the rate of effusive flow through the pinhole opening(9,10). However, open source instruments must be calibrated to atomic oxygen in the laboratory. Such instruments have been exposed to beams of oxygen atoms formed in microwave discharges(11) or on heated filaments(12). Though high velocities and intensities have been obtained for other gases in mass spectrometer calibration experiments(13), the limitations of the atomic oxygen calibrations have been the low energy and intensity of the beam.

Research groups at the NASA Johnson Space Center (JSC), the Los Alamos National Laboratory, and the Air Force Geophysics Laboratory (AFGL) are engaged in a cooperative space flight experiment designed to measure the effects of atomic oxygen on spacecraft materials. The experiment is called Evaluation of Oxygen Interactions with Materials (EOIM)-III (17). AFGL is supplying a mass spectrometer to monitor the flux of oxygen atoms interacting with the EOIM test materials. This instrument will be calibrated at the atomic oxygen high energy beam facility that has recently been constructed at Los Alamos.

AFGL QUADRUPOLE MASS SPECTROMETER

The AFGL Quadrupole Ion/Neutral Mass Spectrometer (QINMS) is a compact, versatile, fast sampling instrument(15). Its primary purpose is to measure the concentration and the identity of each constituent of the

gas entering its sampling orifice. It is sensitive to neutral and positive ionic species, though not to both simultaneously. The spectrometer design is based on similar instruments flown extensively on sounding rockets. QINMS has been used on one Shuttle flight(16).

In addition to the composition information, the instrument collects a fraction of the total ion current on a grid located between the ion source and the entrance aperture to the quadrupole rods. This current is a measure of the total pressure of the neutral gas in the neutral mode and the total density of the ions in the ion mode. The sampling rates of the composition data and the pressure/density data are both fast enough to resolve such transient effects as ionospheric irregularities and spacecraft thruster engine firings.

The ion source of the AFGL instrument is drawn to scale in Fig. 2. This entire assembly is mounted on top of the quadrupole housing, and is contained inside a metal cylinder. An O-ring sealed cover is retracted in flight to expose the top grid of the ion source to the external environment. This ion source is somewhere between the open and closed extremes described above. The grids crossing the path of the incoming oxygen provide some surfaces for recombination, while still allowing some of the oxygen to reach the quadrupole region unimpeded.

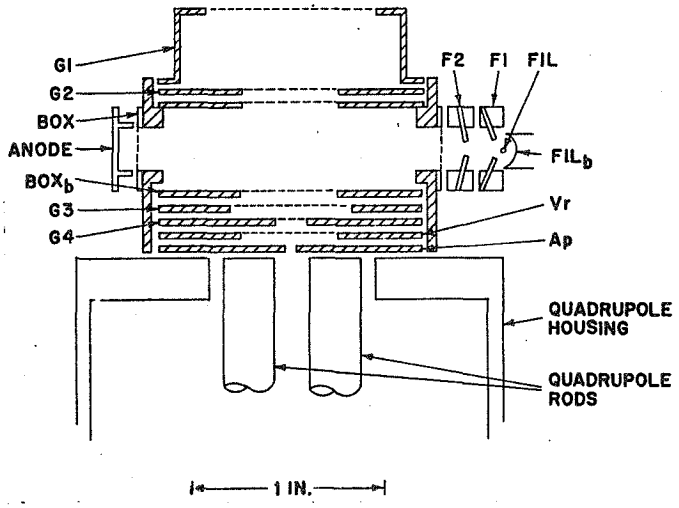

FIG. 2: Scale drawing of the ion source used in the AFGL mass spectrometer. The source incorporates features from both the open and closed designs.

ATOMIC OXYGEN GROUND CALIBRATIONS

The energetic oxygen atom source that has been developed at Los Alamos employs a Continuous Optical Discharge (COD) technique(17,18). A 1.5 kW cw CO_2 laser is focused to a 0.02 cm diameter spot within the throat of a supersonic expansion nozzle. A pulsed CO_2 laser, aligned co-axially with the cw beam, is fired once to start a discharge in the nozzle. The cw

laser then pumps the discharge continuously, maintaining temperatures of 15,000 to 30,000 K within the throat of the nozzle. In the source chamber, molecular oxygen is seeded into a noble carrier gas, such as neon or helium to reduce the power required for breakdown. The oxygen is completely dissociated by the discharge and is accelerated to high velocity by collisions with the carrier gas during the expansion.

The COD atomic oxygen beam source is mounted to the Los Alamos Molecular Beam Dynamics Apparatus (LAMBDA) (19). Three stages of differential pumping separate the source from the primary experiment chamber. LAMBDA is equipped with several sophisticated beam diagnostic tools, including a differentially pumped quadrupole mass spectrometer, a time-of-flight (TOF) chopper, and recently, a spinning sphere absolute pressure gauge(20). Recent advances in the development of the atomic oxygen beam facility are discussed in another paper in this session (Cross et al.).

The most difficult aspect of the calibration experiment is measuring the absolute flux of the oxygen beam. Beam diagnostics such as the differentially pumped mass spectrometer would need calibration in the same way as the flight instrument does. Fig. 3 is a rough sketch of the experimental layout that we have chosen for the mass spectrometer calibration experiments. In essence, the idea is the same as the closed ion source concept. The O-atom beam enters the main chamber from the source on the right. On the far side of the main chamber, approximately one meter away, the beam enters a smaller accommodation chamber through a small aperture of known area. The flight mass spectrometer is mounted on the beam axis on the far side of the accommodation chamber.

FIG. 3: Experimental layout of the Los Alamos atomic oxygen high energy beam facility to be used for the mass spectrometer calibration experiments.

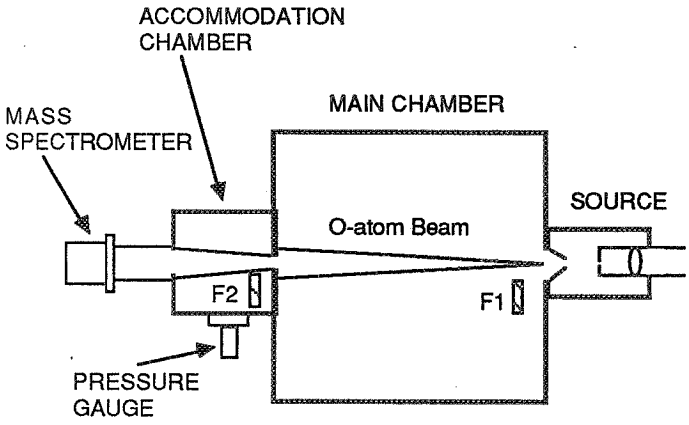

Two beam flags, F1 and F2, can be used to block the beam. F1 is between the first and second differential pumping stages in the source, and is used to turn off the beam completely. F2 is located inside the accommodation chamber and is designed to deflect the incoming beam to the walls. With F2 blocking the beam, the spinning sphere absolute pressure gauge will be used to measure the pressure rise in the accommodation chamber when the beam is turned on. We assume that the atomic oxygen recombines completely and thermalizes on the walls of the accommodation chamber (and choose wall materials to ensure this). The measured pressure rise and the known rate of effusive flow from the small aperture are then used to calculate the absolute intensity of the beam entering the chamber.

Finally, when both flags are removed from the beam, the flight mass spectrometer will be exposed to the full flux of atomic oxygen in the molecular beam. A typical calibration experiment will first involve measuring the absolute intensity and composition of the beam using the LAMBDA beam diagnostics and the techniques described above. Comparison of the known beam characteristics to the intensities of the mass 16 and 32 peaks (O and O_2, respectively) will be used to derive the sensitivity of the flight instrument to atomic oxygen along with the degree of recombination. The effects of surface conditioning and length of exposure to oxygen atoms, as well as the influence of beam velocity, beam intensity, and carrier gas concentration will be observed.

In a preliminary experiment, a thermal beam of oxygen molecules (formed in the supersonic expansion with the laser turned off) was directed into the mass spectrometer ion source. Mass spectra taken with the beam flagged and not flagged appear in Fig. 4. The 32 amu peak is the parent oxygen, and 16 amu is atomic oxygen produced by dissociative ionization. No atomic oxygen was present in the beam. The mass 4 peak is the helium carrier gas. Additional peaks in the spectra are due to vacuum chamber contamination and air leakage. These include water (18, 17 and 16 amu), nitrogen (28 amu) and molecular oxygen (32 amu). When the beam was chopped with a 400 Hz tuning fork chopper and phase sensitive detection of the mass spectrometer signals was used, only beam components were detected.

SUMMARY

The Quadrupole Ion/Neutral Mass Spectrometer, designed and built by the Air Force Geophysics Laboratory, is a versatile instrument well-suited to measurements within the Shuttle environment. Its configuration is derived from similar instruments designed for sounding rocket flights, and successfully collected data during the STS-4 flight. We plan to operate the same instrument on the Evaluation of Oxygen Interactions with Materials (EOIM)-III experiment presently under development by the Johnson Space Center. This experiment is the third in a series of Shuttle-based experiments designed to measure the effects of atomic oxygen on materials and surfaces. The mass spectrometer will measure the flux of atomic oxygen incident on the materials samples, and will also look for surface reaction

products. The data from the experiment will be invaluable in designing spacecraft, such as Space Station, for long duration excursions into the low Earth orbital environment.

A critical part of preparing the mass spectrometer for the flight is calibrating it with a well-characterized high energy beam of atomic oxygen. This will be done at the Los Alamos National Laboratory, where a new source of high energy oxygen atoms has been developed. Using a Continuous Optical Discharge technique, the Los Alamos source produces a beam of oxygen that reproduces many aspects of the space environment accurately. During the calibration experiments, we will investigate the amount of recombination that occurs within the mass spectrometer ion source, the effect of extended exposure to the oxygen beam, and the effects of the beam energy and intensity on the calibrations.

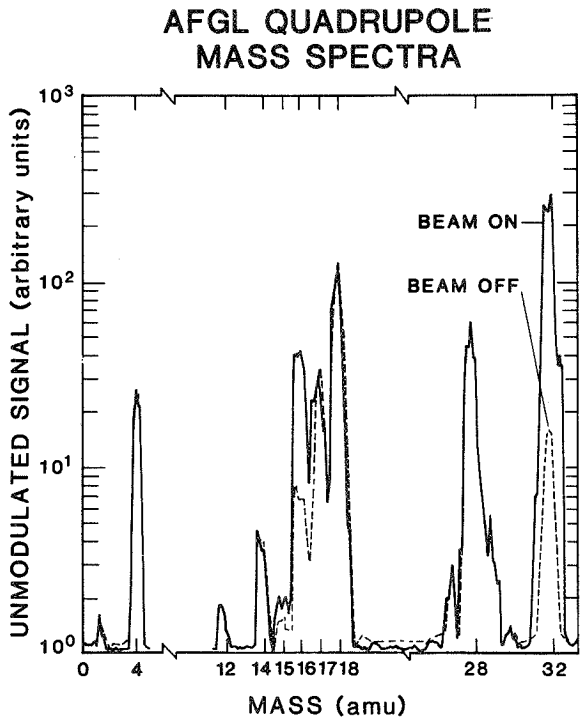

FIG 4: Unmodulated mass spectrometer signals due to a thermal beam of molecular oxygen in helium carrier gas. With the beam off (F1 in beam), the mass spectrometer only sees chamber background species such as water, nitrogen and oxygen. With the beam on (F1 removed from beam) the O_2 and O signals increase markedly. The O species is produced only from dissociative ionization of the parent molecular oxygen.

REFERENCES

1) Leger, L.J., Spiker, I.K., Kuminecz, J.F., Ballentine, T.J. and Visentine, J.T., "STS Flight 5 LEO Effects Experiment-Background Description and Thin Film Results," AIAA Paper 83-2631-CP, Oct. 1983.

2) Leger, L.J., Visentine, J.T., and Kuminecz, J.F., "Low Earth Orbit Atomic Oxygen Effects on Surfaces," AIAA Paper 84-0548, Jan, 1984.

3) Visentine, J.T., Leger, L.J., Kuminecz, J.F. and Spiker, I.K., "STS-8 Atomic Oxygen Effects Experiment," AIAA Paper 85-0415, Jan. 1985.

4) Leger, L.J., Visentine, J.T., and Schliesing, J.A., "A Consideration of Atomic Oxygen Interactions with Space Station," AIAA Paper 85-0476, Jan. 1985.

5) Mende, S.B., Swenson, G.R., Clifton, K.S., Gause, R., Leger, L.J., and Garriot, O.K., "Space Vehicle Glow Measurements on STS 41-D," J. Spacecraft and Rockets, 23, 189-193 (1986).

6) Green, B.D., "Review of the Vehicle Glow," AIAA Paper 85-6095-CP, Nov. 1985.

7) Nier, A.O., Potter, W.E., Hickman, D.R. and Mauersberger, K., "The Open Source Neutral Mass Spectrometer on Atmosphere Explorer -C, -D, and -E," Radio Sci., 8, 271-276 (1973).

8) Pelz, D.T., Reber, C.A., Hedin, A.E. and Carignan, G.R., "A Neutral Atmosphere Composition Experiment for the Atmosphere Explorer -C, -D, and -E," Radio Sci., 8, 277-285 (1973).

9) Horowitz, R. and LaGow, H.E., "Upper Air Pressure and Density Measurements from 90 to 220 Kilometers With the Viking 7 Rocket," J. Geophys. Res., 62, 57-78 (1957).

10) Hedin, A.E., Avery, C.P., and Tschetter, C.D., "An Analysis of Spin Modulation Effects on Data Taken With a Rocket-borne Mass Spectrometer," J. Geophys. Res., 69, 4637-4648 (1964).

11) Narcisi, R.S., Schiff, H.I., Morgan, J.E. and Cohen, H.A., "Calibration of a Flyable Mass Spectrometer For N and O Atom Sensitivity," Space Research III, Proceedings of the Third International Space Science Symposium, Washington, DC, April 30-May 9, 1963, Priester, W., Ed., North-Holland, Amsterdam, 1963, pp. 1156-1167.

12) Lake, L.R., Mauersberger, K., "Investigation of Atomic Oxygen in Mass Spectrometer Ion Sources," Int. J. Mass Spec. and Ion Physics, 13, 425-436 (1974); Sjolander, G.W., "Atomic Oxygen-Metal Surface Studies as Applied to Mass Spectrometer Measurements of Upper Planetary Atmospheres," J. Geophys. Res., 81, 3767-3770 (1976).

13) Ballenthin, J.O., and Nier, A.O., "Molecular Beam Facility for Studying Mass Spectrometer Performance," Rev. Sci. Instrum., 52, 1016-1024 (1981).

14) Visentine, J.T. and Leger, L.J., "Material Interactions With the Low Earth Orbital Environment: Accurate Reaction Rate Measurements," AIAA Paper 85-7019, Nov. 1985.

15) Hunton, D.E., Trzcinski, E., Wlodyka, L, Federico, G. and Dorian, J., "Quadrupole Ion/Neutral Mass Spectrometer for Space Shuttle Applications," AFGL Technical Report 86-0084, #ADA172000.

16) Narcisi, R.S., Trzcinski, E., Federico, G., Wlodyka, L., and Delorey, D., "The Gaseous and Plasma Environment Around Space Shuttle," AIAA Paper 83-2659, Oct. 1983.

17) Cross, J.B. and Cremers, D.A., "Atomic Oxygen Surface Interactions--Mechanistic Study Using Ground Based Facilities," AIAA Paper 85-0473, Jan, 1985.

18) Cross, J.B. and Cremers, D.A., "High Kinetic Energy Laser Sustained Neutral Atom Beam Source," Nuclear Inst. and Methods in Physics, B13, 658-662 (1986).

19) Pack, R.T., Valentini, J.J. and Cross, J.B., "Multiproperty Empirical Anisotropic Intermolecular Potentials for $ArSF_6$ and $KrSF_6$," J. Chem. Phys., 77, 5486-5499 (1982); Bomse, D.S., Cross, J.B., and Valentini, J.J., "The Dynamics of Infrared Photodissociation of van der Waals Molecules containing Ethylene: An Experimental Study," J. Chem. Phys., 78, 7175-7190 (1983).

20) Kern, K., Lindenau, B., David, R. and Comsa, G., "Absolute Determination of Molecular Beam Intensities," Rev. Sci. Instrum., 56, 52-57 (1985).

INTERACTION OF HYPERTHERMAL ATOMS ON SURFACES IN ORBIT: THE UNIVERSITY OF ALABAMA EXPERIMENT

J. C. Gregory

Chemistry Department
The University of Alabama in Hunstville
Huntsville, AL 35899

Abstract

The UAH experiment which flew on the STS-8 mission had several objectives which were mostly of a speculative nature since so little was known of the processes of interest. The experiment provided original, if limited, data on: (a) oxidation of metal surfaces, (b) reaction rates of atomic oxygen with carbon and other surfaces and the dependence of these rates on temperature, and (c) the angular distribution of 5eV atoms scattered off a solid surface. This paper provides a review of the results, with references given to fuller published accounts where these are available.

Introduction

The chemistry of reactions between species with relative kinetic energies in the range of a few eV to a few 10's of eV has only been sparsely studied, principally because of the experimental difficulties and expense of generating beams of usable flux at these energies. The region is of considerable theoretical interest since it overlaps the region of energies of chemical bonds and activation energies. Thus enhancement of reaction rates (over those at ordinary temperatures) is possible and even likely. With this in mind, in 1974 we proposed an experiment for the Long Duration Exposure Facility (LDEF) spacecraft, originally projected to fly in 1978 (Ref. 1). This mission was launched in 1984 and has not yet been recovered from orbit. The early 1980's saw an awakening of interest within NASA in the effect of hyperthermal oxygen atoms on spacecraft materials, and several exposures of materials were made and studied. In 1983 a NASA-wide materials experiment was proposed, for which UAH was invited to provide a modified version of the LDEF hardware. This composite experiment, designated EIOM-2, was flown in September of the same year, which must be one of the shortest completion times for a flight experiment of this size.

The UAH experiment included the following components:

(a) Seven thin (optically-transmitting) metal films deposited on quartz flats. The metals used were Al, Au, Ir, Nb, Ni, Pt and W.

(b) Samples of materials known or suspected to exhibit gross erosion or corrosion effects (C, polymers, Os, Ag). These samples were mounted on heated plates at different temperatures to allow measurement of temperature dependence of rate.

(c) Scatterometers: a passive device of novel design in which the intensity of oxygen atoms reflected from a solid surface was measured.

(d) In addition to the above, carbon specimens were provided to Johnson Space Center experiments designed to measure (i) synergistic effects of solar UV on reaction rates and (ii) effects of atmospheric oxygen ions on those rates.

A short description of the experimental approach and the hardware is given below for each of these components, together with a summary of the results. Orbital exposure data pertinent to the results described here in given in Table I.

TABLE I: STS-8 ATOMIC OXYGEN EXPOSURE DATA

Payload Bay Forward Facing:	t = 41.2 hrs.
Altitude:	120 nautical mi. (225 km)
Velocity:	7.8 km s^{-1}
Mean Oxygen Atom Density (Calculated:	2.65 x 10^{9} cm^{-3}
Surface Impact Frequency:	2.07 x 10^{15} cm^{-2} s^{-1}
Integral Fluence:	3.5 x 10^{20} atoms cm^{-2}

Results

(a) Effects on Optical Surfaces

This investigation was directed to determining some quantitative effects on uncoated optical surfaces. Others have shown that standard optical coatings (where permissible) of metal oxides or metal fluorides are very resistant to atomic oxygen.

The surfaces studied were of two types: high-purity thin films sputtered or evaporated onto 2.54-cm diam $\lambda/20$ fused silica optical flats, and highly polished bulk samples. Films were prepared with optical densities of ~2.5 or less. Measurement of optical densities using a Perkin-Elmer PDS scanning microdensitometer allowed sensitive determination of any changes to these thin films produced by the exposure. By masking one-half of each sample during flight as a control it was possible to measure changes in optical density of ~0.01, corresponding to a few percent change in the thickness of ~10-nm thick films. (No increase in scattering was assumed, since most films became smoother; changes in reflection due to very small oxide thickness increases were

also neglected.) In several cases the sensitivity of the method was ±1 monolayer of surface atoms. Total film thicknesses were accurately measured by step height changes in stylus traces of the film/substrate surfaces using a Tencor Alpha-Step 200 stylus profilometer with a nominal 2-μm radius diamond stylus. Decreases in both the optical density and total film thickness were attributed to metal film removal. A decrease in optical density but an increase in total film thickness was attributed to film expansion due to formation of a non-volatile oxide of lower density than the original film. Topographic measurements were also made on a number of surfaces with an optical heterodyne instrument. These measurements provided an optical determination of surface roughnesses for comparison to stylus results as well as several correlation functions from the same measurement. A fuller account of these measurements is gefen in Ref. 2.

Estimates of metallic film thicknesses in exposed and unexposed areas were calculated from the optical density measurements using equations for transmission and reflection.

A summary of the results is shown in Table II. Al, Ni, Nb and Cu showed small but measurable increases in oxide thickness over that obtained by normal exposure to the atmosphere. Au, Pt and Si showed no measurable effects by these techniques. Os showed massive erosion, and Ag massive corrision. Ir showed evidence of slight erosion.

TABLE II

Material	Nominal Thickness (nm)	Thickness of Metal Converted to Oxide (nm)	Thickness of Metal Lost (nm)
Al film	3.4	0.8	none
Au film	35.5	none	none
Ir film	32.3	none	2.5
Ni film	54.2	0.7	none
Nb film	16.8	1.3	none
Pt film	10	none	none
Os bulk	bulk	none	1100nm
Ag bulk	bulk	>100nm, variable	none
Cu bulk	bulk	~3.5	none
Si bulk	bulk	no measurable effect	

(b) Kinetic Studies on Carbon and Other Highly Erodible Surfaces

The experimental approach used was necessarily very simple as on electro-mechanical devices such as lids, shutters, etc. were available, and no intermediate measurements could be made, i.e., only a single integral effect could be measured for each sample. Samples were nominally one inch discs, with the hot-plate discs only being one quarter-inch diameter. For the case of the erodible materials discussed here, a bar-pattern of small rectangles of niobium was deposited on the surface using a photo-resist technique. The niobium was sputtered on as a uniform film ~200-nm thick. Although it oxidized, it still served to protect the underlying carbonaceous material. The bar-pattern allowed multiple measurements of the step-height to be made using the Tencor stylus profilometer. Amplitudes were checked using SEM micrographs. Half of each sample was covered at all times before and during the flight, and served as a control.

Erodible surfaces studied included single crystal graphite (basal and prismatic planes, vitreous (or glassy) carbon from various manufacturers, polymethyl methacrylate (lucite), bisallyl diglycol carbonate (CR-39, an optical plastic), and diamond.

Erosion observed by this experiment ranged from 75-nm for diamond (which appears to be particularly resistant to oxidation under these conditions), to about 10,000-nm for the poly-carbonate resin, CR-39, which was the most heavily eroded sample reported on any flight exposure.

The temperature dependence of the oxidative effects was measured by conducting the erosion measurements at three temperatures spanning about 120°C. The Arrhenius activation energy, ΔE, was estimated, assuming:

$$r = A\, e^{-\Delta E/RT}$$

where r is the rate of the reaction and A is a constant assumed independent of temperature T. These studies were performed for 6 materials, vitreous carbon, 2 graphites, CR-39, silver, and osmium. All activation energies were small and positive.

The conclusions from the measurements on various forms of carbon exposed in the STS-8 mission appear applicable to organic solids in general. They may be summarized as follows:

1. Measured erosion was linear with total fluence (Fig. 1).
2. No induction time was observed before onset of erosion (Fig. 1).
3. Erosion rate linear with oxygen flux (i.e., reaction probability independent of flux) measured over a small range 1.5 to 2.5 x 10^{15} atoms cm^{-2} s^{-1}.
4. Arrhenius activation energies for the reactions were measured (Fig. 2) as follows:

vitreous carbon	1200 (cal $mole^{-1}$)
graphite (basal plane)	1400
CR-39	1050

5. Reaction probabilities depend on temperature as shown in (4) above. Reaction probabilities for carbons exposed at ~300^{o}K ranged from .1 to .15 where reaction probability equals the number of carbon atoms lost divided by the number of incident oxygen atoms.
6. No effect was observed on the measured erosion rates (at the 5% level) which could be ascribed to the presence for absence either of solar UV or of charged oxygen species.

The silver and osmium data has not been fully analyzed, but it is clear that the apparent activation energy of the rate-controlling step in both the osmium-loss process and for the production of bulk silver oxide under these conditions is positive.

(c) Atom Scattering at Orbital Velocities

When an atom or molecule strikes a surface a number of processes may take place. Some of these are:

1. Accommodation of momentum and energy.
2. Chemical reaction with a surface atom or adsorbed molecule.
3. Recombination, dissociation or excitation of projectile species.
4. Sputtering.

Measurements of the spacial and energy distribution of scattered species provides a probe of the interaction potential existing between the projectile and target species. Understanding of the processes taking place during such an interaction requires some knowledge of this potential.

While the UAH experiment was passive and very simple, it has provided a unique measurement of the angular distribution of oxygen atoms scattered from a polished carbon surface in orbit. It was not capable of measuring the velocity or energy profile of scattered species. The apparatus has been described elsewhere (Ref. 3), and the data has been used to estimate satellite lift and drag parameters (Ref. 4).

The scatterometer, shown in Figure 3, consisted of an aluminum enclosure, a polished vitreous carbon disc mounted so that the stream of fast atoms passing through the entry slit impinged on its center at 55^{o}. Detection of reflected atoms was accomplished by a silvered strip of clear CR-39 plastic mounted in the can like the x-ray film in a diffraction camera.

Silver absorbs oxygen atoms with efficiency ~100% and is converted to clear oxide. Increase in optical transmission measured with a scanning optical densitometer yields reflected O intensity as a function of angle.

The resultant angular distribution of 5eV O atoms is shown in Figure 4. Such a distribution is described as wide lobular with a maximum intensity in the reflection hemisphere 15^{o} from the surface normal.

A calculation of the mass balance for atomic O showed that the silver converted to oxide accounted for at least 80% of atoms incident on the carbon (after deducting those which reacted with carbon).

Conclusions, discussed more fully in Ref. 3, are that the incident atoms are almost, but not quite, fully accommodated at the carbon surface, and that recombination efficiency (to form O_2 molecules is low (<20%). We intend to pursue further studies of scattering in this energy regime both in space and in simulation facilities on the ground.

References

1. J. C. Gregory and P. N. Peters "Interaction of Atomic Oxygen with Solid Surfaces at Orbital Altitudes", unpublished proposal (1975) to Langley Research Center; Proc. 1st LDEF Working Group Meeting, NASA, LaRC, (1981), p48; Experiment A-0114 in "The Long Duration Exposure Facility", p14, NASA SP-473, NASA Headquarters, (1984).

2. P. N. Peters, J. C. Gregory and J. Swann, "Effects on Optical Systems from Interactions with Oxygen Atoms in low Earth Orbits", Applied Optics 25, 1290, (1986).

3. J. C. Gregory and P. N. Peters, "A Measurement of the Angular Distribution of 5eV Atomic Oxygen Scattered off a Solid Surface in Earth Orbit", Rarefied Gas Dynamics 15 (1), 644, (1986).

4. G. R. Karr, J. C. Gregory and P. N. Peters, "Free Molecule Lift and Drag deduced from Shuttle Flight Experiment", Rarefied Gas Dynamics 15 (1), 609, (1986).

Acknowledgements

This work was performed with support from NASA Grants NAGW-823 and 812.

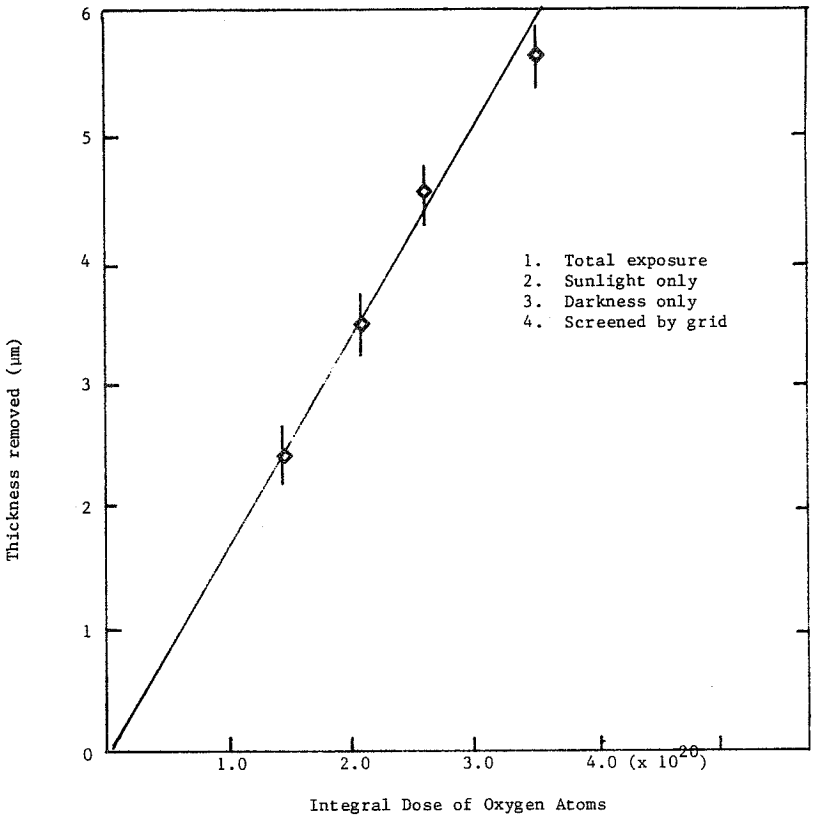

Figure 1. Vitreous Carbon Dosimeter, STS-8 Exposure

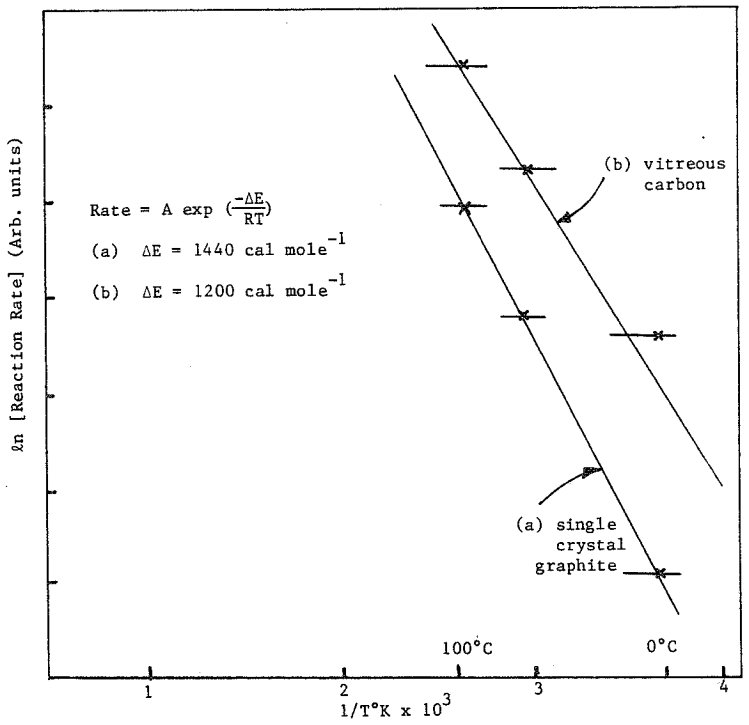

Figure 2. Arrhenius Plots for Carbon Oxidation by 5eV Oxygen Atoms (STS-8 data)

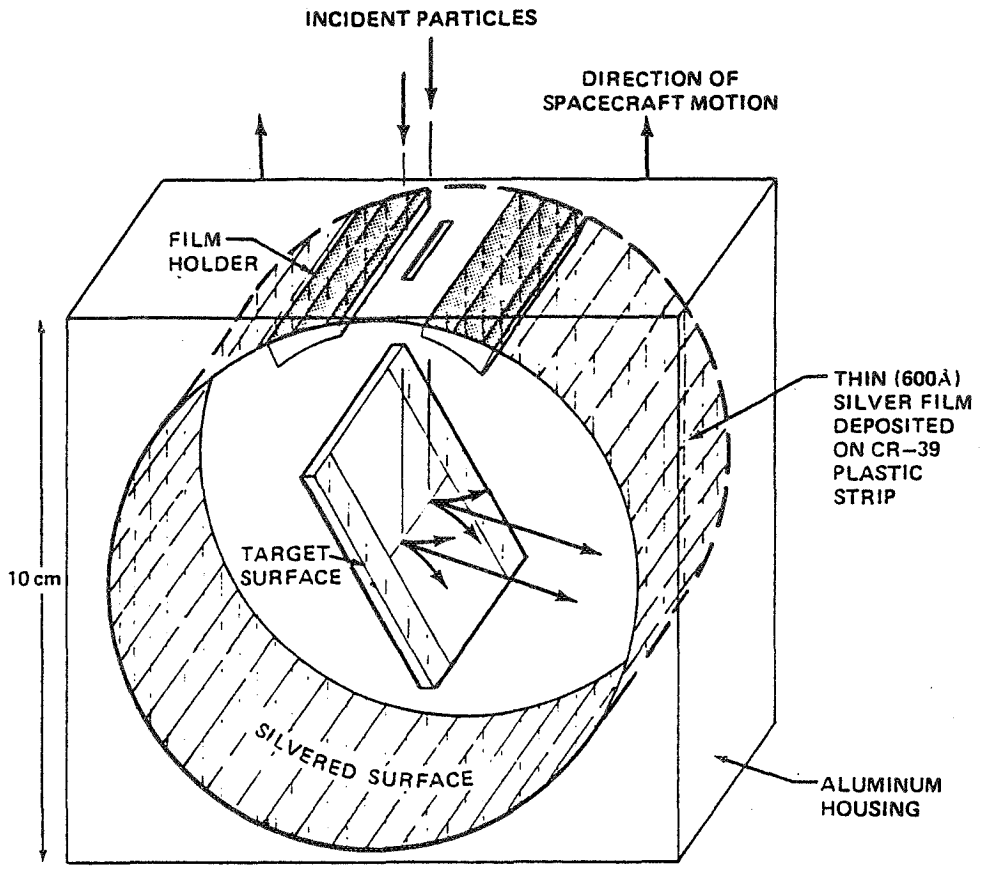

FIGURE 3. THE OXYGEN ATOM REFLECTOMETER FLOWN ON SHUTTLE STS-8 AND THE LONG DURATION EXPOSURE FACILITY

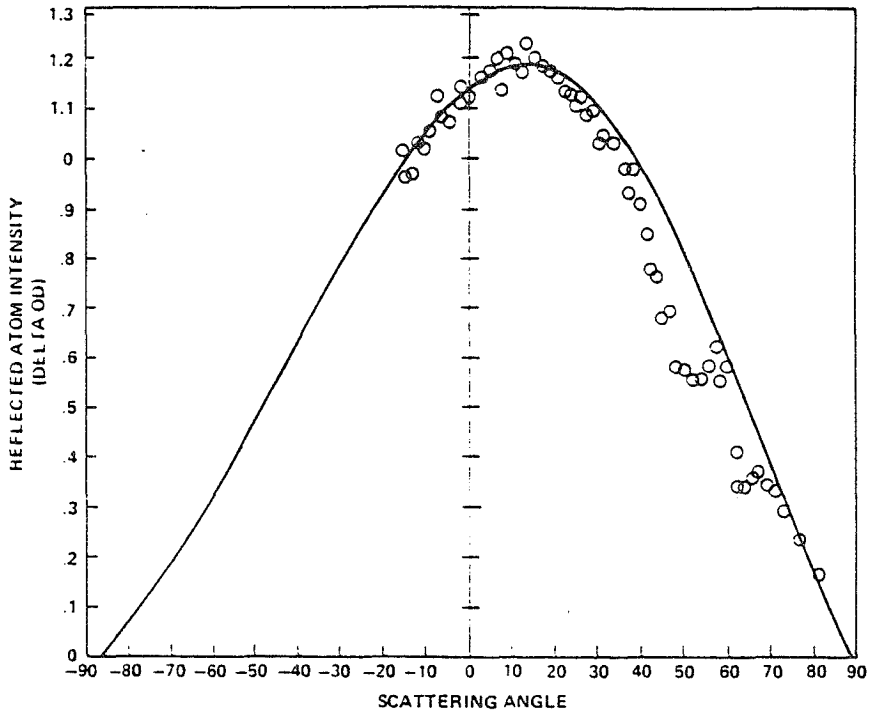

FIGURE 4. FIT USING NOCILLA MODEL TO THE OUTSIDE ENVELOPE OF THE FLIGHT DATA. DISCREPANCIES ASSUMED DUE TO ABSORPTION ARTIFACTS IN THE SILVER FILM θ_r. (NOCILLA) = 40°: S_r = 0.2

Session II:

Atomic Oxygen Interactions

O-Atom Degradation Mechanisms of Materials

Daniel R. Coulter
Ranty H. Liang
Shirley Y. Chung
Keri Oda Smith
Amitava Gupta

Applied Sciences and Microgravity Experiments Section

Jet Propulsion Laboratory
California Institute of Technology
Pasadena, CA 91109

Introduction

Since the earliest flights of the space shuttle (STS I, II and III), it has been recognized that exposure of a wide variety of materials (organic, inorganic and metallic) to the LEO environment has resulted in significant changes in their physical state and/or properties. The observed phenomena have included such things as surface erosion, weight loss, oxidation, changes in absorptivity and emissivity and in some cases even changes in bulk properties (modulus). Over the past few years, literally hundreds of samples have been exposed to the LEO environment on shuttle flights and returned for analysis. Based on the results of these studies it is believed that the observed material degradation is related to the presence of the rarefied atmosphere through which the shuttle flies. In particular, it is postulated that atomic oxygen in the atmosphere is the primary active agent[1]. To date, most of the flight experiments have been directed toward material screening activities. Experiments dedicated to elucidating the mechanisms of the observed degradation have been limited, and in a number of cases, potentially valuable information has been compromised or lost completely due to contamination or sample mishandling. Consequently, the underlying mechanisms of the degradation are still largely unknown. In this paper, we will discuss the LEO environment, the critical issues relating to O-atom degradation, some analytical techniques for studying the problem and some preliminary results on mechanisms. The purpose here is not to give all the answers concerning atomic oxygen degradation; rather it is to state clearly the questions and to point in the direction that we believe must be followed in order to find the answers in the most expeditious manner.

Environment

The LEO environment under consideration is defined by the shuttle orbital flight altitude which generally ranges from 200 to 500 km where the total pres-

sure is $\approx 10^{-7}$-10^{-8} torr corresponding to an atmospheric number density of $\approx 10^{9} cm^{-3}$. The shuttle velocity is $\approx$ 8 km/sec which corresponds to a particle flux of 10^{14}-10^{15} particles/cm^2-sec as the vehicle sweeps through the atmosphere. At this altitude, the atmosphere is primarily comprised of ground state (O^3P) atomic oxygen ($\approx$80%) and molecular nitrogen ($\approx$20%). Helium becomes important only at higher altitudes and the ion concentrations are 10^3 times lower than neutrals. The velocity of the shuttle is almost an order of magnitude greater than the thermal velocities of the atmospheric gasses; therefore, most gas collisions with the spacecraft occur on the forward or ram surfaces. The kinetic energy of the collisions with atmospheric constituents is high ($\approx$5eV for O-atoms) resulting from the high vehicle velocity. It is important to understand that a thermal velocity of 8 km/sec for O-atoms would correspond to a temperature of $\approx$60,000K! Under these conditions, it is not surprising that macroscopic changes in materials have been observed.

Critical Issues and Approach

Several critical issues related to O-atom interactions with materials have been identified. These include questions like:

1) Is the observed loss of material due to ablation or more complex chemistry?

2) What is the energy dependence of O-atom interactions with materials?

3) Is the degradation dependent on the angle of collision with the atmospheric constituents?

4) What is the effect of surface temperature?

5) What are the degradation products and what is their energy distribution?

6) Are the effects confined to the surface or are changes occurring in the bulk?

Fragmented data exists relating to some of these questions. Clearly, a more structured approach is necessary to come to a final conclusion on these issues. A four point approach including

1) carefully planned and executed flight experiments,

2) development of ground based capabilities to simulate the LEO environment,

3) extrapolation (where possible) of data from conventional atomic oxygen studies, and

4) theoretical modeling

is proposed to lead ultimately to a complete mechanistic understanding of the interactions.

The bulk of the efforts in mechanistic investigations to date has involved analysis of flight samples and to a lesser extent, samples exposed to ground based O-atom sources. The techniques applied to study these samples can be divided into two groups, those designed to interrogate the surface and those which can measure bulk properties. Table I lists some of the applicable analytical techniques.

TABLE I. EXPERIMENTAL METHODOLOGY FOR ANALYSIS OF EXPOSED SAMPLES

SURFACE TECHNIQUES	BULK TECHNIQUES
• SEM	• WEIGHT LOSS MEASUREMENTS
• SURFACE ENERGY ANALYSIS	• TRANSMISSION FTIR
• ESCA	• SOL-GEL STUDIES
• FTIR-ATR	• HPLC
• RAMAN SPECTROSCOPY	• STRESS-STRAIN MEASUREMENTS
• UV-VISIBLE REFLECTANCE SPECTROSCOPY	• DYNAMIC MECHANICAL RESPONSE

O-Atom Effects on Polymers

In the early stages of the investigation of O-atom effects on polymers, a key question to be answered was whether the observed loss of material was due to simple ablation or if more complex chemistry was going on. If the mechanism is ablative, then all organics should show approximately the same erosion rate. If more complex chemistry is involved, then the erosion rates should be material specific. There is now considerable evidence that the latter is the case. Table II shows reaction efficiencies for a number of polymers determined from O-atom fluence calculations[2]. The data clearly show that the erosion rates vary by more than two orders of magnitude in going from Teflon® to Mylar®. Furthermore, it is known that metals which form volatile oxides (i.e., osmium) suffer serious erosion as compared to those which do not. Both of these facts point clearly to a chemically based mechanism for erosion.

If indeed chemistry is occurring on the surface, it is important to understand what the reactions are. The study of the reactions of atomic oxygen with organic molecules has been carried out extensively for many years. It is known for example that the interaction of ^3P oxygen with hydrocarbons generally results in hydrogen abstraction while ^1D oxygen usually undergoes insertion. Unfortunately, these data are for low energy O-atom reactions. It is not understood what the effect of 5eV of translational energy will have on

TABLE II. REACTIVITY OF ATOMIC OXYGEN AND MATERIALS

MATERIAL	REACTION EFFICIENCY (10^{-24} cm^3/ IMPINGING ATOM)
TEFLON ®	< 0.03
25% POLYSILOXANE-POLYIMIDE	0.3
POLYVINYLIDENE FLUORIDE	0.6
CARBON	1.2
POLYSTYRENE	1.7
KAPTON ®	3.0
POLYETHYLENE	3.7
MYLAR ®	3.9

the reaction pathways. Preliminary results by Arnold, et al[3] suggest a significant effect of translational energy on erosion of Kapton®.

Predicting reaction pathways on the basis of thermodynamics is not a foolproof method. For example, the enthalpies of several reactions of $O(^3P)$ with aromatic hydrocarbons are shown in Figure 1. The results of molecular beam experiments on reactions of $O(^3P)$ with benzene are shown in Table III [4]. It is seen that the formation of the phenoxy radical is highly favored over the formation of phenol even though the latter is far more thermodynamically stable. Two other relevant pieces of information can be gleaned from this data. First, there is an obvious effect of collision energy on the products, although the conditions still represent very low energies (.1-.3eV) compared to the LEO environment. Secondly, there is a significant isotope effect observed when perdeuterobenzene is used. This again points to the chemical nature of the interactions.

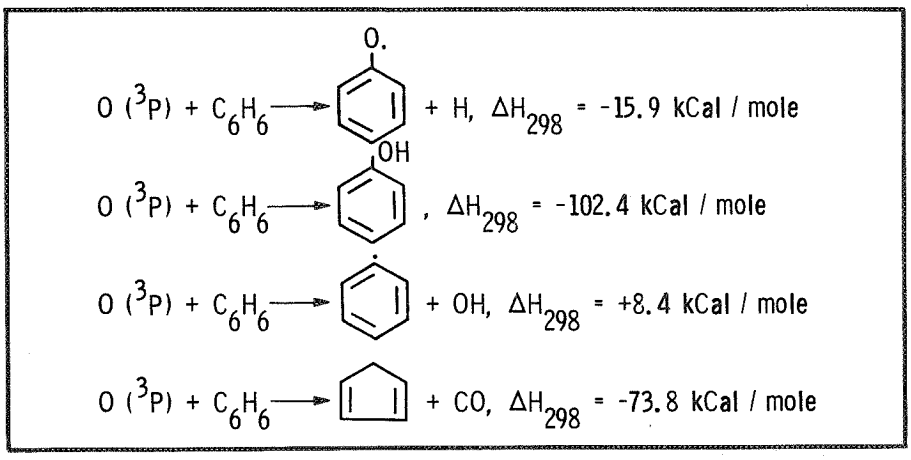

Figure 1. Energetics of several alternate reaction pathways between supersonic beams of $O(^3P)$ atoms and benzene

TABLE III. OBSERVED REACTIONS OF O ATOMS WITH BENZENE

REACTION	PRODUCT	COLLISION ENERGY 0.28 eV	0.11 eV
$O + C_6H_6$	C_6H_5OH	16%	< 5%
	$C_6H_5O\cdot + H\cdot$	84%	> 95%
$O + C_6D_6$	C_6D_5OD	50%	15%
	$C_6D_5O\cdot + D\cdot$	50%	85%

If specific chemistry is going on at the surface of materials, then the question is whether effects will be transmitted to the bulk. Stress-strain measurements have been made on several materials returned from the STS 8 flight. Figure 2 shows this data for PMMA and Udell 1700 Polysulfone®. Clearly, the modulus of the PMMA is unchanged while behavior of the polysulfone is altered considerably after exposure. The question of UV irradiation contributing to this behavior has been investigated in this laboratory, and the results indicate that UV alone cannot be responsible, although potential synergistic effects of UV with O-atoms have not been investigated.

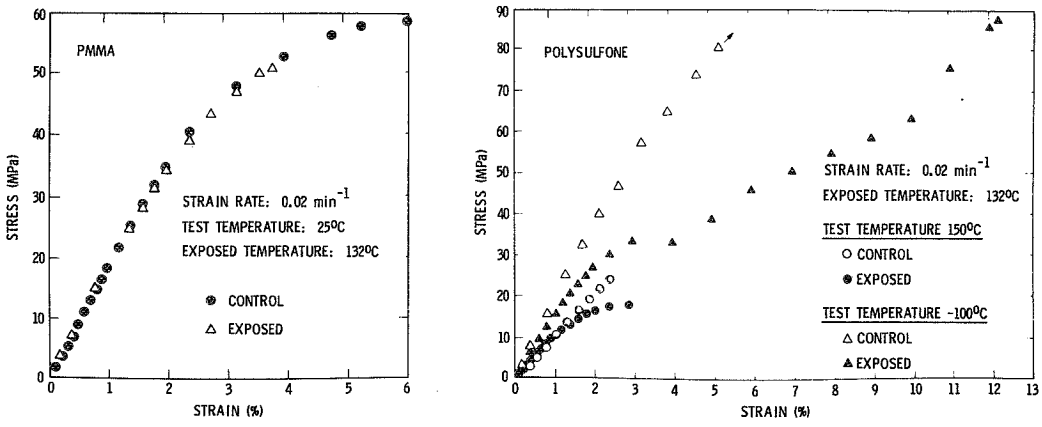

Figure 2. Stress-strain curves for thin (≈5 mil) films of PMMA and Polysulfone exposed to the LEO environment on STS-8

A further indication of bulk material involvement comes from a study of polyethylene (PE) and polyether-etherketone (PEEK) of varying degrees of crystallinity. Samples of both PE and PEEK were prepared from the melts in two ways. One set was fast quenched while the other set was slowly cooled, resulting in otherwise identical samples of lower and higher crystallinity respectively. In both cases, the samples with the higher crystallinity displayed significantly lower erosion rates when exposed to the oxygen atom source at Physical Sciences, Inc.[5] The variation of sensitivity with morphology probably is a sign that diffusion of either the O-atoms themselves or some intermediate is occurring from the surface into the bulk. Slower diffusion of small molecules into the crystalline phase as compared to the amorphous phase in semicrystalline polymers is well known. If diffusion is an important process, then one would expect to see significant temperature effects on the degradation. This has not been observed to date; however, the issue is still open to some debate.

Polyethylene - Case Study of a Flight Experiment

The level to which O-atom interaction mechanisms are understood at this time can be seen by looking at the results of flight exposure studies performed on polyethylene. Thin films flown on the STS-8 shuttle flight showed a weight loss of ≈ 1.3 mg/cm^2. Exposure on this flight was for 40 hours and corresponded to a fluence of $\approx 3 \times 10^{20}$ O-atoms/cm^2 which yields a reactivity of $\approx 4.3 \times 10^{-24}$ gm/impinging atom or $\approx 3.9 \times 10^{-24}$ cm^3/impinging atom. The rate of volatiles leaving the surface can be estimated if an assumption is made about their average molecular weight. Volatile products might be expected to be things like CO, CO_2, H_2O, or CHO which would give an average molecular weight of ≈ 30 gm/mole. Using this value and the measured weight loss data, a value of $\approx 2 \times 10^{14}$ molecules/cm^2-sec can be determined for the rate of volatiles leaving the surface.

The identification of the volatiles leaving the surface is yet to be determined. As of now, the only clues that are available concerning the nature of the chemistry occurring comes from analysis of the exposed surface of the films. Table IV shows the results of ESCA analysis on control and exposed samples.

Clearly, the exposed surface is highly oxidized. Unfortunately, ESCA is not capable of distinguishing between all types of oxides. What can be seen is that there are both CO groups (ketones, ethers and/or alcohols) and COO groups (acids) on the surface. There are apparently no esters remaining on the exposed surface. It is also of interest to determine if significant olefin formation occurs on the surface. To answer this question, control and exposed samples were treated with osmium tetroxide which quantitatively adds to olefins according to the reaction below.

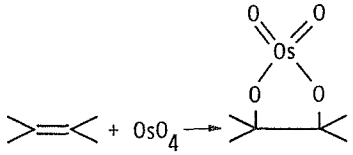

ESCA analysis of the treated surfaces of control and exposed polyethylene showed only a slight increase in osmium binding in the exposed sample (0.3% to 0.6%) thus indicating that olefin formation is not a major process in the case of polyethylene.

TABLE IV. ESCA ANALYSIS OF POLYETHYLENE SURFACE

	C_1	C_2	C_3	O
THEORETICAL	100.0	--	--	--
CONTROL	99.2	--	--	0.8
EXPOSED	81.5	4.5	3.1	9.9

C_1 = -C-C- OR -C = C-

C_2 = -C(=O)-, -C-O-C-, -C-O-H

C_3 = -C(=O)-OH

From the results described above, a strawman degradation model has been developed for O-atom degradation of polyethylene. Such a model is shown in Scheme I. It is likely that the pristine polyethylene surface undergoes primary oxidation resulting in both volatiles and surface oxides. Subsequently, there are secondary oxidation processes resulting in further volatilization and secondary oxide formation. Probably, an equilibrium among the surface oxides is rapidly achieved and maintained as erosion occurs. This is borne out by the fact that analysis of polyethylene samples from several shuttle flights shows similar surface chemistry.

Clearly, a great deal is yet to be understood about the mechanisms of O-atom attack on materials. A considerable effort involving further flight experiments, ground based simulation and theoretical modeling is the only way to achieve this understanding. The results of such an effort will have profound effects on future LEO technology by providing the means to do reliable life prediction and to choose or develop stable materials for that harsh environment.

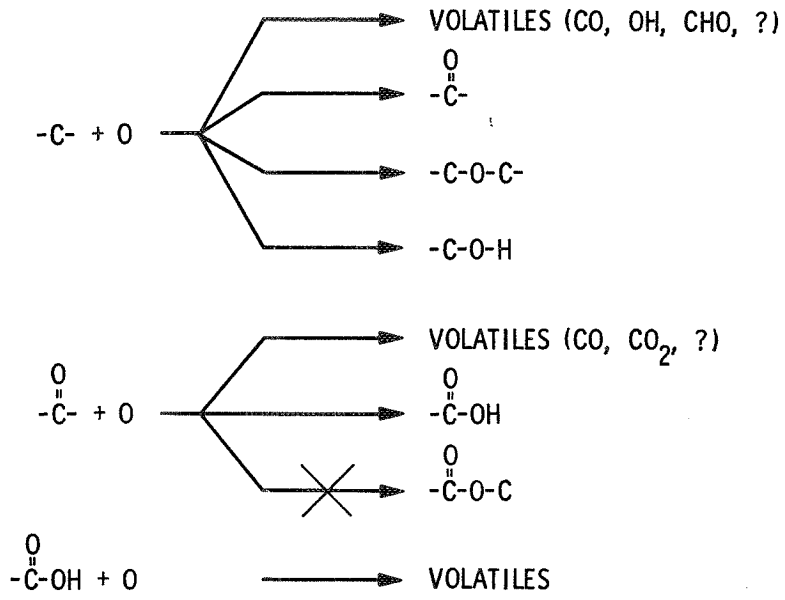

Scheme I

References

1. L. J. Leger, "Oxygen Atom Reactions with Shuttle Materials at Orbital Altitudes," NASA TM-58246, May, 1982.

2. L. J. Leger and J. T. Visentine, J. Spacecraft and Rockets, 23(5), 505 (1986).

3. G. S. Arnold, D. R. Peplinski and F. M. Cascarano, "Translational Energy Dependence of the O-Polyimide Reaction," AIAA Paper 85-7016-CP, November, 1985.

4. S. J. Sibener, R. J. Buss, P. Casavecchia, T. Hirooka and Y. T. Lee, J. Chem. Phys., 72, 4341 (1980).

5. For a description of the beam source see: R. H. Krech and George Caledonia, Int. SAMPE Tech. Conf. Ser., "Materials for Space," 18, 752 (1986).

Kinetics and Mechanisms of Some Atomic Oxygen Reactions

R. J. Cvetanovic

Chemical Kinetics Division
National Bureau of Standards
Gaithersburg, Maryland 20899

Abstract

Mechanisms and kinetics of some reactions of the ground electronic state of oxygen atoms, (O^3P), are briefly summarized. The summary refers to reactions of oxygen atoms with several different types of organic and inorganic compounds such as alkanes, alkenes, alkynes, aromatics, and some oxygen, nitrogen, halogen and sulfur derivatives of these compounds. References to some recent compilations and critical evaluations of reaction rate constants are given.

Introduction

The low lying electronic states of free oxygen atoms are (with their relative energy levels in Kcal/mol given in parentheses): $^3P_2$ (0.0), $^3P_1$ (0.45), ^3P_o (0.65), $^1D_2$ (45.36), and ^1S_o (96.59). The energy differences between the three triplets (^3P) states are quite small and they are usually jointly referred to as the ground electronic state of oxygen atoms. The excitation energy of the first singlet state ($^1D_2$) is 45 Kcal/mol and that of the second singlet state (^1S_o) is 96 Kcal/mol. All these states may play a role in atmospheric chemistry. The present summary of the chemical properties of free oxygen atoms is confined to $O(^3P)$, the ground electronic state, although some differences in the respective chemical behaviors are briefly mentioned.

Several different methods have been used to generate free O atoms for laboratory studies of their chemical behavior, as for example

$$O_2 + e \rightarrow 2O + e \quad (1)$$
$$NO_2 + h\upsilon \rightarrow O + NO \quad (2)$$
$$N_2O + Hg^* \rightarrow O + N_2 + Hg \quad (3)$$
$$O_3 + h\upsilon \rightarrow O + O_2 \quad (4)$$
$$N + NO \rightarrow O + N_2 \quad (5)$$

Over the past three decades, we have made use in our laboratory at the National Research Council in Ottawa, Canada, of all of these methods. After allowance for the specific features of the individual techniques used and the accompanying reaction environments generated, the results obtained were mutually consistent. We have found the mercury photosensitized decomposition of N_2O (Rn. 3) to be particularly convenient and have used it most extensively. N_2 formed in this reaction provides a direct count of the number of the ground state oxygen atoms generated and N_2O itself is likely to react at an appreciable rate with free radicals and atoms only at elevated temperatures.

In the following it will be possible only to present a concise summary of the main features of O atom reactions with different types of chemical compounds and to list several references to more detailed accounts and bibliography. The summary consists of two parts, dealing respectively with 1) the main features of the reaction mechanisms and 2) the trends in the reaction rates under different reaction conditions.

Reaction Mechanisms

Types of primary mechanisms of oxygen atom reactions

Interaction of free oxygen atoms with a molecule of particular type may in principle result in one of the following types of chemical change: 1) "Abstraction" by the O atom of an atom from the compound, 2) "Addition" (attachment) of the O atom to the compound, 3) "Replacement" by the O atom of an atom or atomic group (radical) from the compound. Replacement includes also the isotope exchange reactions of oxygen atoms. The term "Displacement" generally implies that in a "Replacement" process the attachment of the $O(^3P)$ atom and departure of the displaced atom or radical take place simultaneously. A particular type of addition is 4) "Insertion" of the O atom between two bound atoms in the compound (i.e. insertion of the O atom into a chemical bond in the compound). In as much as one of these types of chemical change can be identified and shown to result directly from the chemical interactions in the primary reaction step, it represents the primary reaction mechanism.

Mechanisms of oxygen atom reactions are determined by identifying the primary reaction products. However, a primary reaction product may sometimes be unstable and very short-lived and therefore difficult to observe experimentally. Thus, for example, if an addition is followed rapidly by fragmentation of the adduct, it may simulate an abstraction or a displacement and be classified as such. An example[1] of a mechanistic ambiguity of this kind is provided by the reaction of $O(^3P)$ with H_2S

$$O(^3P) + H_2S \rightarrow [H_2SO]^* \rightarrow \text{products} \qquad (6)$$

which appears to proceed entirely or predominantly by H atom abstraction. In fact, many "Replacement" or "Displacement" reactions may actually be additions followed by rapid fragmentation. Regardless of such ambiguities, discusion of reaction mechanims in terms of basic types of chemical change is generally useful and informative.

Abstraction reactions of O atoms

In the ractions of $O(^3P)$ atoms with alkanes (RH) the reaction products observed (under appropriate conditions to minimize secondary reactions) are H_2O and alkyl radicals (R) formed by abstraction of H atoms by O atoms. The primary reaction mechanism is

$$O(^3P) + RH \rightarrow OH + R \qquad (7)$$

The spin-forbidden insertion to produce an alcohol (ROH) does not occur. In contrast to this, the allowed insertion of the electronically excited singlet $O(^1D_2)$ atoms into the CH bonds of alkanes to form "hot" (vibrationally excited) alcohols occurs readily.[2]

Attack of $O(^3P)$ atoms on aldehydes (RCHO) (and some other alkane derivatives, such as alcohols, thiols, haloalkanes etc) also involves H atom abstraction, e.g.

$$O(^3P) + RCHO \rightarrow OH + RCO \qquad (8)$$

The suggested different reaction path, such as addition of $O(^3P)$ to acetaldehyde to form acetic acid

$$O(^3P) + CH_3CHO \rightarrow CH_3COOH \qquad (9)$$

apparently does not occur.[3,4]

In the case of simple alkenes[5,6], at least at not too elevated temperatures and with $O(^3P)$ atoms not kinetically excited ("hot"), abstraction cannot compete effectively with the very rapid $O(^3P)$ addition to the double bond. However, at sufficiently high temperature, or with sufficiently "hot" $O(^3P)$ atoms, abstraction of H atoms should be expected to become more important.

Addition reactions of O atoms

One of the most important kinetic properties of $O(^3P)$ atoms is their ability to add rapidly to unsaturated CC bonds or to S atoms in some sulfur containing organic compounds.

In the gas phase $O(^3P)$ reaction with alkenes two general types of products due to the initial addition of $O(^3P)$ are observed under normal laboratory conditions: 1) stabilized adducts and 2) the products formed by fragmentation of the initial adducts (including products from secondary reactions of the free radical fragments

formed). The stabilized adducts are of two types: 1) those formed by attachment of O atoms to the double bond (the epoxides) and 2) those formed by molecular rearrangement of the initial adducts, which are almost exclusively carbonyl compounds (aldehydes and ketones). The rearrangement products are formed by 1,2 C to C shift of a H atom (or less frequently radical group) from the C atom to which $O(^3P)$ adds to the other C atom of the original double bond. Formation of epoxides is nonstereospecific: with either cis- or trans-2-butene, for example, both cis- and trans-2-butene oxide are produced and their ratio is different in the two reactions and is also temperature dependent.

The products observed in O-alkene reactions are generalized in a set of "predictive" rules, which define the expected compounds from particular reactions and also define the basic reaction mechanism. It is not possible in a brief summary to present in a satisfactory way all the aspects of the versatile behavior of $O(^3P)$ atom alkene reactions and a detailed reaction mechanism. The subject has been recently discussed in some depth by Cvetanovic and Singleton.[6] The overall sequence of events can be described in a simplified manner using the $O(^3P)$ reaction with cis-2-butene as an example:

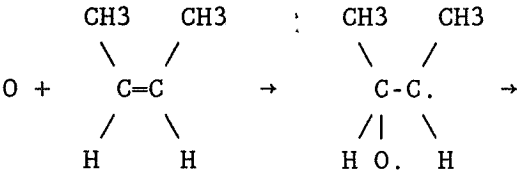

(triplet biradical)

→ cis-1,2-epoxybutane* + trans-1,2-epoxybutane*

→ CH3CH2C(O)CH3* + (CH3)2CHCHO*

→ Pressure independent fragmentation (into CH3, etc)

To explain the observed products, it is necessary to postulate that the initial adduct is a triplet biradical. This intermediate subsequently rapidly rearranges into highly vibrationally excited ("hot") epoxides and carbonyl compounds or undergoes a rapid "pressure independent" fragmentation (which may also include displacements, as defined in an earlier section). The "hot" epoxides and carbonyl compounds undergo at lower pressures a "pressure dependent fragmentation" and tend to be collisionally stabilized at higher pressures. In condensed media[6,7] the pressure dependent fragmentation is suppressed, as expected.

The $O(^3P)$ reaction with cyclopentene illustrates some interesting rearrangement and fragmentation reactions dictated by a particular structure of a structurally constrained system.[8] The initial triplet biradical in this system undergoes partly the usual rearrangement into the "hot" cyclopentene oxide and cyclopentanone but it also undergoes the equivalent of the pressure independent fragmentation (or "displacement") which in this case, because the "displaced" group is part of the original cyclopentene ring, leads to the formation of a ring-opened biradical. The latter undergoes substantial molecular cleveage (into ethylene and acrolein) and a ring closure (mainly into the C4-ring cyclobutyl aldehyde and to a minor extent into the C6-ring dyhydropyrane by incorporating the oxygen atom into the closed ring).

The general mechanism of O atom addition to alkynes[9] resembles that for the addition to alkenes. Fewer mechanistic studies have been done so far for O atom additions to aromatic hydrocarbons. In the $O(^3P)$ reaction with benzene[10] the main product is a non-volatile material difficult to characterize. However, the direct adduct, phenol, is also formed in smaller amounts (about 13% of the benzene consumed). In the reaction with toluene[11], 15-20% of the O atoms reacted are recovered as the direct adduct, cresol. An interesting directional effect is observed: only o-cresol and p-cresol (in a ratio of about 3:1) with very little or no m-cresol are formed. The directional effect is consistent with the electrophilic character of $O(^3P)$ atoms.

$O(^3P)$ atoms rapidly add to S atoms functionally bound in organic sulfides and disulfides,[12,13] as for example in dimethyl sulfide and dimethyl disulfide. Some of the kinetic features of these addition reactions are similar to those in the analogous alkene reactions.

Reaction Rates

Determination of the rate constants of $O(^3P)$ reactions is experimentally demanding and some early measurements were subject to large uncertainties. Determination of relative rates instead of the absolute values proved very useful for probing into the trends in rates as the structure of compounds reacting with oxygen atoms is varied.[6] Reliable techniques are now also available for determination of absolute values of the rate constants. One of these, the phase shift technique for absolute measurements of the rate of $O(^3P)$ atom reactions, was developed and extensively used in our laboratory. Another excellent and much used technique is the resonance fluorescence method. Gratifyingly, comparision of results obtained by these absolute techniques and with the earlier relative rate determinations shows remarkably good agreement.[6]

Several examples of $O(^3P)$ rate constants (in $10^{12}cm^3mol^{-1}s^{-1}$) obtained by these three techniques at 298K are listed bellow.

Reactant	Phase-shift technique	Resonance-fluorescence technique	Relative* rates
Ethylene	0.42	0.49	0.45
Propylene	2.28	2.21	2.6
1-Butene	2.42	2.46	2.6
cis-2-Butene	10.6	10.3	10.6
Isobutene	10.4		11.2
Trimethylethylene	31.1		35.4
Tetramethylethylene	45.8	47.7	45.4
Dimethylsulfide	31.1		33.3
Dimethyldisulfide	60.2		59.9

* Relative rates normalized to absolute values

Trends in the values of rate constants of $O(^3P)$ reactions are reviewed and discussed in a number of publications.[5,6,14-16] The electrophilic trend in the rate constants of $O(^3P)$ reactions with alkenes is demonstrated by the monotonous increase in the rates as the number of alkyl group substituents at the double bond is increased. A number of numerical correlations, such as correlation with the ionization potentials of the olefins or with the rates observed with the same olefins reacting with another electrophilic reagent, provide additional support for the electrophilic character of these atom-molecule reactions.

Data Bases for $O(^3P)$ Reactions

Compilations and critical evaluation of chemical kinetic data for the elementary reactions of $O(^3P)$ atoms with unsaturated hydrocarbons are currently conducted by the Chemical Kinetics Data Center of the National Bureau of Standards. This activity is a part of a larger effort directed towards the development of a comprehensive general evaluated chemical kinetic data base. More specifically, it is a part of an extensive data base, currently developed by the Chemical Kinetics Data Center, which deals with chemical oxidation processes, in particular those involved in thermal combustion and in the atmospheric chemistry. The data bases are intended to provide easily accessible sources of critically evaluated rate data for use in computer modeling and in general research.

The following compilations and critical evaluations have been completed or are currently in progress:

(1) "Chemical Kinetic Data Base for Combustion Chemistry. Part 1. Methane and Related Compounds". W. Tsang and R. F. Hampson, J. Phys. Chem. Ref. Data 15, 1087 (1986).

(2) "Chemical Kinetic Data Base for Combustion Chemistry. Part 2. Methanol", W. Tsang. (Submitted for publication)

(3) "Chemical Kinetics Data Base for Combustion Chemistry. Part 3. Propane, n-Propyl, and i-Propyl", W. Tsang. (In preparation).

(4) "Chemical Kinetic Data Base for Combustion Chemistry. Part 4. t-Butyl, i-Butyl, and i-Butane", W. Tsang. (In preparation).

(5) "Evaluated Chemical Kinetic Data for the Reactions of Atomic Oxygen $O(^3P)$ with Unsaturated Hydrocarbons". R. J. Cvetanovic. (Submitted for publication).

(6) "Evaluated Chemical Kinetic Data for the Reactions of Atomic Oxygen $O(^3P)$ with Sulfur Containing Compounds". D. L. Singleton and R. J. Cvetanovic. (In preparation).

(7) "Evaluated Chemical Kinetic Data for the Reactions of Atomic Oxygen $O(^3P)$ with Saturated Organic Compounds". John T. Herron. (In preparation).

(8) "Compilation of Chemical Kinetic Data for Combustion Chemistry. Part 1. Non-aromatic C,H,O,N, and S Containing Compounds (1971-1982)". Francis Westley, John T. Herron, and R. J. Cvetanovic. (Submitted for publication).

References

1. D. L. Singleton, G. Paraskevopoulos, and R. S. Irwin, "Mechanism of the $O(^3P)$ + H_2S Reaction. Abstraction or Addition?," J. Phys. Chem. **86**, 2605 (1982)
2. H. Yamazaki and R. J. Cvetanović, "Collisional Deactivation of the Excited Singlet Oxygen Atoms and Their Insertion into the CH Bonds of Propane," J. Chem. Phys. 41, 3703 (1964)

3. Cvetanović, R. J., "Reaction of Oxygen Atoms with Acetaldehyde," Can. J. Chem. 34, 775 (1956)
4. H. E. Avery and R. J. Cvetanović, "Reaction of Oxygen Atoms with Acetaldehyde," J. Chem. Phys. 43, 3727 (1965)
5. Cvetanović, R. J., "Addition of Atoms to Olefins in the Gas Phase," Adv. Photochem. 1, 115 (1963)
6. Cvetanović, R. J., and Singleton, D. L., "Reaction of Oxygen Atoms with Olefins," Rev. Chem. Inter. 5, 183 (1984)
7. S-i. Hirokami and R. J. Cvetanović, "Reaction of Oxygen Atoms, $O(^3P)$, with Olefins in Liquid Nitrogen Solution at 77°K," J. Am. Chem. Soc. 96, 3738 (1974)
8. R. J. Cvetanović, D. F. Ring, and L. C. Doyle, "Reaction of Oxygen Atoms with Cyclopentene," J. Phys. Chem. 75, 3056 (1971)
9. Lin, M. C., "Dynamics of Oxygen Atom Reactions," Adv. Chem. Phys., "Potential Energy Surfaces," edited by K. P. Lawley (John Wiley & Sons Ltd.) 42, 113 (1980)
10. G. Boocock and R. J. Cvetanović, "Reaction of Oxygen Atoms with Benzene," Can. J. Chem. 39, 2436 (1961)
11. G. R. H. Jones and R. J. Cvetanović, "Reaction of Oxygen Atoms with Toluene," Can. J. Chem. 39, 2444 (1961)
12. Cvetanović, R. J., Singleton, D. L., and Irwin R. S., "Gas-Phase Reactions of $O(^3P)$ Atoms with Methanethiol, Ethanethiol, Methyl Sulfide, and Dimethyl Disulfide. 2. Reaction Products and Mechanisms," J. Am. Chem. Soc. 103, 3530 (1981)
13. D. L. Singleton, R. S. Irwin, and R. J. Cvetanović, "Mechanism of the reaction of oxygen atoms, $O(^3P)$ with dimethyl disulfide," Can. J. Chem. 61, 968 (1983)
14. Cvetanović, R. J., "Electrophilic Character of Oxygen Atoms," Can. J. Chem. 38, 1678 (1960)
15. Herron, J. T., and Huie, R. E., "Rate Constants for the Reactions of Atomic Oxygen (O^3P) with Organic Compounds in the Gas Phase," J. Phys. Chem. Ref. Data 2, 467 (1973)
16. Warnatz, J., "Rate Coefficients in the C/H/O System," in 'Combustion Chemistry', Ed. W.C. Gardiner, Jr., Springer-Verlag, 1984, p. 197

Product Energy Distributions and Energy Partitioning in O Atom Reactions on Surfaces.

Bret Halpern and Moris Kori Department of Chemical Engineering, Yale University, New Haven, Connecticut 06520

Introduction

Surface reactions involving O atoms are likely to be highly exoergic, with different consequences if energy is channeled mostly to product molecules or surface modes. Thus the surface may become a source of excited species which can react elsewhere, or a sink for localized heat deposition which may disrupt the surface. The vibrational energy distribution of the product molecule contains strong clues about the flow of released energy.

Two instructive examples of energy partitioning at surfaces are the Pt catalyzed oxidations

$$C_{ads} + O_{ads} \xrightarrow{\qquad} CO^{*} \qquad T > 1000\ ^{o}K \qquad \text{I}$$

$$CO_{ads} + O_{gas} \xrightarrow[\text{(Pt oxide)}]{\qquad} CO_2^{*} \qquad T \sim 300\ ^{o}K \qquad \text{II}$$

We recorded the infrared emission spectra of the excited product molecules and from them determined vibrational population distributions. In reaction I, energy appeared to be statistically partitioned between the product CO and several Pt atoms. In reaction II, partitioning was non-statistical; the CO_2 asymmetric stretch distribution was inverted. In gas reactions these results would indicate a long lived and short lived activated complex, and similar pictures may describe these surface reactions.

The experiments and spectra have been described elsewhere (1,2), so the review given here will be abbreviated. A Pt oxide appeared essential in reaction II; we will discuss evidence for it. We will also estimate the fraction of the released energy that is deposited in the catalyst.

Experimental

All experiments were carried out in a large vacuum chamber pumped at a speed of 10,000 lit/sec. High fluxes of atomic and molecular reactants were directed at a Pt foil, and a steady state flux of vibrationally excited product desorbed into background pressures low enough to avoid vibrational deactivation. Radiation from desorbing product molecules was collected and analyzed in in a Fourier Transform Infrared Spectrometer at a resolution of .1 cm^{-1}. The foil temperature, background pressure and reactant flow rates were all under experimental control. The background pressures were adjusted to rotationally cool the emitting species while avoiding vibrational energy loss.

Oxidation of Carbon

Carbon atom targets were supplied by decomposing butane or methane on a Pt foil maintained at $T = 1000\ ^{o}K$ in a simultaneous flux of O_2. Reaction takes place between adsorbed C and adsorbed O. The relative flow of hydrocarbon and oxygen was adjusted so that the steady state coverage of carbon was low in order to avoid graphite formation. The carbon coverage was sensitively

monitored by measuring thermionic electron emission; a monolayer of C increases emission by a factor of 1000. It did not matter if the O atoms were supplied directly from the gas phase or via dissociatively chemisorbing O_2. This is a consequence of the low C atom coverage; the Langmuir - Hinshelwood mechanism is favored so that the origin of the O atom is not important.

The CO emission spectrum exhibited clearly resolved rotational lines from as high as the seventh vibrational level (1). The derived population distribution , at least for $v > 2$, looked nearly Boltzmann, but the plot of ln population versus vibrational quantum number had a downward curvature. The "temperature" for this distribution was approximately 4000 ^{o}K, whereas the surface temperature was at most 1400 ^{o}K. The population of $v = 1$ was higher than expected from the trend of other levels, and we attributed this to vibrational relaxation via conduction electron excitation prior to CO desorption.

The distribution resembled those observed for the excited CO products in a number of gas phase reactions of an O atom and an organic molecule. By analogy we regarded reaction I as proceeding through a complex of bound C, mobile O and a group of n Pt surface atoms. Reaction energy E was randomized in the C-O-Pt complex and partitioned statistically among the various modes of the CO product and the $s = 3n$ vibrations of the Pt atoms. The distribution of vibrational energy in the product CO is given by a prior distribution $P_o(v)$ (3)

$$P_o(v) \sim (1 - \epsilon/E)^{s - 1 + \alpha/2} \qquad [1]$$

where $\epsilon = v\, h\nu$, and $\alpha = 5$ is the number of degrees of translational and rotational freedom. A statistical distribution implies that the C-O-Pt complex is sufficiently long lived to assure energy randomization, but is uncoupled from the surrounding Pt surface during the reaction time.

The number of Pt atoms involved in energy partitioning was found by fitting the experimental distribution to the prior distribution for $v > 2$. The value of E is not precisely known, since it must incorporate an uncertain chemisorption energy for carbon as well as an unknown activation energy. For reasonable values of E from 3 - 5 ev the best fit to the distribution gives s between 8 and 9. Thus, 2 - 3 Pt atoms strongly share in the released energy, and the distribution of vibrational energy appears to be statistical.

Oxidation of CO

The oxidation of CO on Pt is usually carried out by supplying oxygen as O_2 from the gas phase. Modulated molecular beam experiments have established that it is a Langmuir Hinshelwood process (4), and infrared emission spectra have shown that the CO_2 product is vibrationally hotter than the Pt catalyst (5). A $\sim$ 1 ev activation energy is partitioned among the CO_2 product modes and the catalyst. Energy disposal does not favor any internal or translational mode overwhelmingly. There is no evidence for population inversion, and vibrational populations in asymmetric stretch, symmetric stretch, and bending are adequately described by temperatures between 1000 ^{o}K and 2000 ^{o}K. By supplying O atoms directly from the gas phase we make $\sim$ 4.1 ev available for partitioning. Our object was to find out if the vibrational distribution would be significantly changed, and if so, what change in mechanism was responsible.

The product of Reaction I was a highly excited CO_2^* molecule (2). There are several singular points of contrast with the conventional CO oxidation. Reaction took place at room temperature, with zero apparent activation energy. The asymmetric stretch emission spectrum was unusual, suggesting a population inversion and high energy content. The room temperature reaction did not proceed on clean Pt but only on Pt that had been heated to 1700 ^oK and cooled in atomic oxygen. The distinctive features of the excited CO_2 emission spectrum are these:

a) Despite a resolution of .1 cm^{-1} the spectrum is diffuse and shifted to lower frequency from the region about 2350 cm^{-1} where the 001 - 000 transition is located.

b) If the background pressure of O_2, CO, and O atoms is allowed to rise, a resolved spectrum of CO radiating from v = 1 appears superimposed on the diffuse spectrum. The diffuse CO_2 spectrum diminishes in intensity but does not shift.

We interpreted these observations to mean that CO_2 desorbed with an inverted vibrational distribution and high energy content. The spectrum is shifted to lower frequency, coincidentally where CO emits, because the inverted distribution gives a preferential occupation of higher levels where anharmonicity has reduced the level spacing. The spectrum is diffuse because in a highly excited triatomic the large number of contributing transitions produces an overlap of rotational lines that overwhelms the resolution.

The CO emission onset at high pressure may be explained as follows. At first sight it might be ascribed to collisions between desorbing CO_2 and incoming CO, with a near resonant exchange of vibrational energy. This is unlikely to be so. The desorbing CO_2 makes too few collisions between foil and observation zone to permit even near resonant energy transfer. If energy transfer were operative, then the CO_2 emission should have occured from lower levels, rather than merely diminishing in intensity; this was not seen. Collisional energy transfer does not explain the appearance of CO emission. Therefore the CO_2 must have been removed by reaction with one of the available collision partners that were present at sufficient concentration. These include the ground states of O, CO, and O_2, as well as singlet delta molecular oxygen. There are few reactions which may be written with those reactants that might give a CO product at high yield; the only one which is energetically plausible is

$$CO_2 + O \text{ ---------> } CO^* + O_2^* \qquad \text{III}$$

which requires a 2.6 ev activation energy. The only way for reaction III to proceed at room temperature and 10 microns pressure is for the activation energy to be carried in CO_2 vibration. (Calculations indicate that translational energy is not effective in driving reaction III.) If that is true then the vibrational energy content of desorbing CO_2 must be on the average $\sim$2.6 ev.

The participation of reaction III is the only explanation that is consistent with the observations of CO emission, CO_2 destruction, and the improbability of collisional energy transfer. As a consequence we can fix the energy content of the excited product. This is important because the diffuse nature of the emission spectrum makes it difficult to arrive at a unique

distribution of quanta among the three vibrational modes of CO_2. The constraint on the average energy, however, requires that most of the energy resides in asymmetric stretch, since that mode has the largest vibrational quantum. On that basis we derived the approximate distribution of energy in asymmetric stretch shown in Fig. 1 (2).

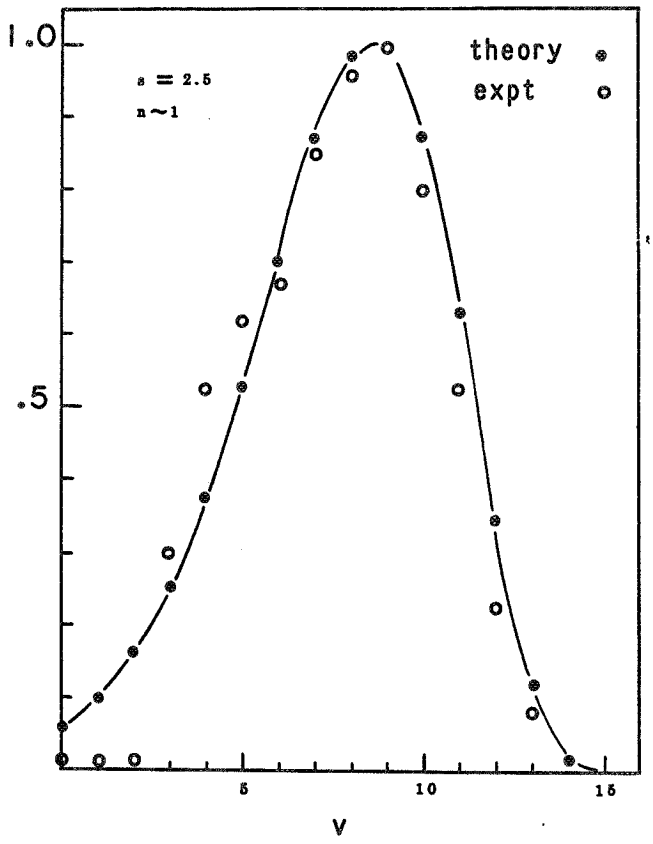

Fig.1 Asymmetric stretch population distribution of CO_2 from reaction II as a function of vibrational quantum number v. The open circles are derived from the infrared spectrum in reference (2). The closed circles are the distribution according to surprisal theory, Equ. 4, as derived in reference (8). The best fit is found for s = 2.5, so that the number of Pt atoms n = 1.

The fact that most of the released energy remains in asymmetric stretch may appear surprising given the high level of excitation. Nevertheless it appears that the asymmetric stretch mode in CO_2 is virtually uncoupled from bending and symmetric stretch, which in turn are closely coupled. This has been demonstrated for CO_2 (6,7) at high asymmetric stretch quantum numbers. It is also plausible that the reaction energy is selectively channeled into asymmetric stretch, since formation involves an adsorbed CO molecule and a nearly free O atom.

We also analyzed the derived population distribution using surprisal theory (3,8). The distribution P(v) resulting from a dynamically constrained, non-statistical partitioning of energy is related to the prior, statistical distribution $P_o(v)$ by

$$P(v) = A\, P_o(v) \exp (\lambda\, v / v_m) \qquad [2]$$

Here, v_m is the highest level that is energetically possible, A is a normalization constant, and λ characterizes the dynamical constraints that distort the prior distribution.

We evaluated $P_o(v)$ for a reaction complex composed of bound CO, a free O

atom, and a cluster of n surface atoms represented by s = 3n harmonic oscillators. The reaction product is CO_2 with most of its energy in the asymmetric stretch mode. If the product were diatomic, rather than CO_2, then the prior distribution P_o would be exactly as it was in Equ. 1. To deal with triatomic CO_2 we treat the asymmetric stretch mode as a diatomic molecule, and regard it as the "product" of reaction, since much of the energy is channeled into that mode, and since it is uncoupled from other CO_2 vibrations. The symmetric stretch and bending modes are represented by three oscillators (two for doubly degenerate bending), which, like the s oscillators of the cluster, can share in reaction energy partitioning. The prior distribution $P_o(v)$ can then be written as

$$P_o(v) = (1- v / v_m)^{s - 1 + \alpha/2 + 3} = (1 - v /v_m)^{s + 9/2} \qquad [3]$$

where again, $\alpha = 5$. The asymmetric stretch distribution P(v) then becomes

$$P(v) = A (1 - v / v_m)^{s + 9/2} \exp(\lambda v / v_m) \qquad [4]$$

For an exoergicity of 4.1 ev the highest level is $v_m = 16$, and the best fit of Equ. 4 to the experimental distribution is found for $\lambda = 15.2$ and $s = 2.5$. The theoretical and experimental distributions are shown in Fig. 1. The value of $s = 2.5$ means that $n \sim 1$, so the number of catalyst atoms involved in energy partitioning is small. In contrast to reaction I, energy partitioning in reaction II is highly non-statistical, and one expects a smaller fraction of released energy to appear in the Pt cluster.

Discussion

We comment on two aspects of reactions I and II. The first is the requirement that Pt be heated in O atoms to promote reaction of atomic O and CO at room temperature. The second is the partitioning of energy to the solid.

The formation of an oxide layer can have several effects. It provides a surface that is "saturated" with oxygen, so that O atoms can only be weakly bound. The energy E = 4.1 ev available for product vibration is then higher than in the Langmuir-Hinshelwood CO oxidation. The oxide layer separates the vibrationally excited CO_2 product and the underlying conduction electron gas; this reduces loss of vibrational energy via electron-hole pair excitation during the brief CO_2 residence time. There is some evidence from high vacuum studies that a silicon impurity within the bulk is required to bind oxygen. That may be true in our work, but our high O atom flux would in any case favor the formation of PtO_2. It is of interest to find other indications of oxide layer formation under conditions similar to those in our infrared experiments. We have done this recently in a fast flow system at 1 torr pressure by means of a novel "chopped fast flow" technique (9).

Chopped fast flow is an adaptation of molecular beam chopping to study heterogeneous kinetics by exploiting the high reactant and product fluxes available in low pressure fast flow systems. In this technique, a catalyst surface is exposed to reactant square waves in a steady carrier flow and the transient response of a surface coverage or a reaction product is monitored. In the experiment of interest, we generated a 5 Hz square wave of O atoms by using a "vibrating needle" gas source (9) to direct a small O_2 flow either

into a microwave discharge or to a line bypassing the discharge. The O and O_2 that periodically left the discharge flowed downstream to a hot Pt filament (1300 ^{o}K < T < 1800 ^{o}K). The Pt filament was thus exposed to a square wave of O atoms and O_2 at low concentration in 1 torr of an inert carrier gas. In addition, the filament was exposed to a steady flow of pentane that did not pass through the discharge. Pentane decomposes on hot Pt to give chemisorbed carbon, which is removed by the adsorbed O atoms supplied either by O or O_2. The rise and fall of carbon coverage was tracked by monitoring thermionic emission with an electrometer whose output was fed to an oscilloscope.

Suppose that the microwave discharge is not activated. If carbon is present on the filament, and the O_2 square wave turns "on", carbon will be oxidized and the emission current will drop. As soon as the O_2 turns "off", impinging pentane will quickly give rise to a monolayer of carbon, and the emission current will increase. The key point is that the desorption time of remaining chemisorbed oxygen is $\sim$ 2 microseconds at T = 1500 ^{o}K. When the oxygen is off, the Pt filament instantly has sites available for pentane adsorption and decomposition; the emission current rises immediately and reflects the prompt buildup of a carbon monolayer. This is seen in Fig. 2.

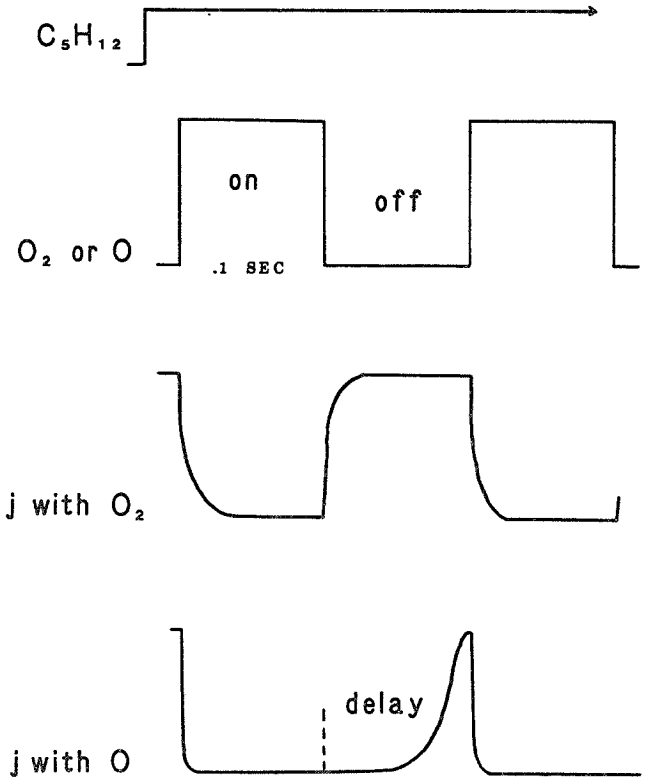

Fig.2 The top two curves are timing diagrams of the O atom 5 Hz "chopped" fast flow and steady pentane flow. The lower curves are oscilloscope traces of the response of the thermionic emission current j to carbon coverage formation and removal by O_2 or O. When O atoms are present, the buildup of carbon, and thus the response of j, is delayed until the oxide layer has decomposed.

The sequence is different when the microwave discharge is activated. Then O atoms as well as O_2 strike the filament in the "on" cycle; carbon is removed and the emission current is low. In the "off" part of the cycle, however, one observes that the onset of carbon deposition, and therefore of emission current, is delayed. If the O atom concentration is increased by increasing the microwave power, the delay becomes longer, as seen in Fig. 2. Evidently reaction of O atoms with Pt at high temperature generates an oxide layer that

decomposes or evaporates relatively slowly. This oxide layer does not catalyze the decomposition of pentane; carbon deposition is then delayed until the oxide disappears and makes available sites on bare Pt. In this way these transient experiments support the idea that reaction of Pt with O atoms at high temperature results in a layer stable at lower temperature.

The fraction of energy E_s/E appearing in the catalyst is of practical and fundamental interest. In reaction I, the CO vibrational distribution was consistent with a statistical partitioning of energy, so we estimate E_s on that basis.

If the diatomic product CO had very closely spaced vibrational levels, and the Pt cluster is treated as a collection of s loosely coupled oscillators, then the average energies E_t, E_v, E_r, and E_s of CO translation, vibration, rotation, and Pt cluster vibration would stand to each other in a ratio given by an equipartition argument as $3/2 : 1 : 1 : s$. The fractions in each mode would then be given by

$$E_t/E = (3/2)/(s + 7/2) \quad E_v/E = E_r/E = 1/(s + 7/2) \quad E_s/E = s/(s + 7/2) \qquad [5]$$

However, the CO vibrational levels are widely spaced; the average energy in vibration is given by a sum over the prior distribution:

$$E_v/E = \frac{\sum (v/v_m)(1 - v/v_m)^{s + 3/2}}{\sum (1 - v/v_m)^{s + 3/2}} \qquad [6]$$

The calculation of the remaining fractions involves integration over densities of states and summations over the CO vibrational levels. The results are

$$E_t/E = (3/2)\, R/(s + 5/2) \quad E_r/E = R/(s + 5/2) \quad E_s/E = sR/(s + 5/2) \qquad [7]$$

where R is given by

$$R = \frac{\sum (1 - v/v_m)^{s + 5/2}}{\sum (1 - v/v_m)^{s + 3/2}} \qquad [8]$$

For the values of s and v_m in the range of interest here, R is about .9. In the limit as v_m tends to infinity, the fractions in Equ. 7 become equal to those for continuous diatomic vibrational levels in Equ. 5. In fact, plots of the various fractions versus the number s of oscillators are very similar for the cases $v_m = 16$ and $v_m =$ infinity. The main difference is that E_v/E is less than E_r/E in the case of widely spaced levels, rather than equal to it

as for continuous levels. Thus the fraction of energy appearing in the catalyst for reaction I can be approximated by

$$E_s/E = s/(s + 7/2) = .72 \quad [9]$$

since s = 9 for a cluster of 3 Pt atoms. The value found from Equ. 7 is only slightly larger. Because E_s/E is so high, it is of interest to determine the probability that sufficent energy can accumulate in one oscillator to induce evaporation or diffusion. We will present the results of that calculation as well as the details leading to Equ. 7 in a future paper.

In reaction II energy disposal was non- statistical. The average energy in CO_2 asymmetric stretch was fixed at roughly 2.6 ev on chemical grounds so that the fraction of energy left for distribution to all other modes is $1 - 2.6/4.1 = .365$. This fraction is to be divided among CO_2 translation and rotation, the three oscillators corresponding to bending and symmetric stretch, and the s = 2.5 oscillators of the catalyst. If this is done statistically, then the fraction of the energy appearing in the catalyst oscillators during reaction II is given by

$$E_s/E = .365 \; s/(s + 11/2) = .11 \quad [10]$$

As expected, this is much smaller than in reaction I.

References

1) M. Kori and B. Halpern Chem. Phys. Letters 98 32 (1983)

2) M. Kori and B. Halpern Chem. Phys. Letters 110 223 (1984)

3) A. Ben-Shaul, Y. Haas, K.K. Kompa, and R.D. Levine
Lasers and Chemical Change, Springer Series in Chemical Physics vol 10
(Springer, Berlin, 1980)

4) C.T. Campbell, G. Ertl, H.Kuipers and J. Segner
J. Chem. Phys. 78 5862 (1980)

5) D.A. Mantell, S.B. Ryali, B.L. Halpern, G.L. Haller, and J.B. Fenn
Chem. Phys. Letters 81 185 (1981)

6) C. Dang, J. Reid, and B.K. Garside Appl. Phys. B 27 145 (1982)

7) D. Bailly, C. Rossetti, and D. Guelachvili
Chemical Physics 100 101 (1985)

8) M. Kori and B. Halpern Chem. Phys. Letters 129 407 (1986)

9) B. Halpern and I. al Mutaz Chem. Eng. Sci. 41 899 (1986)

Acknowledgements

The authors are thankful for the support of the National Science Foundation grant CPE-8114348, Petroleum Research Fund PRF 17006-AC5-C, and Air Force grant OSR F499620-80-C-0026.

THE ROLE OF ELECTRONIC MECHANISMS IN SURFACE EROSION AND GLOW PHENOMENA

Richard F. Haglund, Jr.

Department of Physics and Astronomy and
Center for Atomic and Molecular Physics at Surfaces
Vanderbilt University, Nashville, TN 37235

1. Introduction

Surface erosion and surface glow are textbook examples of phenomena originating in electronic transitions initiated by energetic particle-surface and photon-surface interactions. In the low-earth orbit (LEO) environment, such electronic energy-surface interactions may be triggered by ultraviolet radiation, by electrons and ions, or by low-energy collisions with neutral atomic oxygen and nitrogen. These interactions are particularly efficient in dielectrics because of their capacity to absorb, localize and rechannel electronic energy in ways which lead to the desorption of atoms, molecules, ions and even clusters. And, in the LEO environment, virtually all materials present a dielectric surface to the ambient radiation flux.

Recent research has established that the dominant constituents in electronically induced surface *erosion* are ground-state neutral atoms and molecules. The next most important decay channel for incident electronic energy is through electronic desorption of excited neutral particles which decay radiatively in flight away from the surface -- thus causing a surface *glow*. The rates for both erosion and glow processes are strongly influenced by the presence of surface impurities, as well as by the nominal composition and thermal history of the surface -- all matters of significant concern for assessing the viability of spacecraft materials.

The experimental studies of desorption induced by electronic transitions (DIET) described in this paper are producing an increasingly complete picture of the dynamical pathways through which incident electronic energy is absorbed and rechanneled to produce macroscopic erosion and glow. These mechanistic studies can determine rate constants for erosion and glow processes in model materials and provide valuable guidance in materials selection and development. However, they are not a substitute either for simulations or lifetime studies. Instead, they provide likely clues to the tailoring of materials survive the rigors of the LEO environment, and indeed, establish the scientific context within which the meaning of the simulations and lifetime studies can be accurately assessed.

2. Historical Background

The first DIET experiments, beginning with the pioneering work of Menzel and Gomer [1] and of Redhead [2] in the 1960's, centered primarily on the detection of ions desorbed from surfaces by electrons. This work on electron-stimulated desorption (ESD) established the general understanding that these processes involved electronic excitation to a repulsive potential energy surface. A decade later, Madey and Yates showed that angular distributions of the desorbing ions could provide detailed information about the surface chemical bond [3]. By the late 1970's, the advent of synchrotron light sources had paved the way for photon-stimulated desorption (PSD) experiments and aroused renewed interest in these phenomena, particularly in dielectrics. The first model of a specific electronic desorption in a dielectric came from

Knotek and Feibelman [4], who showed that the unexpectedly large yield of O^+ ions from TiO_2 could be traced to a deep core-level excitation and localized hole-pair formation, leading to a "Coulomb explosion" that ejects the O^+ ions from the near-surface layers.

However, it was clear that ESD/PSD of ions was not an efficient contributor to mass loss from irradiated materials. A new perspective on electronically-induced surface erosion was opened up in 1981, when Tolk *et al.* reported that the ESD yield of excited neutral alkali atoms from alkali halide crystals exceeded the ion yields by some five orders of magnitude [5]. Shortly thereafter, similar results were found in the photon-stimulated desorption of Li from LiF [6]. Since then, it has been established that the yield of *ground-state* neutral alkali atoms from alkali halides, in turn, exceeds the excited-state yields by another one to two orders of magnitude [7]. Efficient, electronically-driven desorption of neutral excited and ground-state atoms is now recognized as the dominant phenomenon whenever dielectric materials are irradiated by photons, electrons, metastable atoms or slow atoms or ions. However, neither the Knotek-Feibelman nor the older Menzel-Gomer-Redhead models can account for the large neutral ESD/PSD yields, so an adequate theory is still under development. At present, then, the search for mechanistic explanations of glow and erosion in the LEO environment must take its cues heuristically from DIET experiments on model materials.

2. Neutral Species Desorption Spectroscopy

A typical neutral-species desorption experiment is configured as in Figure 1. The incident radiation -- photons, electrons, or heavy particles -- desorbs ground- or excited-state atoms and molecules from the sample surface, which is maintained under ultrahigh vacuum conditions (nominally 10^{-10} torr) to allow control of surface contamination. The particles ejected from the surface radiate as free particles as they pass through the region in front of the surface. That radiation is imaged by a focusing lens system through the slit of a spectrometer and onto the

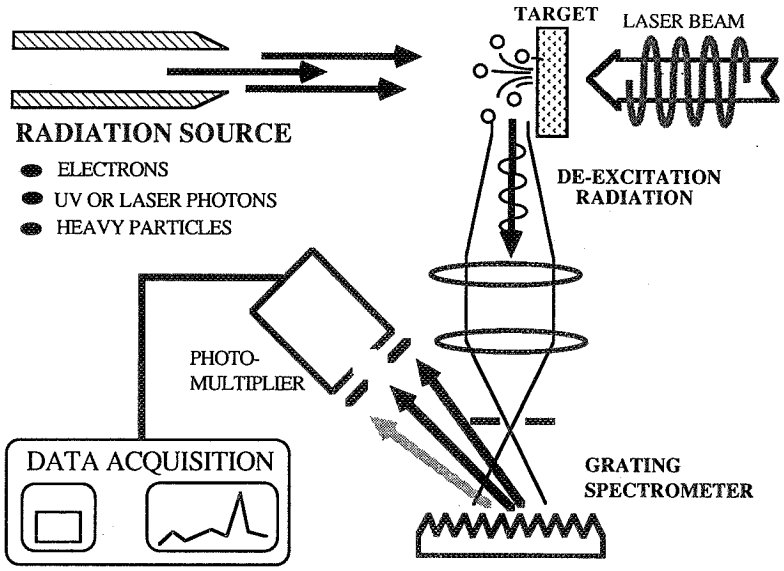

FIGURE 1

Schematic of an experiment using neutral species atomic and molecular spectroscopy to study DIET processes.

entrance port of a photomultiplier tube. Ground-state neutrals are made to fluoresce by the use of a dye laser tuned to the transition frequency of a resonant transition in the species to be identified. By scanning the spectrometer through the appropriate range of wavelengths, radiation from the desorbing species can be identified and relative yields quantified by integrating the spectral lines for each identified atom or molecule. On the other hand, if one wishes to measure velocity distributions, one scans the laser through the range of frequencies appropriate to the Doppler-shifted transition of interest; the atoms absorb at the appropriate Doppler-shifted frequency appropriate to their rest frame, and the de-excitation radiation, when plotted as a function of frequency, reflects the velocity distribution of the desorbing particles. Further details of these optical techniques have been described elsewhere [8].

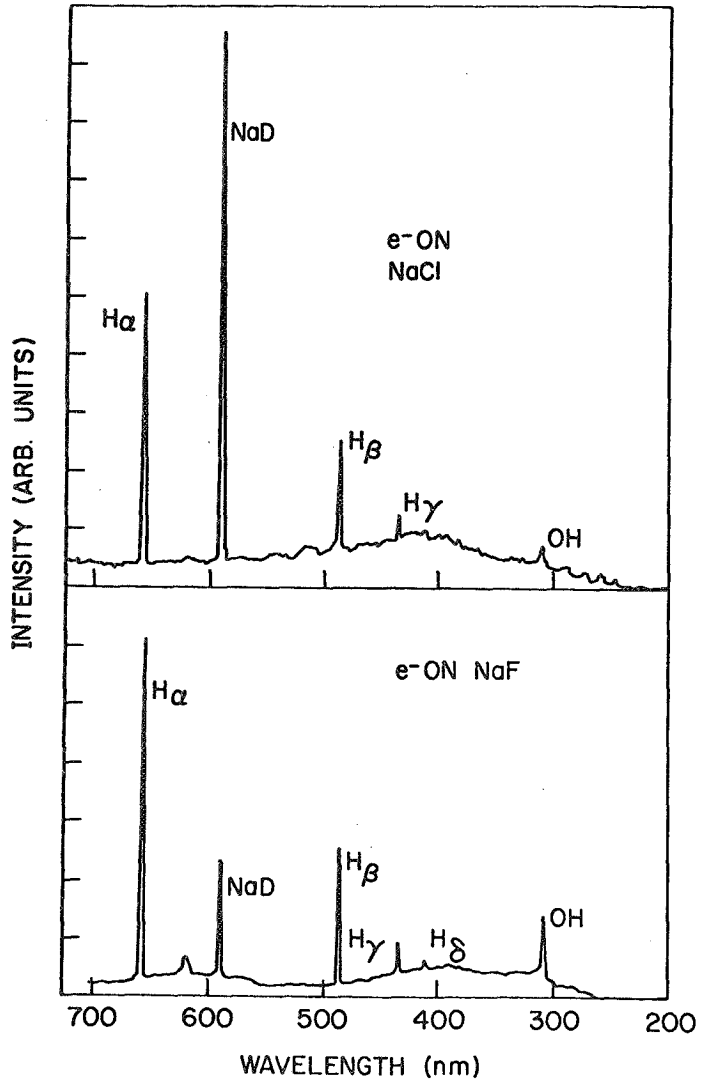

Typical results from a spectrometer scan in such an experiment are shown in Figure 2. The samples of NaF and NaCl were maintained in ultrahigh vacuum, and cleaned prior to electron irradiation by heating for several hours. However, even with this cleaning procedure, there were impurities (H, OH and some unidentified species with a vibrational spectrum reminiscent of molecular radiation) still on the surface which desorbed along with the Na atoms from the substrate.

One of the points of interest in this spectrum is that the amplitude of the Na line is larger relative to the hydrogen lines in the NaCl spectrum. This suggests that desorption of the substrate atoms is less efficient in NaF -- in other words, that the presence of hydrogen or hydrocarbons on the surface may affect the possibility of electron-induced erosion. The vibration-like bands at the right edge of each spectrum have also become objects of considerable interest, since its presence appears to be correlated with a reduction in the desorption efficiency for substrate atoms [9]. It thus appears to be associated with the existence of a protective overlayer whose structure and composition are being investigated in more detail at the present time.

FIGURE 2

Typical spectrometer scans for the experimental geometry of Figure 1 in an ESD experiment on NaF and NaCl single crystals. Note the difference between the relative yields of the desorbing H and Na° atoms for the two different substrates.

4. Photon-Stimulated Desorption Thresholds

The experimental PSD data, typified by those of Figure 3, indicate that there is a broad range of electron and photon energies over which the alkalis are desorbed with significant efficiency from alkali halides by ESD/PSD. In the Figure, the yield of neutral sodium atoms produced by photon bombardment of an NaCl single crystal surface is shown as a function of photon energy. The curve shows some structure at the levels of the 2p and 2s sodium core energy levels, but in general is rather featureless. This result is not surprising in view of the dominant role of defect diffusion in the PSD process for ground-state neutrals (see below). Similar results have been seen for a number of other alkali halides, including NaF, NaCl, NaBr and NaI [10].

However, as Townsend pointed out in his pioneering paper in ESD on alkali halides [11], if the creation of a self-trapped exciton is the first step in electronically stimulated desorption, one needs only the energy requried to create the exciton on the dihalide molecule $(X^-_2)^*$ to initiate the process (typically a few eV). However, nearly all measurements of the stimulated desorption process to date have relied on electrons or uv photons of significantly higher energies than the few electron volts mandated by this requirement. Moreover, until the development of the sensitive optical techniques necessary for tracking neutral desorption, it was not necessarily easy to look for the onset of desorption yields.

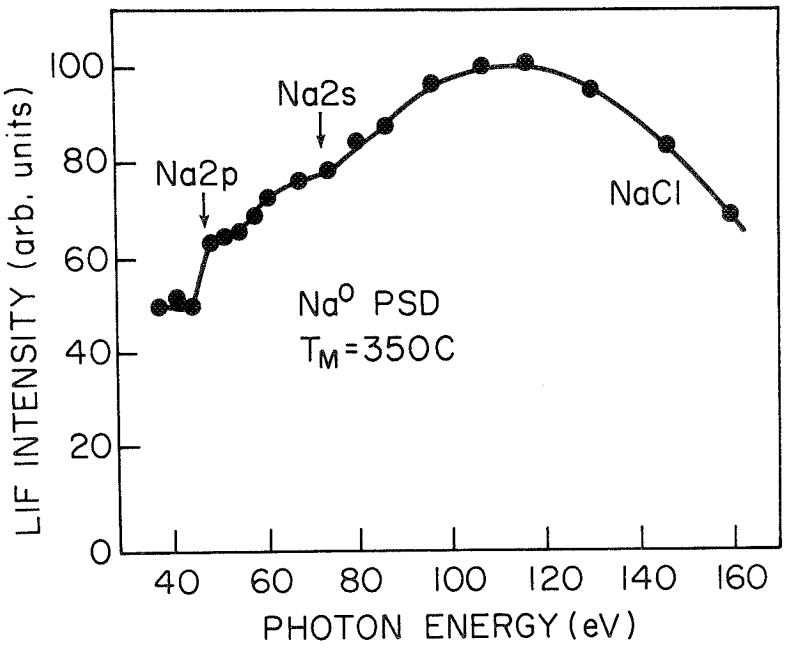

FIGURE 3

Yields of neutral Na atoms in a PSD experiment on an NaCl crystal in ultrahigh vacuum. The yield, in arbitrary units, is plotted as a function of the photon energy in eV. Overall PSD efficiency for these experiments is a few per cent for Na⁰.

Recent measurements using filters to block out different portions of the incident uv photon energy spectrum show that the threshold for PSD of Li^0 from LiF is indeed to be very low. Three spectral bins were chosen: from 0-13.2 eV (LiF filter), 20-90 eV (Al filter), and 0-200 eV, this last representing the full zeroth order spectrum transmitted through the toroidal grating monochromator (TGM) used in this set of measurements. The relative yields were calibrated by the convolution of the raw yield with a trapezoidal-rule integration of the measured response of a gold photodiode to the tuned spectrum of the TGM. After deconvolution of the monochromator efficiency from the raw data, it was found that that some twenty-five *per cent* of the total neutral yield results from photons with energies below the band gap for the LiF filter. This means that such desorption is likely to take place efficiently not only throughout

the spectral range of the primary ultraviolet photons found in LEO, but also that low-energy photons produced in secondary processes may also produce significant effects.The low value of this neutral emission threshold is consistent with results obtained by Schmid *et al.* almost a decade ago using four-photon excitation from a pulsed ruby laser [12]. However, the present results indicate that the process leading to alkali desorption is *not* intrinsically intensity dependent, as the earlier laser results might have led one to believe.

Experimental studies of the thresholds and energy dependence for electron bombardment of alkali halides indicate that the same general picture holds for ESD. For purposes on estimating rates to, say, within an order of magnitude, it is appropriate to assume that the efficiency for ESD/PSD processes producing ground-state neutral alkalis from alkali halides is on the order of a few *per cent*, while the excited-state alkalis are produced with one to two orders of magnitude less efficiency.

4. Temperature Dependence of Electron-Stimulated Desorption Processes

Measurements of desorption as a function of sample temperature can give indications of the degree to which diffusion or other thermally activated processes play a role in desorption [13]. Figure 4 shows a measurement of the fluorescence yield as a function of temperature for Li^0 and Li^* desorbed from the (100) face of a LiF crystal under electron irradiation at an energy of 750 eV. The plot shows that the desorption follows the classic Arrhenius curve, but a logarithmic plot of the data shows two slopes, with activation energies of 1.29 and 1.61 eV, respectively. This may be due to the difference between "direct" desorption of Li^0 following depletion of the halogen on the surface layer and the agglomeration of weakly bound alkali atoms, on the one hand, and for "indirect" Li^0 desorption mediated by diffusion-driven defect migration from the near-surface layers of the bulk material, on the other. At the highest temperatures for which measurements were made, the saturation of the yield curve suggests an equilibrium between the defect production and desorption rates.

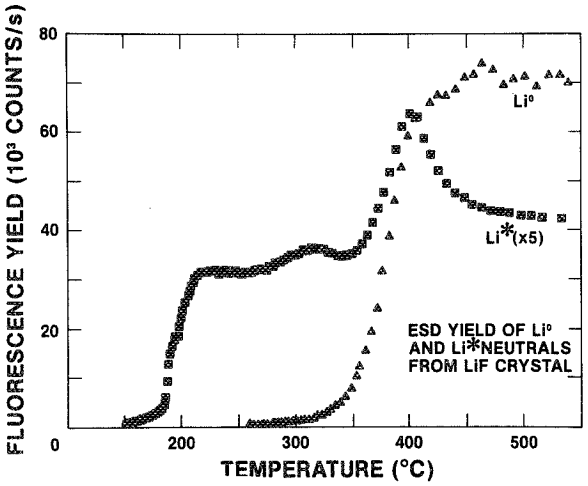

FIGURE 4

Measured yields of Li^0 (triangles) *and Li^** (squares) *desorbed by electron bombardment from the surface of an LiF crystal in ultrahigh vacuum. The electron energy was approximately 750 eV. The Li^* experiment was done in a different geometry than that for Li^0, so that the relative yields cannot be compared from the figure.*

Collateral evidence for the thermal character of ground-state neutral desorption comes from the experimental determination of velocity distributions as a function of surface temperature. Similar results have been obtained for ESD measurements on NaCl and for PSD experiments on NaF, NaCl, NaBr and NaI [11]; in both experiments, it was found that the measured surface and best-fit temperatures were coincident and completely consistent with neutral ground-state alkalis desorbing in thermal equilibrium with the surface.

While the ground-state neutral alkalis exhibit features typical of thermally-desorbed atoms, the excited-state alkalis show characteristics quite at variance with this picture. First of all, the onset in the Li excited-state yield occurs at temperatures far below those necessary to desorb ground-state neutral Li (Figure 4). Moreover, the behavior of the curve above 250° C certainly does not resemble thermal desorption (Arrhenius curve with saturation) as is the case with the Li^0. PSD measurements of Na^* from NaCl show a contrary behavior: The excited state yield *falls off* strongly with temperature in the region where the ground-state yield is increasing most steeply [14]. This behavior may be indicative of fundamental differences between electron- and photon-initiated processes, or it may reflect the short-pulse character of the excitation from the synchrotron radiation source. In any case, however, it is apparent that strongly non-thermal behavior is a general feature of DIET processes leading to the formation of *excited* neutrals.

Although the relative yields of ground-state and excited-state neutrals appear to be within an order of magnitude of each other in Figure 4, the ground-state data were obtained with the laser configured for Doppler spectroscopy, and therefore the fluorescence yields may not reflect the true density of Li^* relative to Li^0 in the focal volume of the spectrometer. This relative yield may provide important clues to the strength of the desorption mechanism.

5. Time Dependence of Electron-Stimulated Desorption

The spectroscopy of excited-state neutrals shows other features which differ sharply from the results of studies on ground-state neutral desorption. For example, measurements of excited-state fluorescence yields as a function of distance from the sample surface for ESD of Na from NaCl have generally been consistent with a kinetic energy of several eV, rather than the thermal velocities characteristic of the ground-state neutrals [9]. Also, time-resolved measurements indicates that another difference between ground-state and excited-state neutral alkali desorption is that the former result from a combination of surface and near-surface-bulk excitations -- mediated by diffusion of electronic defects from the near-surface bulk -- whereas the latter appear to be produced at the crystal surface.

Figures 5 and 6 display the results of time-resolved ESD experiments on LiF which contrast the desorption characteristics of Li^0 and Li^* for the same electron-gun and temperature parameters. In this case, the temperature of the LiF surface was maintained at 400 C, and the gun was chopped at a rate of a few kHz. The laser-induced-fluorescence (LIF) yield was measured for the ground-state Li, and then the laser was turned off to measure the yields of Li^*. In Fig. 5, the LIF yield for Li^0 is shown as a function of time for a pair of electron gun pulses. The yield climbs sharply at first, and then shows a gradual saturation as the contribution from near-surface bulk layers increases. When the electron gun is turned off, the LIF yield is observed to drop sharply at first, and then fall quite slowly until the next electron-gun pulse is turned on. In Fig. 6, on the other hand, the Li^* yield rises on the leading edge of the incident electron pulse just as Li^0, but turns off instantaneously with the trailing edge of the exciting electron beam. Indeed, a measurement of this trailing edge of the Li^* fluorescence pulse with the best time resolution possible with our multichannel analyzer (10^{-7} s) showed that the yield decreases from 0.9 to 0.1 of its maximum value within 100 ns. This means that while the *source* of Li for excited-state Li is the same as that for the ground-state Li, the excitation *mechanism* yielding Li^* must be distinctively different.

The ground-state data are well described by a diffusion model based on realistic electron-energy deposition profiles [15, 16]; preliminary indications are that such a model will be appropriate for describing ground-state PSD of alkalis from alkali halides as well. Similar

behavior is observed for PSD of Li^0 and Li^*, but in this case the time delays for emission of ground-state neutrals are on the order of *seconds* rather than milliseconds.

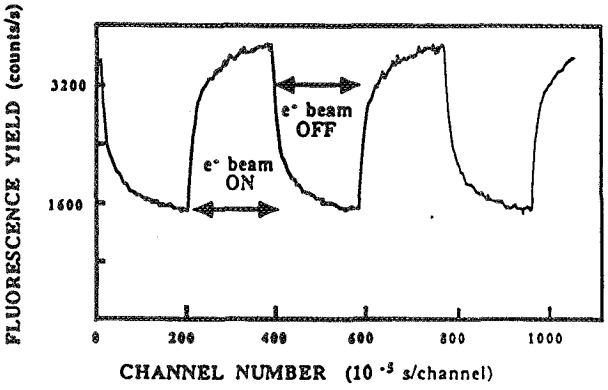

FIGURE 5

Fluorescence yield as a function of time for Li^0 desorbed by electron bombardment of the LiF (100) surface.

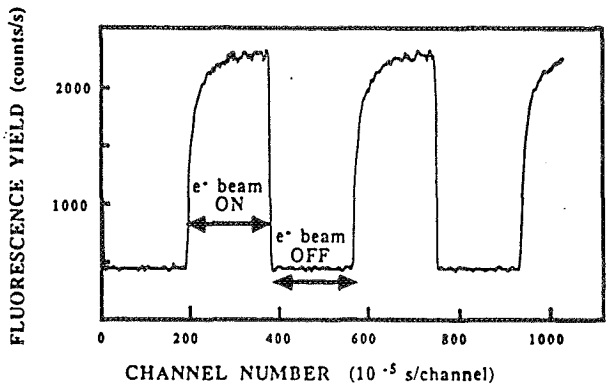

FIGURE 6

Fluorescence yield as a function of time for Li^* desorbed by electron bombardment of the LiF (100) surface.

6. A Model for Defect-Induced Desorption

Electronically stimulated desorption of ground-state neutral alkali atoms from alkali halide crystals exhibits a variety of features consistent with thermal desorption: a nearly Maxwellian distribution of velocities, a characteristic Arrhenius desorption characteristic as a function of surface temperature and a yield vs. bombarding energy characteristic which shows relatively little structure at the known locations of alkali core-hole excitation energies. Differences between ground-state ESD and PSD yields probably reflect, as much as anything, the fact that ESD tends to be a one-step process where PSD can have multi-step effects, including the production of secondary electrons which themselves are capable of effecting ESD. In addition, the time-resolved measurements indicate that diffusion plays a significant role, especially at high temperatures [15].

On the other hand, it has been shown that halogens desorbed from alkali halides under low-energy electron bombardment have suprathermal energies and are emitted preferentially along the halogen "strings" in the crystal [11]. This suggests that the formation and relaxation of H-centers is a likely mechanism for the ejection of the halogens from the surface and near-surface layers of the bulk. This picture is reminiscent of the focussed collision sequence originally proposed by Pooley [17] and Hersch [18], and involves the formation of an H-center (the so-called "crowdion," -- a pair of halogens on a single halogen site) leading to preferential and energetic ejection of halogens along the <110> directions. Simultaneously, by leaving behind an electronic defect and an electron free to bind to the now undercoordinated alkali atoms near the surface (F-center), it provides a mechanism for the generation of neutral alkalis for thermal desorption.

No such simple picture appears possible for the excited-state alkalis, however. To begin with, there is the distinctly non-thermal desorption characteristic already discussed. Also, time-resolved measurements of ESD for excited-state neutrals shows that the yield of these species drops to background level within 0.1 ms of the turn-off time of the electron gun.

Moreover, the fact that excited-state neutral yields are typically two to three orders of magnitude larger than the ion yields indicates that the mechanism must also be relatively simple compared to the Knotek-Feibelman picture involving inter-atomic Auger processes. Finally, there is the fact that only the first excited state of alkalis desorbed from alkali halides has ever been observed for low incident electron energies -- in contrast to the case of hydrogen, for example, where three or four excited states are routinely observed in ESD and PSD experiments (see Figure 2).

Thus recent experiments on ESD and PSD of *ground-state* neutral alkali desorption in the alkali halides appear to confirm early inferences pointing to the formation of self-trapped excitons followed by thermal desorption due to "halogen exhaustion" and defect migration. This sequence of events is representative of a perfectly general mechanism in which the formation of an exciton (electron-hole pair) is followed by relaxation to a mobile, permanent electronic defect whose diffusion leads to selective bond-breaking. Our fascination with the alkali halides as a particularly tractable model material should not be allowed to obscure the more important fact that this generic mechanism operates in many other materials, including many metal oxides, the alkaline earth halides, fused silica and many glasses [19].

7. Electronic Transitions and the Atomic Oxygen Problem

Now, after all these preliminaries, the question must be asked, what has all this got to do with the problem of oxygen-atom-induced erosion the low-earth-orbit environment? The relevance of electronically induced erosion and glow can be considered under at least three headings: changes in surface composition induced by electron bombarbment or UV- photon irradiation in LEO; electronic transitions experienced by the oxygen atom in gas-surface collisions; and possible synergistic or catalytic effects of oxygen, electrons and solar ultraviolet radiation.

Given the efficiency of defect-induced desorption processes, it is clear that electronic mechanisms will play a significant role in the alteration of surface composition and stoichiometric properties. Spacecraft surfaces in LEO are exposed to significant electron and UV photon flux. The fluences is of order $10^{11\text{-}12}$ electrons (photons)/cm^2/sec and the spectrum of both electrons and photons is hard enough to produce ESD and PSD in dielectric materials.

Systematic ESD/PSD experiments on hydrocarbons, polymers, composites and plastics have not been carried out, although it is known that H is desorbed efficiently by both electrons and photons from condensed hydrocarbons [20]. In the case of hydrogen-bearing materials, if there is a significant differential loss of H_2 and/or H, this could change the reactivity of O(^{3}P) with the surface, due to the well-known propensity of this atom to replace hydrogen when it is energetically favorable to do so. Such substitutional events are likely to impact mechanical integrity and alter the electrical and thermal properties of spacecraft material.

Also, in many materials -- alkaline earth halides, alkali halides and metal oxides, for example -- the ESD/PSD events trigger the accumulation of metallic overlayers on the surface which are likely to become oxidized rapidly, again with the likelihood that desirable electrical, optical or thermal properties will be altered. Composites and glasses, with their many and various electron traps, are likely to be particularly difficult to understand -- but their susceptibility as a class to electronically induced radiation damage of this type is well known.

There is at present little or no guidance from either physics or chemistry for predicting quantitatively how electronic transitions will affect the collisions of 5 eV oxygen atoms with

surfaces, although initial measurements using a 2.5 keV beam of atomic oxygen show definite differences between oxygen ions and atoms in measured desorption spectra. Gas-surface interactions with molecular beam sources of the purity requisite for mechanistic studies are generally too low in energy to allow for easy projection of low-energy mechanisms to the 8 km/s characteristic of LEO conditions. In addition, given that the heat of formation of many oxides is on the order of 5 eV, it is quite possible that there are strong threshold effects which make the extrapolation upward from molecular beam energies problematical. Most sputtering theories deal solely with metallic materials, where the collision cascade is the dominant mechanism. However, there is a wealth of evidence showing the importance of electronic mechanisms in the sputtering of insulators and semiconductors, even at relatively high energies. If electronic surface-interaction channels are open, even at low energies, it is unlikely that surface phonon excitations -- prominent though they are in meV noble-gas scattering from surfaces -- play a significant role. Indeed, the demonstrated reativity of O on many surfaces argues against significant coupling to the surface phonon spectrum.

Two phenomena which are likely to contribute to both erosion and glow through radiation-induced electronic excitations are *level-crossing*, on the one hand, and *coupling to defect and impurity states* in dielectric materials, on the other. Space allows only a brief consideration of these two situations.

Level crossings, or curve crossings, as they are also known, occur in adiabatic collisions, and allow two colliding atoms A and S to experience electronic transitions such that one partner in the collision is left in an excited electronic state. Should atom S (for "substrate") be localized in a repulsive energy state, it would be ejected from the material and radiate as a free atom (or molecule) exterior to the material surface -- thus producing erosion and/or glow. In the case of an incident oxygen atom, the electronic energy can be transferred to an ejected surface constituent atom, retained by the bombarding atom as it scatters from the surface, or be absorbed by a molecule (NO, for example) formed in the collision of the oxygen with atoms already on the surface -- depending on the particular features of the atomic-oxygen-induced chemistry.

Coupling between electronic states of an incident atom A and those of surface atoms S can occur because of overlaps between empty states of the atom and filled defect or impurity states in the surface band structure. The energetics are shown schematically in Figure 7. These defect or impurity states occupy levels in the middle of the band gap which would exist in the bulk: the defect states because of the abrupt termination of the bulk material -- in effect, creating a defect located immediately adjacent to every surface atom -- and the impurity states because they likewise cannot occupy any of the electron levels in the filled valence bands of the pure material.

Either of these two types of electronic transitions is capable of producing excited atoms whose radiative decay appears as a surface glow. Ground-state neutral atoms and molecules can also arise efficiently from the operation of either mechanism -- and such neutrals can, as in the Pooley-Hersh model, either be expelled energetically from the material or exist in an unbound configuration suceptible to thermal desorption. Thus the oxygen collisions with the surface can, through the operation of purely electronic mechanisms, give rise to surface erosion. Moreover, synergistic effects, such as those already observed in various LEO experiments, fit neatly into this picture, since the ambient ultraviolet and electron irradiation can change both surface composition and stoichiometry in ways which exacerbates the effects of the atomic oxygen.

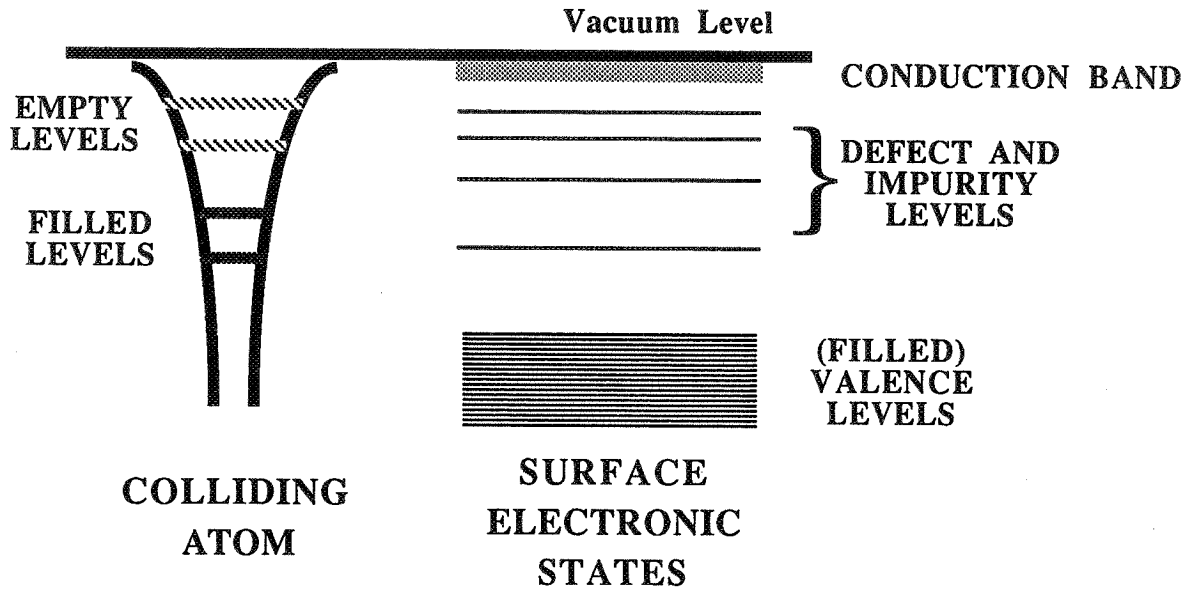

FIGURE 7

Schematic drawing of energy levels for an atom colliding with a surface.

8. Conclusions

Extensive experiments with electron, photon and heavy particle irradiation of alkali halides and other simple model materials have produced a large body of evidence showing that:

- Surface erosion, consisting primarily in the ejection or desorption of ground-state neutral atoms, occurs with large efficiencies for all irradiating species.

- Surface glow, resulting from the radiative decay of desorbed atoms, molecules and clusters in excited electronic states, likewise occurs for all irradiating species.

- The typical mechanism for ground-state neutral desorption is exciton formation, followed by relaxation to a permanent, mobile electronic defect which is the precursor to bond-breaking in the surface or near-surface bulk of the material.

- The mechanisms for excited-atom formation may include curve crossing in atomic collisions, interactions with surface defect or impurity states, or defect diffusion, and are still a subject of active investigation. The phenomena are not explainable at the present time by any physical model.

- The generic features of desorption induced by electronic transitions are characteristic of a broad class of dielectric materials, many of which are important to the construction of space platforms and satellites.

It is only to be expected that further mechanistic studies, particularly those involving the use of atomic oxygen beams at energies typical of the LEO interaction energy, will turn up further interesting examples of the influence of electronic transitions on erosion and glow phenomena.

ACKNOWLEDGEMENTS

It is a pleasure to acknowledge the contributions of my colleagues to the work summarized in this paper. They include Profs. Royal Albridge, Alan Barnes, Marcus Mendenhall and Norman Tolk, all of Vanderbilt University; Dr. Kenneth Snowdon of the University of Osnabrück, Federal Republic of Germany; Drs. Guillermo Loubriel, Thomas Green and Peter Richards of the Sandia National Laboratories; Dr. Ned Stoffel of Bell Communications Research; Dr. John Tully of AT&T Bell Laboratories; Dr. Dennis Newns of the IBM Thomas J. Watson Research Center; and Dr. Richard Rosenberg of the Synchrotron Radiation Center, University of Wisconsin-Madison.

Portions of the work on DIET processes have been supported by research contracts from the Air Force Office of Scientific Research, the Office of Naval Research, the Los Alamos National Laboratory and the Sandia National Laboratories. Vanderbilt's program in surface studies with neutral atomic oxygen beams is supported by the Martin-Marietta Corporation and the Air Force Office of Scientific Research.

REFERENCES

[1] D. Menzel and R. Gomer, J. Chem. Phys. **41** (1964) 3311.

[2] P. A. Redhead, Can. J. Phys. **42** (1964) 886.

[3] T. E. Madey and J. T. Yates, Jr., Surface Sci. **63**, 203 (1977).

[4] M. L. Knotek and P. J. Feibelman, Phys. Rev. Lett. **40** (1978) 964. See also M. L. Knotek, Phys. Today **37** (9), 24 (1984).

[5] N. H. Tolk, L. C. Feldman, J. S. Kraus, R. J. Morris, M. M. Traum and J. C. Tully, Phys. Rev. Lett. **46** (1981) 134.

[6] N. H. Tolk, M. M. Traum, J. S. Kraus, T. R. Pian, and W. E. Collins, Phys. Rev. Lett. **49** (1982) 812.

[7] N. H. Tolk, P. Bucksbaum, N. Gershenfeld, J. S. Kraus, R. J. Morris, D. E. Murnick, J. C. Tully, R. R. Daniels, G. Margaritondo and N. G. Stoffel, Nucl. Instrum. Meth. in Phys. Res. **B2**, 457 (1984).

[8] N. H. Tolk, R. F. Haglund, Jr., M. H. Mendenhall, E. Taglauer and N. G. Stoffel, in: *Desorption Induced by Electronic Transitions: DIET II*, eds. W. Brenig and D. Menzel (Springer-Verlag, Berlin, 1985), p. 152.

[9] D. Cherry, M. Mendenhall, R. Albridge, R. Cole, R. Haglund, W. Heiland, L. Hudson, W. Peatman, H. Pois, P. Savundararaj, M. Shea, J. Tellinghuisen, N. Tolk and J. Ye, Nucl. Instrum. Meth. in Phys. Research B13, 533 (1986).

[10] N. G. Stoffel, R. Riedel, E. Colavita, G. Margaritondo, R. F. Haglund,Jr., E. Taglauer and N. H. Tolk, Phys. Rev. **B32** (1985) 6805.

[11] P. D. Townsend, R. Browning, D. J. Garlant, J. C. Kelly, A. Mahjoobi, A. M. Michael and M. Saidoh, Radiat. Effects **30** (1976) 55.

[12] A. Schmid, P. Bräunlich and P. K. Rol, Phys. Rev. Lett. **35** (1975) 1382. See also N. L. Boling, P. Bräunlich, A. Schmid and P. Kelly, Appl. Phys. Lett. **27** (1975) 191.

[13] R. F. Haglund, Jr., R. G. Albridge, D. W. Cherry, R. K. Cole, M. H. Mendenhall, W. C. B. Peatman, N. H. Tolk, D. Niles, G. Margaritondo, N. G. Stoffel and E. Taglauer, Nucl. Instrum. Meth. in Phys. Research **B13**, 525 (1986). For related (but in some respects contradictory) experimental results for Na desorbed by ESD from NaCl, see M. Syzmonski *et al.*, DESORPTION INDUCED BY ELECTRONIC TRANSITIONS (DIET-II), eds. W. Brenig and D. Menzel (Heidelberg: Springer, 1985) pp. 160-168.

[14] E. Taglauer, N. Tolk, R. Riedel, E. Colavita, G. Margaritondo, N. Gershenfeld, N. Stoffel, J. A. Kelber, G. Loubriel, A. S. Bommanavar, M. Bakschi and Z. Huric, Surf. Sci. **169**, 267 (1986).

[15] G. M. Loubriel, T. A. Green, P. M. Richards, R. G. Albridge, D. W. Cherry, R. K. Cole, R. F. Haglund, Jr., L. T. Hudson, M. H. Mendenhall, D. M. Newns, P. M. Savundararaj, K. J. Snowdon, and N. H. Tolk, Phys. Rev. Lett. **57**, 1781 (1986).

[16] T. A. Green, G. M. Loubriel, P. A. Richards, N. H. Tolk and R. F. Haglund, Jr., Phys. Rev. B, to be published.

[17] D. Pooley, Proc. Phys. Soc. London **87**, 245 (1966).

[18] H. N. Hersh, Phys. Rev. **148**, 928 (1966).

[19] N. Itoh and T. Nakayama, Nucl. Instrum. Meth. in Phys. Res. **B13** (1986) 487.

[20] J. A. Kelber, R. R. Daniels, M. Turowski, G. Margaritondo, N. H. Tolk and J. S. Kraus, Phys. Rev. B **30**, 4748 (1984).

[21] R. G. Albridge, R. K. Cole, A. F. Daech, R. F. Haglund, Jr., C. L. Johnson, H. Pois, P. M. Savundararaj, N. H. Tolk and J. Ye, Nucl. Instrum. Methods in Phys. Res. B, in press.

Potential Energy Surfaces for Atomic Oxygen Reactions: Formation of Singlet and Triplet Biradicals as Primary Reaction Products with Unsaturated Organic Molecules

Richard L. Jaffe
Computational Chemistry Branch
NASA Ames Research Center
Moffett Field, Ca 94035

ABSTRACT

The experimental study of the interaction of atomic oxygen with organic polymer films under *LEO* conditions has been hampered by the inability to conduct detailed experiments *in situ*. As a result, studies of the mechanism of oxygen atom reactions have relied on laboratory O-atom sources that do not fully reproduce the orbital environment. For example, it is well established that only ground electronic state oxygen atoms are present at *LEO*, yet most ground-based oxygen sources are known to produce singlet oxygen atoms and molecules and ions in addition to $O(^3P)$. Engineers should not rely on such facilities unless it can be demonstrated either that these different oxygen species are inert or that they react in the same fashion as ground state atoms.

Ab initio quantum chemical calculations carried out at NASA Ames and elsewhere have been aimed at elucidating the biradical intermediates formed during the electrophilic addition of ground and excited-state oxygen atoms to carbon-carbon double bonds in small olefins and aromatic molecules. These biradicals are critical intermediates in any possible insertion, addition and elimination reaction mechanisms. Through these calculations, we will be able to comment on the relative importance of these pathways for $O(^3P)$ and $O(^1D)$ reactions. The reactions of oxygen atoms with ethylene and benzene will be used to illustrate the important features of the mechanisms of atomic oxygen reaction with unsaturated organic compounds and polymeric materials.

I. INTRODUCTION

The kinetics and mechanisms of the chemical reactions of oxygen atoms with organic molecules have been the subject of intensive study for more than thirty years. Most of these investigations have been carried out in the gas phase as the major impetus for this work has come from the combustion and atmospheric photochemistry research communities. Cvetanovic and Singleton(1) have recently reviewed this work for the case of O-atom olefin reactions. Companion studies have been carried out by Klein and Scherr(2) in low temperature glasses. These studies have been fraught with difficulties, as it is not an easy task to generated a clean, controlled and calibrated source of oxygen atoms. More recently, molecular beam studies of $O(^3P)$ reactions with organic species under single-collision conditions have provided a detailed look at the primary processes in these complicated reactions(3-6). A comprehensive reaction mechanism must be capable of describing these single-collision, gas phase and condensed phase experiments.

The chemistry of atomic oxygen is made especially interesting by that species' triplet ground electronic state and by the existence of a low-lying excited singlet state(7). The following general conclusions can be drawn from this large body of work(1,8,9): **$O(^3P)$ abstracts hydrogen from saturated organic molecules and adds to carbon-carbon double bonds resulting in the formation of carbonyl compounds and epoxides, while $O(^1D)$ tends to form alcohols by inserting into C-H bonds.** These initial products undergo secondary reactions which lead to fragmentation of the reactant molecules. In most cases, the branching ratios for secondary fragmentation products are **statistical**, meaning they are governed by the relative thermodynamic stabilities of the energetically permissible products (or by the relative ease of bond rupture).

Renewed interest in the kinetics and mechanisms of atomic oxygen reactions has been generated during the early flights of the space shuttle by observations that most organic polymeric materials undergo noticeable degradation during exposure to the low Earth orbit (*LEO*) environment(10,11). The most severe damage was observed on surfaces facing the direction of motion in orbit. In this orientation, both the flux and the kinetic energy of the atmospheric species striking the surface are high ($\approx 10^{15} cm^{-2} s^{-1}$ and 5-10 eV). Ground state atomic oxygen is the principal constituent of the residual atmosphere in the 150-250 km altitude range and it seems likely that this species would react readily with most organic materials. Dedicated flight experiments on shuttle flights STS-5 and STS-8 have confirmed these early observations(10), indicating that the degradation is widespread and independent of surface temperature and solar UV/VUV irradiation.

Several laboratory facilities(12) have been constructed in an attempt to simulate the *LEO* environment for kinetic and mechanistic studies and for screening materials proposed for use on the space telescope and space station projects. Unfortunately none of these facilities is capable of completely achieving the desired conditions: a beam of 5 eV $O(^3P)$ atoms of the appropriate flux and without contamination from O_2, O^+, $O(^1D)$ or other reactive species.

As one purpose of this workshop is to assess the current status of laboratory simulation of the *LEO* environment, it is appropriate to examine the differences in the reaction mechanisms of $O(^3P)$ and $O(^1D)$ with organic compounds. It should be pointed out that very little is known about O atom reactions with polymers(13) and there is no certainty that the same mechanisms apply to the reactions of small molecules and polymers. However, it is likely that the initial steps in the reaction mechanisms are the same in both cases. In the present study we consider the reactions of atomic oxygen atoms with unsaturated organic molecules from a theoretical point of view. We describe a previous computational study of the addition of oxygen to ethylene(14) and present the results of new calculations for the reaction of $O(^3P)$ + benzene. These systems are chosen because of the availability of experimental data and because they have features in common with organic polymers being considered for *LEO* applications such as *KAPTON* (a polyimide film) and structural materials such as PEEK and polysulfone. Some of the questions we will attempt to answer are: **"under *LEO* conditions will $O(^3P)$ and $O(^1D)$ react differently?", "are the kinetics affected by the 5 eV O atom energy?", and "how do the degradation rates scale with O-atom flux?".**

II. COMPUTATIONAL DETAILS

In recent years, computational chemistry groups at NASA Ames Research Center and elsewhere have been able to capitalize on the availability of supercomputers such as the Cray XMP and have been performing accurate **"first principles"** calculations of the spectroscopic, kinetic and thermodynamic properties of small molecules. These data arise from solutions of the Schrödinger equation which describes the energy and distribution (*wave function*) of a collection of electrons in the field created by the motionless nuclei of the atoms in a molecule(15). By relaxing the locations of the atoms in a series of calculations, molecular equilibrium geometries and saddle points for chemical reactions can be determined. Collisional and spectroscopic properties are obtained by subsequent calculations in which the nuclei are allowed to move, subject to the forces generated by the gradient of the electronic energies.

The calculations reported herein utilize several "standard" aspects of *ab initio* quantum chemistry codes(15). The molecular wavefunction is expanded in a basis of Gaussian functions which represent atomic orbitals and, at the Hartree-Fock or Self-Consistent Field (SCF) level of calculation, each electron experiences only the average field of the remaining electrons in the molecule. SCF calculations give only an approximate picture of the electron density distribution in a molecule. A more accurate description is obtained by allowing each electron to feel the instantaneous influence of all the other electrons. Various computational schemes have been developed to include these effects, two examples of which are the multiconfiguration self-consistent field (MCSCF) and configuration interaction (CI) methods. These effects are generally of critical importance in the study of chemical bond breaking and formation. However, experience has shown that SCF calculations are quite adequate for the determination of geometries for stable molecules

and reaction intermediates.

In the present study we have used all of the above mentioned methods. The calculations were carried out using Dunning's double-ς atomic orbital basis sets in which 9s and 5p Gaussian functions are contracted to make 4s and 2p orbitals for each carbon and oxygen atom and 5s Gaussians are contracted to 3s orbitals for each hydrogen(16). The molecular geometries were determined by minimizing the norm of the analytic gradient of the SCF energy using a computer code GRADSCF(17). At these stationary points, the analytic second derivatives of the energy were evaluated to determine whether the computed geometries correspond to local minima or to saddle points(18). At the SCF geometries, a variation of MCSCF calculation known as the Complete Active Space SCF method (CASSCF) was employed(19). In these calculations, the oxygen 2p electrons and orbitals and the benzene π electrons and orbitals were included in the "active space" and the interactions between all possible arrangements of those 10 electrons in the 9 orbitals were considered. Finally, contracted CI calculations(20) were performed using the CASSCF orbitals as reference vectors and including single and double excitations from a set of reference configurations comprised of all configurations making important contributions to the CASSCF wavefunction at any of the molecular geometries considered. For O + benzene in C_S symmetry $^3A'$, $^3A''$, $^1A'$ and $^1A''$ states are possible. The sizes of the CASSCF and CCI wavefunctions generated for each of these states are given in Table I.

III. O(^{3}P) + ETHYLENE

The reaction of ground state oxygen atoms with ethylene has been the subject of extensive experimental(1,3-6,8,21-23) and theoretical(14) study. The gas phase kinetics studies demonstrated that O(^{3}P) readily adds to the carbon-carbon double bond, resulting in the formation of a transient biradical species which undergoes triplet-singlet interconversion and rearrangement leading to epoxide and aldehyde products. However, molecular beam experiments under single-collision conditions found rapid hydrogen atom elimination follows the biradical formation almost exclusively (4-6,23). The elimination pathway is favored under these conditions because it does not require a change in electron spin. Carbon-carbon bond rupture to form fragmentation products (either formaldehyde and methylene or, after a 1,2-hydrogen shift, formyl and methyl radicals) is possible, but does not seem to occur. Similarly, the rearrangement to form triplet acetaldehyde is not observed, probably because the hydrogen shift involves surmounting a higher energy barrier than does hydrogen elimination. Figure 1 is a schematic energy diagram (taken from ref. 8) which describes these processes.

One of the important results of the theoretical study is that the singlet and triplet biradicals are nearly degenerate and intersystem crossing should occur readily under multiple collision conditions (*e. g.*, bulk gas or condensed phase). Once the system has been converted to the singlet manifold, rearrangement to form ethylene oxide or acetaldehyde can compete with the still-present elimination channel. The addition products are ex-

tremely stable compared to the biradical ($\approx$ 400 kJ/mol for acetaldehyde), but collisional stabilization is required to prevent their unimolecular fragmentation.

The reactions of $O(^1D)$ can proceed by the same biradical-addition pathway as in the triplet case, or by direct insertion into the C-H bond to form $(C_2H_3)OH$. The latter channel generally dominates the kinetics, however, because it involves much stronger attractive forces between the reactants. The resulting alcohol will undergo fragmentation unless it is collisionally stablized.

Hydrogen abstraction is also possible in the reaction of atomic oxygen with unsaturated compounds, but its occurrence is negligible at room temperature(24). However, at elevated temperatures, it is expected to become increasingly more important. It is possible that it can even compete with the insertion process in the $O(^1D)$ chemistry(9).

The abstraction and elimination pathways lead to the formation of free radical products that will certainly undergo further bimolecular reaction. The unimolecular fragmentation products will also be highly reactive. All of these fragmentation processes will tend to produce statistical product distributions, with the weakest bonds being the ones most frequently broken. The major difference between ultimate abstraction, elimination, addition and insertion products will most likely be in the amount and nature of the oxygen content. Hydrocarbons and water would be formed from abstraction, carbonyl compounds would be formed from elimination and addition, and hydroxyl compounds from insertion.

IV. $O(^3P)$ + BENZENE

The reactions of $O(^3P)$ with benzene and toluene have also been the subject of considerable study(8,25-29). The measured activation energies(8,25,26), 15-20 kJ/mol, are intermediate between the values found for addition to olefins and hydrogen abstraction. For temperatures as high as 950 K(26), no curvature was observed in the Arrhenius plots of the rate constant data and no hydrogen/deuterium isotope effect was seen. Molecular beam experiments(28,29) have clearly demonstrated that elimination products are dominant under single-collision conditions at collision energies between 10.5 and 41.0 kJ/mol. Curiously, however, for the case of $O(^3P)$ + toluene, Lee and coworkers(29) mainly find methyl elimination products (i.e., phenoxy and methyl radicals). It seems unlikely that a localized biradical adduct should form at that site, exclusively. However, the methyl-phenyl bond energy is about 38 kJ/mol less than the H-phenyl bond energy. Perhaps facile 1,2-oxygen shifts take place until the O-atom migrates around the ring to the methyl carbon, permitting cleavage of the weaker methyl-phenyl bond to occur. This 1,2-oxygen shift would involve epoxide-like intermediate structures. As the *ab initio* quantum chemical study of the ethylene-oxygen adduct(14) provided insight into the mechanism of the $O(^3P)$ + ethylene reaction, we have undertaken a similar study for O + benzene(30).

The initial calculations for the $O(^3P,^1D)$ + benzene system involved determination of the equilibrium geometries for the reactant (benzene), biradical adducts, the addition product (epoxide) and insertion product (phenol). SCF gradient calculations were performed for the closed shell benzene, epoxide and phenol molecules, for the triplet and singlet open-shell biradical adducts and for the triplet epoxide intermediate. The geometry of the lowest energy biradical ($^3A'$) is shown in figure 2. It has one radical electron in what is mainly a benzene π orbital ($16a'$) which is localized on the ortho and para carbons. The other unpaired electron ($17a'$) is localized on the O-atom and lies in the O-C-H plane perpendicular to the C-O bond. The O-C-H bond angle is 103° with the O and H atoms evenly distributed above and below the benzene ring plane. The carbon atom involved in the adduct bond is nearly tetrahedral and the C-O and C-C bonds are rather elongated. The individual CASSCF orbital densities are plotted in figure 3 for some of the triplet biradical ($^3A'$) valence orbitals. It can be readily seen that the aromaticity is lost and that one of the unpaired biradical electrons occupies a benzene π orbital while the other is localized on the oxygen atom.

The resulting energies from the SCF, CASSCF and CCI calculations are summarized in Table II. It can be seen that significant differences exist between the experimental energy estimates and the results of the large (MR)-CCI calculations. The approximation that only the benzene π electrons and the O-atom 2p electrons have been correlated is more severe for phenol with its O-H bond than for the biradical. Also a larger basis set would have to be used for more accurate calculations. As was observed for O + ethylene(14), the singlet-triplet energy splittings in the biradicals are quite small. This suggests that interconversion would occur fairly rapidly. The SCF calculations for the $^3A'$ and $^3A''$ biradicals and the $^3A''$ epoxide included determination of the harmonic vibrational force fields and normal mode frequencies. Examination of those results indicated that the structures were all true local minima(18), implying the existence of barriers to the interconversion of biradicals to epoxides or phenols. The locations and heights of these barriers have not been determined in the present study. However, the triplet epoxide is considerably higher in energy than the biradical which makes the possibility of 1,2-oxygen shifts seem unlikely.

The similarity between the energetics for O-atom reactions with ethylene and benzene (or toluene) indicate that the kinetics should also be similar. One expects elimination to dominate under single-collision conditions with addition being most important for bulk gas or condensed phase experiments. At higher energies, hydrogen abstraction would also be expected to play an increasingly more important role. The difference in products between $O(^3P)$ and $O(^1D)$ chemistry under multiple collision conditions is not readily apparent, as the primary addition and insertion products would all undergo secondary fragmentation.

V. IMPLICATIONS FOR POLYMER REACTIONS

It is tempting to extrapolate the reaction mechanisms described above to the case of

O + polymer reactions under thermal and high energy conditions. One expects the initial reaction steps to involve similar abstraction, addition, elimination or insertion processes. However, a polymer can be thought of as the ultimate condensed phase molecule and rapid stabilization and internal conversion should be possible. In general, fragmentation products should be formed based on their thermodynamic stability and the relative weakness of the bonds being broken. For the case of polystyrene, one might expect to observe a loss of hydrogen atoms (due to abstraction) and phenyl groups (due to elimination and fragmentation) from the chain backbone. The resulting alkyl radicals would probably behave similarly to the intermediate formed in the reaction of $O(^3P)$ with polyethylene.

If translationally hot oxygen atoms were present, small energy barriers would not impede reaction and the abstraction process would probably be enhanced compared to addition or elimination. This change in reaction mechanism means that rate constants cannot readily be extrapolated from the thermal to 5 eV O-atom case. Furthermore, the products for $O(^1D)$ reactions would be similar to those for ground state oxygen at higher energies (the reactions are less discriminating) even though they are quite different at lower energies. Also, it is possible that the magnitudes of the rate constants for the $O(^3P)$ and $O(^1D)$ reactions would be similar at high energies if both processes are limited mainly by the collision rate.

Two other critical factors depend on the condensed-phase nature of the polymer films. If the oxygen atoms are accomodated (*i. e., thermalized*) on the solid surface before reacting, the 5 eV translational energy will not be an important factor and the nuances of the thermal reaction mechanisms will be important. Secondly, under the high vacuum conditions encountered in both LEO and molecular beam experiments, volatilization of moderate molecular weight oligomers will occur. If the O + polymer reaction results in a downward shift in the molecular weight distribution of the polymer, enhanced vaporization will take place which will result in a significant contribution to the measured weight loss in vacuum, but not at higher pressures. These concerns, which are beyond the scope of the present theoretical study, need to be addressed if a comprehensive description of atomic oxygen-polymer reactions is to be developed.

REFERENCES

1. R. J. Cvetanovic and D. L. Singleton, Reviews of Chemical Intermediates **5**, 183 (1984).
2. M. D. Scheer and R. Klein, J. Phys. Chem. **73**, 597 (1969); R. Klein and M. D. Scheer, J. Phys Chem. **74**, 613 (1970).
3. H. E. Hunziker, H. Kneppe and H. R. Wendt, J. Photochem. **17**, 377 (1981).
4. R. J. Buss, R. J. Baseman, G. He and Y. T. Lee, J. Photochem. **17**, 389 (1981).
5. K. Kleinermanns and A. C. Luntz, J. Phys. Chem. **85**, 1966 (1981).
6. A. R. Clemo, G. L. Duncan and R. Grice, J. Chem. Soc., Farad. *2* **78**, 1231 (1982); erratum, *ibid.* **79**, 637 (1983).
7. C. E. Moore, "Atomic Energy Levels", NBS Circular 467, 1949.

8. J. T. Herron and R. E. Huie, J. Phys. Chem. Ref. Data **2**, 467 (1974).
9. see, for example: A. C. Luntz, J. Chem. Phys. **73**, 1143 (1980).
10. L. J. Leger, I. K. Spiker, J. F. Kuminecz, T. J. Ballentine and J. T. Visentine, "STS-5 LEO Effects Experiment: Background, Description and Thin Film Results", AIAA Paper 83-2631, Nov. 1983.
11. L. J. Leger, J. T. Visentine and J. F. Kuminecz, "Low Earth Orbit Atomic Oxygen Effects on Surfaces", AIAA Paper 84-0548, Jan. 1984.
12. see for example: G. S. Arnold and D. R. Peplinski, AIAA Jour. **23**, 1621 (1985).
13. R. H. Hansen, J. V. Pascale, T. De Benedictis and P. M. Rentzepis, J. Pol. Sci.: Part A **3**, 2205 (1965).
14. M. Dupuis, J. J. Wendoloski, T. Takada and W. A. Lester, Jr., J. Chem. Phys. **76**, 481 (1982).
15. H. F. Schaefer, III, ed., "Applications of Electronic Structure Theory", Vol. 3 and 4, Plenum, New York, 1977.
16. T. H. Dunning, Jr., J. Chem. Phys. **53**, 2823 (1970).
17. GRADSCF is an *ab initio* gradient program system designed and written by A. Komornicki at Polyatomics Research and supported on grants through NASA.
18. A "stationary" point is defined as a molecular geometry for which all the individual components of the gradient of the energy are zero. At such a point, the second derivatives of the energy correspond to the force constant matrix, the eigenvalues of which are related to the squares of the normal mode vibrational frequencies. If the eigenvalues are all positive, the geometry is a local or global minimum. If one of the eigenvalues is negative, the geometry corresponds to a saddle point.
19. P. E. M. Siegbahn, J. Almlöf, A. Heiberg and B. O. Roos, J. Chem. Phys. **74**, 2384 (1981).
20. P. E. M. Siegbahn, Int. J. Quantum Chem. **23**, 1869 (1983).
21. D. L. Singleton and R. J. Cvetanovic, J. Am. Chem. Soc. **98**, 6812 (1976).
22. R. A. Perry, J. Chem. Phys. **80**, 153 (1984).
23. R. Browarzik and F. Stuhl, J. Phys. Chem. **88**, 6004 (1984).
24. The abstraction reaction in ethane has an activation energy of 26.6 kJ/mol as compared to 4.7 kJ/mol for the activation energy for addition in ethylene(8), but the *A*-factor is 7.6 times larger for ethane than ethylene. At 298 K the rate constants are dominated by the exponential factor and the ethylene addition process is nearly 900 times faster than the ethane abstraction. However, at 500 K the rate constant ratio is reduced to 25.
25. G. R. H. Jones and R. J. Cvetanovic, Can. J. Chem. **39**, 2444 (1961); A. J. Colussi, D. L. Singleton, R. S. Irwin and R. J. Cvetanovic, J. Phys. Chem. **79**, 1900 (1975).
26. J. M. Nocovich, C. A. Gump and A. R. Ravishankara, J. Phys. Chem. **86**, 1684 (1982).
27. T. M. Sloane, J. Chem. Phys. **67**, 2267 (1977).
28. S. J. Sibener, R. J. Buss, P. Casavecchia, T. Hirooka and Y. T. Lee, J. Chem. Phys. **72**, 4341 (1980).
29. R. J. Baseman, R. J. Buss, P. Casavecchia and Y. T. Lee, J. Am. Chem. Soc. **106**, 4108 (1984).
30. Similar study for O + toluene is in progress: R. L. Jaffe, unpublished results.

Table I. Size of the Calculations

Symmetry[a]	CASSCF[b] $N_{config.}$	(MR)-CCI $N^{c}_{ref.}$	$N_{config.}$
$^1A'$	2688	6	368,771
$^1A''$	2604	12	792,295
$^3A'$	3756	9	1,143,225
$^3A''$	3804	13	2,225,971
$^3A''$[d]	3800	8	573,296

[a] Geometries restricted to C_S symmetry (O and two *para* C atoms lie in the symmetry plane).

[b] 9 orbitals (6 a' and 3 a'') and 10 electrons included in the active space (includes O 2p shell and benzene π orbitals).

[c] Number of reference configurations used in the CCI. For each symmetry and multiplicity this includes all CASSCF configurations with coefficients greater than 0.075 for any geometry.

[d] Epoxide calculations (symmetry plane bisects 2 C-C bonds) based on 5 a' and 4 a'' orbitals in the CASSCF active space.

Table II. Computed Energies[a] for C_6H_6 + O (^3P and ^1D)

Symmetry	SCF[b]	CASSCF[c]	(MR)-CCI	EXPT.[d]
Asymptote				
$^3A''$	0	0	0	0
$^1A''$	215.9			188.7
Biradical				
$^3A'$	151.0	41.8	9.6	(-63.)
$^3A''$		54.0	53.6	
$^1A'$	156.9	51.5	22.2	
$^1A''$		59.4	57.7	
Phenol				
$^1A'$ (S_0)	-106.3	-228.4	-280.7	-428.4
$^3A'$ (T_1)	303.3	156.1	100.8	-87.9
$^1A'$ (S_1)				14.2
$^3A''$		274.1	196.2	
$^1A''$		266.1	202.5	
Epoxide				
$^1A'$ (S_0)	138.5			
$^3A''$ (T_1)	306.7	166.1	144.3	

[a] Energies in kJ/mol.
[b] All geometries optimized.
[c] Calculations at SCF-optimized geometries ($^3A'$ for biradicals and $^1A'$ for phenols).
[d] Based on JANAF Tables and ref. 27.

Summary of previous results for C_2H_4

- **Energy map augmented by calculations of Dupuis *et al.***

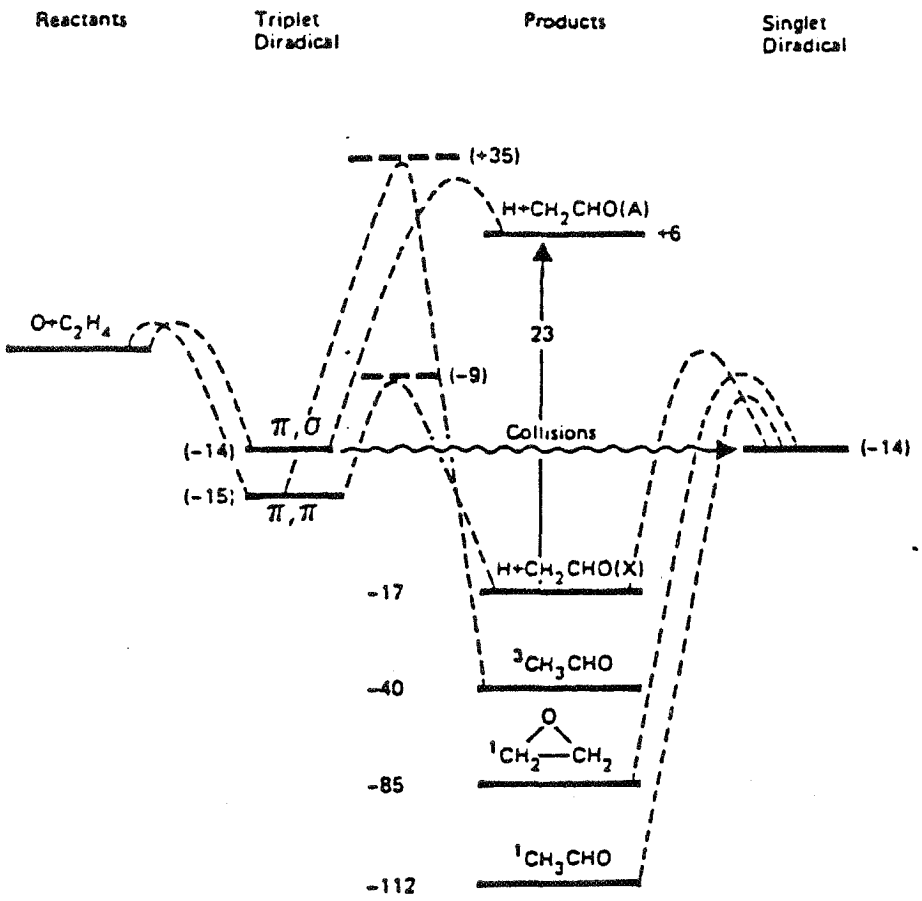

Figure 1.

Benzene-O atom biradical geometry

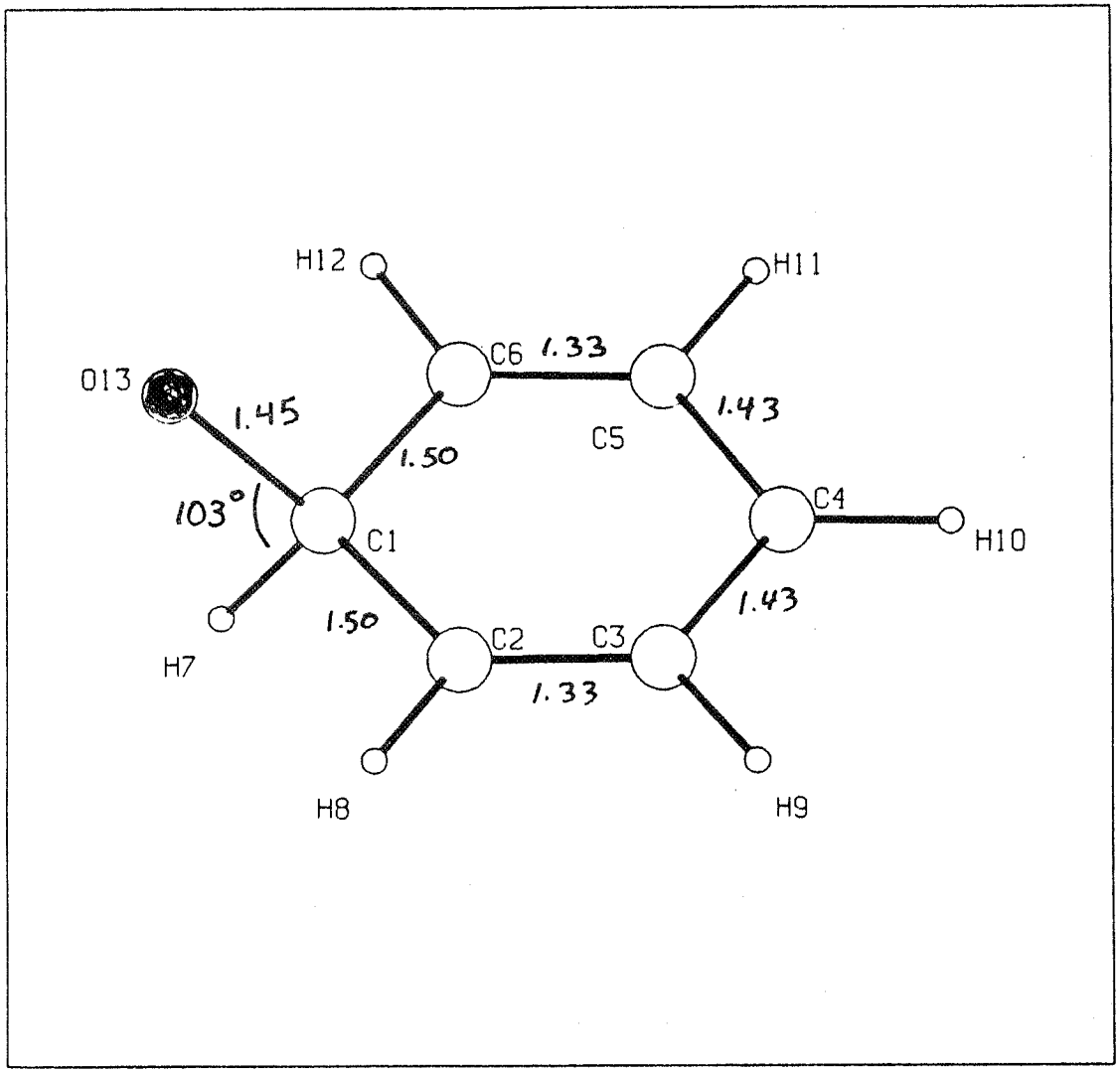

Figure 2.

Selected natural orbitals for $^3A'$ benzene-O atom biradical

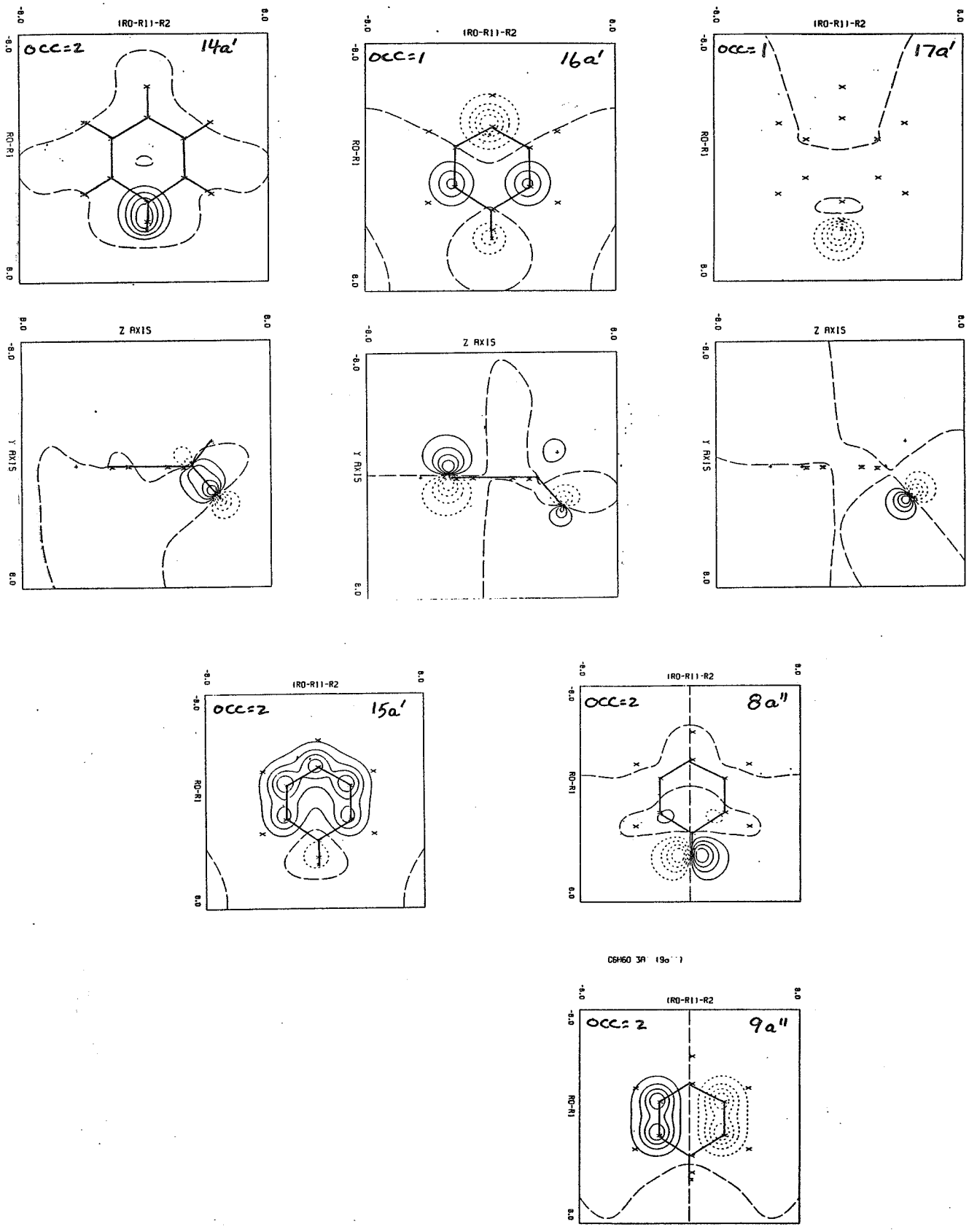

Figure 3.

Abstract

Dynamics of Atom - Surface Interactions

Steven J. Sibener
University of Chicago, Il

The intent of this presentation will be to provide an overview of the many scattering techniques that are currently being used to examine the dynamics and energetics of gas-surface energy exchange processes and gas-surface reaction mechanisms. The talk will in particular highlight recent inelastic scattering measurements which are revealing the microscopic basis for collision-induced gas-surface energy exchange, e.g., which surface vibrational modes actively participate in translational energy accommodation. Reactive scattering and laser desorption experiments which examine energy disposal in volatile products will also be discussed. Finally, if time permits, an efficient atomic oxygen beam source will be described which is suitable for terrestrial studies of gas-surface interactions.

EXPERIMENTAL REMPI STUDIES OF SMALL MOLECULES*

J. L. Dehmer, P. M. Dehmer, S. T. Pratt, M. A. O'Halloran, and F. S. Tomkins
Argonne National Laboratory, Argonne, IL 60439

Resonance Enhanced Multiphoton Ionization (REMPI) utilizes tunable dye lasers to ionize an atom or molecule by first preparing an excited state by multiphoton absorption and then ionizing that state before it can decay. This process is highly selective with respect to both the initial and resonant intermediate states of the target, and it can be extremely sensitive. In addition, the products of the REMPI process can be detected as needed by analyzing the resulting electrons, ions, fluorescence, or by additional REMPI. This points to a number of exciting opportunities for both basic and applied science. On the applied side, REMPI has great potential as an ultrasensitive, highly selective detector for trace, reactive, or transient species. On the basic side, REMPI affords an unprecedented means of exploring excited state physics and chemistry at the quantum-state-specific level. We shall give an overview together with examples of current studies of excited molecular states to illustrate the principles of and prospects for REMPI.

I. INTRODUCTION

Rapid advances in laser and detector technologies are making it possible to investigate molecular photophysics and photochemistry in powerful new ways. For example, resonantly enhanced multiphoton ionization (REMPI) measurements, in which the total (or the mass selected) ion current is monitored as a function of laser wavelength, have yielded extensive and often novel information on the spectroscopy of the resonant intermediate states (1). More recently, several groups have begun to monitor REMPI by measuring the kinetic energy distribution of ejected electrons (2,3), thus directly probing the photoionization dynamics of excited states. These and other experimental approaches, outlined below, are motivated by the prospect of investigating the spectroscopy and dynamics of excited molecular states at the quantum-state-specific level. Moreover, the resulting ability to selectively probe molecular excitation and decay has direct bearing on a variety of applied fields, e.g. ultrasensitive detection of unstable, reactive, or trace species, the characterization of the physics and chemistry of excited states that mediate the effects of ionizing radiation on matter, isotope separation, laser-modified chemistry, modeling of plasmas and the physics and chemistry of the atmosphere in normal and disturbed states.

To illustrate the potential of REMPI, we will outline several different types of experiments that can be carried out using the two-color REMPI excitation processes shown schematically in Figure 1. In Figure 1a, two photons from a "pump" laser with frequency $h\nu_1$ are used to excite an individual rotational (not shown) and vibrational level of an excited electronic state AB^*. An independently tunable "probe" laser of frequency $h\nu_2$ is

*Work supported by the U. S. Department of Energy, Office of Health and Environmental Research, under Contract W-31-109-Eng-38, and by the Office of Naval Research

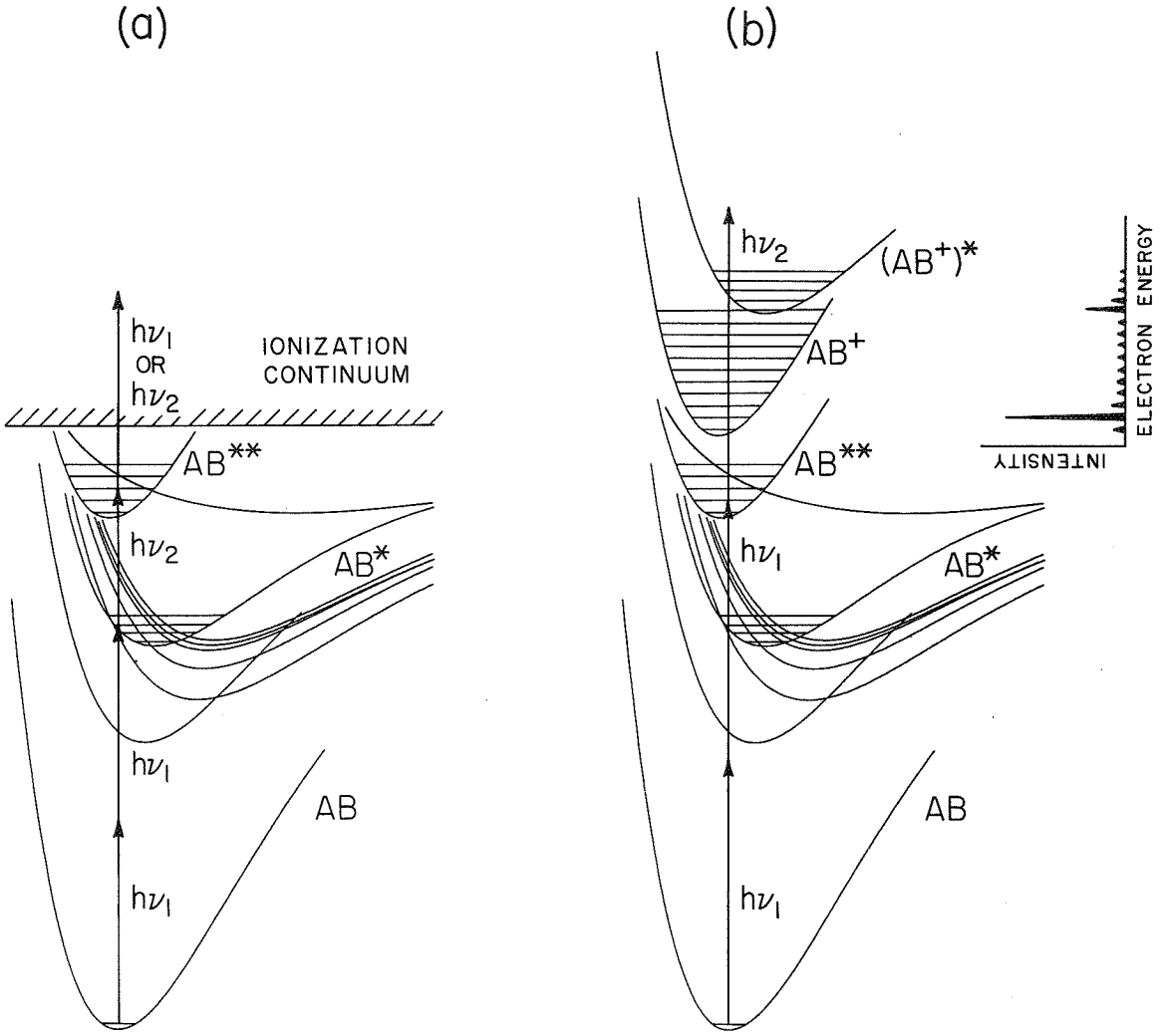

Fig. 1. Schematic potential energy diagram showing two different REMPI processes in a diatomic molecule.

used to further excite the AB^* level to the manifold of rotational-vibrational levels of a higher excited state AB^{**}. A third photon of frequency $h\nu_1$ or $h\nu_2$ is used to ionize AB^{**}. In this case, one is interested in the $AB^* \rightarrow AB^{**}$ transition rather than the ionization step, so the continuum is represented simply by a structureless hatched area. In Figure 1b, a similar process is indicated; however, in this case, the state AB^{**} is produced by two photons of the pump laser, with the probe laser accessing the ionization continuum directly. Here, one is interested in the ionization step itself, and so the accessible ionic states AB^+ and $(AB^+)^*$ are shown explicitly.

The resonant multicolor excitation schemes represented schematically in Figure 1 permit us to address many problems in molecular science which were either very difficult or unimaginable with conventional excitation sources. These include the following. (a) By varying $h\nu_2$ (in Figure 1a) and detecting the total (or mass selected) ion current as a function of wavelength, one

performs optical-optical double resonance (OODR) spectroscopy. This generates spectroscopic information on AB^{**} which typically lies in the vacuum ultraviolet (VUV) with single photon sources, but in the visible or ultraviolet with multiphoton sources. This produces high resolution spectroscopic information without the need of a large vacuum spectrograph. More importantly, the $h\nu_2$ transition originates from a single rotational level of AB^{*}, which greatly simplifies the spectrum. Use of OODR techniques also enables the direct study of states that are dipole forbidden in single photon excitation. (b) If the excited state AB^{**} is predissociated, e.g., by the repulsive curve in Figure 1, it is possible to probe in detail the mechanisms of the dissociation process by analyzing both the internal energy distribution of the photofragments and the time dependence of their formation. In addition, photodissociation often is one of the simplest and most convenient methods of producing open shell atoms, free radicals or transient species for further spectroscopic study. (c) Measurement of the photoelectron energy distribution (indicated by the inset in Figure 1b) will give the relative probabilities of producing alternative ionic states and, thus will directly reflect the photoionization dynamics of individual excited quantum states. It also will be possible to determine photoelectron branching ratios and angular distributions at various points within an autoionizing resonance, which will be an extremely sensitive probe of the interactions between the discrete state and the various ionization continua. At present, such measurements are being performed using synchrotron radiation light sources with modest wavelength resolution (~0.2-0.5 Å); however, this wavelength resolution is rarely sufficient to sample different regions within a single autoionizing resonance. (d) Since the ionization step in Figure 1b is performed with a visible or UV wavelength, simple rotation of a retardation plate will produce a photoelectron angular distribution, which accesses further dynamical information and also reflects the orientation of the excited state AB^{**}, resulting from the multiphoton excitation process. (e) Preparation of an excited state AB^{**}, followed by a delayed laser probe can monitor the time evolution of intramolecular rearrangement and/or decay processes. In molecules more complicated than that indicated in Figure 1, this procedure can monitor the time evolution of vibrational energy redistribution. In this case, picosecond lasers would be required to capture the normally very fast internal rearrangement. Use of a delayed probe beam can also be used to characterize collisional effects on a prepared state. (f) Using the high degree of selectivity, and hence, sensitivity of either excitation mechanism in Figure 1, it is possible to directly probe free radicals, clusters, ions and other transient species which are formed as minor components in complex mixtures. (g) Many possible chemical uses of the general scheme in Figure 1 can also be readily seen. For instance, by suitable selection of AB^{**} in Figure 1b, it is possible to produce AB^{+} or AB^{+*} in particular vibrational and rotational quantum states in order to study the dependence of subsequent chemical transformations on varying degrees of internal energy in different electronic or nuclear modes. Also, by using the selectivity of the excitation process, it is possible to monitor the reactants and products of elementary chemical reactions at the quantum-state-specific level.

This list of possibilities is not exhaustive, but is is ample to show the great scientific potential of REMPI. In what follows, we will present selected examples of REMPI studies in somewhat more detail.

II. PHOTOIONIZATION DYNAMICS OF EXCITED MOLECULAR STATES

A major area of investigation using REMPI-PES is the study of branching ratios following photoionization of excited molecular states. This is a virtually unexplored area, since conventional single photon PES studies have been almost completely limited to ground state ionization. Because of its importance as a theoretically tractable molecule, H_2 has received considerable attention during the past few years, and REMPI-PES studies have been reported for excitation via the B $^1\Sigma_u^+$ (4,5), B' $^1\Sigma_u^+$ (6), C $^1\Pi_u$ (7-9), D $^1\Pi_u$ (6), and E,F $^1\Sigma_g^+$ (10,11) resonant intermediate states. As an example, Figure 2 shows the REMPI-PES obtained along the laser polarization axis ($\theta = 0^o$) at the wavelengths of the resonant three-photon C $^1\Pi_u$, v' = 0-4 ← X $^1\Sigma_g^+$, v" = 0, Q(1) transitions (7); angular distributions were determined for the more intense peaks (8). The most striking aspect of the photoelectron spectra is the dominance of the photoelectron peak corresponding to the $v^+(X\ ^2\Sigma_g^+) = v'(C\ ^1\Pi_u)$ transitions. In addition, the weaker peaks with the greatest intensity are those adjacent to the $v^+ = v'$ peak. This agrees with expectations based on Franck-Condon factor calculations; however, while the qualitative agreement was found to be very good, the quantitative agreement was poor (7). For example, in the spectrum excited via C $^1\Pi_u$, v' = 4, the v^+ = 3, 5, and 6 peaks are too large by factors of 3, 2, and 23, respectively, and the intensity of the $v^+ = 4$ peak accounts for only 43% of the total, rather than the predicted 90%. The most probable reasons for this behavior are the energy and the internuclear distance dependence of the electronic transition moment or the presence of autoionizing states (including doubly excited autoionizing states) in the ionization continuum.

The detail of these and other experimental results on H_2 and other diatomic molecules such as NO (12,13) permits a direct comparison with theory, which allows an assessment of the accuracy of various theoretical models. However, a theoretical analysis of molecular REMPI processes is complicated for two reasons -- (1) the inherent nonlinearity of multiphoton absorption introduces dynamical effects such as saturation, a.c. Stark shifts, alignment of excited states, and the sensitivity of the REMPI probability to the spatial and temporal characteristics of the laser, and (2) the molecular aspects of the problem introduce complications, particularly the multicenter nature of the molecular field and the interaction among the rotational, vibrational, and electronic states. Recently, Dixit et al. (14-20) have begun a theoretical program to analyze REMPI processes in diatomic molecules. Their approach is to calculate the molecular parameters (transition moments, photoionization cross sections, and scattering phase shifts) at an ab initio level and then to carry out the REMPI dynamics. Their calculation (14) of the branching ratios and angular distributions for the (3+1) REMPI of the C $^1\Pi_u$ state of H_2 were in good agreement with the experimental results for the lower vibrational levels, although significant differences were observed for the higher vibrational levels.

Thus, the field of excited state photoionization dynamics is at an early and most interesting stage of development, the first detailed experiments and calculations having been performed very recently. The continuation and expansion of such studies promises to provide a much clearer understanding of REMPI processes.

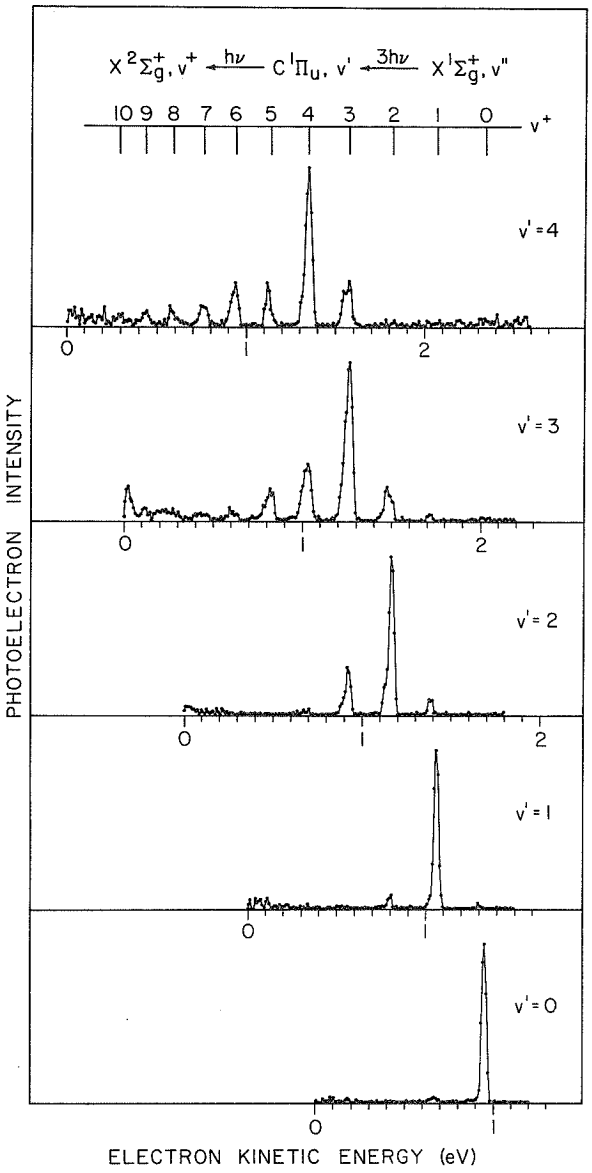

Fig. 2. REMPI-PES of H_2 determined at the wavelengths of the resonant three photon $C\,^1\Pi_u$, $v' = 0 - 4 \leftarrow X\,^1\Sigma_g^+$, $v'' = 0$, $Q(1)$ transitions. Note the dominance of the photoelectron peak corresponding to the $v^+(X\,^2\Sigma_g^+) = v'(C\,^1\Pi_g)$ ionizing transition.

III. REMPI STUDIES OF OPEN SHELL ATOMS

As mentioned in the Introduction, REMPI provides a powerful means for preparing and studying open-shell atoms, free radicals, and transient species via photodissociation. For illustration, we will briefly discuss some recent work on atomic iodine, although several other atoms (e.g., O, C, S) have already been studied and the technique is thought to be quite broadly applicable. During the past few years, considerable progress has been made in the experimental study of photoionization of halogen atoms (21-25); however, the best resolution attained to date in such experiments (~ 20 cm^{-1}) is not sufficient to resolve all of the features of interest. For example, the spectrum of atomic iodine between 1120 Å and 1090 Å contains Rydberg series converging to two ionization limits within this region as well as members of a third Rydberg series converging to a limit at higher energy. Therefore, it is extremely difficult, if not impossible, to sort out the complex structure

(21). For this reason, we investigated the possibility of using laser techniques for the study of this problem. We used two color multiphoton ionization mass spectrometry to determine the spectra of the optically allowed autoionizing states of atomic iodine. In these experiments, the first laser is used to produce atomic iodine by the photodissociation of methyl iodide and to pump the iodine atoms to a low lying $...5p^4 6p$ state via a two photon transition. A second laser is used to probe single photon transitions from these $...5p^4 6p$ states to autoionizing $...5p^4 ns$ and nd Rydberg states converging to the $^1D_2$ ionization limit. Because a total of three photons is used, this process accesses states of the same parity as those accessed by single photon excitation. However, the resolution in the present experiments is limited only by the linewidth of the laser (~ 0.05 - 0.3 cm^{-1}). Thus, it is possible to study the photoionization spectrum of atomic iodine and other open shell atoms with unprecedented detail.

The choice of the resonant intermediate state will determine the manifold of autoionizing states that may be observed. Two primary considerations are useful in deciding which resonant intermediate state should be used. First, transitions that preserve the ion core of the resonant intermediate state are, in general, stronger than those that require a change in the ion core. For example, the transitions $(^1D_2)6p \rightarrow (^1D_2)ns$, nd are expected to be stronger than the transitions $(^3P_1)6p \rightarrow (^1D_2)ns$, nd. Second, by specifying the values of K and J for the resonant intermediate state, it is possible to limit the range of values of K and J of the autoionizing Rydberg states owing to the angular momentum selection rules.

Spectra were obtained by pumping the two photon transition from the $^2P_{1/2}$ state to the $(^1D_2)6p[3]_{5/2}$ and $(^1D_2 6p[1]_{1/2}$ states and probing transitions to the $(^1D_2)ns$ and nd Rydberg series converging to the $^1D_2$ ionization limit. The former spectrum displays three sharp series that can be resolved to high principal quantum numbers (n ~ 35), while the latter spectrum displays a single sharp series and a single broad series. The symmetry of several of these series was deduced from angular momentum coupling rules. Several recent REMPI-PES studies have shown that ionization into a structureless continuum via an unperturbed Rydberg state usually proceeds by the ejection of the Rydberg electron without a change in the electronic or vibrational state of the ion core (3). Thus, in many instances REMPI can be used as a source of state-selected ions. However, the results can be quite different if the resonant intermediate level is perturbed, because the character of the unperturbed level will then be mixed with that of the perturbing level. If the two interacting levels have different ion cores, the perturbation is revealed in the photoelectron branching ratios following REMPI. In this work, REMPI-PES was used to study a perturbation in the odd parity Rydberg series of atomic iodine and to determine the feasibility of producing state-selected I^+ ions using REMPI. It was shown that, while state selected ions can be produced in some cases, the state selecting capability of REMPI is dramatically reduced for perturbed levels. For example, the photoelectron spectra obtained via the $(^3P_2)nf[3]_{5/2}$ levels show the effect of a perturbation by the $(^3P_0)4f[3]_{5/2}$ level.

As a consequence of the small ionization cross sections of the Rydberg levels in these experiments, two processes were observed that compete with REMPI. The first involves fluorescence of the resonant intermediate level to a lower lying level, which is then ionized with greater efficiency, and the

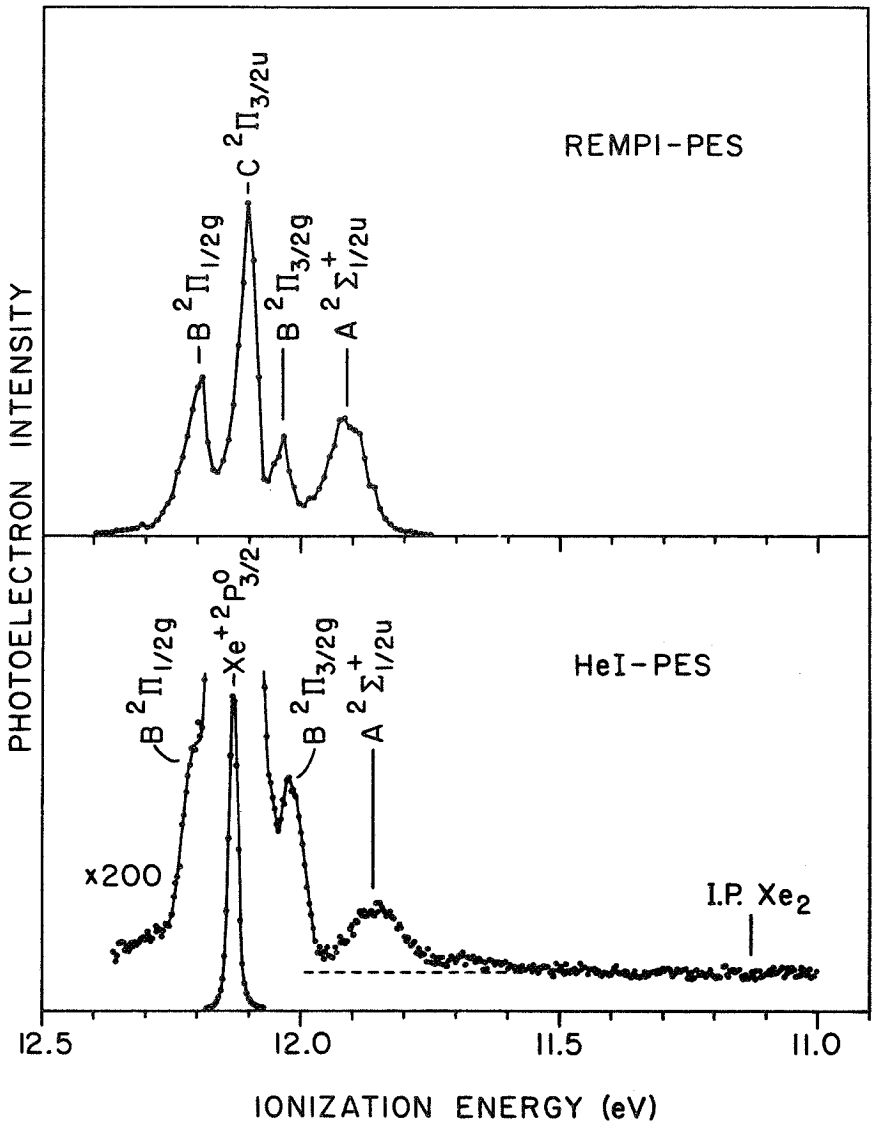

Fig. 3. HeI-PES of Xe_2 (lower trace) and REMPI-PES of Xe_2 determined at the wavelength of the resonant two photon Xe-Xe^* $5d[5/2]^o_2$, v' = 0 ← Xe_2 X $^1\Sigma^+_g$, v" = 0 transition (upper trace). The spectra are shown in the region of the Xe^+ $^2P^o_{3/2}$ atomic ionization limit. Note that atomic ionization is more than 100 times as intense as the molecular ionization in the HeI-PES, but that no atomic ionization is observed in the REMPI-PES, because the energy of the Xe_2 resonant intermediate state does not correspond to an energy level of atomic Xe.

second involves energy transfer (either collisional or radiative) between $I^*\ ^2P_{1/2}$ atoms and the Rydberg atoms. Although these two processes would be indistinguishable from direct REMPI using mass spectrometric techniques alone, the use of REMPI-PES allows the separation of the contributions of these different mechanisms and provides a more complete understanding of the overall process.

IV. REMPI STUDIES OF MINOR COMPONENTS

It is also possible to use REMPI-PES to determine the ionic energy levels of species that are present in small concentrations in the presence of a species with an interfering PES. In this case, REMPI is used to selectively ionize the species of interest, while leaving the interfering species unexcited. For example, the photoelectron spectra of the homonuclear rare gas dimers Ar_2, Kr_2, and Xe_2 were determined several years ago using conventional HeI PES (26,27). However, since the rare gas dimer is present in concentrations of only a few percent in the supersonic molecular beam, the single photon PES of the rare gas dimers were dominated by photoelectrons from photoionization of the free atom. In the case of Xe_2, the atomic photoelectron peaks were found to obscure half of expected photoelectron bands; however, the spectra obtained using REMPI-PES are completely free of these atomic photoelectron peaks. Figure 3 shows an example of a HeI-PES and a REMPI-PES of Xe_2 in the region of the $Xe^+ \ ^2P^o_{3/2}$ ionization threshold. This region of the photoelectron spectrum contains transitions to four molecular states -- the Xe_2^+ A $^2\Sigma_u^+$, B $^2\Pi_{3/2g}$, B $^2\Pi_{1/2g}$, and C $^2\Pi_{3/2u}$ ionic states. The data of Figure 3 show that in the HeI-PES only two of the molecular bands are clearly observed. In the REMPI-PES, however, all four molecular bands are seen, and there is no evidence of atomic photoelectron peaks. These data can be analyzed to determine detailed information on the potential energy curves of the ionic states.

In the above example, the minor component (Xe_2) in the sample was produced in a supersonic expansion; however, trace species or free radicals can also be produced by the pulsed laser and the REMPI-PES determined in the same laser pulse. Frequently, this is one of the best methods for producing and studying radicals or reactive species.

REFERENCES

1. See, for example, P. M. Johnson and C. E. Otis, Ann. Rev. Phys. Chem. 32, 139 (1981), and references therein.
2. K. Kimura, Adv. Chem. Phys. 60, 161 (1985), and references therein.
3. P. M. Dehmer, J. L. Dehmer, and S. T. Pratt, Comments on Atomic and Molecular Physics, in press, and references therein.
4. S. T. Pratt, P. M. Dehmer, and J. L. Dehmer, J. Chem. Phys. 78, 4315 (1983).
5. J.H.M. Bonnie, J.W.J. Verschuur, H. J. Hopman, and H. B. van Linden van den Heuvell, Chem. Phys. Lett., in press.
6. S. T. Pratt, P. M. Dehmer, and J. L. Dehmer, J. Chem. Phys., submitted.
7. S. T. Pratt, P. M. Dehmer, and J. L. Dehmer, Chem. Phys. Lett. 105, 28 (1984).
8. S. T. Pratt, P. M. Dehmer, and J. L. Dehmer, J. Chem. Phys. 85, 3379 (1986).
9. M. A. O'Halloran, J. L. Dehmer, S. T. Pratt, and P. M. Dehmer, in preparation.)
10. S. L. Anderson, G. D. Kubiak, and R. N. Zare, Chem. Phys. Lett. 105, 22 (1984).
11. C. Cornaggia, D. Normand, J. Morellec, G. Mainfray, and C. Manus, Phys. Rev. A 34, 207 (1986).
12. W. G. Wilson, K. S. Viswanathan, E. Sekreta, and J. P. Reilly, J. Phys. Chem. 88, 672 (1984).

13. S. Fredin, D. Gauyacq, M. Horani, Ch. Jungen, G. Lefebvre, and F. Masnou-Seeuws, Mol. Phys., submitted.
14. S. N. Dixit, D. L. Lynch, and V. McKoy, Phys. Rev. A 30, 3332 (1984).
15. S. N. Dixit and V. McKoy, J. Chem. Phys. 82, 3546 (1985).
16. S. N. Dixit, D. L. Lynch, V. McKoy, and W. M. Huo, Phys. Rev. A 32, 1267 (1985).
17. D. L. Lynch, S. N. Dixit, and V. McKoy, Chem. Phys. Lett. 123, 315 (1986).
18. S. N. Dixit and V. McKoy, Chem. Phys. Lett. 128, 49 (1986).
19. R. L. Dubs, S. N. Dixit, and V. McKoy, J. Chem. Phys. 85, 656 (1986).
20. H. Rudolph, D. L. Lynch, S. N. Dixit, and V. McKoy, J. Chem. Phys. 84, 6657 (1986).
21. S. Shahabi, A. F. Starace, and T. N. Chang, Phys. Rev. A 30, 1819 (1984).
22. J. Berkowitz, C. H. Batson, and G. L. Goodman, Phys. Rev. A 24, 149 (1981).
23. B. Ruscić and J. Berkowitz, Phys. Rev. Lett. 50, 675 (1983).
24. B. Ruscić, J. P. Greene, and J. Berkowitz, J. Phys. B 17, L79 (1984).
25. B. Ruscić, J. P. Greene, and J. Berkowitz, J. Phys. B 17, 1503 (1984).
26. P. M. Dehmer and J. L. Dehmer, J. Chem. Phys. 68, 3462 (1978).
27. P. M. Dehmer and J. L. Dehmer, J. Chem. Phys. 69, 125 (1978).

Session IV:

Atomic Oxygen Source Development

Laboratory Studies of Atomic Oxygen Reactions with Solids

Graham S. Arnold and Daniel R. Peplinski
The Aerospace Corporation
El Segundo, CA

Atomic beam experiments have been performed in this laboratory to investigate the rate of atomic oxygen etching of carbon and polyimide films. The main emphasis of these experiments has been on gaining an understanding of the role of atomic oxygen translational energy and substrate temperature in promoting the reactions. A description of the experimental facility and techniques[1] will be presented. Our published results[2-6] will be reviewed.

1. G.S. Arnold and D.R. Peplinski, "A Facility for Investigating Interactions of Energetic Atomic Oxygen with Solids," ATR-84(8540)-3, The Aerospace Corporation, El Segundo, CA, 16 September 1985.

2. G.S. Arnold and D.R. Peplinski, AIAA Journal, 23, 976, (1985).

3. G.S. Arnold and D.R. Peplinski, "Kinetics of Oxygen Interaction with Materials," AIAA Paper #85-0472, AIAA 23rd Aerospace Sciences Meeting, Reno, NV, Jan. 1985.

4. G.S. Arnold and D.R. Peplinski, AIAA Journal, 23, 1621, (1985).

5. G.S. Arnold and D.R. Peplinski, "Translational Energy Dependence of the O+Polyimide Reaction," AIAA Paper #85-7016-CP, AIAA Shuttle Environment and Operations II Conference, Houston, TX, November, 1985.

6. G.S. Arnold and D.R. Peplinski, AIAA Journal, 24, 673, (1986).

HIGH INTENSITY 5 eV ATOMIC OXYGEN SOURCE and LOW EARTH ORBIT SIMULATION FACILITY

J. B. Cross, L. H. Spangler, M. A. Hoffbauer, and F. A. Archuleta
Los Alamos National Laboratory
Chemical and Laser Sciences Division
Los Alamos, NM 87545

Lubert Leger and James Visentine
Lyndon B. Johnson Space Center
Houston, TX 77058

ABSTRACT

An atomic oxygen exposure facility has been developed for studies of material degradation. The goal of these studies is to provide design criteria and information for the manufacture of long life (20 to 30 years) construction materials for use in low earth orbit. The studies that are being undertaken using the facility will provide (1) absolute reaction cross sections for use in engineering design problems, (2) formulations of reaction mechanisms for use in selection of suitable existing materials and design of new more resistant ones, and (3) calibration of flight hardware (mass spectrometers, etc.) in order to directly relate experiments performed in low earth orbit to ground based investigations.

The facility consists of (1) a cw laser sustained discharge source of O-atoms having a variable energy upto 5 eV and an intensity of between 10^{15} - 10^{17} O-atoms s^{-1} cm^{-2}, (2) an atomic beam formation and diagnostics system consisting of various stages of differential pumping, a mass spectrometer detector and a time-of-flight analyzer, (3) a spinning rotor viscometer for absolute O-atom flux measurements, and (4) provision for using the system for calibration of actual flight instruments. Surface analysis equipment (Auger, LEED, XPS, etc.) is available for the characterization of material surfaces before and after exposure to O-atoms.

INTRODUCTION

The reactivities of spacecraft surfaces with the LEO environment which are used to predict surface recession for Space Station materials have been derived by exposing these materials during Shuttle flights of limited duration and low atomic oxygen fluence. These in-flight investigations are important, but the Shuttle is limited in its usefulness in evaluating coating life. For example, even during conditions of maximum solar activity, a 7-day mission at an altitude of 222 km would result in an atomic oxygen fluence of only 1.3×10^{21} atom/cm^2, assuming maximum (normal incidence) exposure. Yet fluences for long-duration missions, such as Space Station, will be in the range of 10^{22} - 10^{23} atom/cm^2. Therefore, ground based studies must be conducted to determine the validity of extrapolation to high fluence conditions using reactivities derived from low

fluence exposures. The facility described here will be used to study: material interaction rates as a function of time, the interaction mechanisms leading to surface recession, the full life (10^{22}-10^{23} atom/cm^2) effects of atomic oxygen on exposed surfaces and protective coatings, and scattering angular distributions and O-atom energy loss both of which will be important parameters in computer modeling of Space Station interaction with the LEO environment. The facility is designed to produce a beam of neutral atomic oxygen at energy levels typical of orbital conditions (5 eV). In addition, it is designed to be capable of producing fluxes in the range of 10^{16}-10^{17} atom/s-cm^2, in order to study reactivities at typical Space Station fluences within reasonable periods of time. Assuming an incident flux as high as 5 x 10^{16} atom/s-cm^2, materials must be exposed for approximately 50 hours to obtain fluence levels typical of Space Station solar inertial surfaces.

The simulation of the LEO environment has focused on the development of intense sources of O-atoms in the energy range of 2 to 10 eV. The limitations of many of these sources can be traced to reactions of the species with the production apparatus and the characteristics of the production methods. For example the source developed by Knuth[1] has been used for the production of atomic oxygen[2] but due to reactions with the electrodes, the oxygen is admitted downstream of the discharge region resulting in a maximum kinetic energy of about 1 eV and an intensity of 3 x 10^{17} s^{-1} sr^{-1}. Radio frequency discharges[3,4] have been used to produce oxygen atoms with kinetic energies of 0.1 to 1.0 eV and intensities of 10^{17-18} s^{-1} sr^{-1}. The production of high mass kinetic energy species is accomplished by seeding and heating in helium[5] expansions but low mass species (<20 amu) are limited to roughly 1 to 2 eV in kinetic energy using this technique. Charge exchange methods excel at energies >100 eV but suffer from space charge limitations[6] below 10 eV producing beam intensities orders-of-magnitude less than the previously mentioned techniques. Due to the low duty cycle of pulsed beams, techniques using pulsed laser breakdown require peak intensities of 10^3 to 10^4 that of cw beams in order to effectively equal cw time averaged intensities. These very high peak intensities can produce gas phase multiple collisions effects in gas-surface experiments which are not occurring at space station altitudes.

LASER SUSTAINED PLASMAS

In the early 1970's, it was hypothesized[7,8] and then demonstrated that a free-standing continuous discharge could be produced by focusing the output of a sufficiently powerful cw-CO_2 laser in inert[9] and molecular[10] gases at one atmosphere or above. The discharge resides near the focus of the laser and operates above the plasma frequency at 30 THz where the electric fields interact with individual electrons and ions to heat the plasma via free-free transitions (inverse Bremsstrahlung).[11] The laser power maintenance threshold depends upon the type of gas, the total pressure, whether the laser beam is horizontal or vertical (convection sweeps the hot gas out of the laser focal volume), the focusability or coherence of the laser beam, and the optical quality of the lens system. For example our work uses a 1-in. focal length ZnSe miniscus AR coated lens operated in the horizontal position with a transverse flow 1.5 kW CO_2 laser. The gases xenon, argon, and neon require 50, 300, and 1300 W, respectively for maintenance of the discharge. Because the focused power of the cw laser is in the range 10^6 to 10^7 W cm^{-2}, several orders of magnitude smaller than typical

breakdown thresholds, a high energy external spark is needed to initiate the discharge. This can be provided by a conventional spark[12] or as in this work a pulsed CO_2 laser. The primary advantages of the laser sustained discharge in creating energetic atomic beams are the high temperatures produced by the high power densities (10^4 W-cm^{-3}), the ability to sustain the discharge independent of nozzle material, and low total input power. Preliminary results using xenon have been reported in ref. 12.

SOURCE CONSTRUCTION AND OPERATION

A cross-sectional view of the source is shown in figure 1 and consists of two portions, the lens holder and nozzle holder. The 1-in.-diam ZnSe AR coated miniscus lens is clamped to the end of a water-cooled copper tube. Indium gaskets are used to cushion and seal the lens as well as to provide maximum heat transfer to the copper. A threaded copper clamping ring is tightened onto the lens while heating the lens, holder, and indium to 50 to 70°C. This procedure provides excellent sealing of the lens onto the indium. The nozzle holder is made entirely of copper with all joints being welded rather than brazed. The nozzle body is made from a 3.2-mm platinum rod 3.2-mm long drilled to within 0.76 mm of one end to a diameter of 2.39 mm. The nozzle body is brazed into the end of the nozzle holder and the 0.2-mm- diam nozzle is then electron discharged machined through the 0.76-mm wall. A 3-mm-thick copper wall separates the platinum nozzle from the water cooling jacket. A double viton O-ring is used to seal the lens and nozzle holders and to locate the lens concentric with the nozzle.

Figure 2 shows the source mounted in the molecular beam scattering apparatus and aligned with both the plasma sustaining cw (maximum power 1.8 kW) and plasma initiating pulsed (0.5 J) CO_2 lasers. The output of the cw laser traverses the length of a 3.2-m laser table and is reflected back and turned 45° to enter the source assembly. Both copper turning mirrors (M1 and M2) are water cooled. The pulsed laser beam is placed nearly coaxial to the cw beam using the set of copper coated glass mirrors (M3, M4, and M5). Initial alignment of the

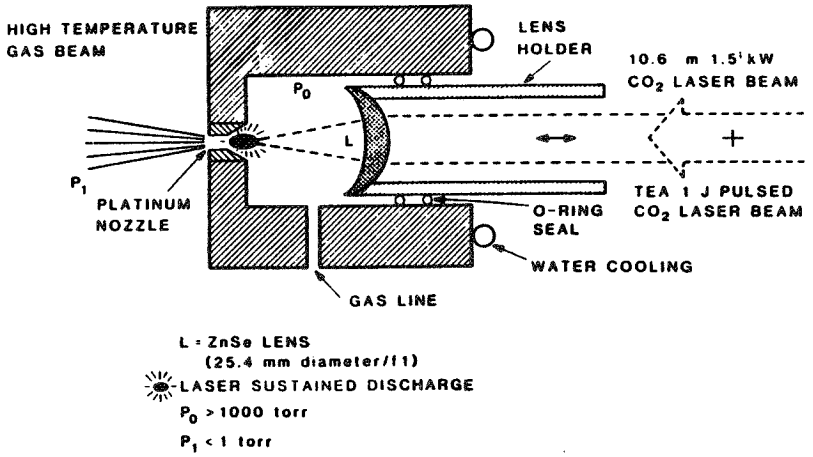

Fig. 1. Laser sustained discharge atomic beam source: discharge is initiated using a pulsed (0.5 J) TEA CO_2 laser and sustained with a 1.5-kW CO_2 laser.

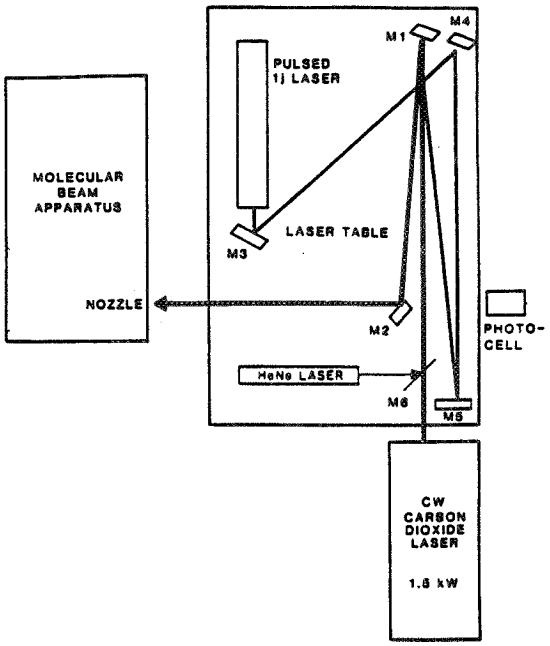

Fig. 2. Alignment of pulsed and cw CO_2 lasers with nozzle. The 5-cm-diam water cooled mirrors M1 and M2 are used to align both the pulsed and cw lasers with the nozzle. Mirrors M3, M4, and M5 are used to align the pulsed laser with the cw laser. Mirror M6 employs a kinematic magnetic mount to place the HeNe laser beam coaxial to the cw laser beam. When operating the cw laser the mirror M6 is removed. The photocell detects the plasma light emitted from the nozzle assembly and interrupts the cw laser operation if the plasma is extinguished.

cw, pulsed, and HeNe laser beams is accomplished by burning a pinhole in a 0.1-mm-thick nickel foil using the cw laser and then adjusting the pulsed laser turning mirrors to place it through the same hole. The cw CO_2 laser is then turned off, the mirror M6 placed in the path of the cw beam, and the HeNe laser is aligned to pass through the pinhole.

Final alignment of the cw laser beam with the nozzle is accomplished through operation of the source with argon and optimizing the time-of-flight distributions for maximum velocity by moving the discharge radially using the final turning mirrors M1 and M2 and axially by movement of the ZnSe lens. After initiating and aligning the discharge using argon, other gases are mixed with the argon to obtain radical species with velocities <5 km/s. If velocities greater than 5 km/s are desired, the argon is replaced with neon yielding velocities <10 km/s.

BEAM CHARACTERIZATION

Beam characteristics are depicted in the TOF distributions of figures 3, 4, and 5. The time-of-flight (TOF) analyzer used for these studies consisted of a 12.5-cm-diam disk rotated at 310 Hz with 8 equally spaced 1-mm slots located on its circumference. The TOF analyzer is calibrated using low pressure (200 torr) room temperature expansions of neon, argon, and krypton gases. The ion energy

in the quadrupole mass spectrometer detector[12] was found to be 10 eV (25-cm path length) and the neutral flight path length was 19.5 cm. The entrance to the detector was a round 0.152-mm-diam hole. Slots (0.2-mm wide) below each 1-mm slot are used to obtain timing signals from a light bulb and photocell detector. This timing signal was used to control a 256 channel multichannel scaler having a 2-μs dwell time/channel which was used to record the time-of-flight (TOF) spectra. The TOF spectra shown have not been corrected for ion flight times, timing mark offset (12 μs), or instrumental broadening. The reported velocities were obtained by correcting for ion flight times and timing mark offsets but not instrumental broadening.

The calculation of molecular dissociation follows that of Lee,[3]

$$R = N_O/N_{O_2} \tag{1}$$

$$= (x_D/x_{O_2})/\eta \; (x_{O_2}/x_O)(I_O - \eta \, I_{O_2})/I_{O_2}$$

$$\% \text{ dissociation} = R/(R+2) \tag{2}$$

where I_O and I_{O_2} are the experimentally observed number density signals at mass 16 and 32 with the discharge on, η is the ratio of number densities of mass 16 and 32 with the discharge off, x_D is the dissociative ionization cross section of O_2 to form O^+, $x_D = 0.88$ A^2, and x_i are the ionization cross sections which we have taken to be,

$$x_{O_2} = 1.52 \text{ Å}, \text{ and } x_O = 1.15 \text{ } A^2 \quad .$$

Figure 3 shows argon TOF distributions with the discharge off and on. The velocities with the discharge on were calculated to be 4.2 km/s for argon and 6.9 km/s for neon with the discharge slightly backed away from the nozzle. Our

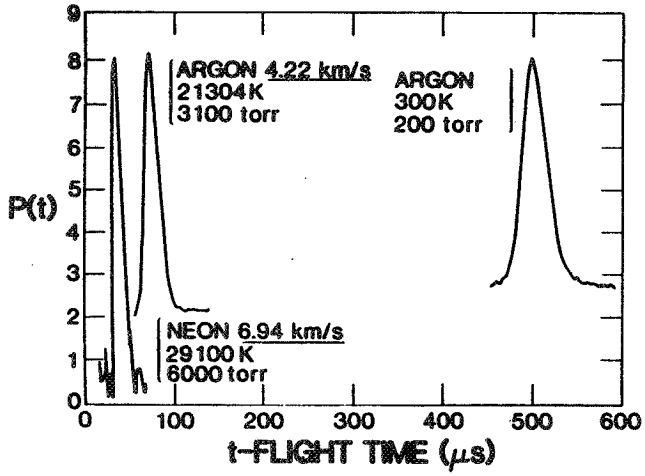

Fig. 3. Argon and neon time-of-flight distributions. Flight times have not been corrected for timing mark offset or detector ion flight times.

previous work[12] with xenon predicted that the argon and neon velocities would be 3.6 km/s and 6 km/s, respectively, indicating that a crude estimate of other gas velocities (V_m) can be obtained using the formula[12]

$$V_m = V_{Ar}(40/m)^{1/2} (T_m/T_{Ar})^{1/2} \quad (3)$$

where m is the mass of the carrier gas, the subscript Ar refers to argon, and T_m is the plasma spectroscopic temperature of the carrier gas.[10]

Figures 4 and 5 show TOF spectra for mass 16 and 32 with oxygen mixtures of 40% and 49%, respectively. Essentially 100% dissociation of O_2 into O-atoms was observed with the 40% oxygen argon mixture while a 49% mixture produces 98% dissociation indicating that increasing amounts of oxygen may produce recombination within the nozzle.

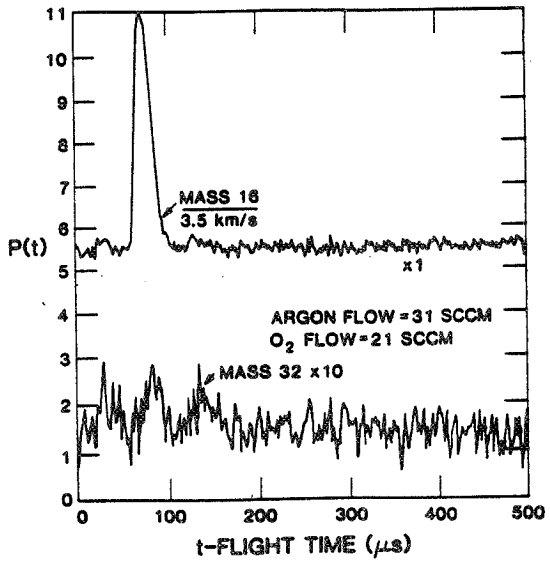

Fig. 4. TOF Distribution of mass 16 and 32 using 40% O_2, 60% argon mixture.

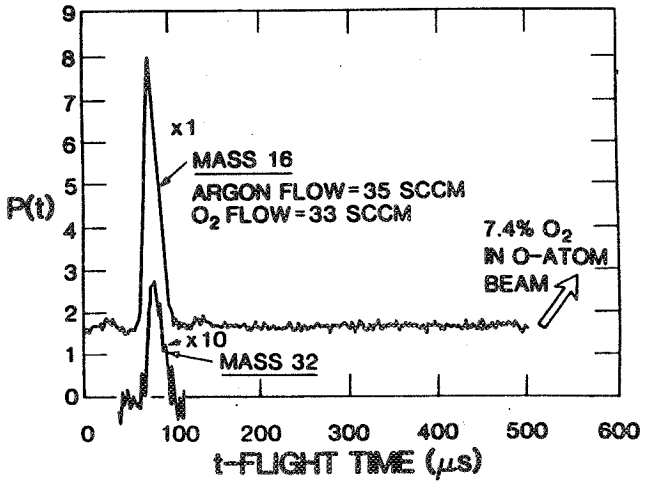

Fig. 5. TOF distribution of mass 16 and 32 using 49% O_2, 51% argon mixture.

The extent of dissociation is highly dependent upon the placement of the discharge within the nozzle; small changes in the radial or axial position can easily produce ratios of O-atoms to O_2 of 50%. Figure 6 shows the effect that a 0.5-mm axial change in the discharge placement in the nozzle has on the gas velocity distribution. As the discharge is moved farther into the nozzle the velocity distribution becomes broader and peaked at higher velocities. The plasma acts as a plug when placed in the nozzle and the initial density (10^{20} cm^{-3}) drops by a factor of roughly 100 to values of 10^{18} to 10^{17} cm^{-3} due to the high temperature of the plasma. At the higher plasma temperature a decrease in the total collision cross section would also be expected.[13] This creates a condition in which the nozzle is operating at a Knudsen number close to unity or in the transition region between hydrodynamic and free molecular flow thus causing a broadening of the velocity distribution. The higher peak velocities are observed because cooler boundary layers in front of the discharge are reduced in intensity.

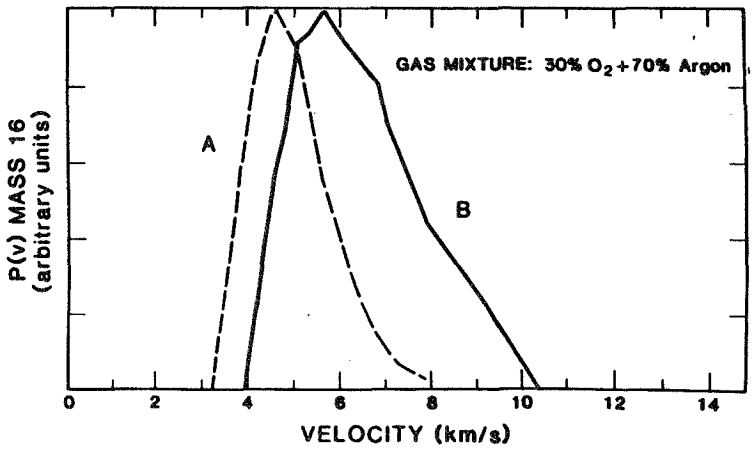

Fig. 6. TOF distributions of mass 16 using a 30% O_2, 70% argon mixture. Distribution A was taken with the plasma at the entrance to the nozzle while distribution B was taken with the plasma moved 0.5 mm farther into the nozzle.

Figure 7 shows the relationship between beam brightness (number of particles/s-steradian), flux density (number of particles/s-cm^2) and distance from the source (L cm). Measurements performed on the laser sustained source show it to be capable of a brightness of 10^{19}/s-sr with a O-atom flux 10% that of the argon carrier (reverse seeding). At a 15-cm distance from the source we calculate a flux density of ~10^{16}/s-cm^2. Upon operation with neon or helium carrier gas we expect a factor of 5-10 increase in flux. When performing surface recession experiments a shorter source to sample may be used to increase flux density.

O-ATOM EXPOSURE FACILITY

Figure 8 shows a diagram of the O-atom beam exposure facility. The beam source is pumped by a 2000 l/s diffusion pump while the two downstream differential pumping chambers are pumped with 500 l/s turbomolecular pumps. The scattering chamber is equipped with a 1500 l/s turbomolecular pump. A water cooled

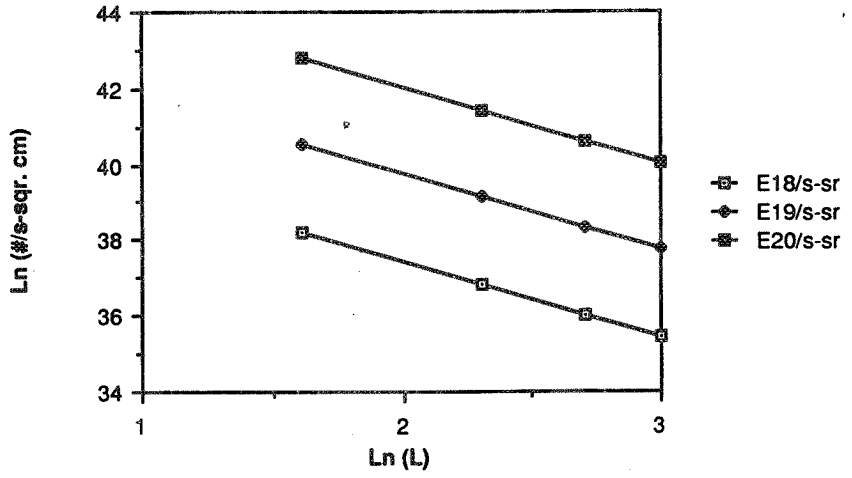

Fig. 7. Plot of flux density (#/s-cm^2) vs distance (L) from source for various brightness (#/s-steradian)

copper skimmer is used to extract the O-atoms from the expansion and to isolate the nozzle chamber from the first differential pumping stage. A remotely operated straight-through valve on the nozzle chamber allows that chamber to be vented for nozzle replacement without venting the remaining apparatus.

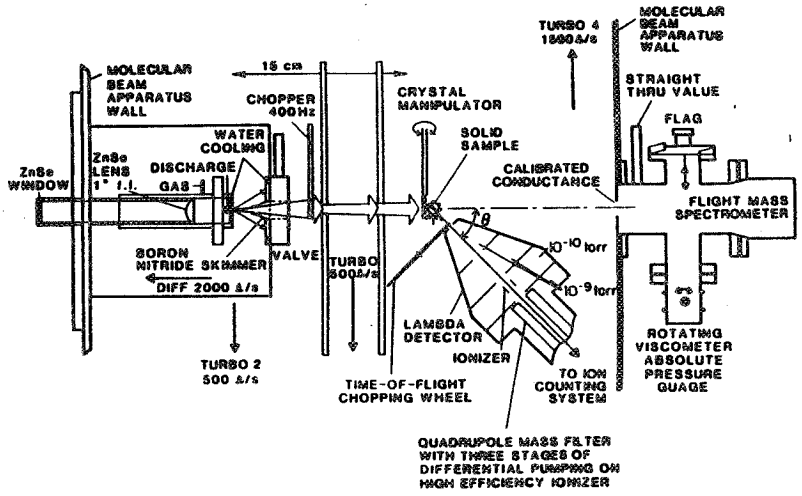

Fig. 8. Los Alamos molecular beam dynamics apparatus: shows the central portion of the instrument including the molecular beam source, and movable detector. The detector is an electron bombardment ionizer-quadrupole mass spectrometer suspended from the rotatable lid of the main vacuum chamber and is used for the measurement of angular distributions. Also shown is a time-of-flight chopping wheel that provides 50% transmission efficiency using cross correlation techniques. Pumping of the system is accomplished by a 1500 l/s turbo on the scattering chamber, a 500 l/s turbo on the differential pumping chambers, a 2000 ℓ/s diffusion pump on the nozzle source and ion pumps on the detector.

A rotatable quadrupole mass spectrometer detector employing a Brink[14] type ionizer is shown along with the time-of-flight chopper. The three-stage, differentially pumped detector has an angular resolution of 1° and a detection sensitivity of 10^{-4}, i.e., one ion is produced for every 10,000 neutrals entering the ionizer.

Figure 9 shows a representative scattering chamber background taken with a residual gas analyzer and with the liquid nitrogen scattering chamber cryoshroud at 100°K. The chamber total pressure was 3×10^{-8} torr. The mass spectrum indicates a small air leak and hydrocarbon background pressures in the range of 10^{-12} torr.

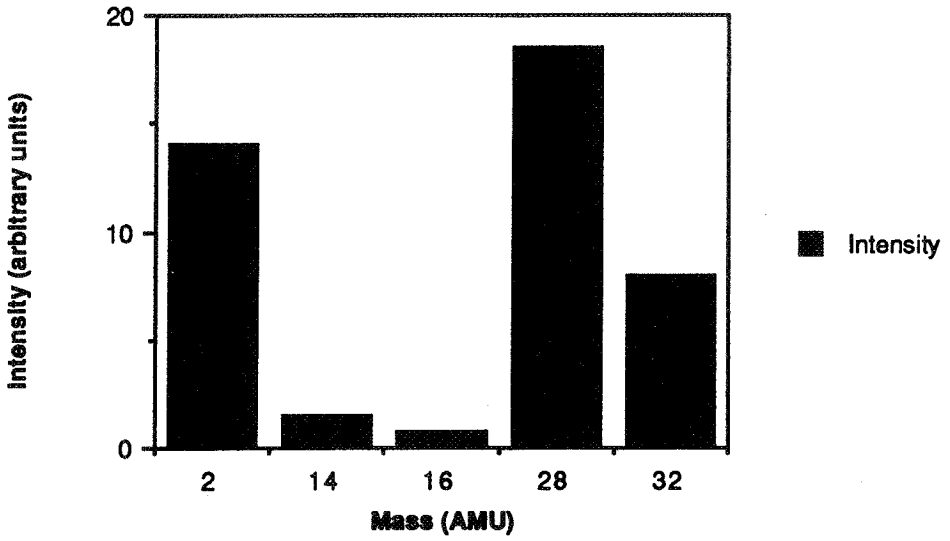

Fig. 9. Background (3×10^{-8} torr) mass spectra taken with Inficon residual gas analyzer. Liquid nitrogen shroud has been cooled to 100 K. Note small air leak is present.

GAS-SURFACE SCATTERING

Initial results of gas scattering from an uncharacterized nickel surface are presented in figures 10 and 11. The molecular beam apparatus described in ref. 12 was used along with a pseudorandom sequence TOF chopper. The TOF detector is operated at 400 Hz with the multichannel scaler operating with a dwell time/channel of 10 μs. Angular distributions were obtained by modulating the direct beam at 400 Hz with a tuning fork chopper while data was accumulated with a phase locked pulse counter. The TOF chopper was kept in operation during angular distribution measurements. Counting times of 2 min/ angle were used for angular distributions and 5 min/angle for TOF acquisition. These initial experiments focused on large incident angle (70°) scattering because of the ease of observing both the direct and scattered beams. The discharge source was operated with a 50% mixture of oxygen and argon with the axial position of the discharge slightly back of the nozzle (velocity was not optimized). Figure 10 shows strong specular scattering of atomic oxygen over the angular range accessible to the detector indicating predominantly direct scattering with surface residence

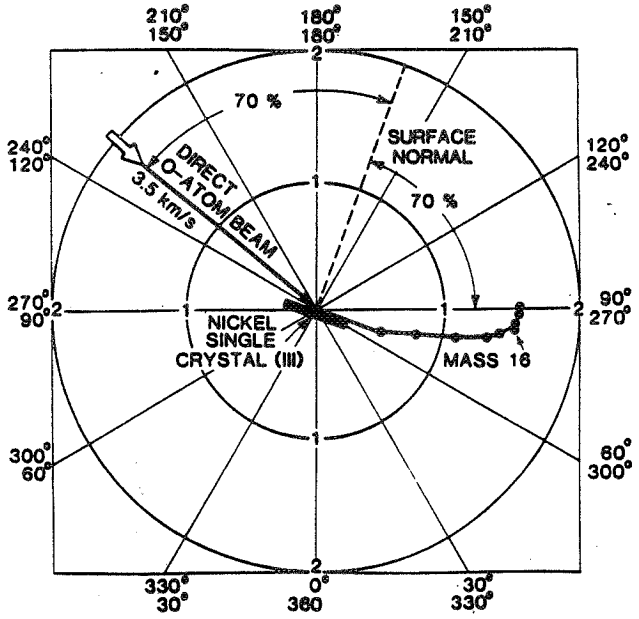

Fig. 10. Angular distribution of O-atoms scattered from uncharacterized nickel crystal. Error bars on data points are the size of the plotting symbol. Surface temperature was 300 K.

times on the order of the collision time. Figure 11 shows TOF spectra taken at the specular angle 70° and at 80° from the surface normal for both atomic and molecular oxygen. The data of figure 11 when converted to translational energy indicates that approximately 1/2 the initial beam energy was lost to the solid. The surface was not characterized but most likely consisted of nickel oxide with overlayers of O_2. Further experiments are in progress to obtain angular distributions near the surface normal to determine the extent of energy accommodation and to fully characterize the surface.

Figure 12 shows preliminary results on reaction product identity produced by interaction of oxygen atoms with kapton held at a temperature of 120°C. The argon (mass 40), O_2 (mass 32) and O-atom (mass 16) were present in the beam while masses 18, 30, and 44 were produced by oxygen interactions with the kapton surface. Preliminary measurement of the velocity distribution shows both the nonreactive scattering and reactive products to be equilibrated with the surface temperature (low velocity and broad distributions). The angular scattering distributions have not been accurately measured but mass 18 product intensity at two angles 20° either side of the specular angle indicate a very broad distribution. These results are in sharp contrast to those obtained from scattering from a metal surface where sharp specular scattering is observed along with modest energy accommodation.

CONCLUSION

An O-atom exposure facility has been described which consists of (1) a cw laser sustained discharge source of O-atoms having a variable energy up to 5 eV and an intensity of between 10^{15}-10^{17} O-atoms s^{-1} cm^{-2}, (2) an atomic beam formation and diagnostics system consisting of various stages of differential

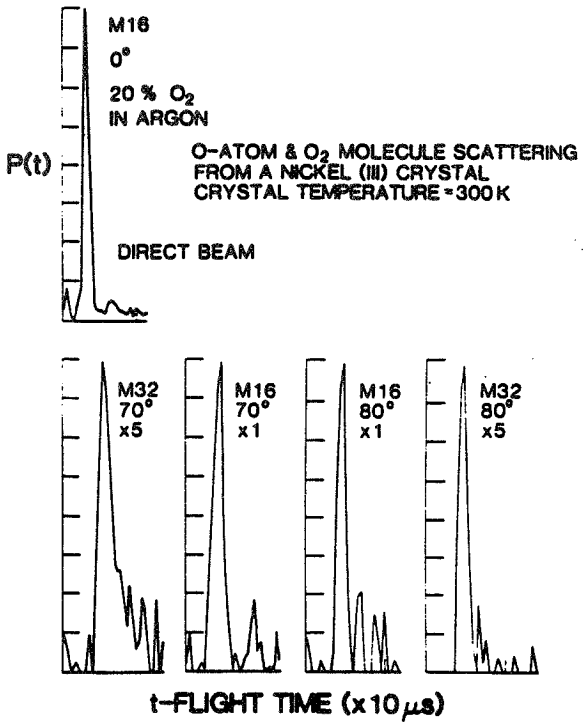

Fig. 11. TOF distributions at 70 and 80° from surface normal. The mass 16 distribution when converted to energy indicates roughly 50% of the energy was transferred to the solid.

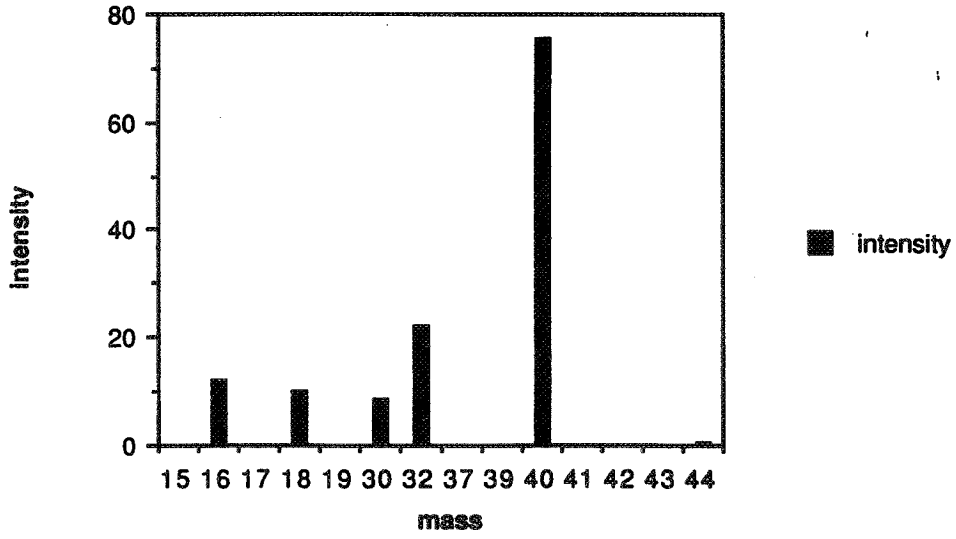

Fig. 12. Reaction products produced by reaction of O-atoms with kapton held at 120°C. Masses 16, 32, and 40 are in the direct beam while masses 18, 30, and 44 are reaction products. Species with mass >44 were not detected at a sensitivity level 100 times that for mass 18.

pumping, mass spectrometer detector and time-of-flight analyzer, (3) a spinning rotor viscometer for absolute O-atom flux measurements, and (4) provision for using the system for calibration of flight instruments.

A new beam source has been described that uses a laser sustained plasma technique for producing high intensity ($>10^{18}$ s^{-1} sr^{-1}) and high translational energy (>2 eV) beams. Data indicates that beam temperatures near the plasma spectroscopic temperature can be obtained and that data from one gas can be used to predict results from others. Atomic oxygen beam energies of 2.5 to 3 eV have been produced with intensities of ~4 x 10^{18} s^{-1} sr^{-1}. Measurements have been taken that show the instrument capable of measuring the extent of energy equilibration produced by high velocity collisions with engineering type surfaces, nonreactive and reactive scattering angular distributions of O-atoms and reaction product identity. These types of information will provide the data base for computer modeling of Space Station interactions with LEO environment.

REFERENCES

1. Knuth, E. L.; Winicur, D. H.: J. Chem. Phys. 46 (1967) 4318).
   Knuth, E. L.; Rodgers, W. E.; Young, W. S.: An Arc Heater for Supersonic Molecular Beams, Rev. Sci. Instr. 40 (1969) 1346.

2. Silver, J. A.; Freedman, A.; Kolb, C. E.; Rahbee, A.; Dolan, C. P.: Supersonic Nozzle Beam Source of Atomic Oxygen Produced by Electric Discharge Heating; Rev. Sci. Instr. 53 (1982) 1714.

3. Lee, Y. T.; Ng, C. Y.; Buss, R. J.; Sibener, S. J.: Development of a Supersonic $O(^3P_J)$, $O(^1D_2)$ Atomic Oxygen Nozzle Beam Source, Rev. Sci. Instr. 51 (1980) 167.

4. Grice, R.; Gorry, P. A.: Microwave Discharge Source for the Production of Supersonic Atom and Free Radical Beams, J. Phys. E12 (1979) 857.

5. Campargue, R.: Progress in Overexpanded Supersonic Jets and Skimmed Molecular Beams in Free-Jet Zones of Silence; J. Phys. Chem. 88 (1984) 4466.

6. Ardenne, M. V.: Tabellen der Elektronenphysik, Ionenphysik and Ubermikroskopie., Veb Deutscher Verlag Der Wissenschafter, Berlin (1956), pg. 507.

7. Razier, Y. P.: The Feasibility of an Optical Plasmatron and It's Power Requirements; ZhETF Pis. Red. 11 (1970) 195 [JETP Lett. 11 (1970) 120].

8. Razier, Y. P.: Subsonic Propagation of a Light Spark and Threshold Conditions for Maintenance of a Plasma by Radiation; Zh. Eksp. Teor. Fiz. 58 (1970) 2127 [Sov. Phys. JETP, 31 (1970) 1148].

9. Razier, Y. P.: Laser Induced Discharge Phenomena. Consultants Bureau, New York (1977).

10. Kozlov, G. I.; Kuznetsov, V. A.; Nasyukov, V. A.: Sustained Optical Discharge in Molecular Gases; Zh. Tekh. Fiz., 49 (1979) 2304 [Sov. Phys. Tech. 49 (1979) 1283].

11. Hughes, T. P.: Plasmas and Laser Light. John Wiley, New York (1975).

12. Cross, J. B.; Cremers, D. A.: High Kinetic Energy (1-10 eV) Laser Sustained Neutral Atom Beam Source; Nuc. Instr. and Methods, B13 (1986) 658.

13. Levine, R. D. and Bernstein, R.B.: Molecular Reaction Dynamics; Oxford University Press, New York (1974), p. 25.

14. Brink, G. O., Rev. Sci. Instrum., 37, 857 (1966).

15. Femerey, J. K.; J. Vac. Sci. Technol., 9, 108 (1972).

A Sputtering Derived Atomic Oxygen Source for Studying Fast Atom Reactions

Richard A. Ferrieri, Yung Y. Chu and Alfred P. Wolf
Chemistry Department, Brookhaven National Laboratory, Upton, NY 11973

ABSTRACT

A novel technique for generation of fast atomic oxygen has been developed. These atoms are created by ion beam sputtering from metal oxide surfaces. Mass resolved ion beams at energies up to 60 KeV are produced for this purpose using a 150 cm Isotope Separator. Studies have shown that particles sputtered with 40 KeV Ar^+ on Ta_2O_5 were dominantly neutral and exclusively atomic. The atomic oxygen also resided exclusively in its ^3P ground-state. The translational energy distribution for these atoms peaked at ca 7 eV (the metal-oxygen bond energy). Additional measurements on V_2O_5 yielded a bimodal distribution with the lower energy peak at ca 5 eV coinciding reasonably well with the metal-oxygen bond energy. The 7 eV source was used to investigate fast oxygen atom reactions with the 2-butene stereoisomers. Relative excitation functions for H-abstraction and π-bond reaction were measured with trans-2-butene. The abstraction channel, although of minor relative importance at thermal energy, becomes comparable to the addition channel at 0.9 eV and dominates the high-energy regime. Structural effects on the specific channels were also found to be important at high energy.

INTRODUCTION

In recent years the Space Shuttle program has enabled scientists to make observations and gather data on the effects of the earth's environment on materials exposed at low orbit attitudes and at orbiting velocities of 8×10^5 cm/s. Such tests have shown materials to undergo extensive degradation which result in surface modification and even mass loss (1-4). Since the earth's atmosphere is dominantly comprised of atomic oxygen at these altitudes, it was thought that the most probable cause for these effects was due to chemistry initiated by the high velocity impact with these atoms. This prompted a recent surge of effort aimed at developing atomic oxygen sources for the purpose of investigating these energetic phenomena under controlled laboratory conditions. Studies of this nature are undoubtedly crucial to the development of new materials that would be more impervious to these effects not only from the standpoint of satisfying immediate interests in obtaining more suitable protective materials for the Shuttle's ram direction surfaces, but also from the standpoint that such long term degradative effects could have a severe impact on the longevity and performance of any future orbiting stations (5).

The present report describes a source of fast atomic oxygen that is derived from ion beam sputtering. This report also describes an application of this source to the investigation of high energy atomic oxygen

chemistry in the gas-phase. It is felt that investigations of this kind provide a sounder foundation through which the chemistry occurring on surfaces can be better understood.

EXPERIMENTAL APPARATUS

The complete system for O-atom generation and reaction is shown schematically in Figure 1. The system utilized a 150 cm isotope separator for the purpose of generating and mass resolving kilovolt ion beams. Ions were generated within a dual plasmatron source then extracted through a 4.45 mm diameter aperture. The source housing along with the aperture plate were electrically floated at the desired acceleration voltage. Acceleration voltages between 5 and 60 KeV were possible. Positive ions were accelerated toward an extraction lens that was biased with +200 v and focused slightly. A strong vertical focussing was also provided by an Einzel lens system while the other two plates were at ground potential. The beam was then subjected to a uniform magnetic field applied by a 90°, 150 cm magnet for momentum analysis. The system has the resolving power of 400. For the majority of the test studies described in this report, a 40 KeV argon ion beam was employed at intensities ranging between 15 and 25 μA after mass resolution and focussing.

The sputtering chamber comprised of a set of focussing lenses, differentially pumped aperture, and reaction chamber. As the ion beam emerged from the magnetic sector, it was focussed through 4.8 mm diameter differential aperture using cylindrical electrostatic lenses. The aperture was cut from a brass disk and vacuum sealed onto a larger aluminum flange that made a vacuum seal between the target chamber and the forechamber holding the focussing lenses. Both chambers were constructed of 15.2 cm inside diameter pyrex pipe. The reaction chamber was 20 cm long. The back-end was also vacuum sealed to a second aluminum flange that provided access to the chamber. All beam monitoring connections fed through this flange were of the type of sealed BNC connectors. A polished brass sleeve, 15.0 cm x 12.7 cm diameter was mounted inside the chamber using teflon rings for electrical isolation. This sleeve was biased with a positive potential in order to draw secondary electrons out of the reaction zone. Holes were cut in the sleeve and aligned with ports on the pyrex chamber to provide access for gas inlets, vacuum monitoring devices, a quadrupole mass analyzer equipped with a differential sampler, and a product collector. Background pressures were typically below 1×10^{-6} torr. Reactant gases were differentially pumped through the target chamber at pressures ranging from 1×10^{-5} to 3×10^{-2} torr.

The sputtering source comprised of a 12.1 cm diameter brass disk mounted on a vacuum sealed rotatable rod. Metal oxide foils, prepared in an anodizing cell (6), were mounted on this disk at a fixed angle incident to the impinging ion beam path. The source could be moved to any distance from the front aperture, and rotated 360°.

The product collector comprised of a 92 cm x 7.6 cm diameter pyrex impact trap that was mounted 90° to the gas flow. The inner surface of

this trap was liquid nitrogen cooled during a run. The entire trap could also be baked-out at about 200°C. During a run, products and substrate gas were condensed onto the inner surface of this trap for later analysis via gas chromatography - mass spectrometry. Non-condensible products, however, were monitored via on-line mass spectrometry. Collected products were processed through a manifold consisting of various solid adsorbents used to concentrate reaction products relative to the substrate gas. The techniques used in this process are similar to those employed in bulk gas processing for atmospheric analysis (7).

Source Characteristics

A principal concern in designing the above system was to minimize the effects of secondary electrons on the resultant atom-molecule chemistry. These electrons were emitted as a result of primary ion collisions with the oxide surface, and also as a result of ion interaction with substrate gases. From tests designed to monitor electron impact effects on gaseous constituents present in the target chamber, it was determined that a sleeve surrounding the reaction zone and biased with a + 90 v potential would minimize these effects.

A study was also carried out to provide information related to the question whether metastable atomic oxygen states are generated through ion beam sputtering. It is well documented that metastable $O(^1D)$ atoms undergo reaction with saturated hydrocarbons via C-H insertion to yield the respective alcohol (8). On the other hand, ground-state $O(^3P)$ atoms only abstract H-atoms to yield water. It was possible to measure the metastable state distribution by measuring the yields of alcohol and water arising from sputtered O-atom reaction with a saturated hydrocarbon molecule. Normal butane gas was used in this test. The following results were obtained: a Ta_2O_5 target showed only a trace amount of alcohol that was below detection limits for quantification; a V_2O_5 target yielded levels corresponding to 1 metastable in 150 atoms. It was concluded that the present conditions for sputtering yielded relatively clean sources of $O(^3P)$ atoms.

The O-atom sputtering yield (atoms/ion) was also determined from the water product yields in the above tests. Results indicated O-atom sputtering yields as high as 76 atoms/ion and 190 atoms/ion for fresh Ta_2O_5 and V_2O_5 surfaces, respectively. This afforded dynamic concentrations of ca 1×10^9 and 2.6×10^9 atoms/$cm^3 \cdot \mu A$, respectively. It may be possible to attain even higher concentrations by increasing the mass, energy, or intensity of the ion beam. Studies have shown that the sputtering yield generally increases as the mass and energy of the impinging ion beam increases (9).

Preliminary measurements were taken on the O-atom translational energy distribution using a quadrupole mass analyzer modified with an energy filter. The energy filter was made from a brass disk with a 6.35 mm aperture that matched the focussing lens to the mass filter. A gold plated tungsten wire mesh (80% transmission) was spot welded across the aperture.

This lens was mounted in the mass filter assembly between the ionizer and focussing lens, and was biased with up to 70 volts using a floated power supply. The entire assembly was mounted at 90° to the axis of the ion beam. The metal oxide target was also fixed in an orientation 60° incident to the axis of the ion beam, but could be rotated on axis to allow for energy distribution measurements to be taken at both forward (150° ± 10) and backward (30° ± 15) scattering angles. In operation, neutral atoms were ionized, energy filtered, then mass filtered. The m/e signal at 16 was recorded as a differential response to increases in the applied energy discrimination potential.

Comparisons were made between the m/e signals at 16 from neutral and ionic particles sputtered from the surface in vacuo by running the ionizer in both the on and off modes. Results showed that the positive ions occupied only a very small fraction (< 1%) of the sputtered material. It was also noted that the m/e signal ratio 16:181 was stoichiometric for Ta_2O_5 suggesting that the sputtered material is also dominantly atomic.

Results from these preliminary energy distribution measurements on neutral O-atoms sputtered from Ta_2O_5 are shown in the histograms in Figures 2a-c. Figures 2a and 2b represent distributions measured in the forward scattered and backscattered directions. While the distribution appears poorer in the later case, the integrated signal in this direction was about a factor of 6 lower than the forward direction. Peak energies in both cases seemed to coincide with the Ta-O bond energy (10). Increasing the mass of the primary ion beam, as seen in Figure 2c, did little to alter the peak energy and distribution. Parallel measurements were taken on V_2O_5. A bimodal distribution was observed for this oxide where the peak energy of the lower energy component roughly corresponded to the V-O bond energy. The higher energy component, ca 12 eV, may be representative of the oxide surface undergoing a stoichiometric change during ion bombardment (6).

GAS-PHASE STUDIES

Since a number of materials of aerospace interest contain carbon-based chemical bonds, and the impact velocities in low earth orbits provide ca 5 eV of collision energy for reaction, it would seem logical that studies on the gas-phase reactions using the fast atomic oxygen source with molecules containing such bonds, could facilitate understanding certain cases of material degradation.

In a recent preliminary study, the 7 eV source was used to measure the effective competition between π-bond reaction and H-abstraction on trans-2-butene. While it is generally accepted that thermal $O(^3P)$ atoms react preferentially, if not exclusively, with the π-bonds of unsaturated hydrocarbon molecules (8), it is not known under what conditions H-abstraction may effectively complete against this channel. Recent studies using substituted alkenes have shown H-abstraction thresholds at ca 1 kcal/mol with rising excitation functions attributing to the significance of this channel at higher energies.

In the present study, collision energies ranging between 7 eV and room temperature were obtained by buffering the target chamber with various pressures of neon. The average energy lost per collision with this buffer was calculated using equations derived from the Estrup-Wolfgang theory (11). Results indicate that the abstraction channel was of minor relative importance at thermal energy, but dominates the high-energy regime. A structural effect between cis- and trans-2-butenes was also observed in this high energy regime. The trans isomer was more susceptible to H-abstraction (relative to π-bond reaction) than the cis isomer. Two explanations are offered for this observation: a true structural effect may indeed be exerted at the point of the atom's approach to the molecule, thereby altering the effectiveness of one channel over the other; a pseudo abstraction channel may also be operative, where H-migration across the C-O bond of the addition complex followed by dissociation yields the same result as direct abstraction. In the later, a structural effect may be exhibited after the fact through varying intermediate stabilities.

SUMMARY

In summary, a system has been described for the generation and reaction of energetic O-atoms through ion beam sputtering. This process produces a clean source of ground-state $O(^3P)$ atoms with translational energies in the range of aerospace interest. High concentrations of atomic oxygen are also available through sputtering. Levels at 2.5×10^{10} and 6.6×10^{10} atoms/cm^3 were obtained using a 25 μA Ar^+ beam on Ta_2O_5 and V_2O_5, respectively. Achieving higher levels should also be possible by increasing the intensity, mass, or energy of the ion beam.

An application of this source was demonstrated in the studies on fast atomic oxygen reactions with unsaturated hydrocarbons. Results not only have shown that the nature of the chemistry is extremely dependent on the collision energy, but suggest that the entrance channels for specific reactions could be sensitive to geometry factors as well.

ACKNOWLEDGEMENT

This research was carried out at Brookhaven National Laboratory under contract DE-AC02-76CH00016 with the U. S. Department of Energy and supported by its Office of Basic Energy Sciences.

REFERENCES

1. L. J. Leger, I. K. Spiker, J. F. Kuminecz and T. J. Visentine, "STS Flight 5 LEO Effects Experiments - Background Description and Thin Film Results," AIAA Paper 83-2631-CP, October 1983.

2. L. J. Leger, J. T. Visentine and J. F. Kuminecz, "Low Earth Orbit Atomic Oxygen Effects on Surfaces," AIAA Paper 84-0548, Presented at the 22nd Aerospace Sciences Meeting, Reno, NV, January 1984.

3. J. T. Visentine, L. J. Leger, J. F. Kuminecz and I. K. Spiker, "STS-8 Atomic Oxygen Effects Experiment," AIAA Paper 85-0415, Presented at the 23rd Aerospace Sciences Meeting, Reno, NV, January 1985.

4. B. D. Green, G.E. Caledonia and T. D. Wilkerson, "The Shuttle Environment: Gases, Particulates and Glow," J. Spacecraft and Rockets, October 1985.

5. L. J. Leger, J. T. Visentine and J. A. Schlensing, "A Consideration of Atomic Oxygen Interactions with Space Station," AIAA Paper 85-0476, Presented at the 23rd Aerospace Sciences Meeting, Reno, NV, January 1985.

6. R. Kelly and N. Q. Lam, Radiation Effects 19, 39 (1973).

7. A. C. Stein (editor) "Air Pollution" (Academic Press, New York 1968) Vol. 3, p. 497.

8. R. J. Cventanovic, "Advances in Photochemistry" (Interscience Publishers, John Wiley and Sons, New York 1963) W. A. Noyer, Jr., G. S. Hammond and J. N. Pittls, Jr. (editors), pp. 117-149.

9. H. F. Winters, "Radiation Effects on Solid Surfaces" ACS Advances in Chemistry Series, Monograph 158 (Am. Chem. Soc., Washington, DC, 1976) pp. 1-29.

10. O. Kubaschewski, E. L. Evans and C. B. Alcock, Metallurgical Thermochemistry (Pergamon Press, Oxford, 1967), p. 303.

11. R. Wolfgang, J. Chem. Phys. 39(11), 2983, 1963.

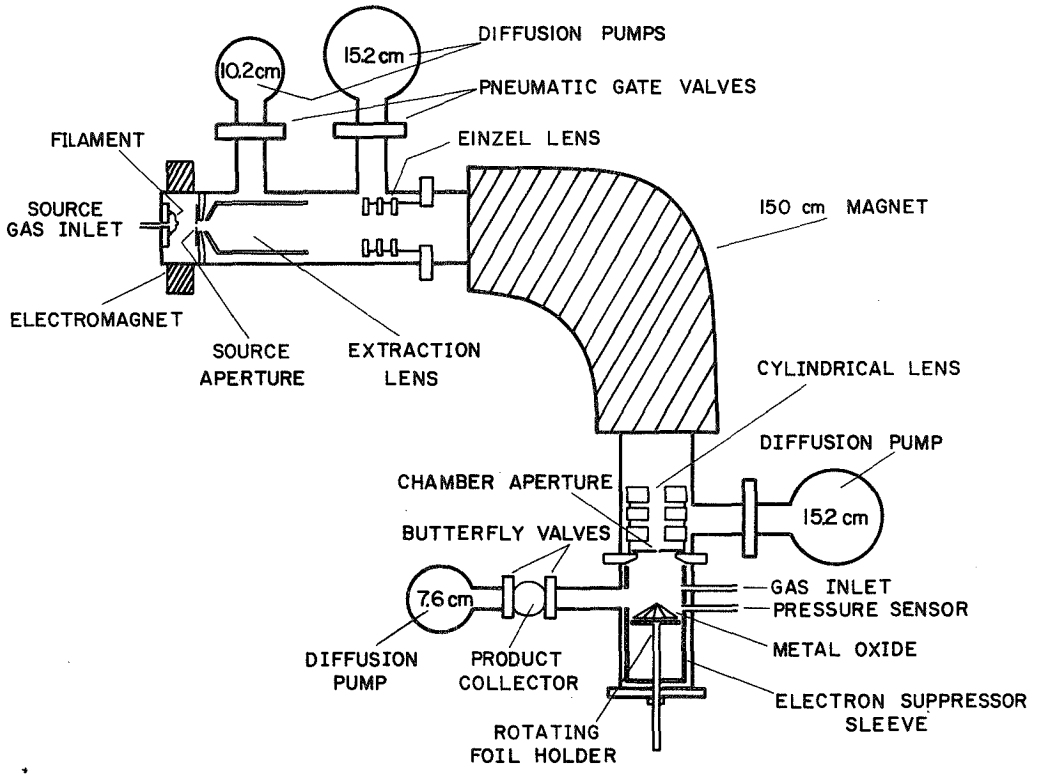

Fig. 1 Schematic view of isotope separator and sputtering chamber.

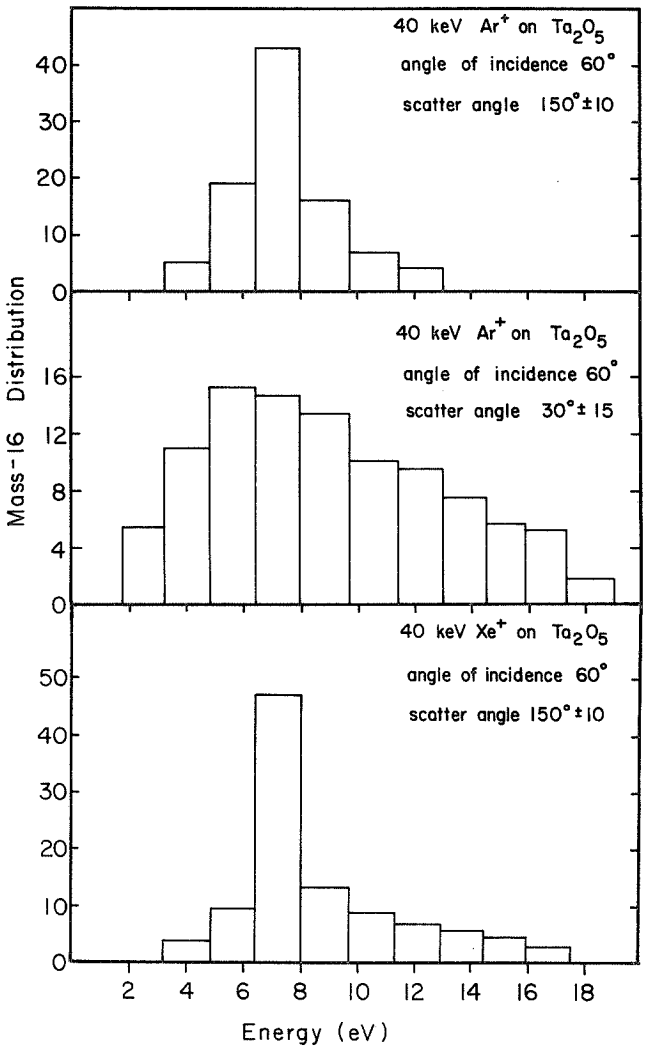

Fig. 2 Translation energy distribution of O-atoms sputtered from Ta_2O_5

Neutral Atomic Oxygen Beam Produced by Ion Charge Exchange for Low Earth Orbital Simulation

by

Bruce Banks and Sharon Rutledge
NASA Lewis Research Center
Cleveland, Ohio 44135

Marko Brdar, Consultant

Carl Olen and Curt Stidham
Cleveland State University
Cleveland, Ohio 44115

Abstract

A low energy neutral atomic oxygen beam system has been designed and is currently being assembled at the Lewis Research Center. The system utilizes a 15 cm diameter Kaufman ion source to produce positive oxygen ions which are charge exchange neutralized to produce low energy (variable from 5 to 150 eV) oxygen atoms at a flux simulating real time low earth orbital conditions. An electromagnet is used to direct only the singly charged oxygen ions from the ion source into the charge exchange cell. A retarding potential grid is used to slow down the oxygen ions to desired energies prior to their charge exchange. Cryogenically cooled diatomic oxygen gas in the charge exchange cell is then used to transfer charge to the oxygen ions to produce a neutral atomic oxygen beam. Remaining uncharge exchanged oxygen ions are then swept from the beam by electromagnetic or electrostatic deflection depending upon the desired experiment configuration. The resulting neutral oxygen beam of 5-10 cm in diameter impinges upon target materials within a sample holder fixture that can also provide for simultaneous heating and UV exposure during the atomic oxygen bombardment.

Introduction

Many spacecraft materials exposed to the Low Earth Orbital (LEO) environment are oxidized by ram impact of atomic oxygen present as a result of photodissociation of the Earth's upper atmosphere (1-3). The rate of oxidation of most polymers and some metals is sufficiently high to be of concern for LEO space missions. As a result, Space Station must utilize protective coatings or alternative durable materials to assure acceptable long term performance of exposed components such as solar array blankets, composite structures, and solar dynamic power system reflector surfaces (4 and 5).

The development and verification of materials durable to the LEO environment will require both ground based laboratory simulation and in-space testing. The economics and convenience of LEO simulation facilities will result in their extensive use provided there is adequate confidence in their ability to simulate the LEO environment and its effects on materials. The LEO environment is reasonably well characterized in terms of the ram energy and flux of the atomic oxygen which is essentially unionized and in the ^3p

ground state. (See Fig. 1) (1 and 6). However, the laboratory production of $O(^3p)$ at these fluxes and energies without the presence of other species not typically present in LEO is difficult. Simulation is even more challenging if one attempts to replicate the synergestic exposure of IR, visible, and UV solar flux; micrometeroid and space debris impact; thermal cycling; wandering ram vector orientation; and residual upper atmospheric species. Thus one must select those aspects of the LEO environment which are relevant to their particular situation and make arguments that the phenomena occurring in the laboratory simulation adequately replicates that which has been found to occur in LEO. The degree to which an atomic oxygen exposure system credibly simulates the mechanisms occurring in LEO can be judged by quantitative comparison of measurements of the surface texture, chemistry, and erosion yield (mass lost per incident oxygen atom) of a variety of materials that possess volatile oxides. Obviously, the closer one simulates the energy, flux, and species present in the LEO environment, the lower risk of producing effects which do not project a realistic simulation mechanism.

Atomic oxygen can be easily produced at low energies (tenths of an eV) but at high fluxes in RF plasma ashers. Plasma ashers have been valuable for qualitative evaluation of candidate LEO materials. All materials that are known to oxidize in LEO also oxidize in plasma ashers. In adddition all materials that are known to be unaffected in space behave the same in plasma ashers. However, the relative rates of oxidation of various materials are not quantifiably in agreement with the LEO results. Thus asher results only allow one to predict that a material will survive or be oxidized in LEO leaving knowledge of the rate of oxidation unknown. This may be a result of differences in energy, flux, metastable states, or species in the plasma. The plasma may contain ions, electrons, diatomic neutrals and atomic neutrals.

This paper presents design considerations for a neutral atomic oxygen beam system currently being assembled at the NASA Lewis Research Center that utilizes ion charge exchange to produce a low energy neutral oxygen beam for LEO simulation.

Vacuum Facility

The vacuum facility layout is shown in Figure 2. It consists of a 60.96 cm diameter by 1.71 m long non magnetic stainless steel chamber to house the neutral atomic oxygen beam system components. The vacuum chamber was specifically designed for the oxygen beam system and has numerous ports for beam characterization probes. It has full diameter access doors at both ends, as well as a large 40.64 cm diameter port to mount a vertically downward oriented ion source within it. The cylindrical vacuum chamber is evacuated by a 25.4 cm diameter 2350 l/sec diffusion pump with its associated cold trap and roughing pump. The pumping system utilizes fomblinized oil to allow chemical stability when pumping oxygen.

Ion Source

The ion source, shown schematically in Figure 3 is a 15 cm diameter electron bombardment ion source. The ion source is used to produce oxygen ions which are to be neutralized by charge exchange as shown in Figure 4. The ion source utilizes a hot wire filament cathode in which Pt or Ir will be used to insure adequate life in the oxygen environment. The ion source will be

operated with one of three candidate gases: O_2, N_2O, or CO_2, depending upon their overall system performance. Molecular oxygen is an ideal source gas in that it does not introduce contaminant gases into the vacuum facility. However, as can be seen in Table I there are numerous excited states of O^+ that would potentially be present and thus accelerated as part of the ion beam. Ideally one would like only the $O^+(^4S)$ ground state ions to be generated in the ion source discharge chamber. However, it is anticipated that ions produced will be 75% O_2^+ and 25% O^+, where the O^+ is comprised of both ground state and metastable states (8).

Measurements of electron impact ionization of O_2 by Neynaber and Magnuson (7) have indicated that the single ions are composed of 65% $O^+(^4S)$ ground state ions; and 25% $O^+(^2D)$ and 10% $O^+(^2P)$ metastable ion states. N_2O and CO_2 source gasses have the potential advantage of producing significantly higher percentages of ground state oxygen ions but have the added complication of introduction of unwanted ion and neutral species.

The ions produced within the discharge chamber are accelerated by the ion optics shown in Figure 3. The energy distribution of the accelerated ions is more depenent upon the potential gradients within the discharge chamber than the applied accelerating potential which can be accurately set. The small potential gradients within the discharge chamber are expected to produce energy uncertainties of the order of leV. Depending upon the choice of ion optics (one, two, or three grids) the oxygen ions will then be accelerated to specific energies up to 150 eV. Single accelerator grid ion optics allows very high current densities to be extracted at low ion energies (9). Average ion current densities of 7 mA/cm^2 have been measured for 50 eV argon ions (10). Single ion optics typically consist of a high open area electroformed metal mesh (usually gold or nickel) which is negatively biased. The mesh spacing is chosen to be smaller than the space charge limited flow acceleration sheath distance. Single grid optics enable high current density ion beams to be produced at low net ion energies which allows the use of lower magnetic fields for beam manipulation. However, the single grid ion beams appear to be quite divergent at these low energies. Two grid ion optics, in which the most upstream grid (the screen grid) is at ion source cathode potential and the downstream grid (the accelerator grid) is negatively biased, must be operated at higher net ion energies to achieve reasonable current densities but their beams are much better aligned. Three grid ion optics utilize the two grid optics but have an additional downstream grounded grid which reduces beam divergence when operated at low voltages with high current densities. The two and three grid optics generally consist of a hexagonal array of 1 to 2 mm diameter apertures in 0.4 mm thick dished molybdenum sheets separated by 0.3-0.5 mm gaps. Final choice of the ion optics type will depend upon their relative ability to provide high current density at the inlet of the charge exchange cell.

The ion beam produced by the ion source is then neutralized (in a bulk plasma sense but not microscopically) by the addition of electrons from a hot wire neutralizer located just downstream of the ion source.

Ion Selecting Magnet

An electromagnet is used to direct the singly charged oxygen ions toward the charge exchange cell as shown in Figures 4 and 5. The electromagnet also

serves to selectively reject O_2^+ and any O^{++} ions from entering the charge exchange cell. The electromagnet is large enough to bend the full 15 cm diameter beam at energies up to 150 eV with a .0415 tesla field in its gap.

Charge Exchange Cell and Retarding Screen

The singly charged oxygen enters a charge exchange cell after first being slowed by passing through a retarding screen shown in Figures 4 and 5. The screen cage within the charge exchange cell is biased to a positive potential such that the net ion energy has been slowed to 4-5 eV. Because positively biased surfaces tend to draw high electron currents it may be necessary to provide a negatively biased electron repeller screen just upstream of the positively biased ion retarding screen. The termination of electron flow along with the ion flow would necessitate their readdition by means of a neutralizer filament within the charge exchange cell cage. Inside the charge exchange cell a low temperature charge transfer gas is present to supply electrons to the oxygen ions and thus produce a fast 4-5 eV oxygen atom beam. Ideally one would like the reaction $O^+(^4S) + O_2 \longrightarrow O(^3p) + O_2$ to occur with a high probability and without trajectory alterations. The probability of charge transfer is increased if one increases the density of the charge transfer gas, as well as, increasing the length of the cell. The cell shown in Figure 5 is $\approx$50 cm long. The O_2 gas density in the cell is elevated by cryogenically cooling its copper walls. The cross-section for $O^+ + O_2 \longrightarrow O + O_2^+$ is approximately 2×10^{-16} cm^2 for ground state ions and 3×10^{-15} cm^2 for metastable ions (11). Based on this charge exchange cell size, the ground state charge transfer cross-section, and an O_2 pressure of 10^{-4} torr, approximately 31% of the incoming ions will be converted to neutral oxygen atoms.

Several charge transfer issues invite the consideration of alternate gases and alternate configurations. The highest probability charge transfer occurs from resonant transfer with atomic oxygen. Because of the complexity of obtaining a high population of cold atomic oxygen one might consider other gases with larger Franck-Condon overlaps with $O^+(4_S)$ at the recombination energy (13.618 eV). Gases which appear to have a high probability of momentumless charge transfer include H_2O, CO_2, CH_2F_2 and CF_4 (12). However, each of these gases will allow nonoxygen species to be back ingested into the ion source thus allowing some probability of their ionization and subsequent acceleration. In the case of CO_2, back injestion may not be a problem if CO_2 is also used as the ion source gas.

The exact degree to which charge transfer can occur with various gases without momentum transfer is not well characterized for oxygen ion beams of 4-5 eV. If the charge transfer occurs and imparts significant trajectory changes to the oxygen ions then a very short single open ended charge exchange cell operated at high pressure would be needed to allow acceptable fluxes to arrive at the target sample surface. A short 5.08 cm long, charge exchange cell option is being fabricated with a small variable diameter entrance hole. The cell utilizes an electrostatic repeller screen to prevent uncharge exchanged ions from impacting the sample surface. The reduced inlet to the cell and lack of an exit port will allow much higher number densities to be achieved within the cell and still enable off axis directed atomic oxygen to impinge on the target sample surfaces.

Ion Deflector Magnet

Uncharge exchanged ions are bent 90^{o} downward from the atomic oxygen beam by an electromagnet located just downstream of the charge exchange cell to prevent their impingement upon the sample surface. This electromagnet will be operated to produce a 0.0076 tesla field over its 12 cm gap.

Sample Holder & Environment

The atomic oxygen impinges upon target samples located just downstream of the ion deflector magnet. The goal of the system is to simulate the atomic oxygen flux (10^{11} - 10^{14} oxygen atoms/cm^2 sec) and energy (4.2 - 4.4 eV) of LEO conditions, as well as the UV and thermal environment. Thus the samples are located in a thermally controlled box with the capability of synergestic UV exposure as shown in Figure 6. Sample rotation is also possible to correctly simulate the changing angle of attack that would occur on solar oriented surfaces.

Simulation Analysis

The energy characterization of the atomic oxygen beam can be inferred by means of retarding potential probing of the oxygen ions which have not charge exchanged. The measurement of the atomic oxygen flux can be accomplished by comparative pressure measurements of a differentially pumped cavity located in the target sample plane. An inlet aperture in the cavity allows both the O_2 from the background vacuum facility and the atomic oxygen to enter a pumped chamber. Because the O_2 is randomly directed it has a high probability of being pumped out while the axially directed atomic oxygen exits through a downstream aperture and enters an absolute pressure measurement cavity. By comparing the pressure in this cavity for beam on and beam off conditions via turning on and off the ion selecting magnet a flux through the sample plane can be calculated.

Because erosion rates of materials exposed to expected Space Station altitude fluxes is low, thin film surface analysis techniques including Rutherford backscattering will be utilized to measure material erosion yields.

Concluding Remarks

A low energy atomic oxygen beam system designed to simulate both the energy and flux of the LEO environment is being assembled at the NASA Lewis Research Center. A variety of design considerations and configuration options are being considered to optimize the quality of the simulation. Synergistic thermal, UV, and angle of attack exposure considerations will be provided with surface analysis techniques used to quantify material loss rates.

Acknowledgements

The authors gratefully acknowledge the helpful suggestions provided by Dr. Jean Futrell of University of Deleware, Dr. Harold Kaufman of Front Range Research and Dr. Paul Wilbur of Colorado State University.

References

1. B. Banks, M. Mirtich, S. Rutledge, and H. Nahra, "Protection of Solar Array Blankets from Attack by Low Earth Orbital Atomic Oxygen," paper presented at the 18th IEEE Photovoltaic Specialists Conference, Las Vegas, NV, Oct. 21-25, 1985.

2. L. Leger, "Oxygen Atom Reaction with Shuttle Materials at Orbital Altitudes," NASA TM-58246, 1982.

3. A. Whitaker, "LEO Atomic Oxygen Effects on Spacecraft Materials," paper presented at the AIAA Shuttle Environment and Operations Meeting, Washington, D.C., Oct. 31-Nov. 2, 1983, AIAA-83-2632-CP.

4. B. Banks, M. Mirtich, S. Rutledge, D. Swec, and H. Nahra, "Ion Beam Sputter-Deposited Thin Film Coatings for Protection of Spacecraft Polymers in Low Earth Orbit," NASA TM 87051, Jan., 1985.

5. D. Gulino, R. Egger, and W. Banholzer, "Oxidation-Resistant Reflective Surfaces for Solar Dynamic Power Generation in Near Earth Orbit," paper presented at the 33rd National Symposium of the American Vacuum Society, Baltimore, MD, Oct. 27-31, 1986.

6. L. Leger, J. Visentine, and J. Schliesing, "A Consideration of Atomic Oxygen Interactions with Space Station," AIAA paper 85-0476, Jan., 1986.

7. R. H. Neynaber and G. D. Magnuson, "Associative Ionization in Collisions between Metastable Helium and Atomic Nitrogen and Oxygen," J. Chem. Phys., Vol. 64, No. 7, April 1, 1976.

8. P. Wilbur, Colorado State University, personal communication.

9. J. Harper, J. Cuomo, and H. Kaufman, "Technology and Applications of Broad-beam Ion Sources Used in Sputtering, Part II Applications," J. Vac. Sci. Technol., Vol. 21, No. 3, Sept./Oct., 1982.

10. J. R. Sovey, NASA Lewis Research Center, personal communication.

11. M. Bortner and T. Baurer, "Defense Nuclear Agency Reaction Rate Handbook," Second Edition, DNA 1984H, Revision No. 8, April, 1979.

12. J. Futrell, University of Delaware, personal communication.

Table I - Oxygen Atom and Ion States

STATE	ENERGY (eV)	MEAN RADIATIVE LIFETIME (SEC)
$O\ (^3P)$	Ground State	∞
$O\ (^1S)$	4.18	.8
$O\ (3_s\,^5S^\circ)$	9.13	.0006
$O\ (3_s\,^3S^\circ)$	9.51	1.8×10^{-9}
$O\ (^1D)$	1.96	148.00
$O^+\ (^4S)$	Ground State	∞
$O^+\ (^2D^\circ_{3/2})$	3.33	5.9×10^3
$O^+\ (^2D^\circ_{5/2})$	3.32	2.1×10^4
$O^+\ (^2P^\circ_{1/2})$	5.01	5.4
$O^+\ (^2P^\circ_{3/2})$	5.01	4.2

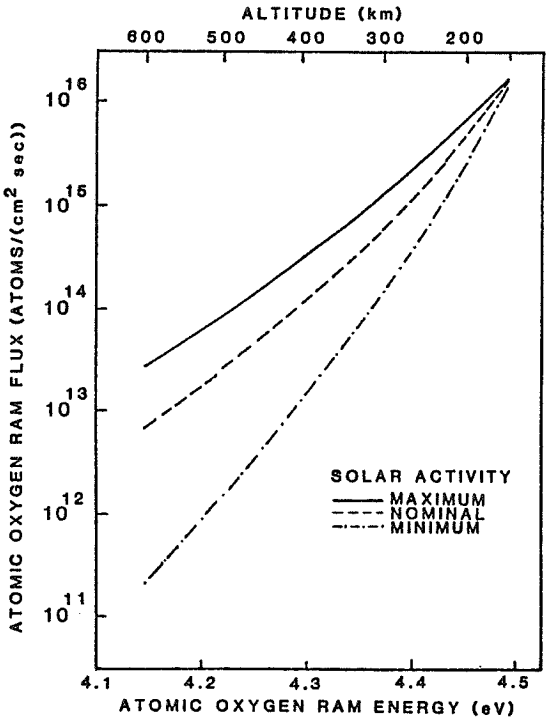

Fig. 1 - Atomic oxygen ram flux and energy as a function of altitude.

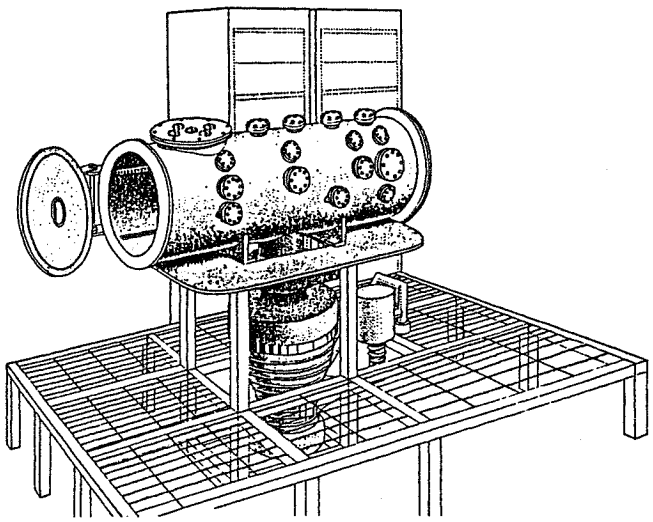

Fig. 2 - Atomic oxygen beam vacuum facility.

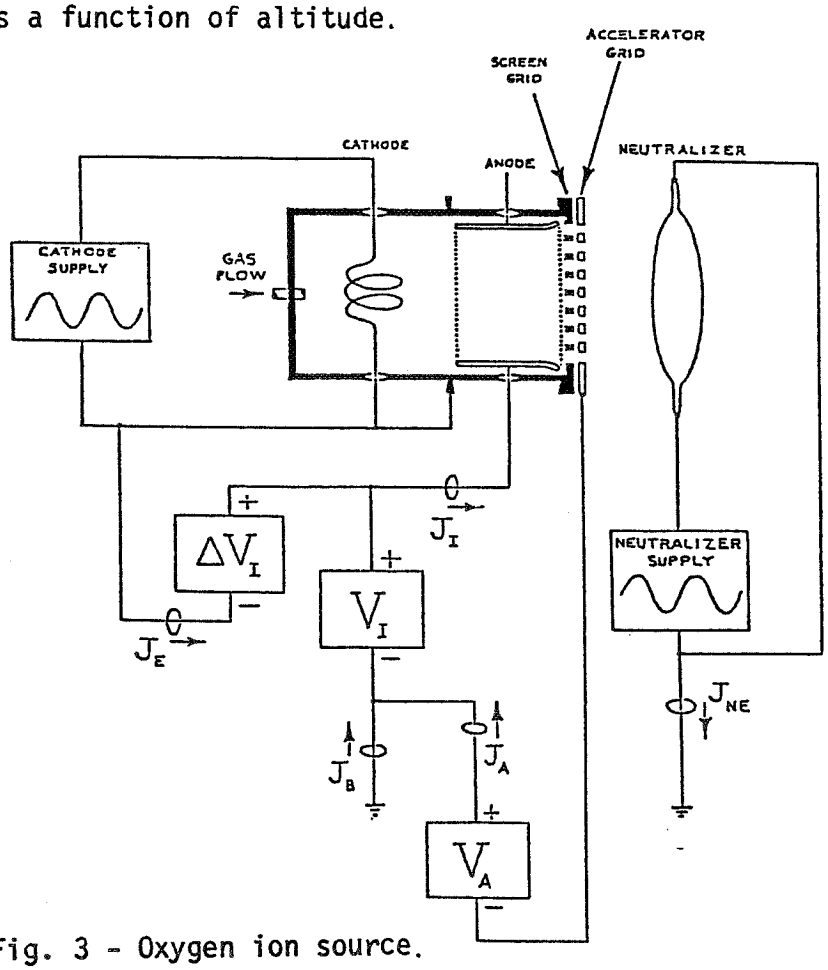

Fig. 3 - Oxygen ion source.

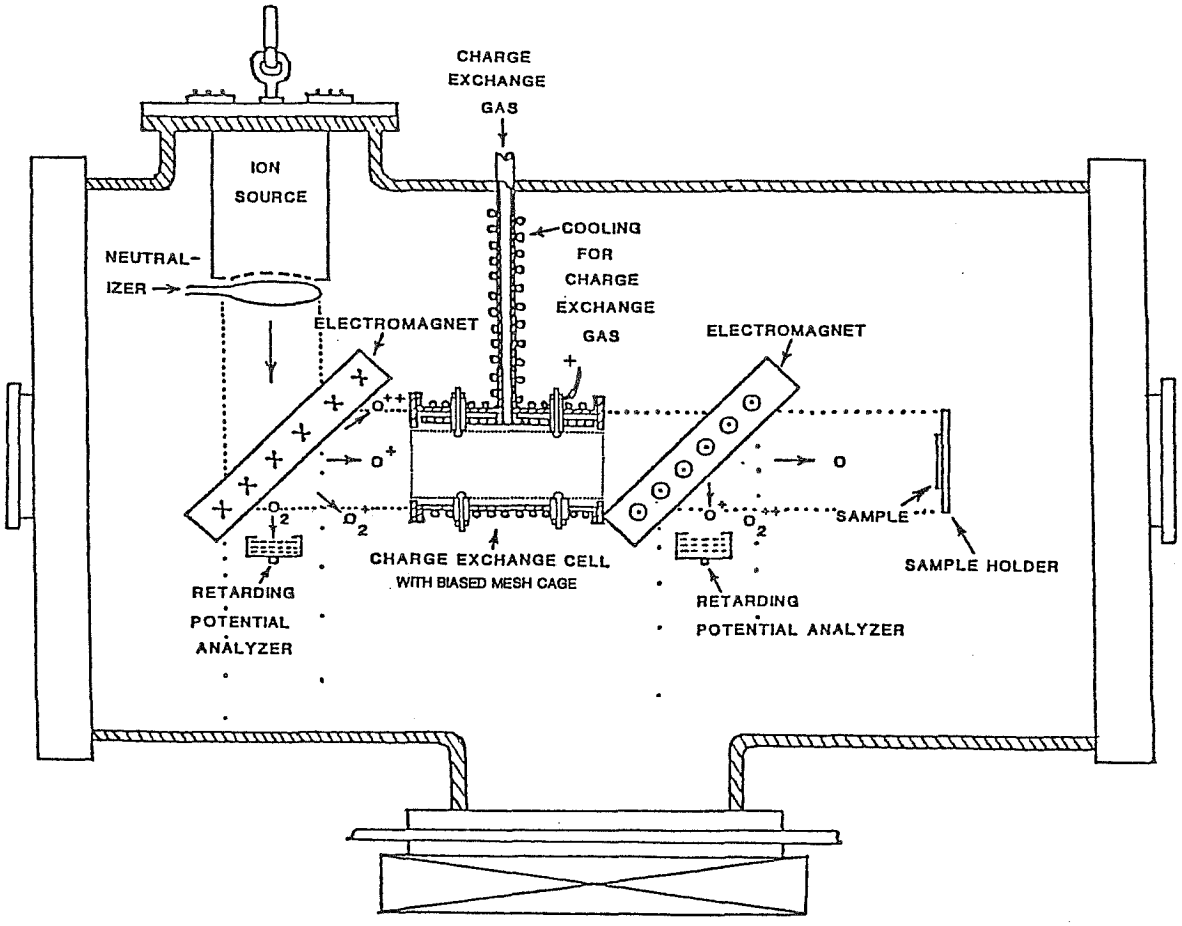

Fig. 4 - Overall schematic of atomic oxygen beam system.

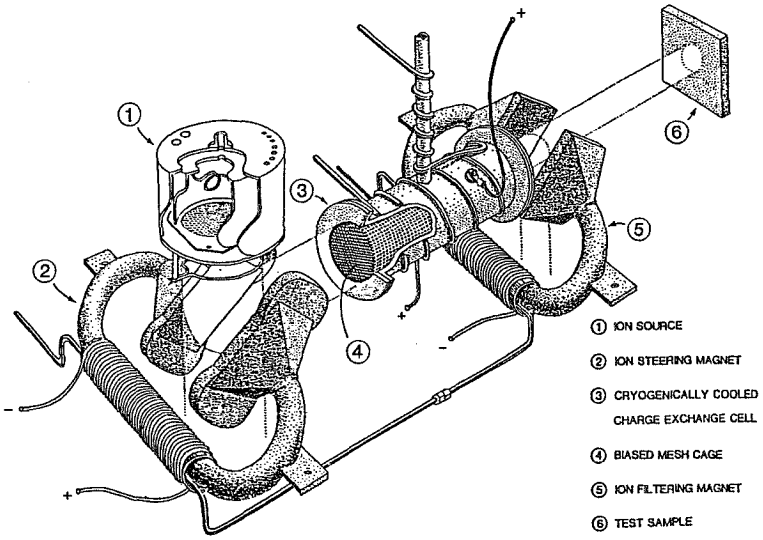

Fig. 5 - Sketch of atomic oxygen beam system components.

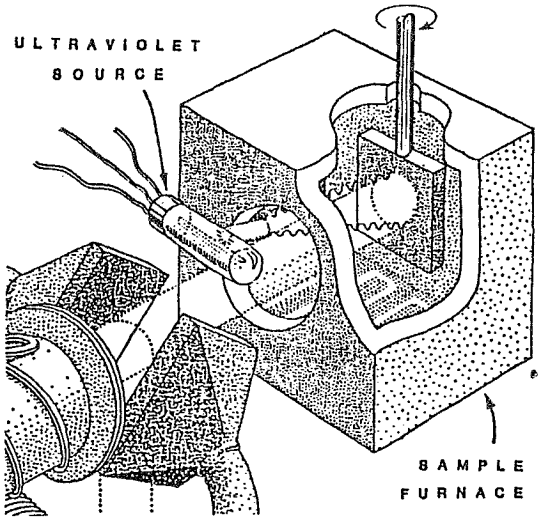

Fig. 6 - Target sample holder configuration.

PULSED SOURCE OF ENERGETIC ATOMIC OXYGEN

George E. Caledonia and Robert H. Krech
Physical Sciences Inc.
Research Park, P.O. Box 3100
Andover, MA 01810

ABSTRACT

A pulsed high flux source of nearly monoenergetic atomic oxygen has been designed, built, and successfully demonstrated. Molecular oxygen at several atmospheres pressure is introduced into an evacuated supersonic expansion nozzle through a pulsed molecular beam valve. An 18J pulsed CO_2 TEA laser is focused to intensities $> 10^9$ W/cm^2 in the nozzle throat to generate a laser-induced breakdown. The resulting plasma is heated in excess of 20,000 K by a laser-supported detonation wave, and then rapidly expands and cools. Nozzle geometry confines the expansion to promote rapid electron-ion recombination into atomic oxygen. We have measured average O-atom beam velocities from 5 to 13 km/s at estimated fluxes to 10^{18} atoms per pulse. Preliminary materials testing has produced the same surface oxygen enrichment in polyethylene samples as obtained on the STS-8 mission. Scanning Electron Microscope examinations of irradiated polymer surfaces reveal an erosion morphology similar to that obtained in low earth orbit, with an estimated mass removal rate of $\sim 10^{-24}$ cm^3/atom. The characteristics of the O-atom source and the results of some preliminary materials testing studies will be reviewed.

INTRODUCTION

Satellites in low-earth orbit sweep at velocities of ~8 km/s through a rarefied atmosphere which consists primarily of atomic oxygen. Experimental pallets flown on Shuttle missions STS-5 and STS-8 clearly demonstrated a dependence of material degradation and mass loss on the ram direction atomic oxygen exposure.(1-4) These experiments indicate that most hydrocarbons and active metals are highly reactive, whereas material containing silicones, fluorides, oxides and noble metals are moderately inert. For Kapton,® an important aerospace polymer, it was observed that about one in ten atomic oxygen interactions lead to mass loss due to chemical reaction.(2,3)

The need for continued material degradation studies has been emphasized in a study by Leger et al.(5) where it was demonstrated that atomic oxygen induced material degradation could have a severe impact on the performance of Space Station. The EOIM-3 material pallet, with sophisticated instrumentation to detect atomic oxygen reaction products and to study reaction mechanisms, is scheduled to be deployed on a future Shuttle mission, and NASA is actively pursuing the development of various hardening techniques to make materials more impervious to the effects of energetic atomic oxygen interactons.

The recent setbacks in launch capability have reemphasized the need for a high flux atomic oxygen source which can be used to study material degradation. Although in-flight experiments provide valuable test data, the large

matrix of materials and test parameters, and uncertain flight scheduling now mandate that most of these studies be performed in a ground test facility.

A high flux source of atomic oxygen has been developed at Physical Sciences Inc. (PSI) based on years of research in the area of pulsed laser propulsion.(6-8) The basic concept is to rapidly introduce a burst of gas into an evacuated nozzle and then to focus the output of a pulsed laser to cause a breakdown at the nozzle throat. The subsequent laser-initiated detonation wave will heat the major portion of the gas during the laser pulse creating a high temperature plasma. This plasma will then expand through a nozzle tailored to allow electron-ion recombination but not atomic recombination. As the gas expands its temperature and density will drop, however, its directed velocity increases correspondingly, producing a thermally "cold," high energy beam of oxygen atoms at the nozzle exit. This technique has been utilized to produce a high velocity O-atom source for material degradation studies. For example with 10^{-4}g of gas and a 5J laser pulse we predict formation of $>10^{18}$ oxygen atoms with a characteristic energy of 5 eV. For comparison with other sources, if the source is pulsed at 10 Hz, an average flux of $>10^{17}$ O-atoms/cm^2-s can be maintained on a 100 cm^2 target.

In our research effort at PSI we have constructed a small test facility to demonstrate that high velocity oxygen atoms can be produced. A series of measurements have been performed to demonstrate the presence of atomic oxygen and the measured velocities agreed with theoretical predictions. Measurements of the material degradation of O-atom irradiated targets are being performed, and these experimental observations are described. The design of a larger O-atom test facility presently under construction is also presented.

FACILITY DESCRIPTION

The present test facility consists of a stainless steel high vacuum chamber in which oxygen gas is rapidly pulsed through a conical expansion nozzle and laser heated by a pulsed CO_2 laser to temperatures above 20,000 K.

A schematic diagram of the apparatus is shown in Fig. 1. The vacuum chamber is a standard 20 cm diameter five-way stainless steel high vacuum cross with Con-Flat flanges. Each sidearm extends 20 cm from the center of the chamber. A sixth 10.0 cm diameter port was welded to the bottom of the chamber for evacuation. The top flange of the vacuum chamber has two radiometers for time-of-flight velocity measurements into the chamber. The pulsed valve/nozzle assembly is mounted on the end flange which also contains vacuum feed-throughs for electrical connections. The opposing flange holds the laser focusing lens. Each side

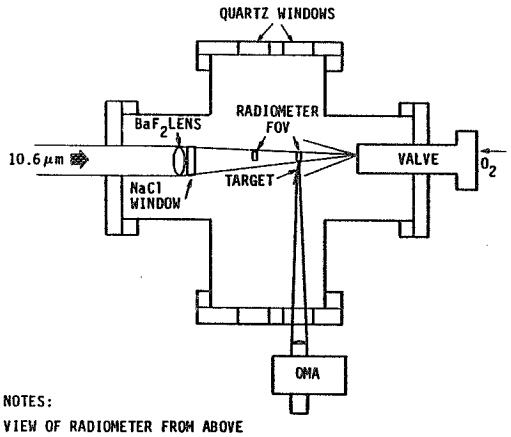

Fig. 1. Schematic diagram of O-atom apparatus

flange has two 5 cm diameter quartz view-ports for visual and spectroscopic observations.

The bottom flange is connected to a 10 cm diffusion pump stack equipped with an ionization gauge readout. The ultimate pressure in the chamber is 3×10^{-5} torr. In operation the chamber pressure is kept below 1×10^{-4} torr, to prevent beam interaction with the background gas. (Mean free path at 10^{-4} torr is 50 cm which is greater than the chamber length and is sufficient to provide a "collision free" environment.) The pumping speed of the vacuum chamber is sufficient to allow introduction of a pulse of 10^{-4}g of oxygen at 1 Hz into a background pressure below 1×10^{-4} torr.

The pulsed valve/nozzle assembly is shown schematically in Fig. 2. The valve is a modified Model BV-100V pulsed molecular beam valve from Newport Research, Inc. This valve allows the generation of short duration pulses of gas at high flowrates which cannot be continuously maintained under high vacuum conditions due to pumping speed limitations. The valve is operated with a 1 mm i.d. orifice plate, and is bolted directly to a 100 mm long, 20 deg full angle aluminum expansion nozzle with a 1 mm i.d. throat. The choked flowrate of the valve/nozzle assembly is 0.19g of oxygen per second per atmosphere stagnation pressure.

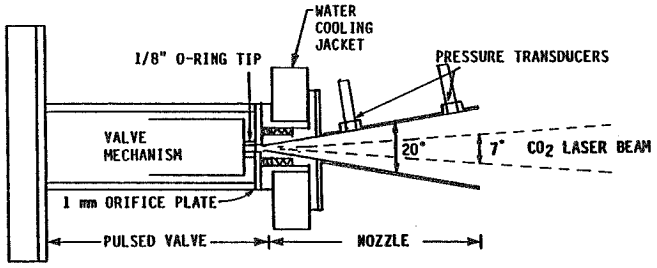

Fig. 2. O-atom source pulsed valve/ nozzle assembly

The nozzle has two flush mounted pressure transducers located 43 and 93 mm from the throat with 1 μs response time and 20 mV/psia sensitivity.

A Laser Applications Limited TEA CO_2 laser is used to generate 18J pulses of 10.6μ radiation. The energy is delivered in a 2.5 μs pulse, with approximately one-third of the energy delivered in the first 200 ns. The radiation in the gain switched spike generates a laser induced breakdown in the high pressure oxygen at the nozzle throat forming a plasma which continues to absorb the radiation as long as the laser is on.

The laser beam is directed to the test chamber by three gold turning mirrors (Fig. 3). A barium fluoride flat between the second and third mirror reflects eight percent of the beam to a calorimeter to monitor the laser energy. A 300 mm focal length barium fluoride lens is used to focus the laser beam to ~1 mm diameter spot size at the nozzle throat.

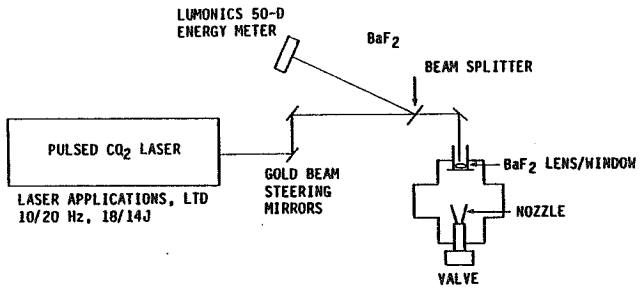

Fig. 3. Laser/optics assembly

BEAM DIAGNOSTICS

Optical measurements have been conducted to characterize the laser initiated O-atom beam. Beam velocities from 5 to 13 km/s were obtained by varying both the stagnation pressure and the laser energy. The velocities were deduced by monitoring the time history of the 777.3 nm atomic oxygen line emission with two filtered radiometers mounted on the top flange of the vacuum chamber.

The spectral measurements of the O-atom beam, and target interactions have been obtained using a Princeton Instruments Optical Multichannel Analyzer (OMA). The OMA head consists of a 1024 photodiode array with a gated S-20R intensifier. The spectrograph is a Jarrel Ash 0.275m MARK X with interchangeable grating, and a maximum resolution of 3Å. The optical field of view in the chamber was restricted to a 0.090 x 0.90 cm rectangle by a collecting telescope matched to the f number of the spectrograph. Glass cut-on filters were used to prevent second and higher order spectra from being recorded.

Spectra are recorded using the OMA in the gated mode. The diode array was gated on 5 μs after the laser trigger to prevent detection of scattered breakdown radiation. A number of spectral scans of the radiation from the expanded oxygen plasma were performed over the wavelength range of 400 to 800 nm. Results were highly reproducible. The strongest signals arose from atomic oxygen emission at 777 nm. No evidence of O_2 emission was identified, however, some atomic hydrogen emission was observed due to laser ablation of the valve tip elastomers, and H_2O impurities in the oxygen feed gas.

Characterization of the beam has been also performed by ballistic pendulum measurements of the cold and hot flows. This has allowed quantization of the atomic flow rate to within a factor of two. Refinements in the larger test facility, primarily a time-of-flight mass spectrometer probe, will further reduce this uncertainty.

PRELIMINARY MATERIAL DEGRADATION STUDIES

Preliminary material degradation studies have been conducted with the small test facility. Materials irradiated have included polyethylene, Teflon®, Kapton® (untreated and oxidation resistant treated samples), Mylar®, PEEK, PBT and Carbon Epoxy composites.

Ground-based testing facilities must produce a surface morphology and mass removal rate similar to that produced on orbit to provide meaningful erosion data. Typical erosion morphology of a polymeric sample is shown in Fig. 4 (graciously provided by J.T. Visentine), for exposure levels of 5 to 9 x 10^{20} O-atom/cm^2, corresponding to ~1 week on orbit. Kapton samples irradiated in our facility to an exposure level of ~3.3 x 10^{20} O-atom/cm^2 show a remarkably similar surface morphology Fig. 5, and measurable mass loss (~1.3 mg). (Fig. 6 shows a sample of Kapton 500H prior to exposure for comparison.) This morphology is not due to kinetic energy alone since another sample of Kapton was bombarded with ~5 eV Ar (Fig. 7) and showed no mass loss. Similar results were obtained with low and high density polyethylene samples.

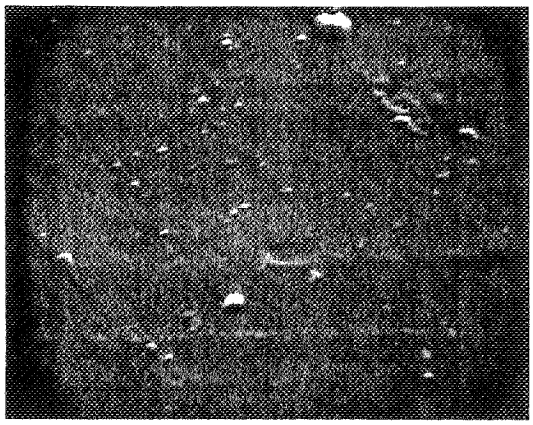

PRIOR TO EXPOSURE
(10,000x)

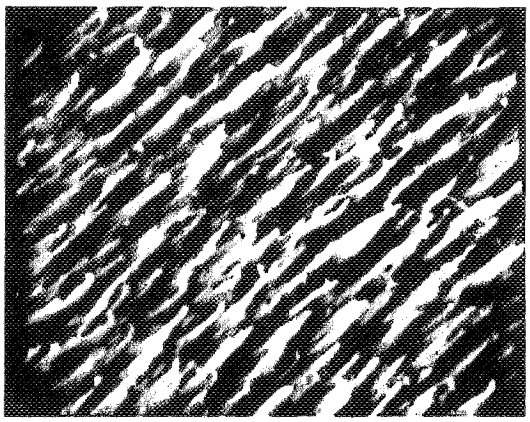

AFTER ATOMIC OXYGEN EXPOSURE
(10,000x)

Fig. 4. SEM photograms of STS-8 Kapton specimens

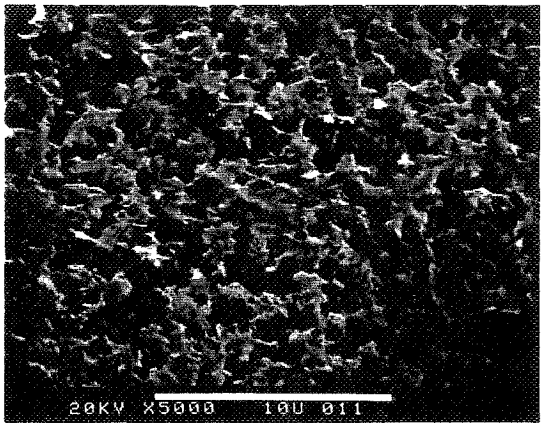

AFTER 12000 PULSES (~$3 \times 10^{20}/cm^2$)

Fig. 5. Kapton 500H after 12,000 pulses (~3 x $10^{20}/cm^2$)

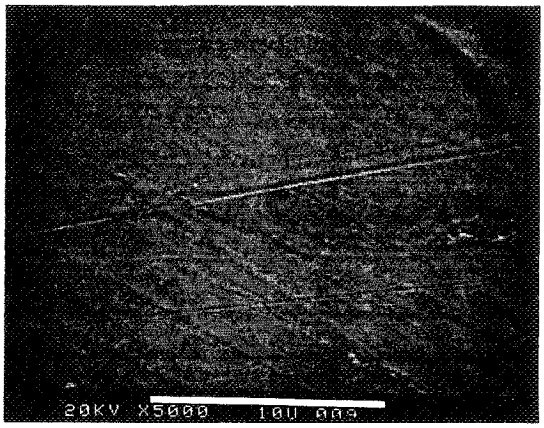

BEFORE EXPOSURE

Fig. 6. Kapton 500H before exposure

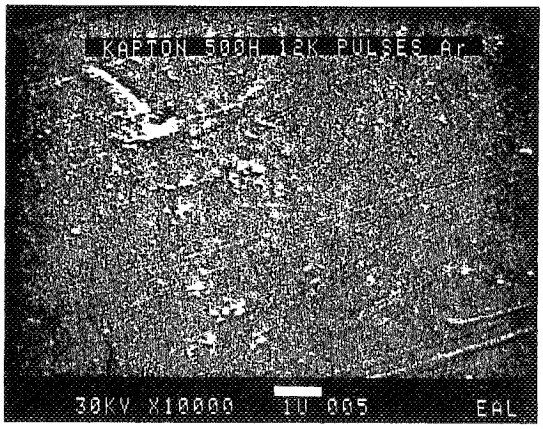

Fig. 7. Kapton 500H irradiated by 5 eV Ar for 12,000 pulses

Current capabilities provide for exposure rates of ~1.5 x 10^{20} atom/cm^2-hr at ~5 eV (~1.6 Hz); and provide an exposure acceleration factor of 50 compared to LEO and 5000 for space station altitudes for ~6 cm^2 samples. A larger facility described below will allow for further accelerated testing.

DESIGN OF LARGE-SCALE TEST FACILITY

The small test facility produces high density O-atom beams, but cannot irradiate large sample areas. Using the same techniques, we are constructing a large chamber to allow the testing of larger samples (~15 cm diameter) at a 10 to 20 Hz pulse rate.

In order to accommodate larger samples, or many smaller ones, the new chamber will be 40 cm o.d. six-way cross assembly. A chamber this size allows for convenient sample access, mass spectrometer probes for beam and target product analysis, in situ mass loss measurement, velocity dependent measurements and target irradiation by a UV solar simulator. A schematic of the chamber is shown in Fig. 8.

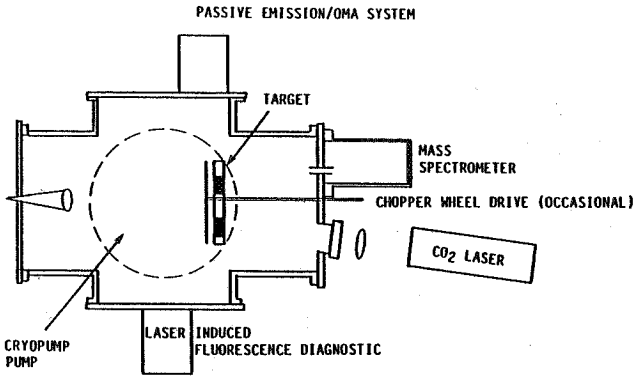

Fig. 8. Schematic of new O-atom facility

A Varian cryopump with a speed of ~3000 ℓ/s will maintain 10^{-4} torr in the chamber with a gas load of 10^{-3} g/s. A cryopump was chosen to eliminate any possible contamination of test samples by back diffusion of pump oil.

Two quadrupole mass spectrometer systems will be coupled to the main chamber. A Balzers QMS 311 will be used to monitor the atomic beam. It will sit in a differentially pumped chamber, separated from the main chamber by a sampling orifice. This QMS will monitor the pulse to pulse reproducibility of the O-atom beam, and when cross calibrated with the laser induced fluorescence diagnostic, will provide a real time quantitative O-atom detector. A second QMS will be suspended from the top flange of the chamber to monitor the reaction products of the atomic oxygen/interaction and will be mounted to allow for rotation with respect to the target for angular product dependence studies.

The pulsed CO_2 laser system was manufactured by Laser Applications Limited and provides 18J per pulse at 10 Hz. This allows a sufficient margin for transmission and reflection losses to process ~10^{-4}g bursts of gas into 5 eV O-atoms. Furthermore an option for 20 Hz operation is available to provide a higher throughput.

A Quantel 10 Hz YAG pump dye laser system will be used for multiphoton laser induced fluorescence detection of atomic oxygen. Approximately 1 mJ at 226 mm can be obtained for the excitation of ground state atomic oxygen

($2p^4{}^3P \rightarrow 2p^3 3p^3P$) with subsequent fluorescence around 845 nm from the $3_p{}^3P \rightarrow 3_s{}^3S$ transitions in atomic oxygen, and the same technique can be used to detect the 1_D and 1_S metastables.

SUMMARY

Our goal is to build a reliable ground based energetic O-atom test facility which will be able to meet the NASA material testing requirements.

The concepts of the design have been demonstrated both experimentally and theoretically, and the technique exploits the characteristics of existing commercially available high power laser technology. At present repetitively pulsed CO_2 lasers provide the most convenient source of laser radiation in terms of reliability, cost and delivered energy.

With a 10 Hz pulse rate, the device will conservatively irradiate a 100 cm^2 area with $>10^{17}$ atoms/cm^2-s. In less than 2 hr of operation under these conditions, energetic oxygen atom fluences of $7 \times 10^{20}/cm^2$ will be possible over the exposed area. For comparison this O-atom fluence is equivalent to that seen by a ram direction shuttle surface for an entire week-long mission in low earth orbit (250 km) and is equivalent to the fluence seen by a ram surface of the Space Station at 500 km altitude during the course of an entire year (during a year of average solar activity). Although questions can be raised by accelerated testing, this new facility will provide the ability to identify materials most affected by O-atoms (which can then be tested further on-orbit), to systematically separate effects of UV irradiation, temperature, and O-atom energy, to study the rate of change of recession/material loss as surfaces change character, and to identify failure points (most susceptible to erosion) in assemblies such as solar cells. The importance of such effects has been clearly demonstrated in recent Space Shuttle flights.(5, 9-11).

With this new test facility we can perform quantitative erosion testing of materials, components, and even small assemblies (such as a solar cell array) in order to determine components or interfaces which are most vulnerable to O-atom erosion. This ground-based facility will allow accelerated testing to identify structures or materials which are in most critical need of protection so that remedial strategies or protective coatings can be developed and even tested in this ground test facility at a fraction of the cost and in a much more timely manner than on-orbit.

REFERENCES

1. Leger, L.J., Spiker, I.K., Kuminecz, J.F., and Visentine, J.T., "STS Flight 5 LEO Effects Experiments--Background Description and Thin Film Results," AIAA Paper 83-2631-CP, October 1983.

2. Leger, L.J., Visentine, J.F., and Kuminecz, J.F., "Low Earth Orbit Atomic Oxygen Effects on Surfaces," AIAA Paper 84-0548, January 1984.

3. Visentine, J.T., Leger, L.J., Kuminecz, J.F., and Spiker, I.K., "STS-8 Atomic Oxygen Effects Experiments," Paper presented at AIAA 23rd Aerospace Sciences Meeting, Reno, NV, January 1985.

4. Green, B.D., Caledonia, G.E., and Wilkerson, T.D., "The Shuttle Environment: Gases, Particulates and Glow," J. Spacecraft and Rockets 22, 5 Sept-Oct 1985, 500-511.

5. Leger, L.J., Visentine, J.T., and Schliesing, J.A., "A Consideration of the Atomic Oxygen Interactions with Space Stations," AIAA 85-0476, January 1985.

6. Simons, G.A. and Pirri, A.N. "The Fluid Mechanics of Pulsed Laser Propulsion," AIAA J. 15, 835 (1977).

7. Rosen, D.I., Pirri, A.N. Weiss, R.F., and Kemp, N.H., "Repetitively Pulsed Laser Propulsion: Needed Research," In progress in Astronautics and Aeronautics Vol. 89 (1985), ed. L.H. Caveny, pp. 95-108.

8. Rosen, D.I. Kemp, N.H., Weyl, G., Nebolsine, P.E., and Kothandaraman, G., "Pulsed Laser Propulsions Studies," Physical Sciences Inc. Technical Report TR-184, 1981.

9. Hall D.F. and Stewart, T.B., "Photo-Enhanced Spacecraft Contamination Deposition," AIAA 85-0953, June 1985.

10. Peterson, R.V. Hanna, W.D., and Mertz, L.O., "Results of Oxygen Atom Interaction with Kevlar and Fiberglass Fabrics on STS-8," AIAA 85-0990, June 1985.

11. Knopf, P.W. Martin, R.J., McCargo, M., and Dammann, R.E., "Correlation of Laboratory and Flight Data for the Effects of the LEO Atomic Oxygen on Polymeric Materials," AIAA 85-1066, June 1985.

ACKNOWLEDGMENT

This work is funded by NASA under Contract NAS7-936 and monitored by the Jet Propulsion Laboratory. The authors appreciate the efforts of Dr. David I. Rosen who acts as a technical reviewer for the program at PSI.

PRODUCTION OF PULSED ATOMIC OXYGEN BEAMS VIA LASER VAPORIZATION METHODS

David E. Brinza, Daniel R. Coulter, Ranty H. Liang and Amitava Gupta

Chemical and Mechanical Systems Division
Jet Propulsion Laboratory
California Institute of Technology
Pasadena, CA 91109

Abstract

Energetic pulsed atomic oxygen beams have been generated by laser-driven evaporation of cryogenically frozen ozone/oxygen films and thin films of indium-tin oxide (ITO). Mass and energy characterization of beams from the ozone/oxygen films have been carried out by mass spectrometry. The peak flux, found to occur at 10 eV, is estimated from the data to be $3 \times 10^{20} m^{-2} S^{-1}$. Analysis of the time-of-flight data indicates a number of processes contribute to the formation of the atomic oxygen beam. The absence of metastable states such as the $2p^3 3s^1(^5S)$ level of atomic oxygen blown-off from ITO films is supported by the failure to observe emission at 777.3 nm from the $2p^3 3p^1(^5P_J)$ levels. Reactive scattering experiments with polymer film targets for atomic oxygen bombardment are planned using a 35" universal crossed molecular beams apparatus.

1. INTRODUCTION

Atomic oxygen-induced degradation of various materials in low earth orbit (LEO) is a problem of current concern for engineers involved with selection of materials for Space Station and other LEO missions[1]. Flight experiments carried out onboard a number of space shuttle flights have attempted to characterize the interaction of atomic oxygen bombarding organic polymeric[2-4], paint[3-4], and metal[5] surfaces with a relative energy of 5 eV and a flux of about $10^{19} m^{-2} S^{-1}$. These flight experiments have provided an engineering database of erosion rates for a wide variety of materials[6], but do not provide much insight into the mechanisms of the gas-surface chemistry involved in the material degradation processes. For the DuPont polyimide Kapton, a thermal blanketing material, preferential attack at the phenyl ring positions by oxygen is indicated from comparison of resonance Raman spectra of exposed and control specimens[2]. A future flight experiment, entitled Evaluation of Oxygen Interaction with Materials (EOIM-3)[7], will attempt to directly detect products of atomic oxygen interaction with selected materials using the AFGL ion-neutral mass spectrometer. Uncertainty in NASA mission planning for the STS in the near future, though, has placed new emphasis on the development of ground-based capability to study the atomic oxygen degradation problem in a detailed fashion.

A number of approaches have shown considerable promise in simulating the effects of atomic oxygen bombardment on materials. A dc arc discharge source has been employed to study the interaction of atomic oxygen with Kapton[8] and amorphous carbon[9-10] at energies up to 1 eV. The results from these studies are encouraging, as the rates of erosion of the materials were found to be in good agreement with those found on the shuttle. The possibility has not been ruled out that a synergism between atomic oxygen bombardment and ultraviolet radiation from the arc, or metastable contamination of the beam may have strongly influenced the measured erosion rates. A source using a CO_2 laser-sustained plasma, under development at Los Alamos[11], has yielded beams of higher kinetic energy but suffers from the

same problem of uv and/or metastable interference. A pulsed source utilizing a CO_2 TEA laser focussed in pure O_2 to initiate a blast wave in the throat of a conical nozzle[12] has been demonstrated to produce $> 10^{18}$ oxygen atoms per pulse at velocities in excess of 11 km S^{-1}. The velocity distribution from this source was determined via monitoring of the 777.3 nm emission from the ^5P level of atomic oxygen, a direct indication of the presence of high-energy metastable atoms in the beam. The spark from the focussed laser also produces intense ultraviolet radiation which may affect the surface chemistry unless the sample is protected from exposure during the laser pulse. Other sources, utilizing charge exchange[13] or electron detachment of ion beams[14], are currently under consideration, but such sources suffer from low fluxes and have therefore not been utilized in material degradation studies.

An alternative scheme for production of energetic atomic oxygen beams involves a technique known as laser blow off. This method has been successfully used to generate pulsed metal atom beams in the 1 – 20 eV energy range[15]. A thin coating of metal on a transparent substrate mounted in vacuum is irradiated by a focussed high energy laser directed at the target film from the substrate side. The metal film is vaporized and an intense pulse of energetic metal atoms is produced. The ion content of beams produced from rear surface irradiated films is greatly reduced compared to that of beams produced by front surface laser evaporation of materials.

This paper describes the extension of the laser blow off technique to produce beams of atomic oxygen from films of frozen ozone/oxygen mixtures or indium-tin oxide. Analysis of the time-of-flight data for the atomic oxygen beams is performed and a physical interpretation of the processes occurring in the ozone/oxygen film is suggested. In a separate experiment, spectroscopic evidence indicating the formation of metastable atomic states of oxygen could not be observed for the laser blow off of ITO films. The utility of the source for future mechanistic studies of the interaction of energetic oxygen atoms is explored.

2. EXPERIMENTAL DETAILS

A schematic representation of the apparatus used for generation of the atomic oxygen beams is shown in Figure 1. An excimer laser (Lumonics Model 861-S), operated with the KrF lasing mixture (248 nm, 100 mJ/pulse), is focussed into the target by a 20 cm focal length quartz lens mounted in tandem with a 45° angle of incidence dielectric turning mirror (CVI, Inc.) on a x-y translation stage. A 1-inch diameter Supracil 1 window transmits the laser radiation into the vacuum apparatus. The vacuum apparatus consists of $2\frac{3}{4}$-inch Conflat flanged fittings attached to a 4-inch diameter chamber containing the quadrupole mass analyzer. A liquid nitrogen trapped 2-inch diffusion pump provides pumping in the region of the cold window. A 50 ℓ S^{-1} ion pump is used in the quadrupole analyzer region to maintain vacuum in the low 10^{-8} torr range.

The target substrate is a $\frac{1}{2}$-inch diameter sapphire window (ESCO Optics, Inc.) supported by a copper mount in thermal contact with the 10K stage of a cryogenic refrigeration unit (CTI Model 21). An Au-Fe/Chromel thermocouple mounted near the cold window permits determination of the temperature of the window during the course of the experiment. The temperature typically will reach 20-25K at the window mount with appropriate shielding of the cold stage. Thin films of ozone/oxygen mixtures are prepared by permitting pre-mixed gaseous ozone and oxygen to flow through the nozzle of a movable doser onto the cold sapphire window. Ozone is collected on silica gel at −78° C after formation in a corona discharge of flowing oxygen (Matheson, Ultra-High Purity). The composition of the film is established by admitting the appropriate partial pressures of ozone and oxygen into a calibrated volume.

The thickness of the film is determined by the quantity of gas allowed to flow through the nozzle of the doser. No independent determination of film thickness is made during the course of the experiment.

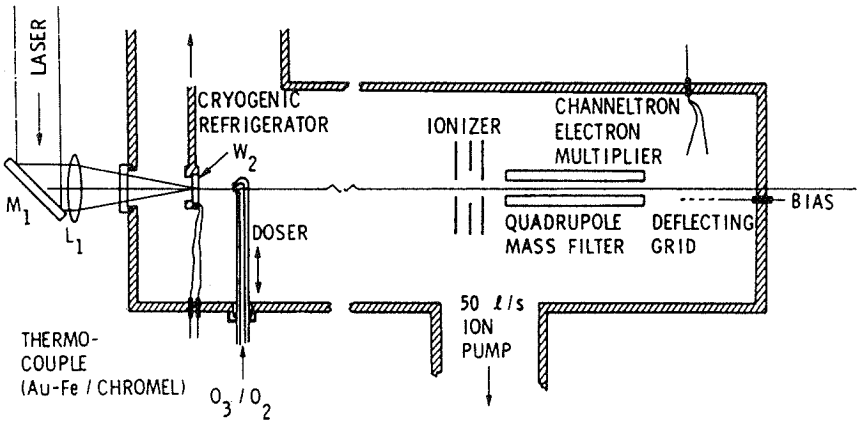

Figure 1. Schematic representation of the apparatus for laser blow off time-of-flight measurements from cryogenic films.

Measurements of the time-of-flight of the individual constituents in the beam are made on a single shot basis. The laser focussing lens is positioned to allow the beam to strike a new spot on the film for each shot. The quadrupole mass analyser (EAI 300), with the ionizer located 30 cm from the target, is tuned to the desired m/e to be transmitted. The transmitted ions are deflected by a biased grid into a channeltron electron multiplier (Galileo Electro-optics CEM 4700) placed off-axis to prevent interference from the laser pulse or fast neutral species unaffected by the quadrupole mass analyzer. A 100 MHz transient waveform recorder (Biomation 8100), triggered by a photodiode monitoring the laser, captures the amplified output of the channeltron electron multiplier. The signal is then output to an X-Y recorder. The recorded time-of-flight traces were digitized at 3 microsecond timebase intervals and the data stored on magnetic disk for subsequent analysis.

For the attempts to observe metastable oxygen emission, a 1-micron thick ITO film deposited on glass (Applied Films, Inc.) was mounted on an x-y translation stage in a 10-inch vacuum cross. A Nd:YAG laser (Quanta-Ray DCR2A-20) operating on the third harmonic (355 nm, 50 mJ/pulse) and focussed by a 40-cm focal length lens was directed into the rear surface of the film through a Supracil 1 window on the chamber. An IP-28 photomultiplier tube (RCA) viewed a region 20-cm downstream from the target film through a 630 nm cut-off filter (Schott) and window on a perpendicular arm of the vacuum cross. The output of the PMT was viewed on an oscilloscope synchronized to the laser pulse.

3. RESULTS

Time-of-flight traces for KrF laser blow-off of an approximately 0.3 micron thick film composed of 20% ozone in solid oxygen are shown in Figure 2. The m/e=16 trace corresponds to signal due to O^+ ion transmitted through the mass filter on a single laser shot. The m/e=32 trace is due to molecular

O_2^+ on a subsequent laser shot. Both traces in the figure have been corrected for transit time through the mass spectrometer according to:

$$(v_1^2 + v_0^2)^{1/2}(tv_1 - d_1) - d_2 v_1 = 0 \tag{1}$$

where v_1 is the initial velocity of the particle prior to ionization, v_0 is the velocity of an ion initially at rest after acceleration by the ion energy potential V (11 eV), t is the total transit time from target to detector, d_1 is the distance from the target to the ionizer (30 cm) and d_2 is the distance from the ionizer to the detector (20 cm). Equation (1) is solved numerically for v_1 at each time-channel in the raw data to obtain the corresponding arrival time at the ionizer. The time-of-flight data is then mapped onto a uniform timebase by linear interpolation of the intensities on the corrected timebase.

The signal detected for m/e=32 indicates some molecular oxygen is present in the beam. Since molecular oxygen undergoes dissociative ionization, there will be a contribution due to molecular oxygen in the m/e=16 time-of-flight trace. The electron-impact ionization processes and corresponding probabilities for molecular oxygen are:

$$O_2 \longrightarrow O_2^+ + e^- \qquad P_{O_2^+} = 0.7 \tag{2}$$

and

$$O_2 \longrightarrow O^+ + O + e^- \qquad P_{O^+} = 0.3 \tag{3}.$$

The contribution of the O_2 dissociative ionization component in the m/e=16 time-of-flight signal may be removed by subtracting m/e=32 data corrected for m/e=16 transit time and scaled by the appropriate factor. This scaling factor is given by the ratio of probabilities for dissociative ionization to simple ionization:

$$\frac{P_{O^+}}{P_{O_2^+}} = 0.43 \tag{4}.$$

The effect of this correction to the m/e=16 data is shown in the lower trace of Figure 3.

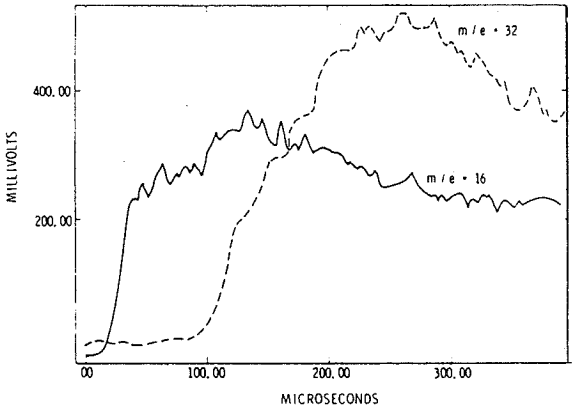

Figure 2. Time-of-flight traces of $m/e = 16$ and $m/e = 32$ for laser blow off from a 0.3 micron film of frozen ozone/oxygen.

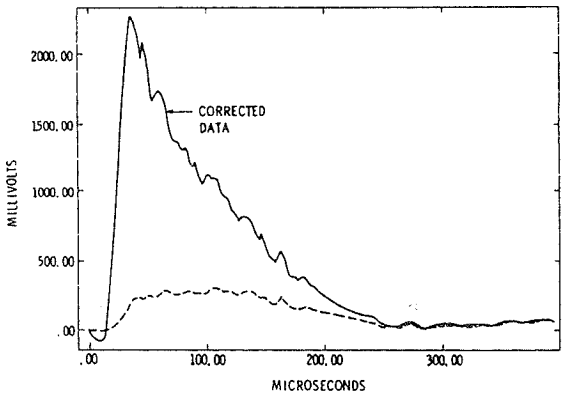

Figure 3. The dashed line corresponds to the $m/e = 16$ signal corrected for dissociative ionization of O_2. The solid line represents the $m/e = 16$ data corrected for finite residence time in the ionizer.

The corrected data now represents a signal proportional to the number density of atomic oxygen in the ionizer as a function of time after the laser pulse. It is desirable to extract from this data the flux of atomic oxygen arriving at the ionizer from this data. This procedure must take into account the dependence of ionization probability upon the residence time in the ionization region of the mass analyzer. The probability of ionization as a function of time would be expected to follow the typical survival equation:

$$P(t) = 1 - \exp(-t/\tau) \tag{5}$$

where τ is some characteristic time of the particular ionizer. Since the efficiency of standard electron-impact ionizers is on the order of 10^{-5}, the series expansion of equation (5) may be cut off at the linear term. In other words, the probability of ionization is inversely proportional to the velocity of the incident neutral. The number density data is converted to an intensity proportional to the flux by multiplying the data by a scale factor proportional to velocity which is set to unity at sufficiently long time ($\approx$ 400 microseconds). Below a minimum cut-off time ($\approx$ 20 microseconds), the scale factor is kept constant to avoid excessive amplification of noise at short times. The result of the conversion of the data is illustrated in Figure 3.

An estimate of the absolute flux of atomic oxygen arriving at the ionizer was made in the following manner. A sensitivity factor for the mass spectrometer was obtained by addition of known pressures of molecular oxygen to the system and summing the signal strengths of the m/e=16 and m/e=32 features for operating conditions identical to those for the time-of- flight measurements. The sensitivity factor is then scaled by the ratio of cross-sections for ionization of atomic oxygen to molecular oxygen. The larger ionization volume for static gas measurements compared to that for beam measurements is also taken into account. Figure 4 illustrates the atomic oxygen intensity plotted against translational energy. The peak flux occurring at 10 eV is estimated (within a factor of five) to be $3 \times 10^{20} m^{-2} S^{-1}$. This flux is comparable to values observed for laser blow-off of metal films [15].

The optical measurements for laser blow off from ITO films showed no indication of emission at the 777.3 nm line of oxygen. A small quantity of nitric oxide (NO) gas was metered into the vacuum chamber to establish the presence of atomic oxygen via recombination glow of the excited NO_2 product:

$$NO + O \longrightarrow NO_2^* \longrightarrow NO_2 + h\nu \tag{6}.$$

The recombination glow was observed downstream from the target after the laser pulse, indicating the production of atomic oxygen in the blow off process.

4. DISCUSSION

The technique of laser blow-off using films of ozone and oxygen is shown to produce intense, energetic beams of atomic oxygen. The energy spectrum of the beam, as graphically illustrated in Figure 4, indicates that the source would be useful in mechanistic studies where effects of varying the translational energy of the incident atomic oxygen on material surfaces are investigated. A simple rotating chopper, synchronized to the laser triggering, would permit the study of the effect of incident energy variation of atomic oxygen across the sample surface. The chopper would obstruct laser light used by the blow off source from striking the portion of the surface under atomic oxygen bombardment. Molecular oxygen would also be prevented from striking a portion of the sample surface since, as can be witnessed in Figure 2, its velocity is considerably less than that of atomic oxygen.

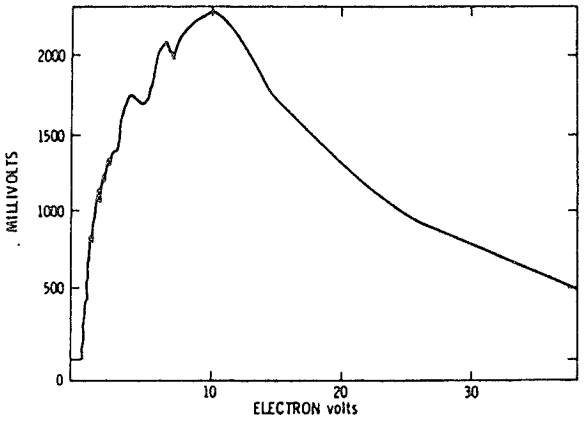

Figure 4. Flux of atomic oxygen plotted against translational energy for laser blow off from an ozone/oxygen film.

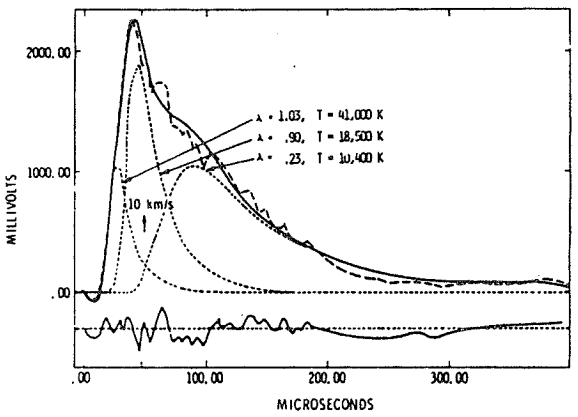

Figure 5. Results of fitting the sum of three components in the form of equation(8) to data observed for blown-off atomic oxygen from a solid ozone/oxygen film.

The observation that molecular oxygen appears to "straggle" behind the arrival of atomic oxygen is somewhat curious. The laser blow off source, as developed by Friichtenicht [15], generates a bubble of expanding gas moving with a center-of-mass flow velocity. As in seeded nozzle beams, little slippage in the velocity of heavier components in the beam is expected. In order to attempt to understand what may be occurring in the blown-off ozone/oxygen films, the time-of-flight data for m/e=16 flux was analyzed according to the model developed by Utterback, *et al.*[16].

The basis for the laser blow off model is a gas bubble expanding spherically in the center-of-mass frame according to a Boltzmann velocity distribution. In the model, the center-of-mass velocity is simply related to the root mean square velocity of this Boltzmann distribution by a multiplier λ:

$$v_{com} = \lambda v_{rms} \tag{7}$$

For on-axis detection, the equation relating the flux arriving at a detector a distance d from the target as a function of time t is:

$$\phi(t) = \frac{N_0}{4\pi}\left(\frac{m}{kT}\right)^{3/2}\left(\frac{2}{\pi}\right)^{1/2} d/t^4 \exp\left\{-\left(\frac{m}{kT}\right)t^{-2}\left[d - \lambda t\left(\frac{3kT}{m}\right)^{1/2}\right]^2\right\} \tag{8}$$

where m is the mass of the species and T is the temperature of the expanding gas bubble. Note that for $\lambda = 0$, equation (8) describes the particle flux from a pulsed source with a Maxwell-Boltzmann velocity distribution. For the molybdenum atom source analyzed by Utterback *et al.*[16] the value of λ was 1.1, indicating a rather well-developed center of mass flow. A non-linear least squares program was written to fit the observed data to equation (8). The equation was found to fit the data poorly. The program was modified to allow the fitting function to be described by a sum of up to three components of the form shown above. The resulting fit to the data is shown in Figure 5. The use of three components to model the data is not intended to represent a unique description of the time-of-flight data; clearly the fit could be improved by including additional components in the model. The point is that the process occuring in the frozen ozone/oxygen film is not well-described by the simple laser blow off model.

Laser blow off of metal films has been characterized by formation of a confined hot plasma which ingests material until the outer surface of the film is breached. There is evidence [15] that the edge of the film is lifted from the substrate somewhat as the gas bubble breaks out into the vacuum. In essence a miniature nozzle is formed which aids in directing the gas flow along the normal to the surface. A frozen ozone/oxygen film would not be expected to behave in such a manner. Solid ozone and ozone/oxygen mixtures will detonate when triggered by mechanical shocks, electrical sparks, etc. Several processes can therefore be envisioned as taking place in the laser driven ozone/oxygen film. The process leading to the initial escape of film material, which should be somewhat analogous to the blow off process in the metal films, is characterized by the highest temperature (41,000 K) and largest λ (1.03). Subsequent loss of film material would be expected to be due to local detonation of the film material followed by evaporation of the mixture over a larger area due to heating of the substrate. This sequence is qualitatively supported by the m/e=16 and m/e=32 time-of-flight traces in Figure 2, as well as the fitted values for the λ's shown in Figure 5.

Other film materials for generation of atomic oxygen beams via laser blow-off are currently under investigation. The initial selection of the ozone/oxygen system was based on the desire to exclude elements other than oxygen and to produce a film which is highly absorbing at the KrF laser wavelength. The disadvantages of this system include the risks associated with the handling of ozone and the fact that cryogenically frozen films suffer from the tendency to condense water, nitrogen and other background components in the vacuum system. The *in situ* prepared films are rather non-uniform as deduced by shot-to-shot flucuations observed in the intensities of the time-of-flight traces. Materials which are stable under ambient conditions, i.e. certain heavy metal oxides, I_2O_5, etc., are strong candidates for film materials. An important factor in material selection seems to be the tendency not to form ionically-bound species. A laser evaporation study of uranium oxide indicated that the vapor was composed chiefly of UO_2 and UO with very little atomic oxygen or uranium detected[17]. Mass spectrometeric characterization of the blow off from ITO and I_2O_5 films will be performed in the near future. If a more suitable film material than cryogenic ozone/oxygen is found, the laser blow off technique should provide an ideal source of fast atomic oxygen for mechanistic studies of material interactions in the low earth orbit environment.

The recent acquisition of a 35" crossed molecular beams apparatus of the design by Y. T. Lee[18], will permit a wide variety of experiments to be performed in support of understanding the gas-surface chemistry occurring in low earth orbit. The rotatable mass spectrometric detector will allow the measurement of energy and angular distributions for products from bombarded surfaces. More fundamental chemistry of fast atomic oxygen reactions with simpler model compounds (i.e. alkanes, substituted benzenes, etc.) may be explored in great detail to permit extrapolation to the initial encounter of atomic oxygen with polymer molecules on a surface. A thorough understanding of the mechanisms for atomic oxygen interaction may prove crucial in the molecular design of highly resistant new materials.

5. ACKNOWLEDGEMENTS

The authors are grateful to Professors Jesse L. Beauchamp and Aron Kupperman for the loan of the mass spectrometer. Professor Kenneth C. Janda graciously provided laboratory space and the use of the excimer laser. This work was performed at the Jet Propulsion Laboratory under contract for the National Aeronautics and Space Administration.

REFERENCES

1. Leger, L.J., Visentine, J.T., and Schliesing, J.A., "A Consideration of Atomic Oxygen Interactions with Space Station," AIAA Paper 85-0476, Jan. 1985.

2. Liang, R.H., Gupta, A., and Coulter, D.R., "Mechanistic Studies of Kapton Degradation in Shuttle Environment," AIAA Paper 83-2656, Nov. 1983.

3. Leger, L.J., Visentine, J.T., and Kuminecz, J.F., "Low Earth Orbit Atomic Oxygen Effects on Surfaces," AIAA Paper 84-0548, Jan. 1984.

4. Park, J.J., Gull, T.R., Herzig, H., and Toft, A.R., "Effects of Atomic Oxygen on Paint and Optical Coatings," AIAA Paper 83-2635, Nov. 1983.

5. Fromhold, A.T., Jr., Whitaker, A.F., Daneshvar, K., and Little, S.A., "Reaction of Metals in Low Earth Orbit during Space Shuttle Flight 41-G," AIAA Paper 85-7018, Nov. 1985.

6. ENVIRONET, the Shuttle Environment Database, lists degradation properties of a large number of materials. Contact: Michael Lauriente, Mail Code 420, NASA/Goddard Space Flight Center, Greenbelt, MD 20771.

7. Visentine, J.T. and Leger, L.J., "Material Interactions with the Low Earth Orbital Environment: Accurate Reaction Rate Measurements," AIAA Paper 85-7019, Nov. 1985.

8. Arnold, G.S. and Peplinski, D.R., "Reaction of Atomic Oxygen with Polyimide Films," AIAA Journal 23(10), 1621 (1985).

9. *ibid.*, "Reaction of High-Velocity Atomic Oxygen with Carbon," AIAA Journal 24(4), 673 (1986).

10. *ibid.*, "Reaction of Atomic Oxygen with Vitreous Carbon: Laboratory and STS-5 Data Comparisons," AIAA Journal 23(6), 976 (1985).

11. Cross, J.B., "Atomic Oxygen Surface Interactions – Mechanistic Studies Using Ground Based Facilities," AIAA Paper 85-0473, Jan. 1985.

12. Caledonia, G.R. and Krech, R.H., "Development of a High Flow Source of Energetic Oxygen Atoms for Material Degradation Studies," AIAA Paper 85-7015, Nov. 1985.

13. Private communication with Dr. Bruce Banks, NASA/Lewis Research Center, Cleveland, OH.

14. Private communication with Dr. Ara Chutjian, Jet Propulsion Laboratory, Pasadena, CA.

15. Friichtenicht, J.F., "Laser-Generated Pulsed Atomic Beams," Rev. Sci. Instrum. 45(1), 51 (1974).

16. Utterback, N.G., Tang, S.P., and Friichtenicht, J.F., "Atomic and Ionic Beam Source Utilizing Laser Blow Off," Phys. Fluids 19(6), 900 (1976).

17. Magill, J., Bloem, J., and Ohse, R.W., "The Mechanism and Kinetics of Evaporation from Laser Irradiated UO_2 Surfaces," J. Chem. Phys. 76(12), 6227 (1982).

18. Lee, Y.T., McDonald, J.D., LeBreton, P.R., and Hershbach, D.R., "Molecular Beam Reactive Scattering Apparatus with Electron Bombardment Detector," Rev. Sci. Instrum. 40(11), 1402 (1969).

Appendix A:

Abstracts for Poster Session

APPENDIX A: ABSTRACTS FOR POSTER SESSION

CONTENTS

THE PRODUCTION OF LOW-ENERGY NEUTRAL OXYGEN BEAMS BY GRAZING-INCIDENCE NEUTRALIZATION

R.G. Albridge, R.F. Haglund, and N.H. Tolk
Department of Physics and Astronomy, Vanderbilt University
Nashville, TN 37235

A.F. Daech
Martin Marietta Michoud Aerospace
New Orleans, LA 70189

The Vanderbilt University neutral oxygen beam facility produces beams of low-energy neutral oxygen atoms by means of grazing-incidence collisions between ion beams and metal surfaces. Residual ions are deflected by applied electric fields. This unique method can utilize initial ion beams of either O^+ or O_2^+ since a very large percentage of molecular oxygen ions are dissociated when they undergo grazing-incidence neutralization. The method of neutralization is applicable to low-energy beams and to all ions. Our research places particular emphasis on O and N_2 beams for simulation of the low earth orbit space environment. Since the beam is a pure O-neutral beam and since measurements of the interaction of the beam with solid surfaces are made spectroscopically, absolute reaction rates can be determined. The technique permits the beams to be used in conjunction with electron and photon irradiation for studies of synergistic effects. Comparisons of optical spectra of Kapton excited by 2.5-keV O, O^+ and O_2^+ show significant differences. Optical spectra of Kapton excited by neutral oxygen beams of less than 1 keV have been recorded.

An Electrically Conductive Thermal Control Surface for Spacecraft Encountering Low-Earth Orbit Atomic Oxygen Indium Tin Oxide-Coated Thermal Blankets

J. L. Bauer

Mechanical and Chemical Systems Division
Jet Propulsion Laboratory
California Institute of Technology

ABSTRACT

Indium tin oxide (ITO) has been coated over an organic black thermal blanket material to prevent blanket degradation in the low-earth orbit (LEO) atomic oxygen environment. The blankets were designed for JPL's Galileo spacecraft destined to orbit and observe Jupiter. Galileo was initially intended for space shuttle launch and would, therefore, have been exposed to atomic oxygen in LEO for between 10 to 25 hours.

Two processes for depositing ITO are described. Thermooptical, electrical, and chemical properties of the ITO film are presented as a function of the deposition process. Results of exposure of the ITO film to atomic oxygen (from a shuttle flight) and radiation exposure (simulated Jovian environment) are also presented. It is shown that the ITO-protected thermal blankets would resist the anticipated LEO atomic oxygen and Jovian radiation yet provide adequate thermooptical and electrical resistance.

Reference is made to the European Space Agency (ESA) Ulysses spacecraft, which also used ITO protection on thermal control surfaces.

Resonant Enhanced Multiphoton Ionization Studies of Atomic Oxygen

S. N. Dixit†, D. Levin‡ and V. McKoy†

†Caltech, Pasadena, CA 91125
‡Institute for Defence Analyses, Alexandria, VA 22311

In Resonant Enhanced Multiphoton Ionization (REMPI), an atom absorbs several photons making a transition to a resonant intermediate state and subsequently ionizing out of it. With currently available tunable, narrow-band lasers, the extreme sensitivity of REMPI to the specific arrangement of levels can be used to selectively probe minute amounts of a single species (atom) in a host of background material. Determination of the number density of atoms from the observed REMPI signal requires a knowledge of the multiphoton ionization cross sections. In the last year, we have been investigating REMPI of atomic oxygen through various excitation schemes that are feasible with available light sources. Using Quantum Defect Theory (QDT) to estimate the various atomic parameters, we have studied the REMPI dynamics in atomic oxygen incorporating the effects of saturation and a. c. Stark shifts. Results will be presented for REMPI probabilities for excitation through various $2p^3(^4S^o)\ np\ ^3P$ and $2p^3(^4S^o)\ nf\ ^3F$ levels.

A High Flux Source of Swift Oxygen Atoms

M. Fink, D.A. Kohl, J.W. Keto and P. Antoniewicz
The University of Texas at Austin
Austin, Texas 78712

A source of swift oxygen atoms is described which has several unique features. A high current ion beam is produced by a microwave discharge, accelerated to 10 keV and the mass selected by a modified Dupont 21-110 mass spectrometer. The O^+ beam exiting the mass spectrometer is focused into a rectangular shape with an energy spread of less than one eV. The next section of the machine decelerates the ion beam into a counterpropagating electron beam in order to minimize space charge effects. After deceleration, the ion beam intersects at 90°, a neutral oxygen atom beam, which via resonant charge exchange produces a mixture of O^+ and O. Any remaining O^+ are swept out of the beam by an electric field and differentially pumped away while the desired O beam, collimated by slits, impinges on the target. In situ monitoring of the target surface is done by XPS or Auger Spectroscopy. Faraday cups provide flux measurements in the ion sections while the neutral flux is determined by a special torsion balance or by a quadrupole mass spectrometer specially adapted for swift atoms. While the vacuum from the source through the mass spectrometer is maintained by diffusion pumps, the rest of the machine is UHV.

Absolute Flux Measurements for Swift Atoms

M. Fink, D.A. Kohl, J.W. Keto and P. Antoniewicz
The University of Texas at Austin
Austin, Texas 78712

While a torsion balance in vacuum can easily measure the momentum transfer from a gas beam impinging on a surface attached to the balance, this measurement depends on the accomodation coefficients of the atoms with the surface and the distribution of the recoil. A torsion balance is described for making absolute flux measurements independent of recoil effects. The torsion balance is a conventional taut suspension wire design and the Young modulus of the wire determines the relationship between the displacement and the applied torque. A compensating magnetic field is applied to maintain zero displacement and provide critical damping. The unique feature is to couple the impinging gas beam to the torsion balance via a Wood's horn, i.e. a thin wall tube with a gradual 90° bend. Just as light is trapped in a Wood's horn by specular reflection from the curved surfaces, the gas beam diffuses through the tube. Instead of trapping the beam, the end of the tube is open so that the atoms exit the tube at 90° to their original direction. Therefore, all of the forward momentum of the gas beam is transferred to the torsion balance independent of the angle of reflection from the surfaces inside the tube.

Hypervelocity Atomic Oxygen Source for the Study Of Atom-Surface Interactions

By

A. Freedman, W. Unkel, and C. Stinespring

Aerodyne Research, Inc.
45 Manning Road
Billerica, MA. 01821

ABSTRACT

We will describe planned improvements in an electric discharge heated atomic oxygen beam source (Ref. Sci. Instrum. 53, 1714 (1982)) which will, if successful, provide 6-7 kms^{-1} beams of atomic oxygen with a flux of $10^{16} cm^{-2} s^{-1}$ at 50 cm distance from the source aperture. A major advance will be the use of a "zone of silence" nozzle-skimmer arrangement which is necessitated by the need for high source flux and performance. It is anticipated that a Phase II program would provide for the fabrication of a two stage vacuum system which would be suitable for bolting on to a UHV surface study apparatus.

This work is supported by the Air Force Office of Scientific Research.

Reactions of Atomic Oxygen [O(^{3}P)] with Polybutadienes and Related Polymers

Morton A. Golub, Narcinda R. Lerner, and Theodore Wydeven
Ames Research Center, NASA, Moffett Field, California 94035

Thin films of the following polymers were exposed at ambient temperature to ground-state oxygen atoms [O(^{3}P)], generated by a radio-frequency glow discharge in O_2: *cis*- and *trans*-1,4-polybutadienes (CB and TB), amorphous 1,2-polybutadiene (VB), polybutadienes with different 1,4/1,2 contents, *trans* polypentenamer (TP), *cis* and *trans* polyoctenamers (CO and TO), and ethylene-propylene rubber (EPM). Transmission infrared spectra of CB and TB films revealed extensive surface recession, or etching, unaccompanied by any microstructural changes within the films, demonstrating that the reactions were confined to the surface layers. Contrary to the report by Rabek, Lucki, and Rånby (1979), there was no O(^{3}P)-induced cis-trans isomerization in CB (or TB). From weight-loss measurements, etch rates for polybutadienes were found to be markedly dependent on vinyl content, decreasing by two orders of magnitude from CB (2% 1,2) to structures with 30-40% 1,2 double bonds, thereafter increasing by half an order of magnitude to VB (97% 1,2). Relative etch rates for EPM and the polyalkenamers were in the order: EPM > CO (or TO) > TP > CB. The sole non-elastomer examined, TB, had an etch rate about six times that of CB, ascribable to a morphology difference. Cis/trans content had a negligible effect on the etch rate of the polyalkenamers. Mechanisms involving crosslinking through vinyl units are proposed for the unexpected protection imparted to polybutadienes by the 1,2 double bonds.

Chemical Interactions in Low Earth Orbit

B. D. Green
Physical Sciences Inc.
Dascomb Research Park
Andover, MA 01810

Although several observations of material changes on-orbit have been reported, mechanistic understanding has not yet become clear because new sets of non-intuitive processes are occurring on orbit. Reactant kinetic energy, low collision rates and surface/adsorbate interactions must be considered in the analysis of these observations. The specific example of oxide formation of elemental materials will be examined in terms of thermodynamics and possible reaction pathways. On the basis of this approach, a rational trend emerges from the orbital behavior of these samples. The role of reactant kinetic energy as opposed to internal energy in chemiluminescent product formation will also be presented. Development of a systematic thermochemical approach may be useful in making screening predictions of long-term material behavior on-orbit.

THEORETICAL APPROACH TO OXYGEN ATOM DEGRADATION OF SILVER

by

Albert T. Fromhold, Jr., Seung Noh, Ronald Beshears
Physics Department, Auburn University, AL 36849

and

Ann F. Whitaker, Sally A. Little
Marshall Space Flight Center, AL 35812

Based on available RBS, PIXE, and ELLIPSOMETRY data obtained on silver specimens subjected to atomic oxygen attack in low earth orbit on Flight 41-G, a theory has been developed to model the oxygen atom degradation of silver. The diffusion of atomic oxygen in a microscopically nonuniform medium is an essential constituent of the theory. The driving force for diffusion is the macroscopic electrochemical potential gradient developed between the specimen surface exposed to the ambient and the bulk of the silver specimen. The longitudinal electric field developed parallel to the gradient is modified by space charge of the diffusing charged species. Lateral electric fields and concentration differences also exist due to the nonuniform nature of the medium. The lateral concentration differences are found to be more important than the lateral electric fields in modifying the diffusion rate. The model has been evaluated numerically. Qualitative agreement exists between the kinetics predicted by the theory and kinetic data taken in ground-based experiments utilizing a plasma asher.

*Research Supported in part by NASA Contract NAS8-36471

Groundbased Studies of Spacecraft Glow and Erosion Caused by Impact of Oxygen and Nitrogen Beams*

W.D. Langer, S.A. Cohen, D.M. Manos, R.W. Motley and S.F. Paul

Princeton Plasma Physics Laboratory, P.O. Box 451, Princeton, NJ 08544

To simulate surface reactions in the space environment we have developed a groundbased facility that produces a very high flux (10^{14} to $10^{16}/cm^2/s$) of low energy (2-20 eV) neutral atoms and molecules. The neutral beams are created using a novel method involving neutralization and reflection of ions from a biased limiter, where the ions are extracted from a toroidal plasma source. We present spectra of emission due to beam-solid interactions on targets of Chemglaze Z-306 optical paint and Kapton. We measured erosion yields for carbon and Kapton targets with low energy ($\sim$ 10 eV) nitrogen and oxygen beams. The reaction rates and surface morphology for the erosion of Kapton are similar to those measured in experiments on STS-5.

*Funded by a research grant from NASA No. NAG8-521.

Potential Surfaces for O Atom-Polymer Reactions

by
B. C. Laskowski
Analatom, Inc., 1977 Concourse Drive, San Jose, CA 95131
and
R. L. Jaffe
NASA-Ames Research Center, Moffett Field, CA 94035

Ab Initio quantum chemistry methods are used to study the energetics of interactions of O atoms with organic compounds. Polyethylene $(CH_2)_n$ has been chosen as model system to study the interactions of $O(^3P)$ and $O(^1D)$ atoms with polymers. Initially we are looking at H abstraction and represent polyethylene by a C3 (Propane) oligomeric model.

The gradient method, as implemented in the GRADSCF package of programs, is used to determine the geometries and energies of products and reactants. The saddle point, barrier, geometry is determined by minimizing the squares of the gradients of the potential with respect to the internal coordinates.

To correctly describe the change in bonding during the reaction at least a two configuration MCSCF or GVB wavefunction has to be used.

Basis sets include standard Pople and Dunning sets, however, increased with polarization functions and diffuse p functions on both the C and O atoms. The latter is important due to the O^- character of the wavefunction at the saddle point and products.

Normal modes and vibrational energy levels are given for the reactants, saddle point and products.

Finally, quantitative energetics are obtained by implementing a small CAS approach followed by limited CI calculations. Comparisons are made with limited available experimental data.

In future work we will be looking at reactions leading to carbon-carbon bond rupture in larger oligomers.

C-3

NASA MARSHALL SPACE FLIGHT CENTER ATOMIC OXYGEN INVESTIGATIONS

by

Physical Sciences Branch
Materials and Processes Laboratory
Marshall Space Flight Center, AL 35812

ABSTRACT

An overview of NASA Marshall Space Flight Center atomic oxygen investigations is provided, including descriptions of flight studies, ground-based testing, contractual efforts, and future focus. Summary results of flight experiments on STS-5, STS-8, and STS-41G are presented. The development of the Marshall Space Flight Center Atomic Oxygen Resistive Monitor for the upcoming EOIM-3 flight experiment is reviewed. Materials characterization work and ground-based testing are described. Contractual efforts, such as the development of atomic oxygen resistant coatings for Space Station, are included. Future emphasis is placed on enhanced ground-based testing via the development and operation of a state-of-the-art atomic oxygen simulation system and on the continuation of flight studies in support of multi-programs.

AN EVALUATION OF CANDIDATE OXIDATION RESISTANT MATERIALS FOR SPACE APPLICATIONS IN LEO

By Sharon Rutledge, Bruce Banks and Michael Mirtich
National Aeronautics and Space Administration
Lewis Research Center
Cleveland, Ohio 44135

Frank DiFilippo, Deborah Hotes and Richard Lebed
Case Western Reserve University
Cleveland, Ohio 44106

Terese Dever and Michael Kussmaul
Cleveland State University
Cleveland, Ohio 44114

ABSTRACT

Atomic oxygen has long been recognized as one of the main causes of degradation for materials such as polyimides and carbon on spacecraft in the low Earth orbital (LEO) environment. The degradation of components such as Kapton® solar array blankets and graphite epoxy structural members is of such magnitude that it could potentially jeopardize the long term durability of Space Station. Radiator surfaces must maintain emittances greater than ≈ .8 while in LEO in addition to maintaining resistance to attack by atomic oxygen at high temperatures. Ground based testing of materials considered for Kapton® array blanket protection, graphite epoxy structural member protection, and high temperature radiators was performed in an RF plasma asher. Ashing rates for Kapton® were correlated with rates measured on STS-8 to determine the exposure time equivalent to 1 year in LEO at a constant density Space Station orbital flux. Protective coatings on Kapton® from Tekmat, Andus Corporation and LeRC were evaluated in a plasma asher and mass loss rates per unit area were measured for each sample. All samples evaluated provided some protection to the underlying surface but ion beam sputter deposited samples of SiO_2 and SiO_2 with 8% polytetrafluoroethylene (PTFE) showed no evidence of degradation after 47 hours of exposure. Mica paint was evaluated as a protective coating for graphite epoxy structural members. Mica appears to be resistant to attack by atomic oxygen but only offers some limited protection as a paint because the paint vehicles evaluated to date were not resistant to atomic oxygen. Four materials were selected for evaluation as candidate radiator materials: stainless steel, copper, niobium-1% zirconium, and titanium-6% aluminum-4% vanadium. These materials were surface textured by various means to improve their emittance. Emittances as high as .93 at 2.5μm for stainless steel and .89 at 2.5 μm for Nb-1Zr were obtained from surface texturing. There were no significant changes in emittance after asher exposure. The protective coatings on Kapton® and candidate radiator materials evaluated so far are promising but further research on protection of graphite epoxy support structures is needed.

Martin Marietta Atomic Oxygen Low Earth Orbit Simulation

by

Gary W. Sjolander and Lyle Bareiss

(Poster Abstract)

An atomic oxygen beam apparatus that produces flux levels and atomic kinetic energy similar to that encountered by spacecraft in low earth orbit (LEO) is coming on line at Martin Marietta Denver Aerospace. The beam appratus consists of an electric discharge ion source, mass filter, decelerator, and neutralizer. Specific design goals include a 1.3 cm beam diamter, a 5 eV beam energy, and a flux density on the order of 1.E+15 cm^{-2} s^{-1}. The total fluence will be on the order of 1.E+19 cm^{-2} for an 8 hour test. The neutral oxygen beam will expose various materials contained with a large target chamber. Within the chamber will be a rather complex suite of instrumentation that will allow real-time studies of material mass loss and reactant species spatial distribution. In addition, a UV solar simulator will aid in the understanding of various synergistic effects.

At present, the AO beam appratus has been checked out through the mass filter. Beam currents in excess of 1 mA at 5000 eV have been measured for nitrogen, oxygen, and hydrogen prior to the mass filter; and beam space charge analysis has been confirmed for a hydrogen beam through the mass filter section. Beam uniformity is 8% across a 1.3 cm diameter atomic oxygen beam at 10 microamperes and 3000 eV. The next phases will include decelerator and neutralizer testing.

Material testing and research in this atomic oxygen environment will include all materials of interest for LEO spacecraft including space station. Results of ground based testing will provide input data to computer modeling of long duration mission analyses of atomic oxygen effects. Ground based testing will also be compared with past and future flight test data through a cooperative effort with Dr. J. Gregory of the University of Alabama in Huntsville as part of the Consortium for Materials Development in Space.

Spacecraft ram glow and surface temperature

G. R. Swenson and S. B. Mende (Both at: Lockheed Palo Alto Research Laboratory, D91-20/B255, 3251 Hanover Street, Palo Alto, Ca. 94304)
E. J. Llewellyn (ISAS, University of Saskatchewan, Saskatoon, Canada)

Space shuttle glow intensity measurements show large differences when the data from different missions are compared. In particular on the 41-G mission the Space Shuttle ram glow was observed to display an unusually low intensity. Subsequent investigation of this measurement and earlier measurements suggest that there was a significant difference in temperature of the glow producing ram surfaces. The highly insulating properties coupled with the high emissivity, of the shuttle tile results in surfaces that cool quickly when exposed to deep space on the night side of the orbit.

The increased glow intensity is consistent with the hypothesis that the glow is emitted fromm excited NO_2. The excited NO_2 is likely formed through three body recombination ($OI + NO + M = NO_2^*$) where ramming OI interacts with weakly surface bound NO. The NO is formed from atmospheric OI and NI which is scavenged by the spacecraft moving through the atmosphere. We postulate that the colder surfaces retain a -thicker- layer of NO thereby increasing the probability of the reaction. It has been found from the glow intensity/temperature data that the bond energy of the surface bound precursor, leading to the chemical recombination producing the glow, is ~0.14 ev. A thermal analysis of material samples of STS-8 has been made and the postulated temperature change of individual material samples prior to the time of glow measurements above respective samples are consistent with the thermal effect on glow found for the orbiter surface.

Comments on the Interaction of Materials with Atomic Oxygen

Larry P. Torre and H. Gary Pippin
Boeing Aerospace Company
P. O. Box 3999 M/S 8Y-70
Seattle, WA 98124

This paper contains an explanation of the relative resistance of various materials to attack by atomic oxygen. An interpretation of previously published data from both ground based and on-orbit experiments, and measurements carried out in Boeing's own laboratories, is presented. The results indicate the importance of bond strengths, size and structure of pendant groups, and fluorination to the resistance of certain polymers to atomic oxygen. A theory which provides a partial explanation of the degradation of materials in low earth orbits due to surface recombination of oxygen atoms is also included. Finally, a section commenting on mechanisms of material degradation is provided.

EFFECT OF LONG-TERM EXPOSURE TO LEO SPACE ENVIRONMENT

by

D. G. Zimcik
Communications Research Centre
Ottawa, Canada

Recent experience with Shuttle flights has shown that certain materials, particularly those of a polymeric base used externally for thermal control, are greatly effected by even short exposure to the environment of low Earth orbit. Since the performance of many of these materials can be crucial to the successful completion of the satellite mission, this discovery has lead to several short-term experiments conducted during Shuttle flights to attempt to characterize the phenomenon of degradation by atomic oxygen. However, since these experiments have generally been designed to maximize the fluence of atomic oxygen over a period of only hours, they effectively constitute accelerated tests, particularly in relation to other environmental effects which are not enhanced. Accordingly, one must be cautious to ensure applicability of the results to a more realistic situation that might occur at higher altitude, for example, where the increased presence of other environmental effects relative to atomic oxygen fluence may lead to enhanced or synergistic degradation. Fortunately, the success of in-orbit repair of satellites from the Shuttle has also provided some long-term exposure data in order to validate experimental data. The most celebrated of these data come from components and materials returned from the Solar Max Satellite Repair Mission.

In the present paper, data obtained from components and materials from the Solar Max Satellite are presented and compared to data for similar materials obtained from the Advanced Composite Materials Exposure to Space Experiment (ACOMEX) flown on Shuttle mission STS-41G. In addition to evaluation of surface erosion and mass loss that may be of importance to very long-term missions, comparison of solar absorptance and thermal emittance measurements for both long and short term exposures were made. Although the ratio of absorptance over emittance can be altered by proper choice of materials to ensure a proper operating environment for the spacecraft, once the thermal design is established, it is important that the material properties not change in order to maintain the operating environment for many payload and bus items such as electronics, batteries, fuel, etc. However, data presented show significant changes after short exposure in low Earth environment. Moreover, the measured changes are shown to differ according to the manner of exposure i.e. normal or oblique, which also affects the resultant eroded surface morphology. These results identify constraints to be considered in development of flight experiments or laboratory simulation testing.

Appendix B:

Panel Discussion on an Atomic Oxygen Effects Test Program

APPENDIX B: MINUTES FROM PANEL DISCUSSIONS OPEN SESSION ON ATOMIC OXYGEN EFFECTS TEST PROGRAM

Co-Chairmen: Michael Greenfield; NASA Headquarters
Bruce A. Banks; NASA Lewis Research Center

Session started with an introduction and summary statement of objectives by Dr. Michael Greenfield. The session was then conducted by Bruce Banks. Five major subject areas were discussed: Objectives, Materials Selection, Exposure Environment Documentation, Surface Interaction Characterization, and Logistics. The discussions for each of these areas are summarized below.

Objectives:

- To compare the LEO simulation characteristics of existing atomic oxygen exposure facilities.
- To utilize the collective data from a multitude of simulation facilities to help understand mechanism and erosion yield dependence upon energy, flux, metastables, charge, and environmental species.

Some questions arose as to whether these are the objectives that should be followed. Some participants wanted to see more mechanistic studies of materials being performed and others wanted to use the program to develop protective materials. The main objective, however, is to compare the LEO simulation characteristics of existing facilities with the reality of LEO, which will require use of some materials that have been tested in LEO. More fundamental mechanistic studies and more applied protective materials evaluations can be and are being done independently by the participants.

The chairmen considered the objectives to be the basic purpose of the proposed test program and felt that they should not be voted on but remain as stated above.

Materials Selection:

Three materials were listed as examples of possible materials for facility comparison test samples: Kapton, PTFE Teflon, and Polyethylene. The floor was opened for discussion and suggestion of materials that the participants would like to see tested. After all suggestions were made, a vote was taken by a show of hands to select materials, each participant allowed to vote for three choices. The results are as follows:

Votes	Material
41	Kapton
14	PTFE Teflon
17	Polyethylene
1	Thermal Control Paint
0	Graphite Metal Matrix

31	Carbon (Thin Film)
17	Carbon Single Crystal
2	Silicone
1	Fluorosilicone
8	Polycrystalline Silicon
14	Silver
2	1,2 Cis-Polybutadiene
1	Silicone Block Copolymer
3	Polystyrene

Some general criteria given by the participants for materials selection were:

> For accurate facility comparison, results should be referenced to a standard such as a flight experiment. So materials should be chosen which are well characterized in flight experiments (Kapton, carbon, polyethylene, silver, etc.).
>
> For comparisons which allow mechanistic studies to be performed a material is needed which is simple and well characterized when it is made, i.e., carbon single crystal, polycrystalline silicon, 1,2 cis-polybutadiene, etc. Kapton was thought, by some participants, to be too complex for mechanistic studies.

Participants were told that the final decision for materials selection would be based on input as a result of their voting. Participants will receive samples of each material that are well characterized and supplied by the same source to assure uniformity of comparison.

Exposure Environment Documentation:

Six potential parameters were suggested as candidates for documentation in these tests: flux, fluence, energy, metastable state distribution, charged species population, and environmental gas species. The floor was opened for discussion and ideas for additional parameters to be added to this list. The purpose was to generate a list of possible parameters but not to vote on them at this time. The list that resulted is as follows:

Flux
Fluence
Energy
Metastable State Distribution
Charged Species Population
Environmental Gas Species
Peak Flux
Energy Distribution
Sample Temperature
Species Partial Pressure
UV Environment
Sample Surface Preparation
Oxygen Purity

Some concern developed as this list grew longer that not all of the facilities would be capable of measuring these parameters and would be excluded from the test program if they could not. They were assured that no facility would be excluded and that these are suggested parameters and the facilities should supply those parameters decided upon which they can measure.

Surface Interaction Characterization:

Three general catagories were suggested as possible characterization areas and one technique was listed under each: Morphology (SEM); Erosion Yield (cm^3/atom); and Chemistry (ESCA). The floor was then opened for discussion to obtain additional characterization areas. The resulting list is given below:

Morphology: SEM

Erosion Yield: cm^3/atom; Surface Recession Measurement

Chemistry: ESCA; EDAX; FDIR; IR (and duration between the atomic oxygen exposure and the specific characterization)
Ejected Species (energy, etc.)
Surface Energy
Dry Run Characterization (sample analysis before and after exposure in chamber with beam off)
In Situ Characterization

Mechanical: Stress/Strain

Optical: Reflectance; Transmittance; Emittance

Logistics:

Common Source of Well Characterized Materials
Data Collection and Distribution
Participant List

Logistics were briefly discussed and participants were informed that these subjects would be covered in the closed NASA session.

NASA CLOSED SESSION ON ATOMIC OXYGEN EFFECTS TEST PROGRAM

Chairman: Michael Greenfield (NASA Headquarters)
Co-Chairman: Bruce Banks (NASA LeRC)

At the conclusion of the open session the closed session was started to determine the logistics for carrying out the test program. The participants were limited to NASA and JPL employees only. Bruce Banks was asked by Michael Greenfield to coordinate the test program.

MATERIALS:

Based on the voting in the open session it was decided by general consensus to choose four of the top ranked materials on the list for testing. The four materials chosen were Kapton, FEP, Polyethylene, and Carbon Single Crystal. Even though thin film carbon was the number two material in the open session it was decided that the carbon single crystal would yield more reliable information because the carbon thin film would be much more variable in production. FEP was chosen as a replacement for PTFE because there is more flight data available for FEB.

How should the materials be supplied?

- As standard commercial materials tried in flight.
- As a special made material which is well characterized.

It was decided to go with commercial supplier and ask if they can send a characterization sheet on the material. Whenever possible we should try to obtain materials as similar as we can to those tested on shuttle flights.

Test Samples

Kapton:	2 mil, DuPont; make sure it is type H, ask for old type H Kapton and not HN.
FEP:	2 mil, DuPont.
Polyethylene:	2 mil, low oxygen content
Graphite:	Highly Oriented Pyrolytic Graphite suggested for surface recession test. Pyrolytic Graphite for weight loss.

EXPOSURE ENVIRONMENT DOCUMENTATION:

Should sample surface preparation be specified?

Panel decided to recommend a cleaning procedure that is optional for the participants. Lubert Leger is going to draft a cleaning procedure.

This brought up the question of surface contamination by shipping of the samples to the participants. Should the participants come to a meeting and pick up their samples? General agreement was that it would be much better to ship the samples. To test for contamination it was suggested that a dummy set of samples be prepared and an ESCA made of the surface then the package shipped round trip and analyzed by ESCA when returned.

Packaging Considered: polyethylene; aluminum foil; or wrap the polymer in layers of itself.

Should everyone be at the same fluence level as STS-8?

Consensus: Yes, there should be a standard suggested fluence level. Preferably the same level as a well documented flight experiment.

Participants should list the estimated uncertainty in all data reported.

Participants should send the data that they can obtain using the environment documentation parameter list as a suggested guideline. No facility will be excluded because it cannot measure all of the parameters on the suggested parameter list. Ashers are welcome also. It was suggested that a special operating parameter list be made up for ashers.

It was also suggested that standardized units be used in reporting all data and that these units be made known to the participants.

The list of exposure environment documentation developed in the open session will be used.

SURFACE INTERACTION CHARACTERIZATION:

List all the tests in this category on a sheet and have them select the ones they can do.

Add birefringence under optical properties.

Otherwise, the list obtained in the open session be used.

LOGISTICS:

Obtain a mailing list of the participants. Jim Visentine will update his facility list and a list of workshop attendees will be obtained. Send a form letter asking potential participants if they would like to participate and if so, what size sample, and which of the four materials they would like to test. Somewhere in one of the letters it should also be stated that participants should not send information that they would not want published.

Should we have a peer review?
General Consensus: No

We should meet as a NASA group or with participants to discuss results and not to decide which facility is better.

When the letters to invite participation are sent out we should specify a time requirement for response. We also should specify a time from the participants' sample receipt date when they should have sent the results from their tests. The possibility exists for having results by the next workshop or having a 6 month progress report.

Have participants retain their samples in case there is further analysis required.

Participants should also keep track of the final date of sample exposure in their facility in case further measurements need to be performed at a later date.

A database may be set up later to compile the data if the response is too large to handle manually.

Appendix C:

Workshop Agenda

APPENDIX C

Program for NASA Workshop on Atomic Oxygen Effects

Monday, November 10, 1986

7:30am Registration, 3rd Floor Pasadena Center

OPENING SESSION
(Room 316C, Pasadena Center)

8:30am Welcome
Donald G. Rea
Jet Propulsion Laboratory

8:40am A Broad-based NASA Program on Atomic Oxygen Effects
Michael Greenfield
NASA Headquarters

9:10am Technical Overview of the Atomic Oxygen Problem
Amitava Gupta
Jet Propulsion Laboratory

SESSION I: SPACE FLIGHT EXPERIMENTS
Chairman: Darrell R. Tenny
NASA Langley Research Center

9:35am Effects of Low Earth Orbital Environment Constituents on Spacecraft Surfaces
Lubert J. Leger
NASA Johnson Space Center

10:15am Material Interactions with the Low Earth Orbital Environment: Accurate Reaction Rate Measurements
James T. Visentine
NASA Johnson Space Center

10:35am Mass Spectrometers and Atomic Oxygen
Donald E. Hunton
Air Force Geophysics Laboratory

10:55am O-Atom/Surface Scattering Flight Experiments
John C. Gregory
Univ. of Alabama - Huntsville

11:25am LEO Surface Contamination and Atomic Oxygen Flight Experiments
Carl R. Maag
Jet Propulsion Laboratory

SESSION IIA: ATOMIC OXYGEN INTERACTIONS: MECHANISMS
Chairman: Amitava Gupta
Jet Propulsion Laboratory

1:30pm O-Atom Degradation Mechanisms of Materials
Daniel R. Coulter
Jet Propulsion Laboratory

2:00pm Kinetics and Mechanisms of Some Atomic Oxygen Reactions
Ratimir J. Cvetanovic
National Research Council of Canada

2:30pm Product Vibrational States in the Reaction of O-Atoms with CO and C on Pt
Bret L. Halpern
Yale University

3:00pm The Role of Electronic Mechanisms in Surface Erosion and Glow Phenomena
Richard F. Haglund, Jr.
Vanderbilt University

SESSION IIB: ATOMIC OXYGEN INTERACTIONS: THEORY AND DIAGNOSTICS
Chairman: Vincent McKoy
California Institute of Technology

3:35pm Potential Surfaces for Atomic Oxygen Reactions
Richard Jaffe
NASA Ames Research Center

4:05pm Dynamics of Atom-Surface Interactions
Stephen J. Sibener
University of Chicago

4:35pm Experimental REMPI Studies of Small Molecules
Joseph L. Dehmer
Argonne National Laboratory

5:00pm SESSION III: POSTER SESSION
(Room 312C, Pasadena Center)

Tuesday November 11, 1986

8:00am Registration, 3rd Floor Pasadena Center

SESSION IV: ATOMIC OXYGEN SOURCE DEVELOPMENT
Chairman: R. C. Tennyson
University of Toronto

8:30am Laboratory Studies of Atomic Oxygen Reactions with Solids
Graham S. Arnold
The Aerospace Corporation

9:00am High Intensity 5eV Atomic Oxygen Source and Low Earth Orbit Simulation Facility
Jon B. Cross
Los Alamos National Laboratory

9:30am A Sputtering Derived Atomic Oxygen Source for Studying Fast Atom Reactions
Richard A. Ferrieri
Brookhaven National Laboratory

10:30am Neutral Atomic Oxygen Beam Produced by Ion Charge Exchange for Low Earth Orbital Simulation
Bruce A. Banks
NASA Lewis Research Center

11:00am A High Flux Pulsed Source of Energetic Atomic Oxygen
George E. Caledonia
Physical Sciences, Inc.

11:30am Production of Pulsed Atomic Oxygen Beams via Laser Vaporization Methods
David E. Brinza
Jet Propulsion Laboratory

1:30pm SESSION V: OPEN PANEL DISCUSSION ON AN ATOMIC OXYGEN EFFECTS TEST PROGRAM
Co-Chairmen: Michael Greenfield
NASA Headquarters
Bruce A. Banks
NASA Lewis Research Center

3:00pm CLOSED DISCUSSION ON NASA ATOMIC OXYGEN EFFECTS TEST PROGRAM (Special Invitation Only)

Appendix D:

List of Workshop Registrants

APPENDIX D

List of Registered Attendees

ARNOLD, Graham S.
Aerospace Corporation
M2-271
P.O. Box 92957
Los Angeles, CA 90009

(213) 647-1935

BANKS, Bruce A.
Lewis Research Center
21000 Brookpark Rd.
Cleveland, OH 44135

(216) 433-2308
(FTS) 297-2308

BARENGOLTZ, Jack B.
Jet Propulsion Laboratory
MS 157-507
4800 Oak Grove Drive
Pasadena, CA 91109

(818) 354-2516
(FTS) 792-2516

BAUER, Jerome
Jet Propulsion Laboratory
MS 157-507
4800 Oak Grove Drive
Pasadena, CA 91109

(818) 354-3726
(FTS) 792-3726

BOMKAMP, Daryl H.
Argonne National Laboratory
9700 S. Cass Avenue
Argonne, IL 60439

(312) 972-5975
(FTS) 972-5975

BOUNDY, Robert A.
Jet Propulsion Laboratory
MS 157-316
4800 Oak Grove Drive
Pasadena, CA 91109

(818) 354-4299
(FTS) 792-4299

BOURASSA, Roger J.
Boeing Aerospace Company
P. O. Box 3999
Seattle, WA 98124-2499

(206) 773-7939

BRINZA, David E.
Jet Propulsion Laboratory
MS 67-201
4800 Oak Grove Drive
Pasadena, CA 91109

(818) 354-6836
(FTS) 792-6836

CALEDONIA, George E.
Physical Sciences, Inc.
Research Park
P. O. Box 3100
Andover, MA 01810

(617) 475-9030

CARDON, Bartley L.
Massachusetts Institute
of Technology
MIT/LL KB-226
P. O. Box 73
Lexington, MA 02173-0073

(617) 863-5500 x2994

CARRUTH, Melvin Ralph, Jr.
NASA Marshall Space Flight Center
EH 12
Marshall Space Flight Center, AL
35810

(205) 544-7647
(FTS) 824-7647

CHINN, Steven D.
Science & Engineering Assoc., Inc.
6535 South Dayton St., Suite 2100
Englewood, CO 80111

(303) 790-1572

CHUTJIAN, Ara
Jet Propulsion Laboratory
MS 183-601
4800 Oak Grove Dr.
Pasadena, CA 91109

(818) 354-7012
(FTS) 792-7012

CORMIA, Robert Douglas
Surface Science Labs
206 Charleston Ave.
Mountain View, CA 94043

(415) 962-8767

COTTRELL, Fred D.
TRW
One Space Park, 01/2210
Redondo Beach, CA 90278

(213) 535-2706

COULTER, Daniel R.
Jet Propulsion Laboratory
MS 67-201
4800 Oak Grove Drive
Pasadena, CA 91109

(818) 354-3638
(FTS) 792-3638

CROSS, Jon B.
Los Alamos National
Laboratory
CLS-2, MSG738
Los Alamos, NM 82545

(505) 667-0511

CVETANOVIC, R. J.
National Bureau of
Standards
Chemical Kinetics Data
Center
222-A147
Gaithersburg, MD 20899

(301)921-2174

DAECH, Alfred F.
Martin Marietta
13800 Old Gentilly Rd.
New Orleans, LA 70124

(504) 255-3617

DEHMER, Joseph L.
Argonne National Laboratory
Environmental Research Div.
9700 S. Cass Avenue
Argonne, IL 60439

(312) 972-4194
(FTS) 972-4194

DIXIT, Sham N.
Lawrence Livermore Lab
Livermore, CA 94550

EVANS, Robin W.
Jet Propulsion Laboratory
Syscon - JPL
2550 Honolulu Ave. #201
Montrose, CA 91020

(818) 249-5252

FERRIERI, Richard A.
Brookhaven National Laboratory
Department of Chemistry
Upton, NY 11973

(516) 282-4391
(FTS) 666-4391

FEWELL, Larry L.
NASA Ames Research Center
Moffett Field, CA 94035

(415) 694-5128
(FTS) 464 5128

FOLTZ, Greg W.
Sandia National Laboratories
P. O. Box 969
Livermore, CA 94550

(415) 422-2801

FRANK, Curtis W.
Stanford University
Dept. of Chemical Engineering
Stanford, CA 94305

(415) 723-4573

FREEDMAN, Andrew
Aerodyne Research Inc.
45 Manning Road
Billerica, MA 01821

(617) 663-9500

FROMHOLD, Albert Thomas
Auburn University
Physics Department
Auburn University, AL 36849

(205) 826-4713
(205) 821-8680

GARVEY, Raymond E., III
Martin Marietta Energy
Systems, Inc.
P. O. Box P, Mail Stop 294
Oak Ridge, TN 37922

(615) 574-9803
(FTS) 924-9803

GILLEN, Keith T.
SRI International
333 Ravenswood Ave.
Menlo Park, CA 94025

(415) 859-3250

GJERDE, Helen B.
Lockheed Missiles &
Space Co., Inc.
Materials & Processes
P. O. Box 3504
Sunnyvale, CA 94088-3504

(408) 742-8244

GOLUB, Morton A.
NASA Ames Research Center
Mail Stop 230-3
Moffett Field, CA 94035

(415) 694-5128
(FTS) 464-5128

GREEN, Byron David
Physical Sciences, Inc.
P. O. Box 3100
Andover, MA 01810

(617) 475-9030

GREENFIELD, Micheal A.
NASA Headquarters
Mail Code RM / B607
Washington, DC 20546

(202) 453-1000

GREGORY, John C.
University of Alabama, Huntsville
4701 University Dr., N.W.
Huntsville, AL 35899

(205) 895-6028

GUPTA, Amitava
Jet Propulsion Laboratory
MS 67-201
4800 Oak Grove Drive
Pasadena, CA 91109

(818) 354-5783
(FTS) 792-5783

HAGLUND, Richard F., Jr.
Vanderbilt University
Dept. of Physics/Astronomy
Nashville, TN 37235

(615) 322-2828

HALE, Robert R.
Jet Propulsion Laboratory
MS 157-507
4800 Oak Grove Dr.
Pasadena, CA 91109

(818) 354-4045
(FTS) 792-4045

HALL, William N.
AF Geophysics Labs
AFGL/PHE
Hanscom AFB, MA 01731

(617) 377-3989

HALPERN, Bret L.
Yale University
Dept. of Chemical Engineering
Box 2159, Yale Station
New Haven, CT 06520

(203) 436-0470

HAMACHER, Hans
DFVLR
Linderhohe,
5000 Koln 90
WEST GERMANY

(02203) 6012330

HEIMBUCH, Alvin H.
NASA Ames Research Center
Mail Stop 230-3
Moffett Field, CA 94035

(415) 694-5408
(FTS) 464-5408

HUNTON, Donald E.
Air Force Geophysics Laboratory
AFGL/LID Hanscom AFB
Bedford, MA 01731

(617) 377-3048

HURLBUT, F. C.
Univ. of California
Mechanical Engineering
Berkeley, CA 94720

JAFFE, Richard L.
NASA Ames Research Center
Mail Stop 230-3
Moffett Field, CA 94035

(415) 694-6458
(FTS) 464-6458

JAMET, Jean F.
Off. Natl. D'Etures et Recherches Aerospatial
Head of Ceramic Corporate Division
29 Av. Division Leclerc
Chatillon, FRANCE

(1) 657 11 60

KEY, Richard W.
Jet Propulsion Laboratory
MS 180-701
4800 Oak Grove Drive
Pasadena, CA 91109

(818) 354-3060
(FTS) 792-3060

KIRKPATRICK, Marc
TRW Space & Technology Group
One Space Park
135/3266
Redondo Beach, CA 90278

(213) 535-8440

KOHL, Denis A.
Univ. of Texas - Austin
Department of Chemistry
Austin, TX 78712

(512) 471-4298

KRECH, Robert
Physical Sciences, Inc.
Research Park, P. O. Box 3100
Andover, MA 01810

(617) 475-9030

KURLAND, Richard M.
TRW Systems
One Space Park
Redondo Beach, CA 90278

(213) 535-0905

LAN, Esther H.
McDonnell Douglas
5301 Bolsa Avenue
Huntington Beach, CA 92708

(714) 896-5244

LANGER, William D.
Princeton Plasma Physics Laboratory
P. O. Box 451
Princeton, NJ 08544

(609) 683-2262
(FTS) 340-2262

LASKOWSKI, Barnard C.
ANALATOM, INC.
1977 Concourse Drive
San Jose, CA 95131

(408) 434-1665

LEE, Charles Y. C.
AF Materials Lab
AFWAL/MLBC
WPAFB, OH 45433

(513) 255-9075

LEGER, Lubert J.
NASA Johnson Space Center
Code ES53
Houston, TX 77062

(713) 483-2059
(FTS) 525-2059

LERNER, Narcinda R.
NASA Ames Research Center
Mail Stop 230-3
Moffett Field, CA 94035

(415) 694-5128
(FTS) 464-5128

LEVINE, Aaron W.
RCA Laboratories
David Sarnoff Research Center
P. O. Box 432
Princeton, NJ 08540-0432

(609) 734-2471

LIANG, Ranty H.
Jet Propulsion Laboratory
MS 67-201
4800 Oak Grove Drive
Pasadena, CA 91109

(818) 354-6314
(FTS) 792-6314

LIFER, Charles E.
Jet Propulsion Laboratory
MS 125-112
4800 Oak Grove Drive
Pasadena, CA 91109

(818) 354-6580
(FTS) 792-6580

LITTLE, Sally A.
NASA Marshall Space Flight Center
Mail Code EH12
NASA Marshall Space Flight Center, AL 35812

(205) 544-5960
(FTS) 824-5960

MAAG, Carl R.
Jet Propulsion Laboratory
MS 157-507
4800 Oak Grove Drive
Pasadena, CA 91109

(818) 354-6453
(FTS) 792-6453

MANSON, Simon V.
21 Squirrel Run
Morristownship, NJ 07960

(201) 539-3893

McCARGO, Matthew
Lockheed Palo Alto Research
0/9240, Bldg 205
3251 Hanover Street
Palo Alto, CA 94304

(415) 424-2382

McCARTY, Kevin F.
Sandia National Labs
P. O. Box 969
Livermore, CA 94550

(415) 422-2067

McCLURE, Donald J.
3 M Company
3 M Center
Bldg. 208-1
St. Paul, MN 55144

(612) 733-9160

McKOY, Vincent
California Institute of Technology
Mail Code 127-72
Pasadena, CA 91125

(818) 356-6545

NAHRA, Henry K.
NASA Lewis Research Center
21000 Brookpark Road
Cleveland, OH 44144

(216) 433-5385
(FTS) 297-5385

NASH, Brian A.
McGhan Nusil Corp.
Research & Development
1150 Mark Avenue
Carpinteria, CA 93013

(805) 689-1289

NEELY, W. C.
Auburn University
Department of Chemistry
Auburn, AL 36830

(205) 826-4043

O'DONNELL, Tim
Jet Propulsion Laboratory
MS 157-507
4800 Oak Grove Drive
Pasadena, CA 91109

(818) 354-3726
(FTS) 792-3726

ORIENT, O.
Jet Propulsion Laboratory
MS 183-601
4800 Oak Grove Drive
Pasadena, CA 91109

OSIECKI, Richard A.
Lockheed Palo Alto Research
0/92-40, Bldg 205
3251 Hanover Street
Palo Alto, CA 94304

(415) 424-2389

OUTLAW, Ronald A.
NASA Langley Research Center
MS 160
Hampton, VA 23665

(804) 865-3781
(FTS) 928-3781

PAILLOUS, Alain
ONERA-CERT-DERTS
BP 4025
Toulouse Cedex, FRANCE 31055

61-55-71-19

PENN, Thomas J.
Jet Propulsion Laboratory
MS 233-302
4800 Oak Grove Drive
Pasadena, CA 91109

(818) 354-4428
(FTS) 792-4428

PETRIE, Brian C.
Lockheed Missiles & Space
Company, Inc.
P. O. Box 3504
Sunnyvale, CA 94088-3504

(408) 742-8244

PIPPIN, H. Gary
Boeing Aerospace Co.
Materials and Processes
M/S 8Y-70
P. O. Box 3999
Seattle, WA 98124

(206) 773-6063

PRICE, Lawrence A.
Martin Marietta
P. O. Box 179
Denver, CO 80201

(303) 977-1874

RAPP, Donald
Jet Propulsion Laboratory
MS 157-316
4800 Oak Grove Drive
Pasadena, CA 91109

(818) 354-4931
(FTS) 792-4931

REA, Donald
Jet Propulsion Laboratory
MS 180-704
4800 Oak Grove Drive
Pasadena, CA 91109

(818) 354-6243
(FTS) 792-6243

RICHTER, Hans-Ewald
DFVLR
Linder Hohe
5000 Koln 90
WEST GERMANY

(02203) 601 23 30

ROSSER, Robert W.
NASA Ames Research Center
Mail Stop 230-3
Moffett Field, CA 94035

(415) 694-5408
(FTS) 464-5408

RUTLEDGE, Sharon K.
NASA Lewis Research Center
Mail Stop 302-1
21000 Brookpark Rd.
Cleveland, OH 44135

(216) 433-2219
(FTS) 297-2219

SIBENER, Steven J.
University of Chicago
James Franck Institute
5640 S. Ellis Avenue
Chicago, IL 60637

(312) 962-7193

SINGH, Bawa
RCA Laboratories
David Sarnoff Research Center
401 Washington Rd.
Princeton, N.J. 08543-0432

(609) 734-2212

SJOLANDER, Gary W.
Martin Marietta
P. O. Box 179
Denver, CO 80201

(303) 977-8686

SLANGER, Tom G.
SRI International
Rm. PS-091
Menlo Park, CA 94025

(415) 859-2764

SLEMP, Wayne S.
NASA Langley Research
Center
MS 183
Hampton, VA 23665

(804) 865-3420
(FTS) 928-3420

SMITH, Mark P.
Lockheed Missiles & Space
B/15F 0/62-92
P. O. Box 3504
Sunnyvale, CA 94088

(408) 756-8631
(408) 756-7603

STRIEPENS, Aloys H.
Rockwell International
Space Transportation
Systems Division
MS DA33
12214 Lakewood Blvd.
Downey, CA 90241

(213) 922-1014

STUCKY, Wayne K.
The Aerospace Corporation
Mail Stop M2-250
P. O. Box 92957
Los Angeles, CA 90009

(213) 336-7389

SWENSON, Gary R.
Lockheed Missiles & Space
Company, Inc.
Dept. 91-20, Bldg 255
3251 Hanover Street
Palo Alto, CA 94304-1191

(415) 424-3297

TENNEY, Darrell R.
NASA Langley Research Center
188M
Hampton, VA 23665-5225

TENNYSON, Rod C.
University of Toronto
Institute for Aerospace Studies
4925 Dufferin Street
Downsview, Ontario
CANADA M3H5T6

(416) 667-7710

TRAJMAR, Sandor
Jet Propulsion Laboratory
MS 183-601
4800 Oak Grove Drive
Pasadena, CA 91109

(818) 354-2145
(FTS) 792-2145

VALLERGA, John V.
Univ. of California/Oakland
Space Sciences Laboratory
Oakland, CA 94602

(415) 643-8165

VAN EESBEEK, Marc
European Space Technology and
Research Center
Keplerwan, Noordwyk
NETHERLANDS 01719-83896

VISENTINE, James T.
NASA Johnson Space Center
Code ES5
Houston, TX 77058

(713) 483-4564
(FTS) 525-4564

WODARCZYK, Frank J.
U. S. Air Force
Office of Scientific Research
AFOSR/NC
Bolling AFB
Washington, DC 20332-6448

(202) 767-4963

YANKIE, Gerald W.
McGhan Nusil Corporation
1150 Mark Avenue
Carpinteria, CA 93013

(805) 684-8780

YILGOR, Iskender
Mercor, Inc.
2448 Sixth Street
Berkeley, CA 94710

(415) 849-0452

ZIMCIK, David G.
Communication Research
Centre
Station H
P. O. Box 11490
Ottawa, Ontario
CANADA K2H 8S2

(613) 998-2187